Semifluxons in long Josephson junctions with phase shifts

Saeed Ahmad, M.Sc.

Thesis submitted to The University of Nottingham
for the degree of Doctor of Philosophy

June 2012

Dedicated to

My beloved late mother

Who taught me the abc of life!

and

My respected late uncle Muhammad Idris (Daa Daa)

Who loved me like his own son!

"Years of hard work
Moments of desperation and hope
My beloved mother and uncle, to both of you"

Abstract

A Josephson junction is formed by sandwiching a non-superconducting material between two superconductors. If the phase difference across the superconductors is zero, the junction is called a conventional junction, otherwise it is unconventional junction. Unconventional Josephson junctions are widely used in information process and storage.

First we investigate long Josephson junctions having two π-discontinuity points characterized by a shift of π in phase, that is, a 0-π-0 long Josephson junction, on both infinite and finite domains. The system is described by a modified sine-Gordon equation with an additional shift $\theta(x)$ in the nonlinearity. Using a perturbation technique, we investigate an instability region where semifluxons are spontaneously generated. We study the dependence of semifluxons on the facet length, and the applied bias current.

We then consider a disk-shaped two-dimensional Josephson junction with concentric regions of 0- and π-phase shifts and investigate the ground state of the system both in finite and infinite domain. This system is described by a $(2+1)-$ dimensional sine-Gordon equation, which becomes effectively one dimensional in polar coordinates when one considers radially symmetric static solutions. We show that there is a parameter region in which the ground state corresponds to a spontaneously created ring-shaped semifluxon. We use a Hamiltonian energy characterization to describe analytically the dependence of the semifluxonlike ground state on the length of the junction and the applied bias current. The existence and stability of excited states bifurcating from a uniform case has been discussed as well.

Finally, we consider 0-κ infinitely long Josephson junctions, i.e., junctions having periodic κ-jump in the Josephson phase. We discuss the existence and stability of ground states about the periodic solutions and investigate band-gaps structures in the plasma band and its dependence on an applied bias current. We derive an equation governing gap-breathers bifurcating from the edge of the transitional curves.

Acknowledgements

All glories and praise be to Allah, The Most Merciful and Mighty, Who created me, raised me, and blessed me with His unlimited bounties. It is just due to His mercy that I have completed this task, otherwise, I would not have had the ability to complete it.

The completion of this thesis would not have been possible without the generous help of many. To list all of them is, unfortunately, not possible here, but still they are not forgotten. I want to thank all of them from the core of my heart. I feel honoured for the supervision of Dr. Hadi Susanto, and Dr. Jonathan Wattis, from The University of Nottingham. This thesis would not have been completed without the help, support, guidance, and efforts of my supervisors. I would like to offer my sincerest gratitude and thanks to Dr. Susanto and Dr. Wattis who have supported me throughout my PhD studies with their patience, and knowledge.

I would like to offer my heartiest gratitude to my wife and best friend, Syeda Saadat Saeed, for her strong moral support and encouragement during this study and throughout my time with her. Thanks are to my brothers Mian Syed Hassan, Mian Noor Hassan, Abid Ahad, Habib Ahmad and Syed Yahya for their encouragement. The sincere love of my beloved sons Saad, Saud, and Asaad, played a key role in the completion of this thesis. I am also grateful to my immediate and extended family for the unflagging support . I must also thank my good friends in the UK and Pakistan, for their constant words of encouragement over the years. It is a pleasure to single out Rais Ahmed, S M Murtaza, M Aamir Qureshi, Liaq Bahadar, and Khuda Bakhsh, who have aided me in more ways than I can possibly acknowledge here. I have no words to thank my respected father, Hafiz Muhammad Zubair, who is dearer to me more than anyone, even myself. Finally, I would like to thank the University of Malakand Chakdara, Dir(L), Pakhtunkhwa, Pakistan for the financial support.

Saeed Ahmad,
Nottingham, United Kingdom, 14th June 2012.

Contents

List of Figures

CHAPTER 1

Introduction

1.1 Superconductivity: a historical development

Material objects are mainly divided into two categories. One of these categories consists of objects (usually metals, e.g., copper, aluminium, etc) that allow electric current to pass through in the presence of a potential difference. Such objects are called *conductors*. A metal consists of a lattice, where atoms are so close to each other that the electrons in the outermost shell are free to dissociate from their parent atoms and move throughout the lattice. Such electrons are called *free* electrons. When a potential difference is applied to such a metal the free electrons move throughout the metal. This movement of free electron in a metal is called an *electric current*. Collisions of electrons with other particles produces *resistance*. Resistance, R, to an electrical current, I, is described by Ohm's Law[1], which states that $R = V/I$, where V is the potential difference applied across the ends of the conductor.

Certain metals, when cooled to a certain critical temperature, have negligibly small electrical resistance. This was first discovered in 1911 by a Dutch physicist, H. Kamerlingh-Onnes, who studied the temperature-dependence of the resistance in mercury. He cooled mercury to about $T_c \sim 4.2K$ $(-452^\circ F, -269^\circ C)$ and observed amazing behaviour. The electrical resistance dropped to zero and remained zero at temperatures less than T_c. This phenomenon of no resistance to electricity was called *superconductivity* by Kamerlingh-Onnes [2]. Soon after the discovery of this phenomenon in mercury, several other simple metals, like aluminium (Al_{13}), indium (In_{49}) and stannum (Sn_{50}) were found to be superconductive. For his wonderful discovery, H. Kamerlingh-Onnes was awarded the 1913 Nobel Prize in Physics.

In 1933 German physicists Walther Meissner and Robert Ochsenfeld discovered that

below a certain critical temperature, a superconducting material will repel a magnetic field, that is, the superconductor exhibits perfect diamagnetism [3]. This great discovery helped in understanding how matter behaves at extremely cold temperatures and is known as the Meissner effect. Theorists have to resort to quantum mechanics to explain this effect since it is unexplainable by classical physics.

In 1935, two German physicists and brothers Heinz and Fritz London proposed equations [4] which gave the first explanation of the Meissner effect. These equations predict how far a magnetic field penetrates into a superconductor. The understanding of superconductivity became more sophisticated in 1950 with the Ginzburg-Landau theory [5], which gave a macroscopic explanation of superconductivity and provided a derivation of the London equations.

In the same year a German-born British physicist Herbert Fröhlich observed that under certain circumstances there can be an attractive interaction between electrons of a material and quanta of crystal lattice vibrational energy [6]. The quanta of crystal lattice vibrational energy are called *phonons*. This opened a remarkable gateway towards the microscopical understanding of superconductivity. In 1956 Leon Cooper, an American physicist, extended these ideas and showed that there can be a small attraction between electrons in a metal. This attraction causes bound pairs of electrons, called *Cooper pairs*, to form. Cooper showed that with these pairs of 'bound' electrons, the ground state of a material is unstable [7]. In low temperature superconductors, Cooper pairs form due to the interaction of an electron in the positively charged lattice and a phonon, and can overcome Coulomb repulsion.

In the year 1957 the first widely accepted theoretical understanding of superconductivity was proposed by American physicists John Bardeen, Leon Cooper, and John Schreiffer [8]. Based on Cooper's 1956 work, this theory, known as the BCS theory, explained superconductivity at temperature close to absolute zero. The theory reveals that Cooper pairs can condense into the same energy level and this explains the perfect diamagnetism, the dependence of critical temperature on isotopic mass, and the effect of zero electrical resistivity. For the development of this theory, Bardeen, Cooper and Schreiffer won the 1972 Nobel Prize in Physics.

In 1962 a British physicist Brain David Josephson predicted the possibility of the tunnelling of the Cooper pairs from one superconductor to anther through a nonsuperconducting (or an insulating) barrier in the absence of voltage difference across the barrier (Josephson [9]). Later on his work was confirmed experimentally and won him a share

of the 1973 Nobel Prize in physics. The phenomenon of tunnelling of the Cooper pairs through the nonsuperconducting barrier in the absence of a potential difference across it, called *Josephson tunnelling* or *the Josephson effect*, and has since attracted the attention of many researchers.

Up to 1980, the highest theoretical critical temperature for the superconductive transition of a material was thought to be $30K$. In 1986 a German physicist J. Georg Bednorz together with a Swiss physicist K. Alexander Müller studied the conductivity of lanthanum barium copper oxide ($La_{2-x}Ba_xCuO_4$) ceramic. Ceramics were considered to be insulators. Bednorz and Müller not only discovered the superconductivity of ceramic materials but also showed that their superconductive transition occurred at a critical temperature of $T_c = 35K$, which was greater than the presumed critical high temperature [10]. This discovery classified superconductors into two types, namely the low, and the high temperature superconductors. In high temperature superconductors the total orbital momentum of the paired electrons is nonzero. This is called a *d-wave state*. In low temperature superconductors the orbital momentum of the paired electrons is zero and forms an *s-wave state*.

One year later, Bednorz and Müller discovered the superconductivity of yttrium barium cuprate (Y Ba_2 Cu_3 O_7) with $T_c = 93K$. For their important breakthrough in the discovery of ceramic superconductors, Bednorz and Müller were awarded the 1987 Nobel Prize in Physics.

In 1993 A. Schilling and his team reported the superconductivity of mercury barium cuprate (Hg $Ba_2Ca_2Cu_3O_{8-\delta}$) with $Tc \approx 134K$ [11], which is the highest T_c superconductor discovered so far. In 2006, a group of Japanese researchers discovered an iron-based layer superconductors [12]. The exact mechanism which causes the superconductivity in them is still a mystery. Research on the development of superconductivity is a dynamic and rich field which will hopefully bring fascinating discoveries.

Work on superconductivity has been awarded the Nobel Prize in Physics on four occasions in nearly hundred years. Superconducting-based technology has presented valuable products having applications in medicine, in the improvement of magnetic resonance imaging (MRI). Superconductor magnets are used to eliminate friction between magnetic levitation trains and track and causes the high speed of Maglev trains. Superconducting Quantum Interference Devices (SQUIDS) are used to remove land mines and detect even the weakest magnetic fields. Efforts are in progress to use superconductors to make ultra fast computers and for the more efficient generation of

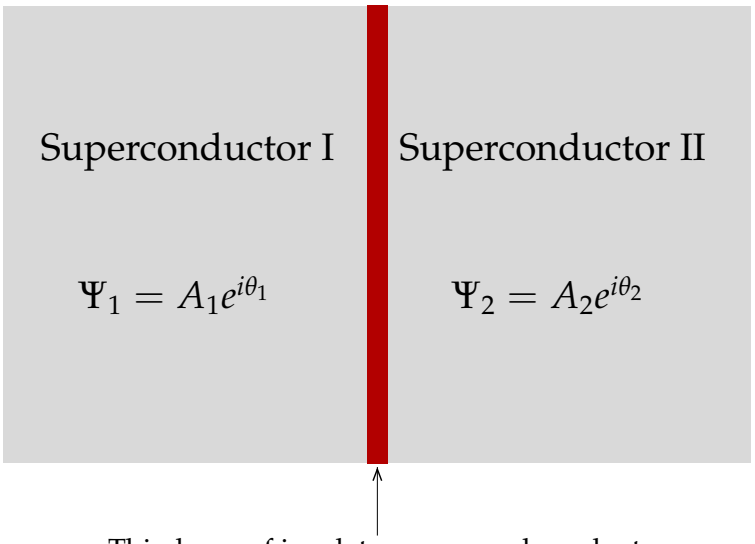

Figure 1.1: A sketch of a Josephson junction

electricity.

1.2 Josephson junctions and related terms

In this thesis, we are mainly concerned with Josephson junctions, therefore, it is advantageous to begin with an introduction to Josephson junctions and related terminology. Named after its inventor, B. D. Josephson, a Josephson junction (also called Josephson transmission line) is a simple macroscopic quantum system that consists of two superconducting layers separated by a non-superconducting layer (or a weak link) as shown in Fig. 1.1. The non-superconductor layer normally acts as a barrier to the flow of conducting electrons from one superconductor to the other. If the barrier is sufficiently thin– about $30 \times 10^{-10} m$, if it is insulator, see Kittel and McEuen [13] , or (up to) some microns $(10^{-6} m)$, if it is a normal conductor, see e.g., Remoissenet [14]– it is possible for electrons that impinge on the barrier to pass from one superconducting layer to the other. This flow of electrons between the two superconductors across the barrier is called tunnelling.

The flow of electrons between the superconductors in the absence of an applied voltage is known as *Josephson current* and the movement of electrons across the barrier is called *Josephson tunnelling*. A Josephson junction is said to be in the *ground state* when no external currents or magnetic fields are applied to it.

1.2.1 Some basic definitions

In quantum mechanics, a wave function is a function that gives a mathematical description of the wave nature of a particle of a physical system. At a given point of the space and time the value of the wave function of the particle is associated with the probability of the presence of the particle at that time.

Let $\Psi_1 = A_1 e^{i\theta_1}$ and $\Psi_2 = A_2 e^{i\theta_2}$ represent the wave functions that describe the two superconductors of a Josephson Junction respectively (see Fig. 1.1), where A_1, A_2 are related to Cooper pair densities of the two superconductors respectively, and θ_1, θ_2 are the internal phases of the superconductors. The difference between the internal phases of the two superconductors

$$\phi = \theta_2 - \theta_1, \tag{1.2.1}$$

is known as *Josephson phase*. In superconducting circuits, the Josephson phase plays a role similar to that of electrostatic potential difference in conventional circuits and controls the current through the device.

A Josephson junction is said to be a $0-$junction if the Josephson phase ϕ in the ground state (the lowest energy state) is zero. Likewise if $\phi = \pi$, the Josephson junction is said to be a π-junction.

A measure of the distance, generally ranging from $50nm$ to $500nm$, within which a magnetic field penetrates a superconductor is called *London penetration depth*. Let m_e denotes the mass of an electron and q_e be its charge, then the London penetration depth is given by, see for instance, Kittel and McEuen [13] and Vasiliev [15]

$$\lambda_L = \sqrt{\frac{\epsilon_0 mc^2}{n_s q^2}}, \tag{1.2.2}$$

where $\epsilon_0 = 1/4\pi$, n_s is the number density, and c is the velocity of light.

A length that gives a measure of a typical distance over which an externally applied magnetic field penetrates a Josephson junction is called a *Josephson penetration depth* and is generally denoted by λ_J. Let d denote the thickness of the sandwiched barrier between the two superconducting electrodes of the junction, then the Josephson penetration depth (λ_J) is given by the relation (see Tinkham [16])

$$\lambda_J = \sqrt{\frac{\Phi_0}{2\pi\mu_0 d' J_c}}, \tag{1.2.3}$$

where $\mu_0 = c/4\pi$, $\Phi_0 = h/2e \approx 2.07 \times 10^{-15} Wb$ is the magnetic flux quantum, $h = 6.26 \times 10^{-34} Js$, is Planck's constant and $e = 1.6021765 \times 10^{-19} C$, is the charge

on electron. The term d' in Eq. (1.2.3) is the sum

$$d^{'} = d + 2\lambda_L, \tag{1.2.4}$$

such that λ_L is the London penetration depth, and J_c is the critical current density, the current density below which transport current is carried without any resistance. The quantity $\mu_0 d'$ is the inductance of the superconducting electrodes of the junction.

On the basis of the Josephson penetration depth, λ_J, Josephson junctions are classified into *short* and *long* Josephson junctions. A long Josephson junction is one whose dimensions are large compared with λ_J. A short Josephson junction, on the other hand, is a junction having dimensions smaller than λ_J. In this thesis, we restrict ourselves to problems related to long Josephson junctions only.

Long Josephson junctions (LJJs) are widely studied by a number of authors who illustrate their practical application in the real world, see, for instance Ioffe et al. [17], and Yamashita et al. [18]. These junctions are intensively studied to realize Cooper-pair box qubit [19], phase qubit [20] or flux qubit, which consists of a superconducting loop with three Josephson junctions [21]. Here, a qubit is a basic element via which the information is stored in the quantum computer (an innovative device which makes it possible to solve problems that take a very long time on classical computers [22]). Qubit can be physically realized using various systems, e.g., solid state devices.

Electric current that passes through the superconductors of a Josephson junction without dissipation is termed a *supercurrent* and is denoted by I_s. The maximum current that can be supported by a Josephson junction is called the *critical current* and is represented by I_c. The value of the critical current depends upon the properties of the Josephson barrier.

1.3 A short review of some important results

In this section, we review the recent developments in Josephson junctions.

In his classical paper [9], Josephson showed that the electron flow tunnelling (i.e., Josephson current) across the barrier is proportional to the sine of the phase difference of the wave functions of the two superconductors of the Josephson junction. Mathematically, if $\phi(x,t)$ represents the Josephson phase, where x and t denote the spatial and temporal variables along the junction respectively, I_s is the super current across the barrier, then the Josephson phase (ϕ) and I_S are related through a $2\pi-$periodic relation,

called "the Josephson current phase relation"

$$I_s = I_c \sin(\phi), \tag{1.3.1}$$

where $I_c > 0$ is the critical current that depends on the properties of the weak link. Eq. (1.3.1) shows that when there is no current flowing across the junction, then $I_s = 0$, and we have $\sin(\phi) = 0$. Thus Eq. (1.3.1) has two stationary uniform solutions, given by

$$\phi = 0,\ \pi \mod(2\pi). \tag{1.3.2}$$

The solution $\phi = 0$, represents the zero phase difference between the two superconductors of the Josephson junction (see Eq. 1.2.1). It is straightforward to show that the solution $\phi = 0$ is stable and corresponds to the minimum of energy of the junction [23].

As shown in Rowell et al. [24], the Josephson energy is given by

$$E_J = (\Phi_0/2\pi)\, I_c \cos(\phi + \pi), \tag{1.3.3}$$

where Φ_0 is the magnetic flux quantum and I_c is the critical current through the junction. Thus $\phi = 0$ is the ground state. Similarly, the solution $\phi = \pi$ of Eq. (1.3.1) is unstable and corresponds to the energy maximum. We note that the Josephson phase, satisfying Eq. (1.3.1) is a continuous function of the spatial variable x. Such junctions are called conventional Josephson junctions.

A magnetic field that is applied parallel to the barrier of a conventional long Josephson junction penetrates the junction in the form of vortices which carry single quantum of magnetic flux. Such quantized vortices are called fluxons. Fluxons, from a mathematical point of view, are solitons which can move freely along the junction.

1.3.1 Josephson junctions with a π-phase shifts

It is natural to ask, what happens if one can produce a discontinuity in the Josephson phase $\phi(x,t)$ by creating an arbitrary shift, say, $\theta(x)$ in it? It was Bulaevskiĭ [25], who, first of all, theoretically suggested that if the Josephson barrier is of ferromagnetic nature, one can create a phase shift $\theta(x) = \pi$, in the Josephson phase. In such a case, the current phase relation becomes

$$I_s = I_c \sin(\phi + \pi) = -I_c \sin(\phi). \tag{1.3.4}$$

This modified Josephson relation given by Eq. (1.3.4) shows that π-junction behaves as if it were a conventional Josephson junction with negative critical current. Again,

as with Eq. (1.3.1), it can be deduced, that for a Josephson junction in the absence of a supercurrent ($I_s = 0$), Eq. (1.3.4) suggests two uniform solutions, namely $\phi = \pi, 0 \mod(2\pi)$. It can be seen that the stability of the constant solutions is reversed. That is, for a phase jump of π, the uniform solution $\phi = \pi$ corresponds to the energy minimum and is stable. The solution $\phi = 0$ is unstable and corresponds to the energy maximum.

As mentioned earlier, π-junctions were proposed more than 30 years ago, yet their remarkable properties are verified in experiments only recently, see, for instance, Van Harlingen [26], Baselmans et al. [27], and Ryazanov et al. [28].

1.3.1.1 Experimental fabrication of π-junctions

Because of their potential application in electronics, as described in Terzioglu et al. [29], Terzioglu and Beasley [30]), and digital circuits (see Testa et al. [31]), π- junctions are widely studied using a variety of different technologies. These include superconductor-ferromagnet-superconductor (SFS) technology which is considered by Ryazanov et al. [28], Sellier et al. [32], Ryazanov et al. [33], Bauer et al. [34], Blum et al. [35], etc.

As is clear from the name, the Josephson barrier in such junctions is of ferromagnetic nature and is sandwiched between the two superconductors. It was shown by Buzdin [36, 37] that the formation of the π- shift in (SFS) Josephson junctions is due to the sign reversing and oscillating superconducting order parameter in the Josephson barrier. If the length of the ferromagnetic barrier is of the order of the wavelength of this oscillation, there will be no change in the superconducting order parameters of the two superconductors. On the other hand, if the barrier's thickness is chosen to that of the order of half of an oscillation's wavelenth, different signs of the order parameter can occur at the two banks of the junction. This change of order corresponds to a sign change in the energy and super current of the junction, and hence, a π-shift is created. It was reported in[37], that besides the thickness of the barrier d_F, the sign of the critical current (I_c) and the Josephson phase (ϕ) also depend upon the temperature T. A drawback of this technology is that it is highly over damped and cannot be applied to the case where low dissipation is needed.

Another way to fabricate a π-junction is to sandwich an insulator-ferromagnetic barrier between the superconductors, known as superconductor-insulator-ferromagnet-superconductor (SIFS) technology , see Kontos et al. [38], and Weides et al. [39]. The junction so formed is an obvious way to decrease damping. In such junctions the cri-

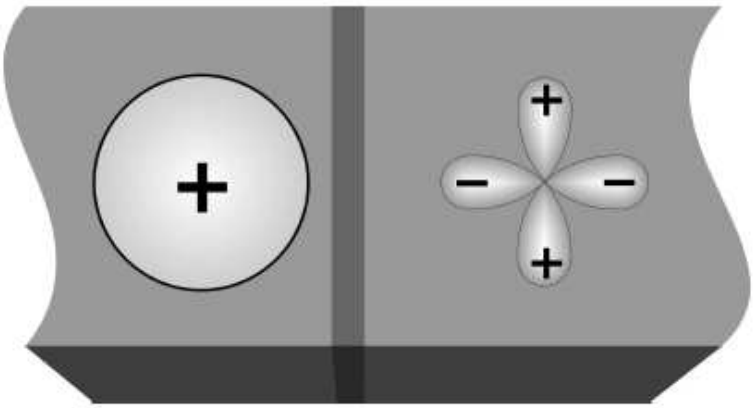

Figure 1.2: A sketch of a Josephson junction formed by s-wave and d-wave superconductors. Such a configuration gives rise to a π-Josephson junction because the phase difference is π. The positive lobe of the s-wave superconductor coincides with the negative lobe of the d-wave superconductor.

tical current is an oscillating function of the barrier thickness. By choosing a certain thickness of the ferromagnetic barrier, the sign of the critical current changes from one superconductor to the other, giving rise to a π-shift in the Josephson phase.

Baselmans et al. [27] reported that a π- junction can be fabricated by enclosing a normal metal between two superconductors, called the superconductor - normal metal-superconductor (SNS) technology. This can be achieved by controlling the energy distribution of the current carrying states in the Josephson barrier (which is a normal metal in the present case).

π-junctions were also realized by using d-wave symmetry of the order parameter in the high temperature (T_c) superconductors (see Tsuei and Kirtley [40, 41], Barash et al. [42], and Il'Ichev et al. [43]). One of the superconductors of the long Josephson junction in such a configuration is of s-wave order and the other is of d-wave order. The junction formed by such a configuration can have an intrinsic shift of π in its phase. The Cooper pair can tunnel from the negative lobe of the d-wave order parameter in one side of the junction to the positive lobe of the s-wave on the other side and a π-junction is formed as shown in Fig. 1.2. It may be noted that, in a Josephson junction formed by such a configuration, the Josephson energy (E_J) is minimized by the phases of the order parameters on both sides of the junction, if the phase difference between the two superconductors is set to π. To obtain a π-junction, the junction is made in such way that there is no possibility of minimizing the Josephson energy in all parts of the junction.

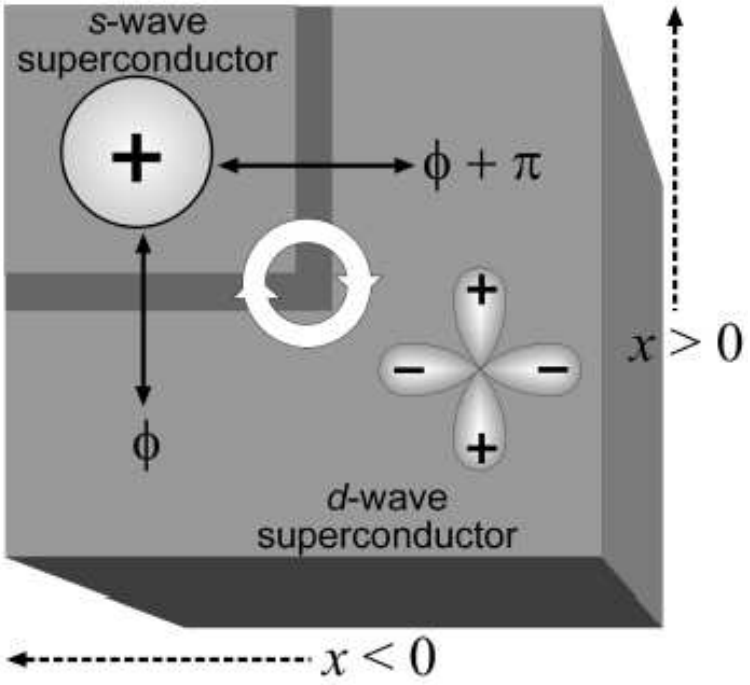

Figure 1.3: The formation of π-phase shift in Josephson junction formed by s-wave and d-wave superconductors, the so-called corner junction.

π-junctions can also be made by constructing a so-called "corner junction" as considered by Van Harlingen [26], Smilde et al. [44], H Hilgenkamp and Tsuei [45]. In such junctions the wave function of the conventional (s-wave) superconductor simultaneously overlaps with a part of the unconventional (d-wave) superconductor wave function with different signs as depicted in Fig. 1.3.

Recently, Goldobin et al. [46] showed that a π-discontinuity can be created in a Josephson junction by using a pair of current injectors. The configuration they used is shown in Fig 1.4, where Δw denotes the width of each current injector and Δx is the distance between the two current injectors. It was shown that if Δx and Δw are sufficiently small and are well below the Josephson penetration depth (λ_J), an artificial phase shift of π can be created in the Josephson phase using this configuration. Among all 0-π Josephson junctions technologies available nowadays, only SFS or SIFS technology allows the fabrication of the 0-π boundary of arbitrary shape. Indeed, recently 0-π long Josephson junctions with 0-π boundary forming a loop were successfully fabricated and the supercurrent transport in them was visualized, see Gulevich et al. [47].

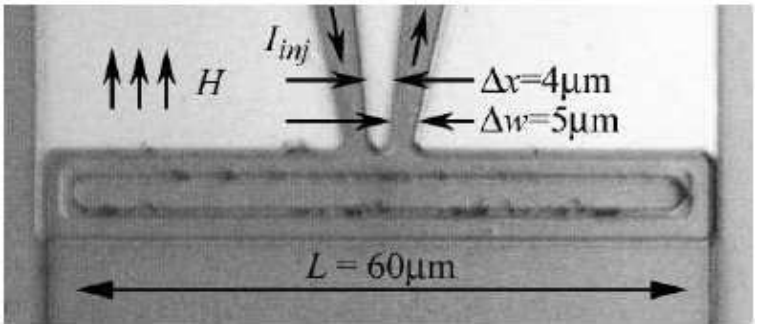

Figure 1.4: An optical microscopic image of the long Josephson junction with two current injectors, where the width of the junction is $5\mu m$. A π-phase shift can be created by junction with such a configuration. This figure is taken from [46].

1.3.2 Uses of π-Josephson junctions

There are several applications of π-Josephson junctions. Braunisch et al. [48] and Sigrist and Rice [49] have proposed π-junctions in high-T_c superconductors to explain the positive paramagnetic Meissner effect. It has been conjectured by Ortlepp et al. [50], and Pegrum [51] that π-junctions have promising applications in information storage and processing. The use of the half vortices created in π-junctions in superconducting memory and logic devices, has previously reported by Kuklov et al. [52]. They demonstrated that by the application of an external current to the junction, the orientation of the half vortex in the π-junction can be changed.

1.3.3 Unconventional long Josephson junctions

A Josephson junction having uniform phase difference across its superconductor is termed as *conventional* Josephson junction. A junction whose different parts having different phase difference is, therefore, termed an *unconventional* junction. In such junctions there is discontinuity in the Josephson phase. The point where the two parts combine is called a point of discontinuity.

In this section, we will concentrate on unconventional Josephson junctions, and in particular, a junction having a π-discontinuity in its phase. As we will see later, an interesting situation can be obtained if one considers such Josephson junctions.

The possibility of a Josephson junction with half portion behaving as a 0- junction and the other half as a π- junction, i.e. a so called 0-π Josephson junction, was first investigated by Bulaevskiĭ [53]. They reported that when the lengths of the 0 and π parts

are the same, equal amount of critical currents flow through them. The supercurrent through the zero part has a positive direction [see Eq. (1.3.1)] while that through the π-part is flowing in the opposite direction [see Eq. (1.3.4)]. These supercurrents, with opposite directions, circulate around the 0-π boundary and create a vortex around the discontinuity. In other words, the ground state of a 0-π Josephson junction corresponds to a spontaneous generation of a vortex of super currents. Such a vortex carry a magnetic flux with magnitude $|\Phi| = \pm\Phi_0/2$, (half of the magnetic flux quanta) and is, therefore, called a *semifluxon* or a *fractional fluxon* (see e.g. [54, 55]). Here $\Phi_0 = h/2e \approx 2.07 \times 10^{-15} Wb$ is a single magnetic flux quantum carried by vortices in long Josephson junctions and are called *fluxons*.

A long Josephson junction with alternating 0 and π facets was numerically studied by Goldobin et al. [56] and analytically by Susanto et al. [57]. They showed that if the length L of the junction is very large compared with the Josephson penetration length λ_J, a single semifluxon may be generated at the point of discontinuity in the junction and is pinned there. They also showed that such semifluxon can have both positive and negative polarities. Semifluxons with a negative polarity carry a magnetic flux equal to the negative of the half magnetic flux quanta. For a very long Josephson junction, the size of the spontaneously generated vortex (semifluxon) is proportional to λ_J. Kirtley et al. [58] have studied the size of the semifluxon for different values of L. They reported that if $L \leq \lambda_J$, (i.e., short Josephson junction) then vortex will not "fit" into the junction and the flux Φ inside the junction is much less than that of the semifluxon ($\Phi_0/2$).

Semifluxons are different from integer fluxons in the sense that fluxons are solitons while semifluxons are not. Semifluxons are automatically generated and are attached to the discontinuity in a 0-π Josephson junctions. Hence, they correspond to a ground state of the system. This ground state is degenerate, that is, there are two ground states corresponding to negative and positive spontaneously generated half flux, which corresponds to the counterclockwise and clockwise circulating supercurrent respectively. Fluxons on the other hand, are generated externally and manually in experiments and correspond to an excited state. Due to this property, semifluxons are attractive for their application in information storage and classical and quantum devices. It was reported by Goldobin et al. [56] the semifluxons in a Josephson junction cannot be moved by a bias current if its value lies between zero and $2I_c/\pi$, with I_c being given by $I_c = J_c wL$ (L, and w respectively represent the length and width of the junction and J_c is the critical current density.)

Semifluxons are experimentally observed in various types of $0-\pi$ long Josephson junctions. Kirtley et al. [59, 60] have observed semifluxons using Superconducting Quantum Interference Device (SQUID) microscopy in yttrium barium copper oxide ($YBa_2Cu_3O_{7-\delta}$) high-T_c superconductive Josephson junctions. Sugimoto et al. [61] reported the presence of the half flux quantum at the tricrystal grain boundary of a thin superconducting film. Tsuei and Kirtley [40] observed semifluxons for the first time using d-wave superconductors at so-called tricrystal grain boundary and later on in $YBa_2Cu_3O_7$-Nb ramp zigzags by H Hilgenkamp and Tsuei [45]. The π-shift does not take place inside the Josephson barrier in all these systems but occurs inside the d-wave superconductors.

Gürlich et al. [62] have observed semifluxons in superconductor-insulator-ferromagnet-superconductor (SIFS) junctions by using low-temperature scanning electron microscopy (LTSEM). Farhan-Hassan and Kusmartsev [63] have recently presented a novel type of semifluxons arising in a T-shaped conventional long Josephson junctions (LJJ). They showed that such semifluxons in Josephson junctions are movable, i.e, they are not pinned at the discontinuity. They also showed that such semifluxons can be created by flux cloning phenomenon arising in the T-shaped junctions. The interested reader is referred to see e.g., the report of Gulevich and Kusmartsev [64] for the detail of flux cloning in Josephson junctions. Most recently Chen and Zhang [65] have investigated a long Josephson junction with two identical iron based superconductors (Fe pncitides) that are separated by a thick vacuum barrier. They observed semifluxons in niobium polycrystal loop.

Because of difficulties in a fabrication of 0-π junctions, semifluxons are not widely studied experimentally. The classical properties of semifluxons are, however, understood (see, for instance [66, 67]), and their possible applications in quantum domain still need to be studied.

1.4 Mathematical model

In the following, we derive the model which we use to describe the dynamics of the Josephson junctions.

Let E_1 and E_2 be the ground state energies of the two superconductors of width a that are separated by a nonsuperconducting barrier of thickness d forming a Josephson junction. Assume ϕ_1, and ϕ_2 be the internal phases of the two superconductors of

the Josephson junction. If ρ_1, and ρ_2 are the pair densities of the two superconductors respectively then the wave functions of the two superconductors, defined in section 1.2.1 take the form

$$\Psi_1 = \sqrt{\rho_1}e^{i\phi_1}, \quad \Psi_2 = \sqrt{\rho_2}e^{i\phi_2}. \tag{1.4.1}$$

In the absence of external potential difference, the junction is in the ground state. If a potential difference V is applied to the junction, the energy difference becomes $\Delta E = E_1 - E_2 = 2eV$, where $2e$ is the charge of a pair. If we define $E_1 = eV$ and $E_2 = -eV$, then the zero energy level can be defined halfway between the values of E_1 and E_2. It can be then shown that Ψ_1 and Ψ_2 satisfy the following linearly coupled Schrödinger equations (see Remoissenet [14] for detail)

$$i\hbar\frac{\partial\Psi_1}{\partial t} = eV\Psi_1 + K\Psi_2, \quad i\hbar\frac{\partial\Psi_2}{\partial t} = -eV\Psi_2 + K\Psi_1, \tag{1.4.2}$$

where $\hbar = h/2\pi$, is the reduced Plank's constant and $K \in \mathbb{R}$ represents the coupling of the superconductors.

Plugging Eqs. (1.4.1) into Eqs. (1.4.2) one can easily write

$$i\hbar\left(\frac{1}{2\sqrt{\rho_1}}\frac{\partial\rho_1}{\partial t} + i\sqrt{\rho_1}\frac{\partial\phi_1}{\partial t}\right) = eV\sqrt{\rho_1} + K\sqrt{\rho_2}e^{i\phi}, \tag{1.4.3a}$$

$$i\hbar\left(\frac{1}{2\sqrt{\rho_2}}\frac{\partial\rho_2}{\partial t} + i\sqrt{\rho_2}\frac{\partial\phi_2}{\partial t}\right) = -eV\sqrt{\rho_2} + K\sqrt{\rho_1}e^{-i\phi}, \tag{1.4.3b}$$

where $\phi = \phi_2 - \phi_1$ is the Josephson phase. Comparing the real parts on both sides of Eqs. (1.4.3), we obtain

$$-\hbar\frac{\partial\phi_1}{\partial t} = eV + K\sqrt{\frac{\rho_2}{\rho_1}}\cos(\phi), \tag{1.4.4a}$$

$$-\hbar\frac{\partial\phi_2}{\partial t} = -eV + K\sqrt{\frac{\rho_1}{\rho_2}}\cos(\phi). \tag{1.4.4b}$$

Practically the supply of the excess charges ρ_1, ρ_2 through the source of external voltage remains constant, i.e. one can assume $\rho_1 = \rho_2 = \rho_0$ say. In this case Eqs. (1.4.4), after a simple algebra, yield

$$\frac{\partial\phi}{\partial t} = \frac{2e}{\hbar}V = \frac{2\pi}{\Phi_0}V, \tag{1.4.5}$$

which is one of the basic equations explaining the Josephson effect. Here $\Phi_0 = h/2e$ is the magnetic flux quantum and $\hbar = h/2\pi$.

By equating the imaginary parts on both side of Eqs. (1.4.3), one may write

$$\hbar\frac{\partial\rho_1}{\partial t} = 2K\sqrt{\rho_1\rho_2}\sin(\phi), \tag{1.4.6a}$$

$$\hbar\frac{\partial\rho_2}{\partial t} = -2K\sqrt{\rho_1\rho_2}\sin(\phi). \tag{1.4.6b}$$

Again, since ρ_1 and ρ_2 are the density of pairs in the two superconductors, the quantities $\partial\rho_1/\partial t$ and $\partial\rho_2/\partial t$ represent the current densities J_1 and J_2 in the two superconductors respectively. As a result Eqs. (1.4.6) give

$$J = J_0 \sin(\phi), \tag{1.4.7}$$

with $J_0 = -4K\rho_0/\hbar$ and $\rho_0 \approx \sqrt{\rho_1\rho_2}$.

Eq. (1.4.7) represents the Josephson tunnelling (also called the quantum mechanical tunneling (QMT)) of the superconducting electron pair through the Josephson barrier [68].

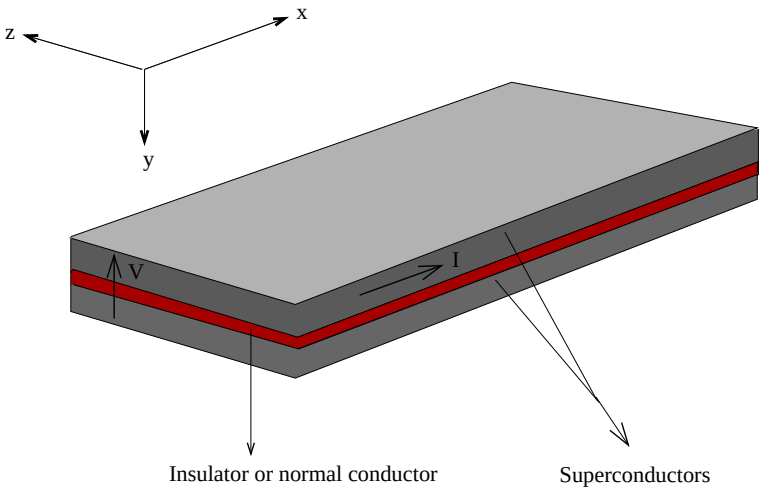

(a) Josephson junction

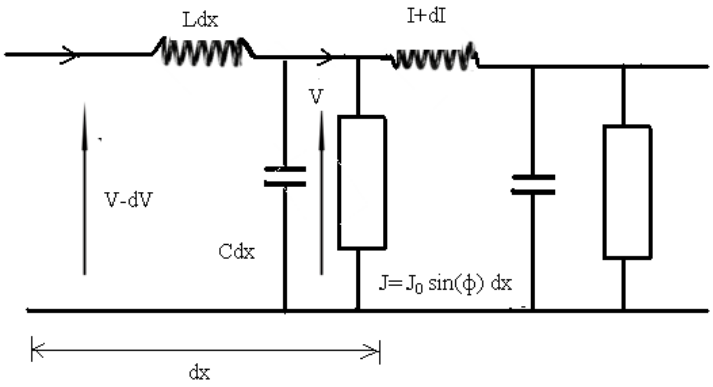

(b) Non dissipative Josephson transmission line.

Figure 1.5: (a) Schematic representations of a Josephson junction and (b) an electrical equivalent of a Josephson transmission line.

Next, we want to find a relation for the Josephson phase ϕ in terms of the spatial va-

riable x and the time t. For this purpose, we consider a Josephson junction shown in the upper panel of Fig. 1.5, and assume the width of the junction is small enough and neglect dissipation in the junction. We consider the gradient of electromagnetic field in the Josephson barrier to be uniform in one space, therefore, the y direction is considered small when compared to the x direction. In the lower panel of the same figure, we consider an electrical equivalent to the Josephson junction under consideration.

Let L be the inductance, the ability of the junction to oppose any change in the current, per unit length of the junction; C be its capacitance, and J_B is the bias current– a current that is fed to a device to ensure its functions with desired characteristics– applied to the junction. Applying Kirchhoff's voltage and current laws [14, 69] to the model given in Fig. 1.5, one may write

$$\frac{\partial V}{\partial x} = -L\frac{\partial I}{\partial t}, \tag{1.4.8a}$$

$$\frac{\partial I}{\partial x} = J_B - C\frac{\partial V}{\partial t} - J_0\sin(\phi) - \frac{V}{R}. \tag{1.4.8b}$$

Differentiating Eq. (1.4.5) partially with respect to x and t and assuming the continuity of the partial derivatives, we respectively obtain

$$\frac{\partial V}{\partial x} = \frac{\Phi_0}{2\pi}\frac{\partial}{\partial t}\left(\frac{\partial \phi}{\partial x}\right), \quad \frac{\partial V}{\partial t} = \left(\frac{\Phi_0}{2\pi}\right)\frac{\partial^2 \phi}{\partial t^2}. \tag{1.4.9}$$

Substituting the first equation in Eq. (1.4.9) into Eq. (1.4.8a), integrating with respect to t and neglecting the integration's constant, we can write

$$I = -\left(\frac{\Phi_0}{2\pi L}\right)\frac{\partial \phi}{\partial x}. \tag{1.4.10}$$

Differentiating Eq. (1.4.10) partially with respect to x, plugging the resulting equation along with Eqs. (1.4.5) and (1.4.9) and into Eq. (1.4.8b) and dividing throughout by J_0, we can obtain

$$\left(\sqrt{\frac{\Phi_0}{2\pi L J_0}}\right)^2\frac{\partial^2 \phi}{\partial x^2} - \frac{1}{\left(\sqrt{\frac{2\pi J_0}{C\Phi_0}}\right)^2}\frac{\partial^2 \phi}{\partial t^2} = \sin(\phi) - \frac{J_B}{J_0} + \left(\frac{\Phi_0}{2\pi J_0}\right)\frac{\partial \phi}{\partial t}. \tag{1.4.11}$$

Let us define

$$\lambda_J = \sqrt{\frac{\Phi_0}{2\pi L J_0}}, \quad \omega_p = \sqrt{\frac{2\pi J_0}{C\Phi_0}}, \quad \gamma = \frac{J_B}{J_0}, \quad \alpha = \frac{\Phi_0}{2\pi J_0},$$

where λ_J is the Josephson penetration depth (see, for instance, [70]), ω_p represents the Josephson plasma frequency [68] and the parameter γ describes the normalized bias current. In experiments, the bias current, γ, is a controllable parameter with typical

values $0 \leq \gamma < 1$. The dimensionless parameter α represents the damping due to quasi-particle tunnelling with a typical value $0 \leq \alpha \ll 1$.

The product of the Josephson penetration depth and the Josephson plasma frequency is called Swihart velocity ([71]) and is denoted by c, that is,

$$\lambda_J \omega_p = \frac{1}{LC} = c,$$

where $c \approx c_0 \times 10^{-2}$ (c_0 is the velocity of light in free space) represents the velocity of electromagnetic wave in a Josephson junction. From the above notation, it is straightforward to derive a relation between the dissipation α and ω_p as

$$\alpha = \frac{1}{\omega_p C}.$$

Measuring the time and distance in the units of ω_p^{-1} and λ_J respectively, the last equation reduces to the normalized equation

$$\phi_{xx} - \phi_{tt} = \sin(\phi) + \alpha\phi_t - \gamma, \tag{1.4.12}$$

where the subscripts denote the partial derivatives. Eq. (1.4.12) is called a *perturbed* sine-Gordon equation. This equation is the most frequently used equation that models the dynamics of various types of the Josephson junctions. One has to choose the boundary conditions according to the geometry of the Josephson junction.

Besides Josephson junctions, the sine-Gordon equation describes the dynamics of various physical systems, e.g., nonlinear optics, and dislocations in crystals where the kink and breathers were found by Seeger et al. [72]. In 1962, this equation was used as a one-dimensional model for a scalar field theory [73].

In practice, the perturbation parameters $\alpha \ll 1$ and $\gamma < 1$ are small. With $\alpha = \gamma = 0$, Eq. (1.4.12) reduces to the *unperturbed* sine-Gordon equation

$$\phi_{xx} - \phi_{tt} = \sin(\phi). \tag{1.4.13}$$

We call this equation the $(1+1)$-dimensional sine-Gordon equation to indicate that one of the dimensions is spatial and the other is temporal. Such a model is integrable with exact solutions in the form of solitons and breathers, as explained in Drazin and Johnson [74] and Rajaraman [75]. It may be noted that perturbations to the sine-Gordon model correspond to external forces and inhomogeneities, and spoil its integrability, and the equation can not be solved exactly. However, if their influence is small enough, the equation can be solved using perturbation techniques. Eq. (1.4.13) was, first of all,

used by Enneper [76] while they were dealing with the differential geometry of surfaces having a constant negative Gaussian curvature.

By using a sine-Gordon equation, Lomdahl et al. [77] has theoretically investigated the propagation of a kink (fluxon)in long Josephson junctions. Dueholm et al. [78] obtained the kink experimentally in a long Josephson junction.The quantum effects of a fluxon through interference effects and macroscopic quantum tunnelling are reported respectively by Hermon et al. [79] and Kato and Imada [80].

1.5 Excitations in the unperturbed sine-Gordon equation

In this section, we look for the travelling wave solution (the exact solution) of the unperturbed sine-Gordon model (1.4.13). Let the required solution be of the form $\phi(x,t) = \phi(\widetilde{\xi})$, where $\widetilde{\xi} = x - vt$, and $0 \leq v < 1$ is the velocity of the wave. Substituting $\phi(x,t) = \phi(\widetilde{\xi})$ into the unperturbed equation (1.4.13) and using the chain rule for differentiation, we can write

$$\left(1 - v^2\right) \phi_{\widetilde{\xi}\widetilde{\xi}} = \sin(\phi).$$

The introduction of a new variable ξ by $\widetilde{\xi} = \sqrt{1 - v^2}\xi$, reduces the last equation into the normalized form $\phi_{\xi\xi} = \sin(\phi)$. Multiplying throughout by ϕ_ξ and integrating with respect to ξ, we arrive at

$$\frac{d\phi}{d\xi} = \pm\sqrt{2\left\{C - \cos(\phi)\right\}},$$

where C is an arbitrary constant of integration. Separating variables and integrating again with respect to ξ we obtain

$$\xi = \pm \int \frac{d\phi}{\sqrt{2\left\{C - \cos(\phi)\right\}}} \tag{1.5.1}$$

This equation is of the type $F[\phi] = \xi$, where F is the *Jacobian elliptic function* [81].

In a particular case, when $C = 1$, using the identity $1 - \cos(\phi) = 2\sin^2(\phi/2)$ and integrating Eq. (1.5.1) we obtain

$$\xi = \ln\left\{\csc\left(\frac{\phi}{2}\right) - \cot\left(\frac{\phi}{2}\right)\right\} + C_1.$$

where C_1 is the constant of integration. Using trigonometric identities, this can be cast into the form $\xi = \pm \ln\tan\left(\frac{\phi}{4}\right) + C_1$. Solving for ϕ, one may write $\phi = 4\arctan\left[\exp\left(\pm(\xi - C_1)\right)\right]$. Returning to the original variables, we arrive at

$$\phi_{1,2}(x,t) = 4\arctan\left[\exp\left(\sigma\frac{x - vt - x_0}{\sqrt{1 - v^2}}\right)\right], \tag{1.5.2}$$

where $x_0 = \sqrt{1-v^2}C_1$, and $\sigma = \pm 1$ is called the topological charge.

To insure that the solutions given by Eq. (1.5.2) are real, one has to impose the condition $v^2 < 1$, on the speed of the travelling wave. Figure 1.6 shows four frames of the

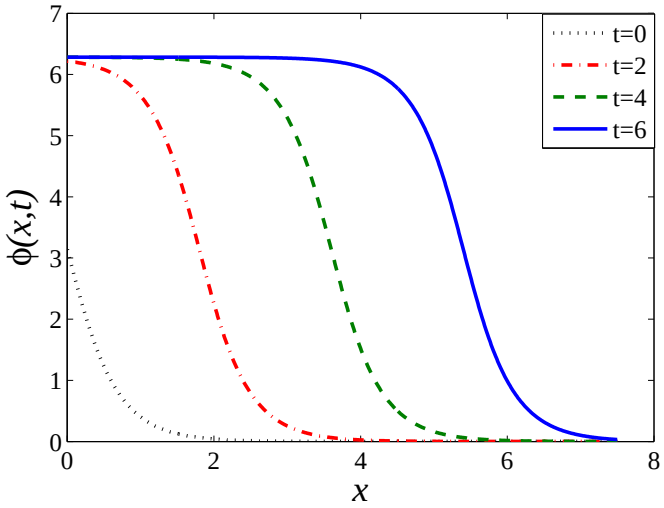

Figure 1.6: One of the traveling wave solutions given by Eq. (1.5.2) of the unperturbed sine-Gordon equation (1.4.13). Here we have taken $v = 0.9$, $x_0 = 0$ and $t = 0, 2, 4, 6$.

travelling wave solution $\phi_2(x,t)$ of Eq. (1.4.13), from which it is clear that $\phi_2(x,t) \to 2\pi$ as $x \to -\infty$. Also Eq. (1.5.2) shows that $\phi_2(x,t) \to 0$ whenever $x \to +\infty$.

1.5.1 The kink (anti-kink) solution

The solution $\phi_1(x,t)$, presented by Eq. (1.5.2) with $\sigma = 1$, is called a *kink* or *soliton* solution and $\phi_2(x,t)$, with the negative sign ($\sigma = -1$), is known as *anti kink* or *anti-soliton* solution (see Ustinov [82]). In Figure 1.7 the plot of kink and anti kink solutions of Eq. (1.5.2), for a particular case when $V = x_0 = 0$, are depicted. It is clear that when x approaches $\pm\infty$, the profile $\phi(x,t)$ asymptotes to 2π or 0 respectively. Thus the Josephson phase difference for a kink (anti kink) solution is 2π.

Solitons can be further divided into two categories. A soliton $\phi(x,t)$ is said to be *non-topological* if $\lim_{x\to-\infty} \phi(x,t) = \lim_{x\to\infty} \phi(x,t)$. In the case where $\lim_{x\to-\infty} \phi(x,t) \neq \lim_{x\to\infty} \phi(x,t)$, the soliton is said to be *topological*. The *kink* solution is therefore a topological soliton.

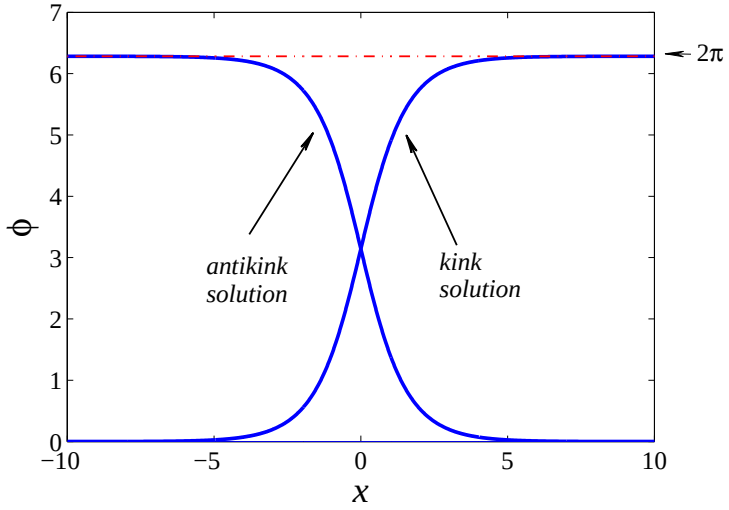

Figure 1.7: Plots of the kink and anti-kink solutions of the unperturbed sine- Gordon equation (1.4.13). These curves are obtained by substituting $x_0 = 0$ and $v = 0$ in Eq. (1.5.2).

It is easy to verify (by direct substitution) into the sine-Gordon equation (1.4.13) that

$$\phi(x,t) = 4\arctan\left[\frac{\sinh\left(vt/\sqrt{1-v^2}\right)}{v\cosh\left(x/\sqrt{1-v^2}\right)}\right], \tag{1.5.3}$$

is another solution. This solution is called a "particle-antiparticle" collision. Four frames of animation of this solution, for different (nonzero) values of t are shown in Fig. 1.8. It is clear from Eq. (1.5.3) that, for any t, the profile $\phi(x,t)$ approaches zero as $x \to \pm\infty$. As time increases, the kink and antikink move in opposite directions.

It can also be verified that Eq. (1.4.13) admits another type of a solution which is spatially localized and oscillates in time. This solution is of the type

$$\phi(x,t) = 4\arctan\left[\frac{\sqrt{1-\omega^2}\sin(\omega t)}{\omega\cosh\left(\sqrt{1-\omega^2}x\right)}\right], \tag{1.5.4}$$

and is called breather solution. The breather solution of the sine-Gordon equation (1.4.13) can be considered as bound state of kink and antikink. The kink and antikink (the particle-antiparticle) oscillate with respect to each other with a certain period $T = 2\pi/\omega$, where ω is the frequency of internal breathing oscillation.

Physically, a kink (antikink) solution of a sine-Gordon equation represents a Josephson vortex (antivortex). The investigation of fluxons (Josephson vortices) in a long Josephson junction has been an important topic of many researchers because of their

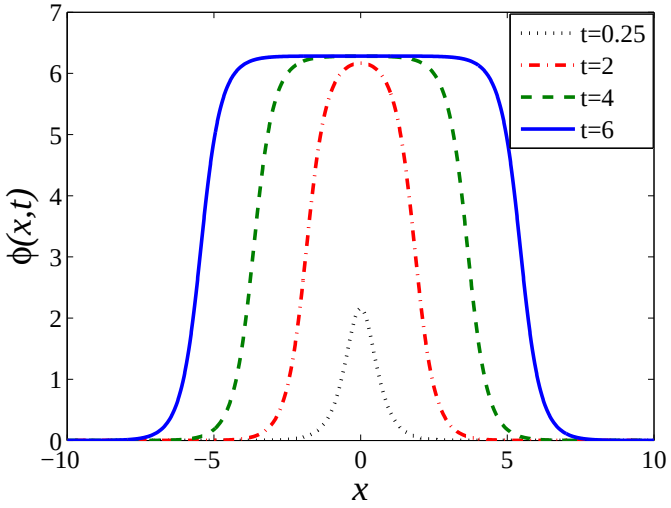

Figure 1.8: Frames of animations of the solutions given by Eq. (1.5.3) of the unperturbed sine-Gordon equation (1.4.13). Here we have taken $v = 0.9$ and $t = 0.25, 2, 4, 6$.

interesting nonlinear nature and potential applications in high-temperature superconductivity, as described by Wallraff et al. [83]. Bugoslavsky et al. [84] reported that Josephson vortices may be used to determine the properties (e.g. critical current density J_c) of a superconducting material. Josephson vortices could be used for the removal of noise-producing trapped magnetic flux in superconducting-based devices, making diodes and lenses of quantized magnetic flux, etc (cf. Savel'Ev and Nori [85]). In addition, a number of physical applications of fluxons are discussed in the excellent book of Likharev [86] and in the extensive literature review of Ustinov [87].

1.5.2 Sine-Gordon equation with phase shift

A Josephson junction with any arbitrary phase shift $\theta(x)$ in the phase, can be described by a sine-Gordon equation with an additional term $\theta(x)$ in the nonlinearity. That is, to study the dynamics of a Josephson junction with an arbitrary phase jump $\theta(x)$, we use

$$\phi_{xx} - \phi_{tt} = \sin\left[\phi + \theta(x)\right] + \alpha\phi_t - \gamma. \tag{1.5.5}$$

In order to solve (1.5.5), appropriate (boundary) conditions are required according to the geometry of the Josephson junction under consideration and the magnetic field applied to the junction, see for instance, Lonngren and Scott [88], McLaughlin and Scott [89], Pedersen [90], Parmentier [91]. In such a case, the fundamental current-phase relation (1.3.1) reduces $I_s = I_c \sin\left[\phi + \theta(x)\right]$.

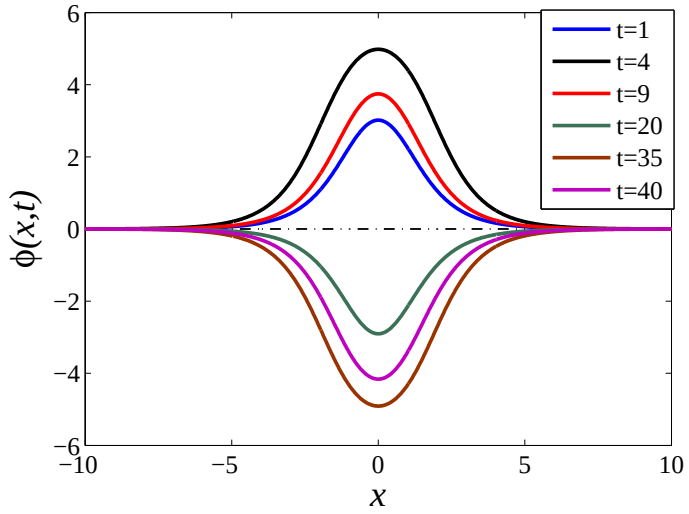

Figure 1.9: Breather solution (1.5.4) of the sine-Gordon equation Eq. (1.4.13) at different values of the temporal variable t.

1.5.3 Phase portrait of the static unperturbed sine-Gordon model

In this subsection we discuss the stability of the uniform solutions with respect to the spatial variable x of the unperturbed sine-Gordon equation (1.4.13). For this purpose we study the behavior of the *equilibrium points* in the *phase plane*, that is, we consider

$$\phi_{xx} = \sin(\phi). \tag{1.5.6}$$

Define $\phi_x = u$ so that $\phi_{xx} = u_x = \sin(\phi)$. Now consider

$$\frac{\phi_x}{u_x} = \frac{d\phi}{du} = \frac{u}{\sin(\phi)},$$

which upon integration, with a constant of integration C, gives

$$u = \phi_x = \pm\sqrt{2(C - \cos(\phi))}. \tag{1.5.7}$$

This first order differential equation in $\phi(x)$ cannot be solved by the elementary methods [92, 93], if $C \neq 1$. However, it is possible to know about the main properties of its solutions without solving it. We select the Cartesian axes ϕ and $u = \phi_x$ which form the *phase plane*. By using different values of C, we plot different family of curves, called the *phase paths* given by Eq. (1.5.7) and obtain the *phase diagram*. On the paths joining $(0, 0)$ and $(2\pi, 0)$ we have $C = 1$. The path inside and outside these curves are respectively given by $-1 < C < 1$ and $C > 1$. The arrowheads indicating the directions of proceeding along the phase curves are determined from $\phi_x = u$. For $u > 0$, the direction of the arrowheads is from left to right in the upper half plane. The direction

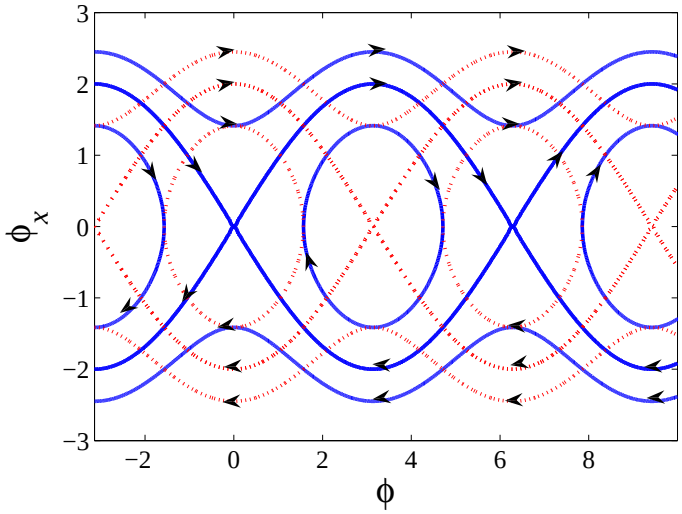

Figure 1.10: Phase portrait of the unperturbed sine- Gordon equation (1.4.13). The phase curves are obtained by assigning different values to C in the Eq. (1.5.7). Here $C < 1$ corresponds to closed loops oscillating about $\phi = \pi$ and $\phi = 0$ and $C > 1$ corresponds to curves entirely in $\phi > 0$ or $\phi < 0$, while $C = 1$ corresponds to hetroclinic connections to $\phi = 2n\pi$, and $u = 0$.

is always from right to left in the lower half plane (when $u < 0$). A point P presenting a pair of values (ϕ, u) on the phase diagram is known as *state of the system*. A given state (ϕ, u) represents a pair of initial conditions for the original differential equation (1.5.6). Equation (1.5.7) reveals the $2\pi-$ periodicity in ϕ as shown in Fig. 1.10.

If the initial state of the solution $\phi = 0$ is slightly displaced, it will fall on a phase trajectory and will be taken away from the initial state. That is, a small change in the initial state of the solution $\phi = 0$ produces a significant change in its initial state. We call the solution $\phi = 0$ *unstable*. On the other hand, if the initial state of the solution $\phi = \pi$ is slightly displaced from its initial state, it will fall on one of the nearby closed phase paths and will oscillate around its initial state. That is, a slight displacement in the initial state of the solution $\phi = \pi$ causes a small change in its initial state. Such type of solution is described as *stable*.

The stability discussed so far was with respect to the spatial variable x for our time-independent sine-Gordon model (1.4.13). For the time-dependent stability we consider the spatial independence, so that Eq. (1.4.13) becomes $\phi_{tt} = -\sin(\phi)$. Following the same steps we arrive at

$$u = \phi_x = \pm\sqrt{2(C + \cos(\phi))}. \tag{1.5.8}$$

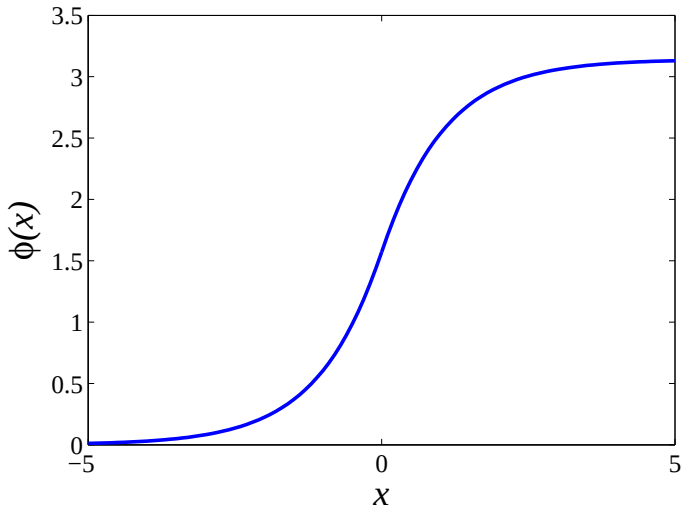

Figure 1.11: Semifluxon solution ((1.5.9)) of the static sine-Gordon equation Eq. (1.4.13) for the case when $\gamma = 0$.

Giving the same arguments, it is clear from the phase portrait of Eq. (1.5.8) (displayed by dotted lines in Fig. 1.10) that the uniform solution $\phi = 0$ is stable while $\phi = \pi$ is not.

1.5.4 Semifluxons solution in sine-Gordon equation

Xu et al. [55] and Goldobin et al. [54] considered a long Josephson junction composed of a zero and π junctions. Such a junction is described by a sine-Gordon equation having a phase shift of π for $x > 0$. Under certain continuity conditions, they derived an expression for a static semifluxon given by

$$\phi(x) = \begin{cases} 4\arctan\left[\exp\left(x - \widehat{x}_0\right)\right], & x < 0, \\ 4\arctan\left[\exp\left(x + \widehat{x}_0\right)\right] - \pi, & x > 0, \end{cases} \tag{1.5.9}$$

where $\widehat{x}_0$ is an integration constant which is determined by the continuity conditions as $\widehat{x}_0 = \ln\left(1 + \sqrt{2}\right)$.

The solution given by Eq. (1.5.9) is plotted in Fig. 1.11. It is clear from this figure that $\phi(x)$ approaches zero as $x \to -\infty$, and when $x \to \infty$, $\phi(x) \to \pi$. In other words $|\phi(\infty) - \phi(-\infty)| = \pi$, hence Eq. (1.5.9) represents a π-vortex solution of the sine-Gordon equation, which is centered at the discontinuity point $x = 0$, of the junction.

The sine-Gordon model (1.5.5) with different phase shifts and continuity (boundary) conditions opens a new field with open problems.

1.6 Objective of the thesis and structure

The main objective of this thesis is to study the dynamics of the Josephson phase in long Josephson junctions with different phase shifts. To do so, we use the sine-Gordon model (1.5.5) as our main model with appropriate continuity (boundary) conditions.

In Chapter 2, we study a long Josephson junction with two π-discontinuity points in the infinite domain. This junction has a π-phase shift of length $2a$ between two zero shift parts, the so-called $0-\pi-0$ long Josephson junction. We show that there exists a critical facet length a_c for the constant zero solution which is only stable for $a < a_c$, and for $a > a_c$ the zero solution is unstable. The uniform π solution is unstable everywhere. In the instability region ($a > a_c$) both the constant solutions are unstable, and the ground state of the system is a non-constant solution. There are two ground states that bifurcate from the zero solution at $a = a_c$, in the case when there is no bias current applied to the system. We use asymptotic analysis to construct the ground states and derive the absolute maximum of the ground states as a function of the facet length a, for a close to the critical facet length a_c. We show that the nonuniform ground state correspond to a semifluxon solution. We then consider the case when an external bias current is applied to the junction and find two critical forces $\pm\gamma_{c,0}$ and $\pm\gamma_{c,\pi}$. For $-\gamma_{c,0} < \gamma < \gamma_{c,0}$, the above mentioned two ground states still exist. There is no static solution in the case $|\gamma| > |\gamma_{c,\pi}|$. An asymptotic analysis is used to calculate $\gamma_{c,0}$, when $|a - a_c| \ll 1$. When $a < a_c$, there is only one non-constant ground state of the system such that $\gamma_{c,0}$ with the above definition is present here. We use asymptotic analysis to discuss the ground state as a function of $\gamma_{c,0}$. We calculate the critical force $\gamma_{c,\pi}$ numerically.

In Chapter 3, we investigate a finite 0-π-0 long Josephson junction, i.e., we extend the ideas of Chapter 2 into a finite domain. We show that the main difference between the infinite domain and finite domain is that the uniform π solution can be stable, when the facet length a exceeds a critical value $a_{c,\pi}$. The zero background state is still stable for $a < a_{c,0}$. We discuss the non-constant ground state solution in the region where both the solutions are unstable. This is done using a perturbation technique and a Lagrangian approach. We also discuss the critical eigenvalues of the constant solutions.

In Chapter 4, we consider a (2+1)-Dimensional 0-π sine-Gordon equation with phase shift $\theta = \pi$ in some region and zero otherwise. First we consider the infinite domain problem and then investigate the junction in the finite domain. Due to the geometry of the junction, we use polar co-ordinates to convert our problem to an effective one-

dimensional problem. We extend the ideas of Chapters 2 and 3 into two dimensions. Beside the ground state solution we discuss the excited state as well.

A sine-Gordon equation having an arbitrary periodic discontinuity $\kappa > 0$ in the nonlinearity is considered in Chapter 5. This equation models a long Josephson junction with a periodic discontinuous phase difference, i.e., a 0-κ long Josephson junction. We discuss the existence and stability of the two types of periodic solutions of the system both in the absence and presence of an external force. Critical values of the discontinuity and an applied bias current are investigated, beyond which a solution switches to its complementary counterpart.

Due to the periodic discontinuity in the phase, the system admits regions of allowed and forbidden bands. We analytically investigate the Arnold tongues, separating the region of allowed and forbidden bands and discuss the effect of an applied bias current on the transitional curves, using a perturbation technique.

Next, we take the stable solution of the system and find the breather solution of the sine-Gordon model, bifurcating from the Arnold tongues. This is done by using a multiple scale expansion method, and a rotating wave approximation approach.

We conclude in Chapter 6 with a brief discussion of the work carried out in this thesis. We also propose several interesting and important problems for further study. Appendices are given at the end of the thesis.

CHAPTER 2

Existence and stability analysis of 0-π-0 long Josephson junction in infinite domain

2.1 Introduction and Overview of the Chapter

In the previous chapter, we discussed some of the technological advances related to create artificial shifts in the Josephson phase, such that the sign of the critical current depends on the spatial variable. We noted that many interesting properties of semi-fluxons in 0-π long Josephson junctions have been observed by a number of authors (see Chapter 1).

The next simplest possible configuration of a long Josephson junction with phase shifts is a junction having two π-discontinuities, i.e., a 0-π-0 long Josephson junction. The existence of Josephson half vortices (semifluxons) and their dependence on the length of the π junction and an applied bias current is the next interesting question to consider. The magnetic flux carried by such vortices and its dependence on the inter-vortex distance need to be investigated analytically. Such a junction has a negative critical current for $|x| < a$, and a positive critical current where $|x| > a$, where $2a$ is the total length of the π-junction and x the spatial variable. As suggested in Kirtley et al. [59], such a 0-π-0 long Josephson junction may be realized in systems like grain boundary Josephson junctions.

In this chapter, we give a theoretical investigation of the existence and behaviour of such half vortices in an infinite long Josephson junction (LJJ) with two π-discontinuity

points. We reconsider the model considered by Kato and Imada [94], namely the 0-π-0 sine-Gordon equation on an infinite domain, and study the existence and stability of the stationary solutions of the governing equation.

The present chapter is organized as follows. In Section 2.2, we discuss the mathematical model that we use to describe the problem under consideration. We show in Section 2.3 that when there is no bias current applied to the junction, the equation has two static and constant solutions that satisfy the continuity conditions. In Section 2.4, we derive an eigenvalue problem to discuss the linear stability of the uniform solutions and discuss the role of dissipation on the linear stability of the uniform backgrounds. Due to the phase-shifts, there is a region of facet lengths, in which both the uniform solutions are unstable. In Section 2.5, we use a perturbation technique, the so-called Poincare-Lindstedt method, to analytically discuss the ground states in the instability region, and show that a non-constant ground state emerges from the uniform solutions, i.e. the ground state of the system is a pair of semifluxons. We also study the dependence of such semifluxons on the facet length. We discuss the effect of an applied bias current on the nonconstant ground state. We compare our analytical approximations with the corresponding numerical simulations. We then briefly summarize the results of the Chapter in Section 2.6.

2.2 Mathematical model

In Section 1.4, we introduced a basic equation, the sine-Gordon equation, which can be used to study various systems. In the system of condensed matters, it is usually used for the description of the tunnelling of Cooper pairs across a barrier between the two superconductors of a long Josephson junction (LJJ) [9]. Due to an arbitrary phase shift $\theta(x)$ in the phase difference (the Josephson phase), one can use Eq. (1.5.5) with appropriate continuity (boundary) conditions.

To study the dynamics of a long Josephson junction with two π-discontinuity points, we use the perturbed sine-Gordon equation (1.5.5) (see, for example, Goldobin et al. [54]). In the present problem, we consider the case of the spatial variable $-\infty < x < \infty$. Note that Equation (1.5.5) is written after rescaling the spatial variable x and time variable t to the Josephson penetration length λ_J and the inverse plasma frequency ω_p^{-1}, respectively. The function $\theta(x)$, representing the presence, or absence, of the additional

π-phase shift, is given by

$$\theta(x) = \begin{cases} 0, & -\infty < x < -a, \\ \pi, & |x| < a, \\ 0, & a < x < \infty, \end{cases} \tag{2.2.1}$$

where $2a$ is the length of the π junction, which we refer to as the facet length. This is our primary bifurcation parameter in the ensuing problem.

For the solutions to be physically meaningful, the eigenfunction $\phi(x,t)$ and the magnetic flux $\phi_x(x,t)$ must be assumed continuous at the discontinuity $x = a$. In other words, we study equation (1.5.5) subject to the continuity conditions

$$\phi(\pm a^-, t) = \phi(\pm a^+, t),\ \phi_x(\pm a^-, t) = \phi_x(\pm a^+, t). \tag{2.2.2}$$

The governing equation (1.5.5), subject to the conditions (2.2.2), can be derived from the Lagrangian (see Section 7.1 in appendix for detail)

$$\mathcal{L} = \int_0^\infty \int_{-\infty}^\infty \left[\frac{1}{2}\phi_t^2 - \frac{1}{2}\phi_x^2 - 1 + \cos(\phi + \theta) - \gamma\phi\right] dxdt, \tag{2.2.3}$$

As we mainly consider static semifluxons, the existence of the solutions will be studied through the time-independent version of (1.5.5), namely

$$\phi_{xx} = \sin\left[\phi + \theta(x)\right] - \gamma,\ -\infty < x < \infty, \tag{2.2.4}$$

as originally proposed by Kato and Imada [94], and Owen and Scalapino [95].

2.3 Existence and stability of uniform solutions

It is obvious that Eq. (2.2.4) admits two static and uniform solutions i.e., fixed points (modulo 2π), which are obtained by considering the equation

$$\sin\left[\phi + \theta(x)\right] - \gamma = 0, \quad -\infty < x < \infty.$$

Solutions of this equation, in general form, are

$$\widetilde{\phi} = \arcsin\gamma + 2n\pi, \quad (2n+1)\pi - \arcsin\gamma,$$

for $a < |x| < \infty$, $n \in \mathbb{Z}$ and

$$\widetilde{\phi} = \arcsin\gamma + (2m-1)\pi, \quad 2m\pi - \arcsin\gamma,$$

for $0 < |x| < a$, and $m \in \mathbb{Z}$.

Hence, in order for the uniform solutions to satisfy the continuity condition $\phi(\pm a^-) = \phi(\pm a^+)$ in (2.2.2), one has to consider two possibilities.

The first one is to assume

$$\arcsin(\gamma) + 2n\pi = \arcsin(\gamma) + (2m+1)\pi,$$

and

$$(2n-1)\pi - \arcsin(\gamma) = 2m\pi - \arcsin(\gamma).$$

These respectively yield

$$n = m - \frac{1}{2}, \quad \text{and} \quad m = n + \frac{1}{2}. \tag{2.3.1}$$

As mentioned earlier that m, $n \in \mathbb{Z}$, hence, (2.3.1) do not hold at all. It follows that the first possibility is invalid.

Thus, in order for the continuity conditions to be satisfied by the constant background solutions, the only possibility is

$$\arcsin(\gamma) + 2n\pi = 2m\pi - \arcsin(\gamma),$$

and

$$(2n+1)\pi - \arcsin(\gamma) = \arcsin(\gamma) + (2m-1)\pi.$$

It can be easily verified that the above equations hold if and only if $\gamma = 0$. Thus we come across the conclusion that when $\gamma \neq 0$, there is no uniform solution satisfying the continuity conditions (2.2.2). As solutions on the whole domain must satisfy the continuity conditions (2.2.2), it can be concluded that uniform solutions exist only when $\gamma = 0$, and hence we obtain

$$\widetilde{\phi} \equiv 0 \mod(2\pi), \tag{2.3.2a}$$

$$\widetilde{\phi} \equiv \pi \mod(2\pi). \tag{2.3.2b}$$

In the following subsections, we investigate the stability of the uniform backgrounds $\widetilde{\phi}$, given by (2.3.2), in the absence of the forcing term, that is, $\gamma = 0$.

2.3.1 The eigenvalue problem

Let $\epsilon \ll 1$ be a perturbation parameter. In order to determine the linear stability of a uniform solution $\widetilde{\phi}$, we consider $\epsilon e^{\lambda t} V(x)$, a small perturbation from the uniform

solution and substitute the stability ansatz

$$\phi(x,t) = \widetilde{\phi} + \epsilon e^{\lambda t} V(x), \quad -\infty < x < \infty \tag{2.3.3}$$

into Eq. (1.5.5). Neglecting the higher order terms in ϵ, one obtains an eigenvalue problem in the form of the following linear Schrödinger equation

$$V_{xx} = \left[E + \cos\left(\widetilde{\phi} + \theta(x)\right)\right] V, \quad -\infty < x < \infty \tag{2.3.4}$$

where

$$E = \lambda^2 + \alpha\lambda. \tag{2.3.5}$$

The function $V(x)$ is also subject to the continuity conditions

$$V(\pm a^-) = V(\pm a^+), \quad V_x(\pm a^-) = V_x(\pm a^+). \tag{2.3.6}$$

From the stability ansatz (2.3.3), it is clear that the constant background $\widetilde{\phi}$ is linearly

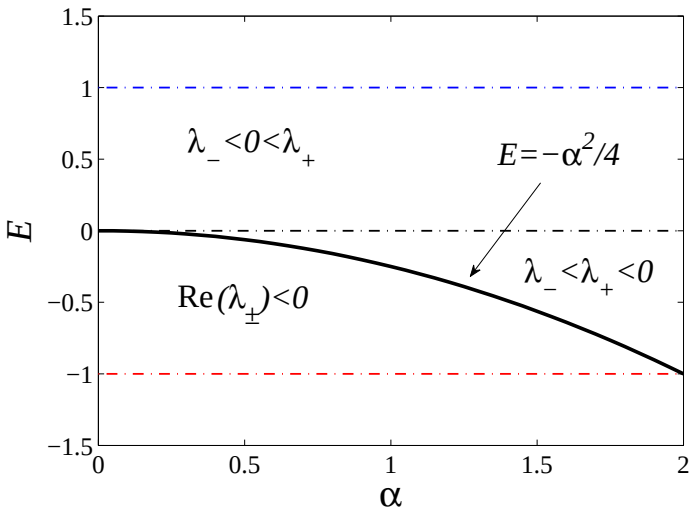

Figure 2.1: Parametric plot of the spectral parameter E as a function of the dissipative parameter α.

stable if and only if λ has nonzero real parts, that is, if λ is pure imaginary and is unstable if $\mathrm{Re}(\lambda) > 0$.

Solving Eq. (2.3.5) for λ, we obtain

$$\lambda_\pm = \frac{1}{2}\left(-\alpha \pm \sqrt{\alpha^2 + 4E}\right), \tag{2.3.7}$$

which describes the growth (decay) rate of the instability (stability). Here E is the spectral parameter in the scattering problem and α is strictly positive.

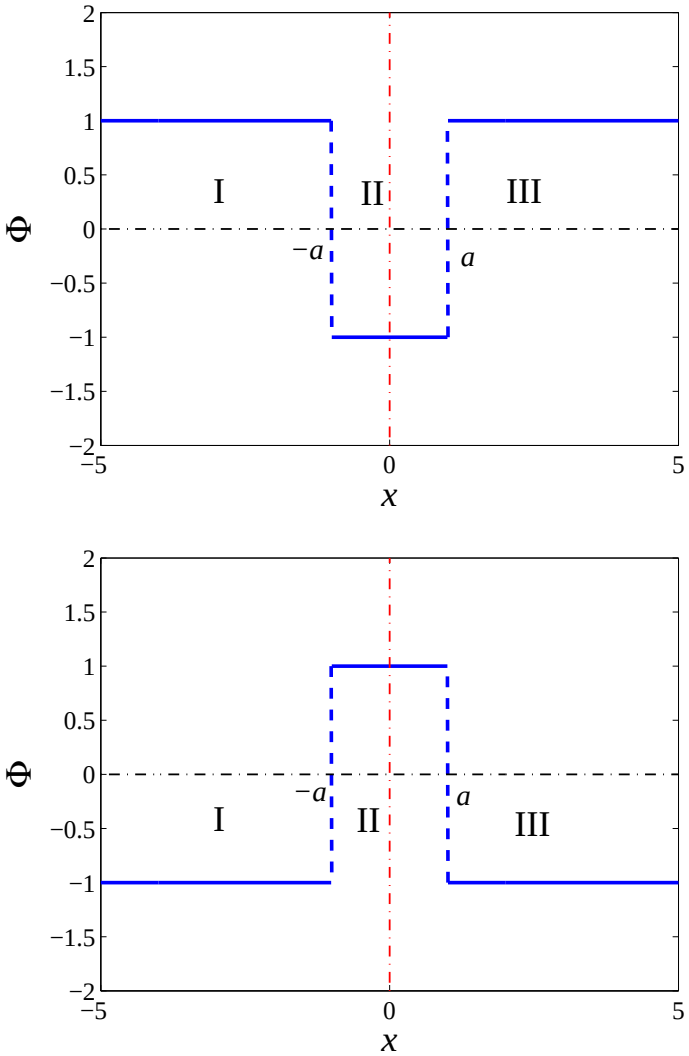

Figure 2.2: Plot of the potential $\Phi = \cos\left[\widetilde{\phi} + \theta(x)\right]$ in the eigenvalue problem (2.3.4) for $\widetilde{\phi} = 0$ (top) and $\widetilde{\phi} = \pi$ (bottom).

2.3.1.1 The effect of the dissipation α on the stability of a uniform background $\widetilde{\phi}$

In the following, we discuss the stability of the uniform solution $\widetilde{\phi}$ first in the presence and then in the absence of the dissipative parameter (α) and show that the stability only depends on the sign of the spectral parameter E and it does not depend upon the parameter α. First consider the case where $\alpha > 0$, i.e., the system is dissipative. Now when $E < 0$, then the $(\alpha, E)-$plane is divided into two regions where $\mathrm{Re}(\lambda_{\pm}) < 0$ and $\lambda_- < \lambda_+ < 0$. The two regions are separated by a line $E = -\alpha^2/4$ (see Fig. 2.1). In both regions the eigenvalues are negative, so that the stability ansatz (2.3.3) implies the stability of the uniform solution.

Also when $E > 0$, then we observe that $\mathrm{Re}(\lambda_\pm) \geq 0$ in the (α, E) region. Again the stability ansatz (2.3.3) shows that the uniform solution is unstable.

Now we suppose the system is non-dissipative, that is, we consider the case where $\alpha = 0$. Eq. (2.3.7) then yields $\lambda_\pm = \pm\sqrt{E}$. Thus if $E < 0$, then $\mathrm{Re}(\lambda) = 0$, i.e. λ is pure imaginary, and hence $\tilde{\phi}$ is stable. Again if $E > 0$, then $\mathrm{Re}(\lambda) \neq 0$, which shows that the solution $\tilde{\phi}$ is unstable.

From the above discussion, it is clear that a uniform solution is stable in the region where $E < 0$ and is unstable whenever $E > 0$. In other words the stability of a uniform solution depends only on the sign of E and not upon the value of α. Therefore, without losing generality, we can set $\alpha = 0$, unless otherwise stated. As a result, Eq. (2.3.7) reduces to

$$E = \lambda^2. \tag{2.3.8}$$

2.4 Linear stability of the uniform solutions

Before proceeding further, we need to point out some basic properties of the differential operator involved in the eigenvalue problem (2.3.4), which are useful to know about the nature of the solution of the eigenvalue problem.

It is simple to show that the differential operator

$$\mathcal{D} = \partial_{xx} - \cos\left[\widetilde{\phi} + \theta(x)\right], \quad (\infty < x < \infty), \tag{2.4.1}$$

is self-adjoint (for a proof, please see Section 7.2 in appendix). Thus, using a property of self-adjoint operators, one can easily deduce that the eigenvalue problem (2.3.4) has real eigenvalues (see Section 7.3 in appendix for a proof). In other words the spectral parameter E, in the eigenvalue problem (2.3.4) is real.

We are particularly interested in two different sets of eigenvalues (or spectral parameter, E) of the eigenvalue problem (2.3.4). One type of the eigenvalues is that for which the problem (2.3.4) admits solutions which are bounded in the regions where $x \to \pm\infty$. In the following, and throughout this thesis, we call such set of eigenvalues, the continuous spectrum of a constant background solution, see Kato [96]. From a mathematical point of view, the continuous spectrum is the set of eigenvalues that constitute a delocalized mode of a solution. These solutions are, in fact, not square-integrable solutions of the eigenvalue problem (2.3.4).

The second type of eigenvalues we are interested in, is that for which a solution V

of the eigenvalue problem (2.3.4) is *bounded* and *decaying* in regions $x \to \pm\infty$. Such solutions is the set of all square integrable solutions of the eigenvalue problem (2.3.4) and constitute localized modes. A set of such eigenvalues, we call the discrete spectrum of a stationary solution.

In the following, we discuss these two spectra corresponding to each stationary solution separately.

2.4.1 Linear stability of the constant background $\widetilde{\phi} = 0$

To investigate the linear stability of the uniform solution $\widetilde{\phi} = 0$, we first discuss the corresponding continuous spectrum

2.4.1.1 Continuous spectrum

Let V be a solution of the eigenvalue problem (2.3.4) which is bounded and has a small amplitude in the limit $x \to \pm\infty$. In other words, those values of E which make $V(x)$ satisfy

$$V_{xx} = \left[E + \cos\left(\widetilde{\phi} + \theta(x)\right)\right] V, \tag{2.4.2}$$

bounded, constitute the continuous spectrum of a constant solution $\widetilde{\phi}$. Now, with the help of the phase-shift (2.2.1), the solution of (2.4.2), for the uniform $\widetilde{\phi} = 0$, reduces to

$$V_{xx} = (E + 1)\, V, \tag{2.4.3}$$

where E is given by Eq. (2.3.8).

It is clear that $V(x)$, satisfying Eq. (2.4.3), is bounded if and only if

$$E < -1. \tag{2.4.4}$$

Hence Eqs. (2.3.8) and (2.4.4) imply that λ is pure imaginary, and the continuous spectrum of the constant zero background solution lies in the region $E < -1$. Therefore, by defining $\lambda = \mu i$, where $\mu \in \mathbb{R}$, we can say that the continuous spectrum of the uniform solution $\widetilde{\phi} = 0$ lies in the region where $\mu < -1$ or $\mu > 1$. Again, from the stability ansatz (2.3.3), it is clear that there is no unstable eigenvalue in the continuous spectrum. Although we know that there is no unstable eigenvalue in the continuous spectrum, still the linear stability of $\widetilde{\phi} = 0$ cannot be, as yet, implied by the continuous spectrum.

2.4.1.2 The discrete spectrum

To determine the linear stability of the uniform $\widetilde{\phi} = 0$ solution, one needs to determine the spectrum that complements its continuous spectrum, which is the discrete spectrum of the stationary zero solution.

From the discussion in Section 2.4.1.1, it is clear that the discrete spectrum lies in the region where

$$E > -1. \tag{2.4.5}$$

From this result, and the stability ansatz (2.3.3), we come to the conclusion that the source of instability, for the uniform zero solution, comes from the discrete spectrum. This implies that if there is no point spectrum, we will have no instability.

As discussed above, the discrete spectrum is formed from those values of the parameter E, for which the solution of the eigenvalue problem (2.3.4) is square integrable. In other words, to determine the discrete spectrum of the uniform solution $\widetilde{\phi} = 0$, we seek for the eigenfunctions V, satisfying the eigenvalue problem (2.3.4), for which the inner product $< V, V >$ is finite, that is

$$\int_{-\infty}^{\infty} V^2 dx < \infty. \tag{2.4.6}$$

As depicted in the upper panel of Figure 2.2, we note that for a static stationary solution $\widetilde{\phi} = 0$, the cosine term in the eigenvalue problem (2.3.4) represents a potential well. We note that belongs to the classical scattering problem [74]. This problem has been well discussed in quantum mechanics (see, for example, Landau and Lifshitz [97] and Liboff [98]) where $\cos\left[\widetilde{\phi} + \theta(x)\right]$ is the potential function. This potential function divides the plane into three regions, namely $|x| > a$ and $|x| < a$. For the sake of simplicity we denote the regions $-\infty < x < -a$, $|x| < a$ and $a < x < \infty$, by I, II, and III, respectively. The governing equations in regions I, II, and III are the same, however we select different solutions due to the boundary conditions at $x \to \pm\infty$.

By embedding Eq. (2.2.1) into the static sine-Gordon equation (2.3.4), and considering the case of $\widetilde{\phi} = 0$, we obtain

$$V_{xx} - (1 + E)\, V = 0, \quad |x| > a, \tag{2.4.7a}$$

$$V_{xx} + (1 - E)\, V = 0, \quad |x| < a. \tag{2.4.7b}$$

First consider Eq. (2.4.7a), whose general solution has the form

$$V = A_1 e^{\widehat{\alpha} x} + \widetilde{A}_1 e^{-\widehat{\alpha} x},$$

where we have defined

$$\widehat{\alpha} = \sqrt{1+E}, \tag{2.4.8}$$

and A_1, $\widetilde{A}_1$ are constants of integration. Let V_1 denote the solution in region I. The term $\widetilde{A}_1 e^{-\widehat{\alpha}x}$ grows without bound when $x \to -\infty$. In order that V_1 satisfies the condition (2.4.6), we need to set $\widetilde{A}_1 = 0$. Thus a square integrable solution of the self adjoint eigenvalue problem corresponds to a bounded and decaying solution in region I, and is given by

$$V_1 = A_1 e^{\widehat{\alpha}x}. \tag{2.4.9}$$

In a similar way, it can be shown that a solution V_3, in region III, satisfying (2.4.6) is of the form

$$V_3 = A_4 e^{-\widehat{\alpha}x}, \tag{2.4.10}$$

where, again, A_4 is a constant of integration.

To solve Eq. (2.4.7b) in region II, we consider two cases, viz $E < 1$ and $E > 1$. If we assume $E > 1$, it follows that Eq. (2.4.7b) in region II has solution of the form

$$V_2 = A_2 \sin\left(\widehat{\beta}x\right) + A_3 \cos\left(\widehat{\beta}x\right), \tag{2.4.11}$$

where A_2 and A_3 are constants of integration and

$$\widehat{\beta} = \sqrt{1-E}. \tag{2.4.12}$$

From Eqs. (2.4.9), (2.4.11) and (2.4.10), we come to the conclusion that the discrete spectrum, or the point spectrum, of the uniform $\widetilde{\phi} = 0$ solution corresponds to bounded and decaying solutions in the regions I, III and is oscillatory in the region II. Thus, the discrete spectrum of the constant solution $\widetilde{\phi} = 0$ is given by

$$V(x) = \begin{cases} A_1 e^{\widehat{\alpha}x}, & -\infty < x < -a, \\ A_2 \sin\left(\widehat{\beta}x\right) + A_3 \cos\left(\widehat{\beta}x\right), & -a < x < a, \\ A_4 e^{-\widehat{\alpha}x}, & a < x < \infty. \end{cases} \tag{2.4.13}$$

Applying the continuity conditions (2.3.6) to the system (2.4.13), one obtains a system of four homogeneous equations of the form

$$F_1 \begin{pmatrix} A_1 \\ A_2 \\ A_3 \\ A_4 \end{pmatrix} = 0, \tag{2.4.14}$$

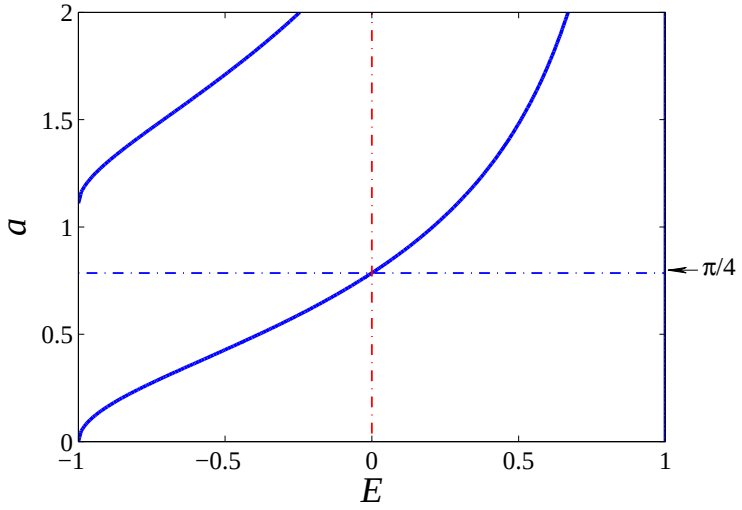

Figure 2.3: Plot of the 'discrete' spectrum of $\widetilde{\phi} = 0$ as a function of the π junction length.

where the coefficient matrix F_1 is given by

$$F_1 = \begin{bmatrix} e^{-\widehat{\alpha}a} & \sin\left(\widehat{\beta}a\right) & -\cos\left(\widehat{\beta}a\right) & 0 \\ \widehat{\alpha}e^{-\widehat{\alpha}a} & -\widehat{\beta}\cos\left(\widehat{\beta}a\right) & -\widehat{\beta}\sin\left(\widehat{\beta}a\right) & 0 \\ 0 & \sin\left(\widehat{\beta}a\right) & \cos\left(\widehat{\beta}a\right) & -e^{-\widehat{\alpha}a} \\ 0 & \widehat{\beta}\cos(\widehat{\beta}a) & -\widehat{\beta}\sin(\widehat{\beta}a) & \widehat{\alpha}e^{-\widehat{\alpha}a} \end{bmatrix}. \tag{2.4.15}$$

To obtain a nontrivial solution of the system (2.4.14), we require

$$\det(F_1) = 0. \tag{2.4.16}$$

Figure 2.3 shows the plot of the zeros of the condition (2.4.16), i.e., the discrete spectrum, in the (E, a) plane. From the figure, one can easily observe that there is a value of the facet length $a = \pi/4$, below which the spectral parameter E is negative. Equivalently, the eigenvalue λ of the eigenvalue problem (2.3.4) is purely imaginary. Thus, the stability ansatz (2.3.3), guarantees the stability of the uniform solution $\widetilde{\phi} = 0$ in the region where $a < \pi/4$. At the point $a = \pi/4$, the spectral parameter E is zero. When the facet length a exceeds $\pi/4$, the spectral parameter E becomes positive, and hence, (2.3.3) shows that the solution $\widetilde{\phi} = 0$ is unstable. Thus, we conclude that $a = \pi/4$ is the critical value of the facet length a at which the spectral parameter E changes its sign and, consequently, the stability of the static solution $\widetilde{\phi} = 0$ changes thereat. We denote this critical value of the facet length a by $a_{c,0}$ and call it the *critical facet length.* That is,

$a_{c,0} = \pi/4$. This agrees with the value of the critical zero facet length calculated Kato and Imada [94], and Susanto et al. [57].

Next, if we consider the case $E > 1$ in region II, the required solution of Eq. (2.4.7b) will be in terms of exponentials. By following the same steps, one can observe that the region $E > 1$ does not contribute to the spectra of the uniform solution. This is because by considering solutions for $E > 1$, the determinant of the matrix obtained by the application of the continuity conditions (2.3.6) to the solutions in the three regions, is sign-definite, that is, has no zero for all $E > 1$. In the context of quantum mechanics, this region corresponds to the continuum of energies of unbounded state (see Chapter 8 in Liboff [98])[1].

2.4.2 Linear stability of the uniform $\widetilde{\phi} = \pi$ solution

To investigate the linear stability of the constant solution $\widetilde{\phi} = \pi$, we first discuss the corresponding continuous spectrum.

2.4.2.1 The continuous spectrum of the uniform π-solution

For the π-background solution, the potential $\cos\left[\widetilde{\phi} + \theta(x)\right]$, in the eigenvalue problem (2.3.4) represents a barrier, as shown in the lower panel of Figure 2.2. Introducing $\widetilde{\phi} = \pi$, and Eq. (2.2.1) into (2.4.2), we find that the continuous eigenfunction of the uniform solution $\widetilde{\phi} = \pi$, as $x \to \pm\infty$, is given by

$$V_{xx} = (E - 1)\, V, \tag{2.4.17}$$

where we have used the fact that $\lim_{x\to\pm\infty} \cos\left[\theta(x)\right] = 1$. Note that the solution $V(x)$ of Eq. (2.4.17) is bounded if and only if

$$E < 1. \tag{2.4.18}$$

Thus the continuous spectrum of $\widetilde{\phi} = \pi$ lies in the region where $E < 1$, or equivalently in the regions $-1 < \lambda < 1$ and on the imaginary axis. This clearly indicates that for some λ, $\mathrm{Re}(\lambda) \neq 0$. That is, there exists a region in the continuous spectrum of the constant π solution where the eigenvalue λ is not purely imaginary. Therefore, the stability ansatz (2.3.3) implies that $\widetilde{\phi} = \pi$ is unstable. Thus the portion of the continuous spectrum corresponding to $0 < E < 1$ gives rise to an instability

[1] To calculate the discrete spectrum of a uniform solution $\widetilde{\phi}$ throughout this thesis, we shall only consider the region $E < 1$.

In order to get square integrable solutions of the scattering problem (the discrete spectrum), we need $E > 1$. A nonempty discrete point spectrum will also contribute to instability and we always have instability.

2.5 Ground states in the instability region $0 < a - a_{c,0} \ll 1$

From our discussion in the previous sections, it is clear that there are two uniform and static solutions admitted by the sine-Gordon model (1.5.5), namely $\widetilde{\phi} = 0$ and $\widetilde{\phi} = \pi$. We also know that there is a critical facet length $a_{c,0} = \pi/4$, below which the uniform zero background solution is stable. The uniform π solution, on the other hand, is unstable for any value of the facet length. This means that there is an instability region $a > a_{c,0}$, where both the uniform solutions are unstable. A non-constant ground state is expected in this instability region, the investigation of whose dynamics is of particular interest, as we will see later.

In this section, we discuss the ground state solutions of the Josephson junction in the instability region where the facet length a is close to the critical facet length $a_{c,0}$, i.e., in the region $0 < a - a_{c,0} = \epsilon \ll 1$. First we derive the system describing the dynamics of the Josephson phase using an effective Hamiltonian method. This method was first considered by Kato and Imada [94] in their paper.

2.5.1 Ground states using a Hamiltonian approach

Kato and Imada [94] consider the eigenvalue problem (2.3.4) and assume $E = 0$, where then a assumes its critical value $a_{c,0}$. One may verify that the bounded solution of the eigenvalue problem in the three regions is given by

$$\phi_0(x) = \begin{cases} C_1 e^{x}, & -\infty < x < -a, \\ C_2 \cos(x), & |x| < a, \\ C_3 e^{-x}, & a < x < \infty, \end{cases} \tag{2.5.1}$$

where C_i are constants of integration.

Applying the continuity conditions (2.2.2) to the system (2.5.1), we obtain

$$C_1 = e^{a} C_2 \cos(a), \quad C_3 = e^{a} C_2 \cos(a). \tag{2.5.2}$$

Eqs. (2.5.2) gives two results, namely

$$C_1 = C_3, \quad \text{and} \quad C_1^2 + C_3^2 = 2C_2^2 e^{2a} \cos^2(a). \tag{2.5.3}$$

From (2.5.3), it is easy to verify that

$$C_1 = C_3 = e^a \cos(a) C_2. \tag{2.5.4}$$

Thus, by substituting values from (2.5.4) into the system (2.5.1), one can write

$$\phi_0(x) = C_2 \begin{cases} \cos(x), & |x| < a, \\ \cos(a) e^{-(|x|-a)}, & |x| > a. \end{cases} \tag{2.5.5}$$

Assuming $\epsilon > 0$, a small parameter, then the facet length a defined by the relation $a = \pi/4 + \epsilon$ represents a small instability region to the right of the critical facet length $a_{c,0}$. Let $C_2 \ll 1$, and suppose

$$\phi = C_2 \phi_0, \tag{2.5.6}$$

be the nonuniform ground state solution, with a small amplitude, in the instability region. By substituting for ϕ into the Hamiltonian

$$H(\phi) = \int_0^\infty \left[\frac{1}{2}\phi_x^2 + 1 - \cos[\phi + \theta(x)] + \gamma\phi \right] dx, \tag{2.5.7}$$

and using Taylor series expansion, up to the fourth order, we obtain

$$H = \sqrt{2}\gamma C_2 - \frac{\epsilon}{2} C_2^2 + \frac{C_2^4}{256}\left(2 + \pi + \frac{16}{3}\epsilon\right). \tag{2.5.8}$$

Note that the integral in (2.5.7) is taken from zero because of the symmetry of the solutions in regions I and III. The stationary points of Eq. (2.5.7) are given by $g(C_2) = dH/dC_2 = 0$, namely

$$\sqrt{2}\gamma - \epsilon C_2 + \frac{C_2^3}{64}\left(2 + \pi + \frac{16}{3}\epsilon\right) = 0. \tag{2.5.9}$$

2.5.2 Ground state in the absence of an external current

Considering the undriven case, i.e., $\gamma = 0$, it is easy to verify, by a formal series expansion of the expression (2.5.9) about the small perturbation parameter $\epsilon = a - \pi/4$, that the nonzero values of C_2 are given by

$$C_2 = \pm 8\sqrt{\frac{1}{\pi + 2}}\left(a - \frac{\pi}{4}\right)^{1/2}. \tag{2.5.10}$$

Substituting C_2 from Eq. (2.5.10) into (2.5.6), with the help of the system (2.5.5), we are now in a position to find an approximate expression of the magnetic flux $\Delta\phi = \phi(0) - \phi(\pm\infty)$, through the junction in the undriven case as[2]

$$\Delta\phi = C_2, \tag{2.5.11}$$

[2]The authors in [80] have got wrong value for the ground state solution at the point $x = 0$, which has also been pointed out in [99].

where $\phi(\pm\infty) = \arcsin(\gamma) = 0$. The approximation to the magnetic flux, given by (2.5.11), in terms of the half of the length of the π junction, is depicted by the dashed line in figure 2.5 and is compared with the corresponding numerical counterpart (solid line). We observe that when a is close to its critical value, the approximation (2.5.11) well approximates the corresponding numerical calculation.

To check our analytical results, we perform numerical calculations and simulations. We numerically solve the time-independent governing equation (2.2.4), subject to boundary conditions (2.2.2) using a Newton-Raphson method, where we discretize the problem using central differences with a relatively fine spatial discretization. To numerically study the stability of a solution, we then discretize and solve the corresponding linear eigenvalue problem (2.3.4) (see also Section 7.4 in the Appendix).

2.5.2.1 Ground state in the presence of an external current

Next, we consider the driven case, $\gamma \neq 0$. By differentiating Eq. (2.5.9) with respect to C_2, and solving the resultant expression gives critical values of C_2 as

$$C_{2,c} = \pm 8\sqrt{\frac{a - \pi/4}{3\,(\pi + 2)}}. \tag{2.5.12}$$

By inserting the critical values of C_2, from Eq. (2.5.12) into Eq. (2.5.9), and Taylor expanding the resulting equation about ϵ, by ignoring the smaller terms, we obtain the critical value of the applied bias current

$$\gamma_c = \pm\sqrt{\frac{128}{27\,(\pi + 2)}}\left(a - \frac{\pi}{4}\right)^{3/2}. \tag{2.5.13}$$

At this critical value of the applied bias currentγ, one of the local minima of Eq. (2.5.7) disappears. The profile of this critical bias current γ_c, is presented by a dashed line in the upper panel of Figure 2.7. The approximation is compared with the corresponding numerical simulation (solid line) in the same figure. It can be observed that γ_c is zero in the region where the uniform zero solution is stable. γ_c increases in the instability region ($a < a_{c,0}$), and asymptotically approaches $2/\pi$ as a gets sufficiently large.

2.5.3 Ground state in the instability region by perturbation

Besides the Hamiltonian calculation of Kato and Imada [94], given in Section 2.5.1, we investigate the ground state in the instability region using a perturbation technique.

Let us suppose $\phi^{(1)}$, $\phi^{(2)}$ and $\phi^{(3)}$ be the bounded solutions of Eq. (2.2.4) in the regions I, II and II respectively.

First, we consider the region I, where $\theta(x) = 0$. Substituting values into Eq. (2.2.4), assuming $\phi^{(1)} \ll 1$, neglecting smaller terms, by formal series expansion we obtain

$$\phi^{(1)}_{xx} - \phi^{(1)} = -\gamma.$$

It is straight forward to show that a bounded solution of this equation in the region under consideration is given by

$$\phi^{(1)}(x) = A_5 e^x + \gamma, \tag{2.5.14}$$

where A_5 is a constant of integration. This solution has a maximum value at the point $x = -a$, where $\phi^{(1)}(-a) = A_5 e^{-a} + \gamma$. Therefore, to satisfy $\phi^{(1)}(x)$ being small, we require $A_5 e^{-a} + \gamma$ small.

Now consider the region II, where now $\theta(x) = \pi$. Inserting values into the static sine-Gordon equation (2.2.4), we obtain

$$\phi^{(2)}_{xx} = -\sin(\phi^{(2)}) - \gamma.$$

From a Taylor series expansion, the last equation, up to the second correction term, yields

$$\phi^{(2)}_{xx} + \phi^{(2)} + \widehat{\epsilon}(\phi^{(2)})^3 + \gamma = 0, \tag{2.5.15}$$

where we have taken $\widehat{\epsilon} = -1/6$. In order to solve this equation we follow the Lindstedt-Poincaré method, see, for example, Nayfeh and Mook [100]. Let

$$X(\tau) = X_0(\tau) + \widehat{\epsilon} X_1(\tau) + \widehat{\epsilon^2} X_2(\tau) + \ldots, \tag{2.5.16}$$

be a series solution of Eq. (2.5.15), where

$$\tau = \omega x, \quad \text{and} \quad \omega = 1 + \widehat{\epsilon}\omega_1 + \widehat{\epsilon}^2\omega_2 + \ldots. \tag{2.5.17}$$

By applying the chain rule for differentiation, we find that $X_x = \omega X_\tau$ and $X_{xx} = \omega^2 X_{\tau\tau}$. Consequently Eq. (2.5.15) reduces to

$$\omega^2 X_{\tau\tau} + X + \widehat{\epsilon} X^3 + \gamma = 0. \tag{2.5.18}$$

Plugging Eqs. (2.5.16) and the second expression in (2.5.17) into Eq. (2.5.18), and equating the coefficients of $\widehat{\epsilon}$ on both sides, we obtain

$$X_0'' + X_0 = -\gamma, \tag{2.5.19a}$$

$$X_1'' + X_1 = -2\omega_1 X_0'' - X_0^3. \tag{2.5.19b}$$

The general solution of Eq. (2.5.19a) is

$$X_0(\tau) = A_6 \cos(\tau) + A_6^* \sin(\tau) - \gamma,$$

where the integration constants A_6 and A_6^* are to be determined. To evaluate these, we impose the initial conditions, say, $X(0) = B$, where $B \ll 1$, $X^{'}(0) = 0$. Application of these initial conditions respectively yield $A_6 = B + \gamma$ and $A_6^* = 0$. As a result, the last equation reduces to

$$X_0(\tau) = (B + \gamma) \cos(\tau) - \gamma. \tag{2.5.20}$$

We substitute Eq. (2.5.20) into Eq. (2.5.19b) to obtain

$$X_1{}'' + X_1 = 2\omega_1 (B + \gamma) \cos(\tau) - \{(B + \gamma) \cos(\tau) - \gamma\}^3. \tag{2.5.21}$$

Equation (2.5.21), upon expansion and using the identities

$$4\cos^3(\tau) = \cos(3\tau) + 3cos(\tau), \quad 2\cos^2(\tau) = 1 + \cos(2\tau),$$

can be cast into the simplified form

$$\begin{aligned} X_1{}'' + X_1 = \quad & \frac{3}{2}\gamma (B + \gamma)^2 + \gamma^3 + (B + \gamma) \left[2\omega_1 - \frac{3}{4}(B + \gamma)^2 - 3\gamma^2\right] \cos(\tau) \\ & + \frac{3}{2}\gamma(B + \gamma)^2 \cos(2\tau) - \frac{1}{4}(B + \gamma)^3 \cos(3\tau). \end{aligned} \tag{2.5.22}$$

The homogenous solution of (2.5.22) is

$$X_{1,h} = A_7 \cos(\tau) + A_7^* \sin(\tau),$$

and the particular solution is of the form

$$X_{1,p} = A_8 \tau \cos(\tau) + A_9 \tau \sin(\tau) + A_{10} \cos(2\tau) + A_{11} \sin(2\tau) + A_{12} \cos(3\tau) + A_{13} \sin(3\tau).$$

Thus Eq. (2.5.22), after some simple algebra, can be written as

$$\begin{aligned} & -2\, A_8 \sin(\tau) + 2\, A_9 \cos(\tau) - 3\, A_{10} \cos(2\,\tau) - 3\, A_{11} \sin(2\,\tau) - 8\, A_{12} \cos(3\,\tau) \\ & -8\, A_{13} \sin(3\,\tau) = \frac{3}{2}\gamma (B + \gamma)^2 + \gamma^3 + (B + \gamma) \left[2\omega_1 - \frac{3}{4}(B + \gamma)^2 - 3\gamma^2\right] \cos(\tau) \\ & + \frac{3}{2}\gamma(B + \gamma)^2 \cos(2\tau) - \frac{1}{4}(B + \gamma)^3 \cos(3\tau). \end{aligned} \tag{2.5.23}$$

Equating the coefficients of like terms on both sides of Eq. (2.5.23) gives

$$A_8 = A_{11} = A_{13} = 0,$$

and

$$\begin{aligned} A_9 &= \omega_1(B+\gamma) - \frac{3}{8}(B+\gamma)^3 - \frac{3}{2}(B+\gamma)\gamma^2, \\ A_{10} &= -\frac{1}{2}\gamma(B+\gamma)^2, \quad A_{12} = \frac{1}{32}(B+\gamma)^3. \end{aligned} \tag{2.5.24}$$

The general solution of Eq. (2.5.22) is, therefore, given by

$$\begin{aligned} X_1 = \quad & A_7\cos(\tau) + A_7^*\sin(\tau) + A_9\tau\sin(\tau) + A_{10}\cos(2\tau) + A_{12}\cos(3\tau) \\ & + \frac{3}{2}(B+\gamma)^2\gamma + \gamma^3. \end{aligned} \tag{2.5.25}$$

Next, to determine A_7 and A_7^*, we use the initial conditions $X_1(0) = 0$, and $X_1'(0) = 0$. As a result we obtain

$$A_7 = -\gamma\left\{1 + (B+\gamma)^2\right\} - \frac{1}{32}(B+\gamma)^3, \quad \text{and} \quad A_7^* = 0.$$

Inserting these values into Eq. (2.5.25), we observe that when τ increases, the term $A_9\tau\sin(\tau)$ grows without bound, making the solution $X_1(\tau)$ unbounded. Such types of term, which make a solution unbounded, are called *secular* terms. To make our solution $X(\tau)$ bounded, we must avoid secular terms, which can be achieved by putting $A_9 = 0$.

Comparing the coefficients of $\cos(\tau)$ on both sides of Eq. (2.5.23), using the condition $A_9 = 0$, and solving for ω_1, we find

$$\omega_1 = \frac{3}{8}(B^2 + 2B\gamma + 5\gamma^2). \tag{2.5.26}$$

Substituting the value of ω_1 from Eq. (2.5.26) along with $\widehat{\epsilon} = -1/6$ into the second equation of (2.5.17), it is easy to verify that

$$\omega = 1 - \frac{1}{16}(B^2 + 2B\gamma + 5\gamma^2). \tag{2.5.27}$$

Inserting the expression for τ from (2.5.17) and neglecting smaller terms, Eq. (2.5.16) gives the required solution (up to the leading term) in the region $|x| < a$, as

$$\phi^{(2)}(x) = (B+\gamma)\cos(\omega x) - \gamma. \tag{2.5.28}$$

From Eq. (2.5.28), it is clear that $(B+\gamma)\cos(\omega a) - \gamma$ is the minimum value of the above solution which is attained by the solution at the points $x = \pm a$. The maximum solution, which is attained at the point where $x = 0$ is $\phi^{(2)}(0) = B$.

In a fashion similar to Eq. (2.5.14), a bounded solution $\phi^{(3)}(x)$ of Eq. (2.2.4), in the region $a < x < \infty$, is

$$\phi^{(3)}(x) = A_{14}e^{-x} + \gamma, \tag{2.5.29}$$

where A_{14} is a constant of integration.

By the help of Eqs. (2.5.14), (2.5.28) and (2.5.29), we are now able to express the bounded solutions of Eq. (2.2.4) in all the three regions in the form of the following system

$$\phi(x) = \begin{cases} A_5 e^x + \gamma, & -\infty < x < -a, \\ (B+\gamma)\cos(\omega x) - \gamma, & |x| < a, \\ A_{14} e^{-x} + \gamma, & a < x < \infty, \end{cases} \tag{2.5.30}$$

Applying the continuity conditions $\phi(-a^-) = \phi(-a^+)$ and $\phi_x(-a^-) = \phi_x(-a^+)$ to the first two equations of the system (2.5.30), we respectively obtain

$$A_5 e^{-a} = (B+\gamma)\cos(\omega a) - 2\gamma, \tag{2.5.31a}$$

$$A_5 e^{-a} = (B+\gamma)\,\omega \sin(\omega a). \tag{2.5.31b}$$

From Eq. (2.5.31a), one may write

$$A_5 = e^a\left[(B+\gamma)\cos(\omega a) - 2\gamma\right]. \tag{2.5.32}$$

A similar result can be obtained by applying the continuity conditions $\phi(a^-) = \phi(a^+)$ and $\phi_x(a^-) = \phi_x(a^+)$ to the last two equations of the system (2.5.30). As a result, one may write

$$A_{14} = e^a\left[(B+\gamma)\cos(\omega a) - 2\gamma\right]. \tag{2.5.33}$$

Comparing Eqs. (2.5.32) and (2.5.33), one can write

$$A_5 = A_{14}. \tag{2.5.34}$$

Dividing Eq. (2.5.31a) by Eq. (2.5.31b), a simple manipulation gives

$$\frac{1}{\omega}\cot(\omega a) - \frac{2\gamma \csc(\omega a)}{\omega(B+\gamma)} = 1, \tag{2.5.35}$$

with ω being given by Eq. (2.5.27). Thus, the amplitude B, of the solution in the second region is given by the implicit relation

$$B = \frac{2\gamma}{\cos(\omega a) - \omega \sin(\omega a)} - \gamma. \tag{2.5.36}$$

2.5.3.1 Ground state solutions in the absence of external current

The analytical work in the above section helps us to discuss the ground state solutions in the small instability region in the vicinity of the critical zero facet length, i.e., in the region

$$a - a_{c,0} = \epsilon, \tag{2.5.37}$$

with $\epsilon \ll 1$.

First we discuss the limiting solutions in the instability region when a is close to $a_{c,0}$, in the case when there is no external current applied to the system. Inserting $\gamma = 0$, into Eq. (2.5.27), the relation between ω and the amplitude B, takes the form

$$\omega = 1 - \frac{B^2}{16}. \tag{2.5.38}$$

Putting Eq. (2.5.38) into Eq. (2.5.35) and rearranging, we have

$$\cot\left[\left(1 - \frac{B^2}{16}\right)a\right] = 1 - \frac{B^2}{16}. \tag{2.5.39}$$

Our goal is to express B as a function of the small parameter ϵ. For this purpose, we introduce the relation (2.5.37) into Eq. (2.5.39), using a Taylor series expansion by assuming ϵ small, neglecting the smaller terms and solving the resultant equation for the amplitude B, simple manipulation gives

$$B(\epsilon) = \pm 8\sqrt{\frac{\epsilon}{\pi + 2}} = \pm 8\sqrt{\frac{a - a_{c,0}}{\pi + 2}}, \tag{2.5.40}$$

which is the same as the maximum of the ground state solution (2.5.11).

Substituting values from Eqs. (2.5.32), (2.5.33) and (2.5.40) into Eq. (2.5.30), we obtain two sets of bounded solutions of the system (2.2.4). These two sets of solutions correspond to the different signs of B. Thus we obtain the ground state solutions in the instability region in the undriven case, i.e., when there is no external current applied to the system.

Let ϕ_1 and ϕ_2 respectively denote the ground state solutions corresponding to the positive and negative value of B, given by Eq. (2.5.40). The profiles of ϕ_1 and ϕ_2, as a function of the spatial variable x, are depicted in the upper panel of Figure 2.4. As is clear from the system (2.5.30), in the absence of external current γ, both $\phi_1(x)$ and $\phi_2(x)$ approach zero when $x \to \mp\infty$ respectively, while at the point $x = 0$, in region II, the ground state solutions $\phi_1(x)$ and $\phi_2(x)$ respectively attain values B and $-B$.

2.5.3.2 Vortices and antivortices in the junction

Consider the ground state solution $\phi_1(x)$. As reported by Josephson [9], by scaling the critical current I_c to unity, the relation (1.3.1) between the supercurrent I_s and the Josephson phase ϕ_1 in region reduces to (see also Section 1.3)

$$I_s = \sin(\phi_1). \tag{2.5.41}$$

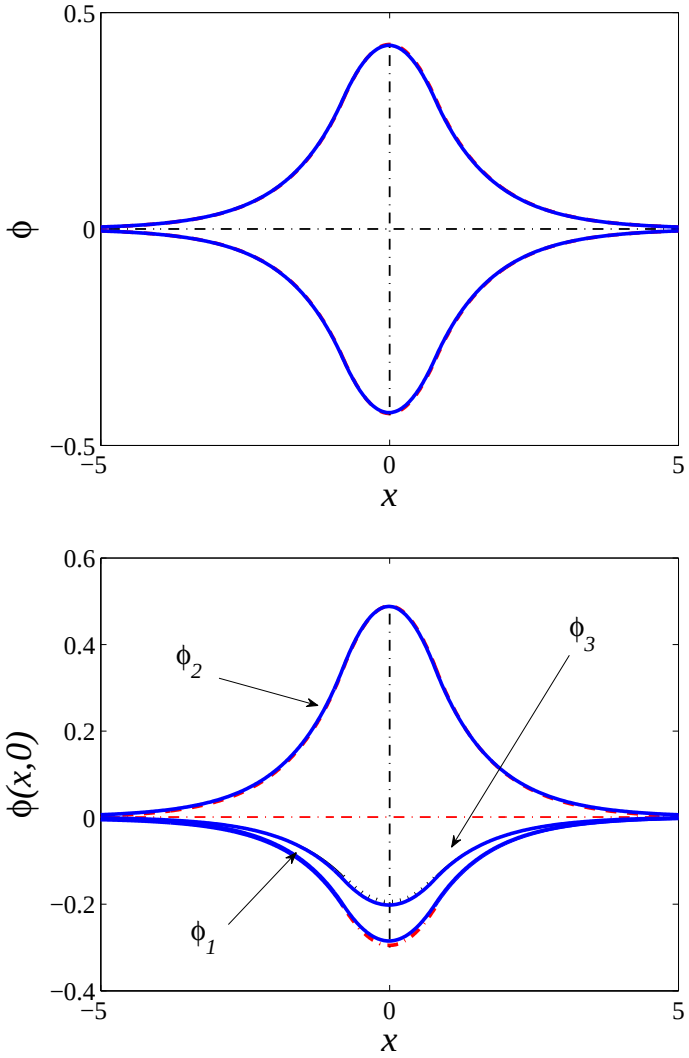

Figure 2.4: Plot of the zero ground state solutions given by system (2.5.30) and Eq. (2.5.40), in the instability region $a - a_{c,0} \ll 1$, as a function of the spatial variable x in the undriven case for $a = 0.8$ (the upper panel). Above the line $\phi = 0$ is the profile of ϕ for the positive value of B while the lower one corresponds to the negative value of B. The lower panel represents the same profile, where $\widehat{B}^{(n)}$ is given by Eq. (2.5.47), for the driven case where $\gamma = 0.0016$ and $a = 0.8$. The dashed lines, dashed dotted lines and dotted lines represents the profiles of the solutions given by (2.5.30), that correspond to $B^{(1)}$, $B^{(2)}$ and $B^{(3)}$ respectively. The solid lines in both the panels represent numerical solutions.

As in region I, the ground state solution ϕ_1 is small. i.e., $0 \leq \phi_1 \ll 1$. Hence, (2.5.41) implies that the supercurrent I_s is positive. Similarly, using Eqs. (2.2.1) and (1.3.4), the

supercurrent in region II is given by [25]

$$I_s = -\sin(\phi_2), \tag{2.5.42}$$

which is negative for $0 < \phi \ll 1$. As result a vortex of supercurrent is produced at the phase discontinuity point $x = -a$. Giving similar reasons, it can be concluded that an antivortex is generated at the second phase discontinuity point $x = a$.

It has been already reported by Kogan et al. [101], that these vortices carry the magnetic flux equal to $\pm\Phi_0/2$, where Φ_0 is a single flux quantum and are called half vortices. The directions of the supercurrent carried by the vortices at the phase discontinuities $x = \pm a$ are opposite. Such type of vortices are known to be *mirror* symmetric.

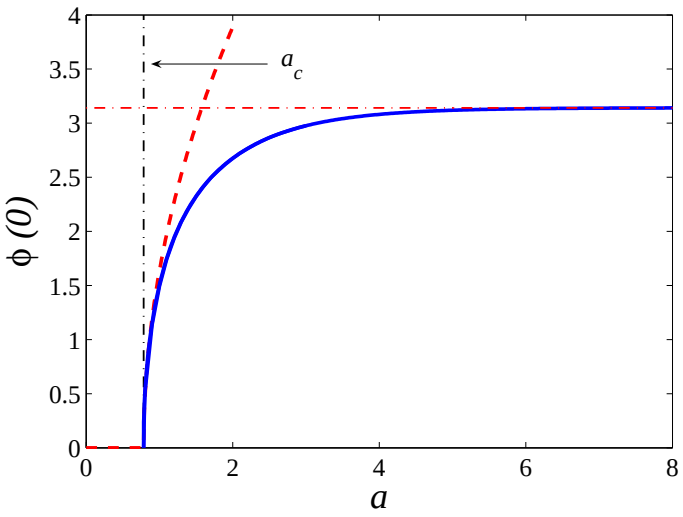

Figure 2.5: Plot of the zero ground state solution given by system (2.5.30) and Eq. (2.5.40) as a function of the π junction length. Solid line represents the numerically obtained ground state and the dashed line is its corresponding approximations. We have taken the positive value of B, as the negative one is just its reflection.

The approximation to the ground state solution close to the critical zero facet length, given by the system (2.5.30) and Eq. (2.5.40) as a function of the facet length a is depicted by the dashed line in Figure 2.5. It is clear from (2.5.30) that when there is no external current applied to the junction, we have $\phi(\pm\infty) = 0$. Thus, the magnetic flux $\Delta\phi$ is the same as the ground state solution at the origin $\phi(0)$. From Fig. 2.5 it is clear that the magnetic flux is zero in the region where $a \leq a_{c,0}^{\infty}$. It means that whenever the distance between the vortex and antivortex decreases, the vortices disappear. The magnetic flux increases in the instability region, where $a \geq a_{c,0}$, and approaches π for large

a, as suggested by the solid line in the same figure, which is obtained from numerical simulations. For a close to $a_{c,0}$, the approximation to $\phi(0)$ is close to the numerically obtained ground state. As we notice that for the ground state solution, investigated above, we have

$$|\phi(0) - \phi(\pm\infty)| = \pi,$$

when $a \to \infty$. This solution, mathematically, represents a *semifluxon* or a *fractional fluxon*. Thus a region has been investigated in which the semifluxons are spontaneously generated.

2.5.3.3 Limiting solutions in the driven case

Now we take into account the situation where the bias current γ is nonzero, that is, we study the static properties of the solution in the presence of an external current γ.

We notice that Eq. (2.5.35) contains three parameters, namely a, B and γ. While expanding this equation in terms of a small parameter ϵ, it would be useful to obtain the leading order term that contains all the three parameters. For this we need a scaling in terms of the small parameter $\epsilon = a - \pi/4$. It can be verified that to obtain the desired first order term, having one parameter family, one must make the following substitutions

$$a = \frac{\pi}{4} + \epsilon, \quad B = \widehat{B}\sqrt{\epsilon}, \quad \gamma = \widehat{\gamma}\epsilon^{3/2}. \tag{2.5.43}$$

Inserting the assumed scaling, from Eq. (5.3.4) into Eq. (2.5.35), and using the Taylor series expansion, with the assumption of ϵ being small, we obtain

$$f(B) = (\pi + 2)\widehat{B}^3 - 64\widehat{B} + 64\widehat{\gamma}\sqrt{2}. \tag{2.5.44}$$

Next, we solve the cubic polynomial Eq. (2.5.44), for $\widehat{B}$, by using the Nickalls' method [102]. Let $N(x_N, y_N)$ be a point on the curve of the polynomial $c_3x^3 + c_2x^2 + c_1x + c_0$, such that for the transformation $z = x - x_N$, the sum of roots of the reduced cubic polynomial $f(z)$ is zero. In such a case $x_N = -c_3/3c_1$ and N is the point of symmetry of the cubic polynomial. Assume δ and h are the horizontal and vertical distances from N to a turning points respectively (see Fig.1 of [102]), then

$$\delta = \sqrt{\frac{c_2^2 - 3c_3c_1}{3c_3^2}}, \; h = 2c_3\delta^3. \tag{2.5.45}$$

By making the transformation $z = 2\delta\cos(\Theta)$, where Θ is the angle which the horizontal line through N makes with the first root of the cubic equation (see Figure 2 in [102]),

Nickalls has shown that the second equation of the Eq. (2.5.45) implies

$$\cos(3\Theta) = -\frac{y_N}{h}. \tag{2.5.46}$$

Applying these ideas to our cubic equation (2.5.44), we find

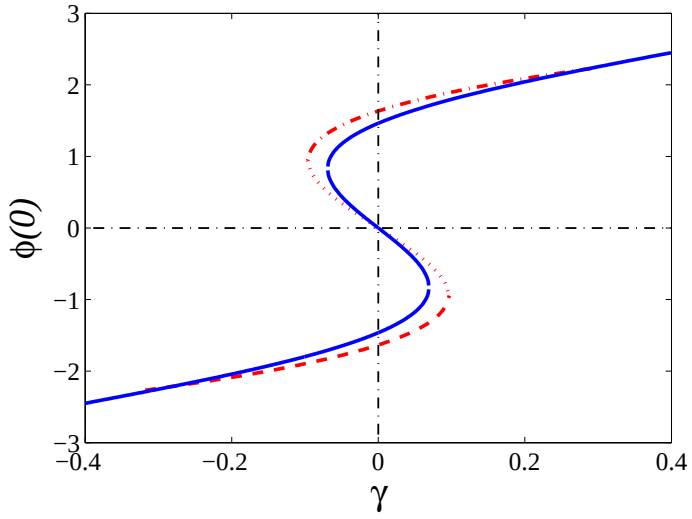

Figure 2.6: Comparison of the numerically obtained zero ground state as a function of the applied bias current and the corresponding approximations given by Eq. (2.5.47). The three roots are represented by the dashed lines, dashed-dotted lines and dotted lines respectively. Here, the value of the facet length a is taken to be unity.

$$x_N = 0, \quad \delta = \frac{8}{\sqrt{3(\pi+2)}}, \quad h = \frac{1024}{3\sqrt{3(\pi+2)}}, \quad y_N = 64\widehat{\gamma}\sqrt{2}, \quad \Theta = \frac{1}{3}\arccos\left(-\frac{y_N}{h}\right),$$

and the roots of Eq. (2.5.44) are, then, given by

$$\widehat{B}^{(n)} = 2\delta\cos\left[\Theta + 2(n-1)\frac{\pi}{3}\right], \text{ n} = 1, 2, 3. \tag{2.5.47}$$

Using these roots, the profile $\phi(0)$, given by Eq. (2.5.30), as a function of the external current γ is depicted in Fig. 2.6. One can observe that the profile of $\phi(0)$ is symmetric about the horizontal line $\phi(0) = 0$. It is clear from the same figure that when γ is zero, we have two nonzero values of $\phi(0)$, which correspond to the solutions $\phi_1(x)$ and $\phi_2(x)$ respectively and a solution for which $\phi_3(x)$ is zero. One can observe a good relation between the approximation and the corresponding numerical solutions.

When $\gamma \neq 0$, there are three nonzero values of $\phi(0)$. If we further increase γ, a stage comes where the solution $\phi_1(x, \gamma)$ coincides with $\phi_3(x, \gamma)$ at a saddle node bifurcation. This critical value of the applied current, at which the coalescence of ϕ_1 and ϕ_2 occurs,

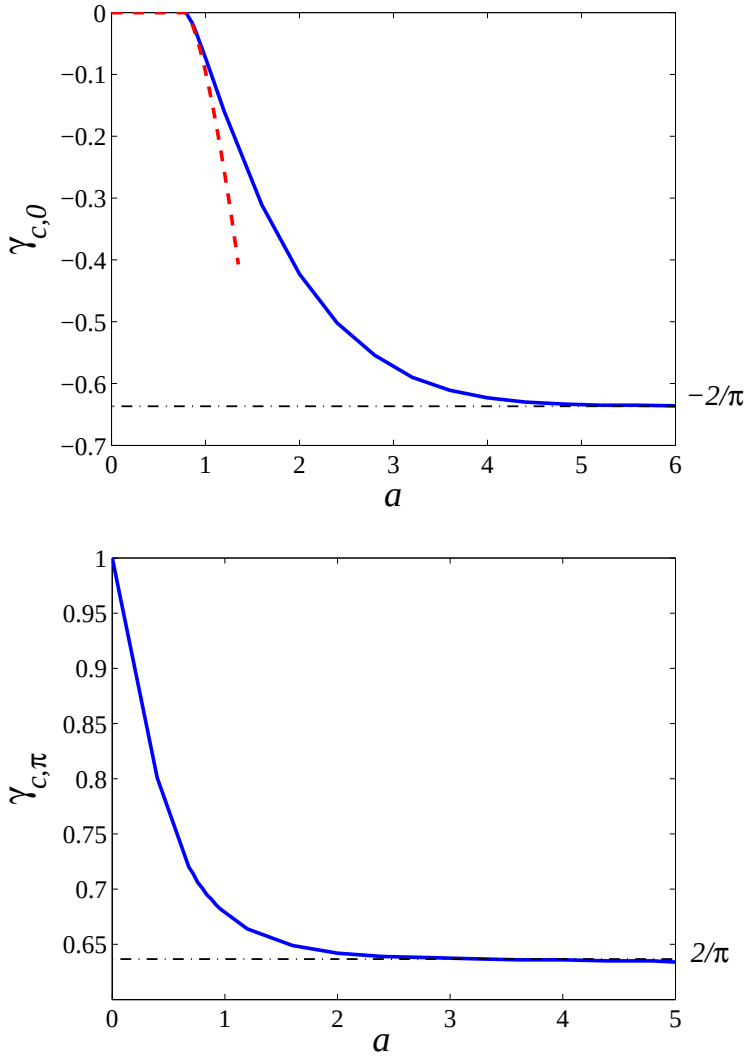

Figure 2.7: The top panel represents a comparison between the approximation of the critical bias current about the uniform $\widetilde{\phi} = 0$ solution, given by Eq. (2.5.50) (dashed line), and the corresponding numerical counterpart (solid line), as a function of the half length of the π-junction. The lower panel shows the numerically obtained $\gamma_{c,\pi}$ as a function of the facet length a.

is denoted by $\gamma_{c,0}$. For $a = 1$ we obtain $\gamma_{c,0} \approx 0.0969$. A same situation is obtained by starting from the solution $\phi_2(x)$ at $\gamma = 0$ and reducing γ (that is, moving to the left of the top solution from the point $\gamma = 0$), until we reach a value of γ where solution $\phi_2(x, \gamma)$ and $\phi_1(x, \gamma)$ coincide. This transition occurs at the point where $\gamma = -\gamma_{c,0}$.

The critical value of γ can be approximated as follows.

The stationary points of Eq. (2.5.44) are given by $f'(\widehat{B}) = 0$. This gives

$$\widehat{B}_{1,2} = \pm\sqrt{\frac{64}{3(\pi+2)}}. \tag{2.5.48}$$

It is obvious that $\widehat{B}_1$ and $\widehat{B}_2$ correspond to the maximum and the minimum values of f respectively. Inserting the values of $\widehat{B}$ from Eq. (2.5.48) into Eq. (2.5.44) and solving the equation so formed for $\widehat{\gamma}$, we find

$$\widehat{\gamma}_{1,2} = \pm\sqrt{\frac{128}{27(\pi+2)}}. \tag{2.5.49}$$

Thus, the scaling $\gamma = \widehat{\gamma}\epsilon^{3/2}$ in the (5.3.4) gives

$$\gamma_{1,2} = \pm\sqrt{\frac{128}{27(\pi+2)}}\left(a - \frac{\pi}{4}\right)^{3/2}. \tag{2.5.50}$$

The approximation to the ground states given by the system (2.5.30) with B being given by (2.5.47), as function of the external current γ are compared with the corresponding numerics in Fig. 2.6. For γ close to $\pm\gamma_{c,0}$, we observe a close agreement between our approximation and the numerical counterparts.

The lower panel of Fig. 2.4 shows the dynamics of (2.5.30) in the presence of an applied bias current as a function of the spatial variable x. The three different solutions correspond to values of $B^{(n)}$ given by Eq. (2.5.47). When $x \to \pm\infty$, the ground state solutions approach $\arcsin(\gamma)$.

In the top panel of Fig. 2.7, a comparison between the approximation to the critical current $-\gamma_{c,0}$ given by Eq. (2.5.50) (dashed line), as a function of the parameter a, and the corresponding numerics (solid line) is displayed. We note that the critical current $-\gamma_{c,0}$ is zero in the region of the stability of the constant solution $\widetilde{\phi} = 0$, where $a \leq a_{c,0}$. In the instability region, where a is close to $a_{c,0}$, the approximation is close to the corresponding numerical simulations. For $a \gg 1$, the critical current $-\gamma_{c,0}$ approaches $-2/\pi$.

We have numerically calculated $\gamma_{c,\pi}$ from Eq. (2.2.4) using a simple Newton Raphson method. The plot of this second critical current, as a function of the parameter a is depicted in the lower panel of the Fig. 2.7. When a is zero, this current has a maximum value. It may be noted that when a increases, that is when the distance between the two vortices decreases, $\gamma_{c,\pi}$ gradually decreases. For $a \gg 1$, we see that $\gamma_{c,\pi}$ asymptotically approach $2/\pi$.

2.6 Conclusions

We have studied an infinitely long Josephson junction having two π-discontinuities in the phase, that is, the so-called 0-π-0 long Josephson junction, in an infinite domain using a perturbed sine-Gordon equation. We have shown that there are two types of constant solutions admitted by the static version of the model under consideration. It is proved that when there is no bias current, the two static solutions satisfy the continuity conditions.

The stability of the two uniform solutions as a function of the facet length a is discussed. We have demonstrated that there is a critical facet length $a_{c,0} = \pi/4$ above which the zero background solution is unstable and that the uniform π solution is unstable for any value of the facet length a.

It is also shown that the ground states of the system is nonuniform in the instability region. We have investigated solutions in this instability region, where it is concluded there are two ground states bifurcating from the zero background. An asymptotic analysis has been used to construct the ground states and their absolute maximum in the vicinity of the critical facet length in the region of instability.

The effect of an applied bias current on the ground states has been studied as well. It is demonstrated that the region with no stable solution, there exist two critical currents $\pm\gamma_{c,0}$ and $\pm\gamma_{c,\pi}$. It is shown that the ground states exist in the region where $-\gamma_{c,0} < \gamma < \gamma_{c,0}$ and that there are no static solutions in the region where $|\gamma_{c,\pi}| < |\gamma|$. We have calculated critical force $\gamma_{c,0}$ in the small instability region using a perturbation technique. The critical current $\gamma_{c,\pi}$ has been calculated numerically. Numerical simulations are presented to confirm our analytical work.

CHAPTER 3

Existence and stability analysis of finite 0-π-0 long Josephson junctions

Parts of this chapter have been published in Ahmad et al. [103].

3.1 Introduction

In Chapter 2, we analytically studied an infinite domain long Josephson junction with two π-discontinuities in the Josephson phase using a perturbed sine-Gordon equation with π-discontinuity in the nonlinearity. An infinite domain 0-π-0 long Josephson junction was first investigated by Kato and Imada [80], where they showed that there is a stability window for the length of π-junction in which the uniform zero solution is stable, while the constant π-solution is unstable everywhere. In the instability region, where both the uniform solutions are unstable, the ground state is a nonuniform solution, which corresponds to a pair of antiferromagnetically ordered semifluxons. Later, it was shown by Zenchuk and Goldobin [104] and Susanto et al. [57] that there is a minimum facet length of the π-junction, above which a nontrivial ground state exits, which corresponds to the minimum facet length needed to construct such solutions, that is, the bifurcation is supercritical.

The possibility of employing 0-π-0 junctions for observing macroscopic quantum tunneling was discussed by Goldobin et al. [99]. In the presence of an applied bias current, a 0-π-0 Josephson junction has a critical current above which one can flip the order of the semifluxons as shown by Kato and Imada [94], Dewes et al. [105] and Boschker [106]. It has also been reported, first by Kuklov et al. [52, 107] and later by Susanto et al. [57], that there is another critical current in the junction, above which the junc-

tion switches to the resistive state, i.e., there is a critical value of the bias current above which static semifluxons do not exist. Goldobin et al. [108, 109] have also broadened the study of 0-π-0 junctions to 0-κ-0 junctions, where $0 \leq \kappa \leq \pi \pmod{2\pi}$. In those reports, they have studied the possible ground states of semifluxons formed at the arbitrary κ-discontinuities in the Josephson phase.

Here, we limit ourselves to discuss 0-π-0 junctions only, but extend it to the case of a finite domain. This is of particular interest, especially from the physical point of view, as such junctions have been successfully fabricated recently by, for example, Dewes et al. [105] and Boschker [106], making a finite length analysis more relevant.

3.2 Overview of the Chapter

This chapter has the following structure. In Section 3.3, we briefly discuss the mathematical model used for the description of the problem under consideration. In Section 3.4, we examine the existence and stability of the constant background solutions of the model. We show that there is a critical value of the facet length a, at which the stability of a stationary solution changes. Subsequently, we derive the relations between the critical facet lengths of the constant backgrounds and the length of the junction. By studying of the stability diagrams of the uniform solutions, we demonstrate that there is a symmetry between the stability diagrams of the two solutions of the system. In Section 3.5, we discuss this symmetry. Like the infinite domain problem discussed in Chapter 2, we show that there exists an instability region in the finite domain as well, where the two uniform backgrounds of the system are unstable. In Section 3.6, by using perturbation analysis, we investigate the ground states corresponding to the two constant solutions both in the absence and presence of an applied bias current. This is carried out using a Lindstedt-Poincareé method and a modified Lindstedt-Poincareé approach. In Section 3.6.5, we discuss obtaining the nonuniform ground state solutions both in the undriven and the driven cases using a Hamiltonian energy characterization. In Section 5.4, we discuss the stability analysis of the critical eigenvalues of the semifluxons corresponding to the constant solutions. Finally, in Section 5.7, we present a short summary of the main results achieved in this chapter.

3.3 Mathematical Model

In the previous chapter, we discussed the dynamics of an infinitely long Josephson junction with two π-discontinuities in its phase. In this chapter, we extend the ideas to the case where the domain is finite.

To describe the dynamics of a finite Josephson junction, we use the sine-Gordon model (1.5.5) and restrict the spatial variable x to lie in the region $-L \leq x \leq L$, where $2L$ is the total length of the junction. That is, we use

$$\phi_{xx} - \phi_{tt} = \sin\left[\phi + \theta(x)\right] - \gamma, \; -L \leq x \leq L. \tag{3.3.1}$$

The Josephson phase given by Eq. (2.2.1) (see Section 2.2), for the present problem, is modified to

$$\theta(x) = \begin{cases} 0, & L > |x| > a, \\ \pi, & |x| < a, \end{cases} \tag{3.3.2}$$

where $2a$ is the length of the π-junction.

Again we suppose that the eigenfunction and the magnetic flux are continuous at the phase discontinuity points $x = \pm a$ and the magnetic flux at the boundaries $x = \pm L$ is zero.[1] In other words, we study the system given by Eqs. (3.3.1) and (3.3.2), subject to the following continuity and boundary conditions

$$\phi(a^-, t) = \phi(a^+, t), \quad \phi_x(a^-, t) = \phi_x(a^+, t), \quad \phi_x(\pm L, t) = 0. \tag{3.3.3}$$

For the region $-L \leq x \leq L$, the infinite Lagrangian (2.2.3) reduces to

$$\mathcal{L} = \int_0^\infty \int_{-L}^{L} \left\{ \frac{1}{2}\phi_t^2 - \frac{1}{2}\phi_x^2 - 1 + \cos\left[\phi + \theta(x)\right] - \gamma\phi \right\} dxdt, \tag{3.3.4}$$

from which the model under consideration (3.3.1), subject to the boundary conditions (5.2.4) can be derived.

As in the infinite domain case, here, we concentrate on the investigation of static semi-fluxons, for which we use the static version of Eq. (3.3.1), that is,

$$\phi_{xx} = \sin\left[\phi + \theta(x)\right] - \gamma, \quad -L < x < L. \tag{3.3.5}$$

[1] In fact, from the physical point of view, one should assume that the magnetic flux at the boundaries $x = \pm L$ is equal to the externally applied magnetic flux H. We limit ourselves to the case of $H = 0$.

3.4 Existence and stability analysis of uniform solutions

As discussed in the previous chapter, the system under consideration admits two stationary and uniform solutions at $\gamma = 0$

$$\widetilde{\phi} = 0, \quad \text{and} \quad \widetilde{\phi} = \pi. \tag{3.4.1}$$

To discuss the stability of the constant solutions, we proceed into the following.

3.4.1 Derivation of the eigenvalue problem

In the following, we discuss the linear stability of the two uniform solutions. By using the stability ansatz (2.3.3), with the new restriction of the variable x, we obtain the eigenvalue problem

$$V_{xx} = \left\{E + \cos\left[\widetilde{\phi} + \theta(x)\right]\right\} V, \quad -L \leq x \leq L, \tag{3.4.2}$$

where $E = \lambda^2$, and $V(x)$ is subject to the continuity and boundary conditions

$$V(a^-) = V(a^+), \quad V_x(a^-) = V_x(a^+), \quad V_x(\pm L) = 0. \tag{3.4.3}$$

Because the eigenvalue problem (3.4.2) is self-adjoint, it follows that the corresponding spectral parameter E is real valued.

Due to the finite size of the domain, $-L \leq x \leq L$, the eigenvalue problem (3.4.2) has only discrete spectra, which, on the basis of the limit $L \to \infty$, can be categorized into two types: the set of eigenvalues that constitutes the continuous spectrum in the limit $L \to \infty$ which for simplicity we denote as the "continuous" spectrum and the set of eigenvalues that complement the "continuous" spectrum in the infinite domain limit, which we call the "discrete" spectrum.[2]

To determine the "continuous" and "discrete" spectra in the finite domain, we seek the same type of solutions as in the infinite domain.

3.4.2 Linear stability of $\widetilde{\phi} = 0$

To study the linear stability of the uniform zero background solution, we first discuss the so-called "continuous" spectrum.

[2] In the infinite domain problem discussed in Chapter 2, we know that the continuous spectrum corresponds to the non-square integrable solutions of the eigenvalue problem in the regions where $x \to \pm\infty$. Thus, by definition, the discrete spectrum is constructed by solutions of the eigenvalue problem which are square-integrable in regions where $x \to \pm\infty$.

3.4.2.1 The"continuous" spectrum

By using (3.3.2) and plotting the term $\cos\left[\widetilde{\phi}+\theta(x)\right]$ in the eigenvalue problem (3.4.2) versus the spatial variable x, the domain under consideration is divided into three regions $-L<x<-a$, $|x|<a$ and $a<x<L$. For the sake of brevity, we denote these regions by I, II and III respectively.

We know that the continuous spectrum of a constant background solution in the infinite domain, corresponds to solutions of the eigenvalue problem which are bounded and have small amplitudes in the regions $x\to\pm\infty$. Therefore, to find the "continuous" spectrum of the uniform zero solution, we seek solutions of (3.4.2) which are bounded and have small amplitudes in the limit of a sufficiently large domain.

Let V_1 be the required solution of the eigenvalue problem (3.4.2) in region I. With the help of Eq. (3.3.2), (3.4.2) reduces to

$$V_{1xx}-(E+1)\,V_1=0. \tag{3.4.4}$$

A bounded V_1 satisfying Eq. (3.4.4) is of the form

$$V_1=\widehat{B}_1\cos(\widehat{\zeta}x)+\widetilde{B}_1\sin(\widehat{\zeta}x), \tag{3.4.5}$$

where

$$\widehat{\zeta}=\sqrt{-1-E}, \tag{3.4.6}$$

and $\widehat{B}_1$, $\widetilde{B}_1$ are constants of integration to be determined using the boundary condition $V_x(-L)=0$. As a result, Eq. (3.4.5) gives

$$\widetilde{B}_1=-\widehat{B}_1\tan\left(\widehat{\zeta}L\right). \tag{3.4.7}$$

Plugging the value of $\widetilde{B}_1$, from Eq. (3.4.7) into Eq. (3.4.5), we obtain

$$V_1=\frac{\widehat{B}_1}{\cos(\widehat{\zeta}L)}\left[\cos\left(\widehat{\zeta}x\right)\cos\left(\widehat{\zeta}L\right)-\sin\left(\widehat{\zeta}x\right)\sin\left(\widehat{\zeta}L\right)\right].$$

By defining $B_1=\widehat{B}_1/\cos(\widehat{\zeta}L)$, the bounded solution takes the following simple form

$$V_1=B_1\cos\left[\widehat{\zeta}\,(x+L)\right]. \tag{3.4.8}$$

It is simple to show that the bounded solutions of the eigenvalue problem (3.4.2) in regions II and III are respectively given by

$$V_2=B_2\cos\left(\widehat{\beta}x\right)+B_3\sin\left(\widehat{\beta}x\right), \tag{3.4.9}$$

$$V_3 = B_4 \cos\left[\widehat{\zeta}\,(x-L)\right], \tag{3.4.10}$$

where B_2, B_3 and B_4 are integration constants, the solution V_3 is subject to the boundary condition $V_x(L) = 0$ and $\widehat{\beta}$ is the same as given by Eq. (2.4.12).

By the help of Eqs. (3.4.8), Eq. (3.4.9) and (3.4.10), we are now in a position to express the bounded solution of the eigenvalue problem (3.4.2) by the following system

$$V(x) = \begin{cases} B_1 \cos\left[\widehat{\zeta}(x+L)\right], & -L < x < -a, \\ B_2 \cos(\widehat{\beta}x) + B_3 \sin(\widehat{\beta}x), & |x| < a, \\ B_4 \cos\left[\widehat{\zeta}(x-L)\right], & a < x < L. \end{cases} \tag{3.4.11}$$

Applying the continuity and boundary conditions (5.2.4) to (3.4.11), we obtain a system of four equations with four unknowns

$$F_2 \begin{pmatrix} B_1 \\ B_2 \\ B_3 \\ B_4 \end{pmatrix} = 0, \tag{3.4.12}$$

where the coefficient matrix F_2 is as follows

$$F_2 = \begin{bmatrix} \cos\left[\widehat{\zeta}(L-a)\right] & -\cos(\widehat{\beta}a) & \sin(\widehat{\beta}a) & 0 \\ \widehat{\alpha}\sin\left[\widehat{\zeta}(L-a)\right] & -\widehat{\beta}\sin(\widehat{\beta}a) & -\widehat{\beta}\cos(\widehat{\beta}a) & 0 \\ 0 & \cos(\widehat{\beta}a) & \sin(\widehat{\beta}a) & -\cos\left[\widehat{\zeta}(a-L)\right] \\ 0 & -\widehat{\beta}\sin(\widehat{\beta}a) & \widehat{\beta}\cos(\widehat{\beta}a) & \widehat{\zeta}\sin\left[\widehat{\zeta}(a-L)\right] \end{bmatrix}. \tag{3.4.13}$$

The necessary condition for the system (3.4.12) to have a nontrivial solution is

$$\det(F_2) = 0. \tag{3.4.14}$$

In other words, the "continuous" spectrum of the constant zero background solution of the system is given by the zeros of the relation (3.4.14). An implicit plot of these zeros in the (a, E)-plane is depicted in the top panel of Fig. 3.1, where we have taken $L = 1$. It is observed, numerically, that there is no unstable eigenvalue in the "continuous" spectrum, that is, $E < 0$ for all a. The distribution of E will become dense, as expected, when we increase the length L.

Although, there is no unstable eigenvalue in the "continuous" spectrum, still one can not conclude about the linear stability of the uniform solution. To discuss the linear stability, we proceed to the following subsection.

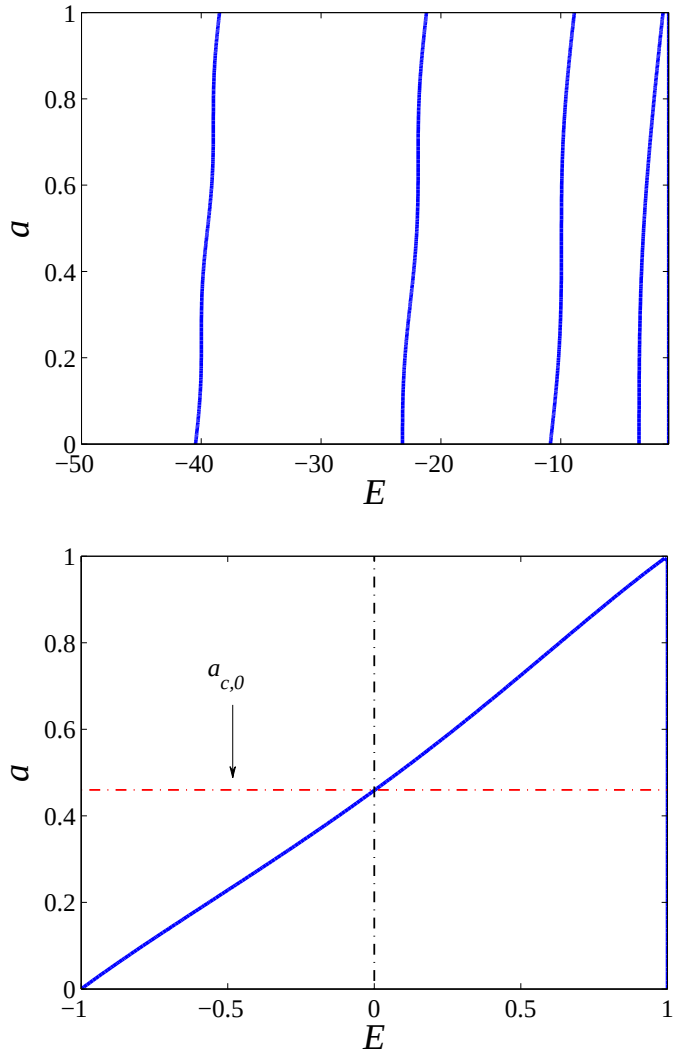

Figure 3.1: Plot of the "continuous" spectrum (top), given by the zeros of the condition (3.4.14) and the "discrete" spectrum (bottom) of the uniform $\widetilde{\phi} = 0$ solution, given by the zeros of (3.4.22) as a function of half of the $\pi-$ junction length a for $L = 1$.

3.4.2.2 The "discrete" spectrum

As discussed in Section 2.4.1.2, the discrete spectrum in the infinite domain corresponds to bounded and decaying solutions in the regions $|x| > a$ and a bounded solution in the region $|x| < a$. Therefore, to determine the "discrete" spectrum of a constant background solution, we find the same type of solution of the eigenvalue problem (3.4.2) in the three regions.

Let us assume that V_1 is a solution of the eigenvalue problem (3.4.2) in the region I

where $\theta = 0$. Consequently, (3.4.2) reduces into

$$V_{1xx} - (1 + E)\, V_1 = 0,$$

whose general solution is

$$V_1 = C_1 e^{-\widehat{\alpha} x} + C_2 e^{\widehat{\alpha} x}, \tag{3.4.15}$$

with C_1 and C_2 being arbitrary constants of integration and $\widehat{\alpha}$ is given by Eq. (2.4.8). This solution must satisfy the boundary condition $V_x(-L) = 0$, in which case we obtain $C_2 = C_1 e^{2\widetilde{\alpha} L}$. Thus, the solution V_1, after a simple manipulation, yields

$$V_1 = \frac{C_1}{e^{\widetilde{\alpha} L}} \left[e^{\widehat{\alpha}(x+L)} + e^{-\widehat{\alpha}(x+L)} \right].$$

Since C_1 is arbitrary, so by defining $B_5 = 2C_1 / e^{\widetilde{\alpha} L}$, Eq. (3.4.15) can be written as

$$V_1 = B_5 \cosh\left[\widehat{\alpha}(x + L)\right]. \tag{3.4.16}$$

Similarly, one can show that the general solution V_3 of (3.4.2) in the region III, subject to the boundary condition $V_x(L) = 0$, has the form

$$V_3 = B_8 \cosh\left[\widehat{\alpha}(x - L)\right]. \tag{3.4.17}$$

By keeping the discussion in Section 2.4.1.2, we assume that $E < 1$ and find the solution V_2 of the eigenvalue problem (3.4.2) in the region II, has the form

$$V_2 = B_6 \cos\left(\widehat{\beta} x\right) + B_7 \sin\left(\widehat{\beta} x\right), \tag{3.4.18}$$

where $\widehat{\beta}$ is given by (2.4.12) and B_6, B_7 are constants of integration to be determined.

Thus, a general solution V of the eigenvalue problem (3.4.2) in all the three regions is given by

$$V(x) = \begin{cases} B_5 \cosh(\widehat{\alpha}(x + L)), & -L < x < -a, \\ B_6 \cos(\widehat{\beta} x) + B_7 \sin(\widehat{\beta} x), & |x| < a, \\ B_8 \cosh(\widehat{\alpha}(x - L)), & a < x < L. \end{cases} \tag{3.4.19}$$

Again, the application of the continuity and boundary conditions (5.2.4) to the system (3.4.19), leads to a system of four homogenous equations of the type

$$F_3 \begin{pmatrix} B_5 \\ B_6 \\ B_7 \\ B_8 \end{pmatrix} = 0, \tag{3.4.20}$$

where the coefficient matrix, F_3, is given by

$$F_3 = \begin{bmatrix} \cosh\left[\widehat{\alpha}(L-a)\right] & -\cos\widehat{\beta}a) & \sin(\widehat{\beta}a) & 0 \\ \widehat{\alpha}\sinh\left[\widehat{\alpha}(L-a)\right] & -\widehat{\beta}\sin(\widehat{\beta}a) & -\widehat{\beta}\cos(\widehat{\beta}a) & 0 \\ 0 & \cos(\widehat{\beta}a) & \sin(\widehat{\beta}a) & \cosh\left[\widehat{\alpha}(a-L)\right] \\ 0 & -\widehat{\beta}\sin(\widehat{\beta}a) & \widehat{\beta}\cos(\widehat{\beta}a) & \widehat{\alpha}\sinh\left[\widehat{\alpha}(a-L)\right] \end{bmatrix}. \quad (3.4.21)$$

Again, the "discrete" spectrum of the uniform solution $\widetilde{\phi} = 0$ is then given by the roots of the condition

$$\det(\mathrm{F}_3) = 0. \quad (3.4.22)$$

An implicit plot of the zeros of the expression (3.4.22), i.e., the "discrete" spectrum of the stationary solution $\widetilde{\phi} = 0$ in the (a, E)-plane, for $L = 1$ is shown in the bottom panel of Fig. 3.1.

It can be observed from Fig. 3.1 that for a given L, there is a critical a above which the lowest E becomes positive, i.e., the solution $\widetilde{\phi} = 0$ becomes unstable. In the following, we denote such a critical a by $a_{c,0}$. For $L = 1$, it is found that $a_{c,0} \approx 0.46$. Similarly for $L = 2$ and $L = 3$, we respectively obtain $a_{c,0} \approx 0.7$ and $a_{c,0} \approx 0.78$. As L increases, $a_{c,0}$ will asymptotically approach $\pi/4$. This can be shown by assuming L large, substituting $E = 0$ into (3.4.22) and solving for $a_{c,0}$. This agrees with the critical facet length in the infinite domain calculated in Section 2.4.1.2. This is shown by the lower horizontal dashed line in Fig. 3.3.

3.4.2.3 Relation between the length of the junction L and $a_{c,0}$

In the following, we express the critical facet length $a_{c,0}$, as a function of the length L in the case where L is large. As we observed from the "discrete" spectrum (see the lower panel in Fig. 3.1), that the critical value $a_{c,0}$ is the point where the lowest eigenvalue becomes zero, that is, at $a = a_{c,0}$ the system has a minimum energy. This minimum energy corresponds to the fundamental even state of the ground state solution (3.4.19), see for example, Liboff [98].

We substitute $E = B_7 = 0$, and $a = a_{c,0}$into (3.4.19), apply the continuity condition at the point $x = -a_{c,0}$ and solve for B_5 to obtain

$$B_5 = \frac{B_6\cosh(a_{c,0})}{\cos(L - a_{c,0})}. \quad (3.4.23)$$

Similarly, by applying the continuity condition at $x = a_{c,0}$, we find that $B_8 = B_5$.

Now, substituting values into Eq. (3.4.22), using trigonometric and hyperbolic identities, and solving for $a_{c,0}$, we observe that $a_{c,0}$ and L are related by the smallest positive root of the implicit relation

$$\cot(a_{c,0}) \tanh(L - a_{c,0}) = 1. \tag{3.4.24}$$

This equation implicitly relates the critical zero facet length, $a_{c,0}$, to the length L of the junction. This relation is graphically expressed by the lower bold line in Fig. 3.3. Above this line the uniform solution $\widetilde{\phi} = 0$ becomes unstable.

3.4.2.4 The case when the length of the junction is small

Next, we assume that the length of the junction is small, and Taylor expand Eq. (3.4.24), it is easy to verify that the coefficients of the first and third order terms are respectively given by $1/2$ and $-1/24$. In other words, for small L, the smallest positive root of Eq. (3.4.24) can be approximated by

$$a_{c,0} = \frac{L}{2} - \frac{1}{24}L^3 + \mathcal{O}(L^5). \tag{3.4.25}$$

This gives an approximation to the relation between $a_{c,0}$ and L, for a small L. The relations given by Eqs. (3.4.24) and (3.4.25) are compared in Fig. 3.3. We note that for a small L, the approximation (3.4.25) well approximates the relation (3.4.24).

3.4.3 Linear stability of the uniform π solution

To discuss the linear stability of $\widetilde{\phi} = \pi$, we first consider the so-called "continuous" spectrum.

3.4.3.1 The "continuous" spectrum

Following the same steps we used in the stability analysis of the constant zero background solution, one can find that the bounded solution V of the eigenvalue problem (3.4.2) that corresponds to the "continuous" spectrum is given by

$$V(x) = \begin{cases} B_9 \cos(\widehat{\beta}(x + L)), & (-L < x < -a), \\ B_{10} \cos(\widehat{\zeta}x) + B_{11} \sin(\widehat{\zeta}x), & (|x| < a), \\ B_{12} \cos(\widehat{\beta}(x - L)), & (a < x < L). \end{cases} \tag{3.4.26}$$

By the application of the continuity conditions (5.2.4), we arrive at a system, given in matrix form by

$$F_4 \begin{pmatrix} B_9 \\ B_{10} \\ B_{11} \\ B_{12} \end{pmatrix} = 0, \tag{3.4.27}$$

with B_i integration constants and F_4, the coefficient matrix, given by

$$F_4 = \begin{bmatrix} \cos(\widehat{\beta}(L-a)) & -\cos(\widehat{\zeta}a) & \sin(\widehat{\zeta}a) & 0 \\ \widehat{\beta}\sin(\widehat{\beta}(L-a)) & -\widehat{\zeta}\sin(\widehat{\zeta}a) & -\widehat{\zeta}\cos(\widehat{\zeta}a) & 0 \\ 0 & \cos(\widehat{\zeta}a) & \sin(\widehat{\zeta}a) & -\cos(\widehat{\beta}(a-L)) \\ 0 & -\widehat{\zeta}\sin(\widehat{\zeta}a) & \widehat{\beta}\sin(\widehat{\beta}a) & -\widehat{\beta}\sin(\widehat{\beta}(a-L)) \end{bmatrix}. \tag{3.4.28}$$

One then finds that the ”continuous” spectrum is given by the zero of

$$\det(F_4) = 0. \tag{3.4.29}$$

A plot of the "continuous" spectrum in the (E, a)-plane is shown in the upper panel of Fig. 3.2 , from which it is clear that the continuous spectrum also only consists of stable eigenvalues.

3.4.3.2 The ”discrete” spectrum

To find the "discrete" spectrum of the uniform solution $\widetilde{\phi} = \pi$, we seek a solution, V, of the eigenvalue problem (3.4.2), which is bounded in region II[3] and decaying in regions I and III. After simple manipulation, it is easy to show that V is given by

$$V(x) = \begin{cases} B_{13}\cos(\widehat{\beta}(x+L)), & (-L < x < -a), \\ B_{14}\cosh(\widehat{\alpha}x) + B_{15}\sinh(\widehat{\alpha}x), & (|x| < a), \\ B_{16}\cos(\widehat{\beta}(x-L)), & (a < x < L), \end{cases} \tag{3.4.30}$$

where B_i are to be determined and $\widehat{\alpha}$, $\widehat{\beta}$ being respectively given by Eqs. (2.4.8) and (2.4.12) (see Chapter 2).

Due to the boundary conditions (5.2.4), we again obtain a system of four homogenous equations

$$F_5 \begin{pmatrix} B_{13} \\ B_{14} \\ B_{15} \\ B_{16} \end{pmatrix} = 0, \tag{3.4.31}$$

[3]See also Section 2.4.1.2

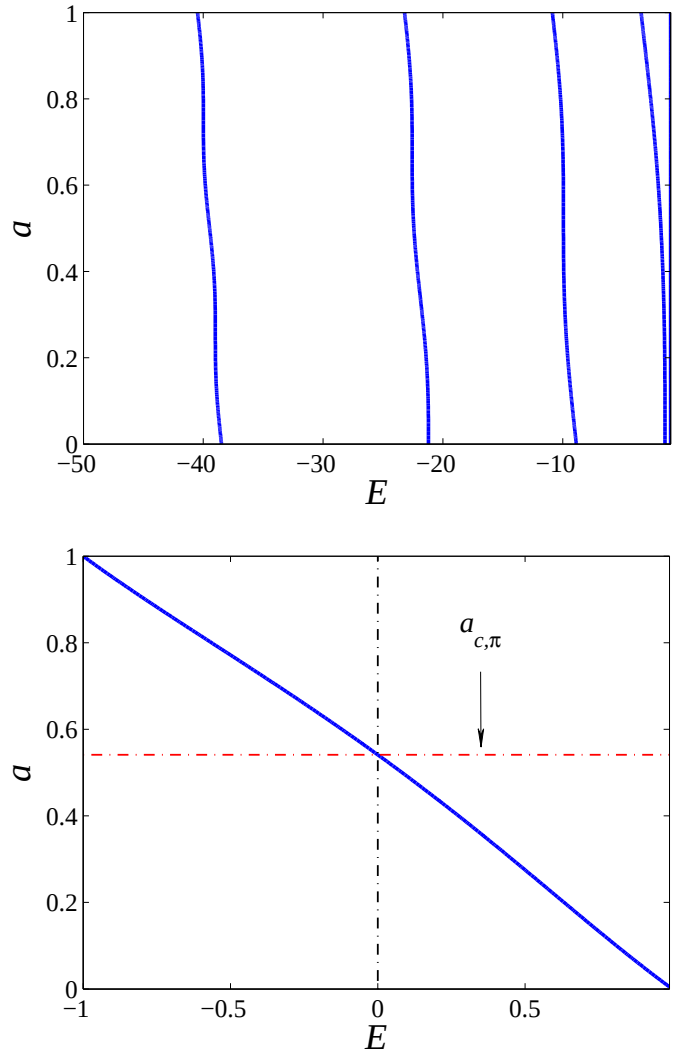

Figure 3.2: Plot of the "continuous" spectrum (top) and discrete spectrum (bottom) of the uniform $\widetilde{\phi} = \pi$ solution as a function of half of the $\pi-$ junction length a for $L = 1$.

with a coefficient matrix F_5, given by

$$F_5 = \begin{bmatrix} \cos(\widehat{\beta}(L-a)) & -\cosh\widehat{\alpha}a & \sinh(\widehat{\alpha}a) & 0 \\ \widehat{\beta}\sin(\widehat{\beta}(L-a)) & \widehat{\alpha}\sinh(\widehat{\alpha}a) & -\widehat{\alpha}\cosh(\widehat{\alpha}a) & 0 \\ 0 & \cosh(\widehat{\alpha}a) & \sinh(\widehat{\alpha}a) & -\cos(\widehat{\beta}(a-L)) \\ 0 & \widehat{\alpha}\sinh(\widehat{\alpha}a) & \widehat{\alpha}\cosh(\widehat{\alpha}a) & \widehat{\beta}\sin\widehat{\beta}(a-L) \end{bmatrix}. \quad (3.4.32)$$

A nontrivial solution of the system (3.4.31) exists if and only if

$$\det(F_5) = 0. \quad (3.4.33)$$

The bottom panel of Figure 3.2 shows the plot of the zeros of (3.4.33) in the (E, a)-plane, i.e., the "discrete" spectrum of $\widetilde{\phi} = \pi$, where we have taken $L = 1$. We observe that

for a close to zero, the spectral parameter $E > 0$, i.e., $\widetilde{\phi} = \pi$ is unstable. Yet, there is a critical value of a above which E becomes negative and the uniform solution π becomes stable. We denote this critical value of the facet length by $a_{c,\pi}$, which for $L = 1$ is approximately equal to 0.54.

This is one of the main differences between the problems of an infinite and a finite domain 0-π-0 long Josephson junctions. In Chapter 2, we have shown that the uniform solution $\widetilde{\phi} = \pi$ is unstable everywhere, while in the present case, one can have a region of stability of the constant π-background.

In the following, we derive expressions relating the critical π-facet length and the length the π-junction, considering large and small values of L.

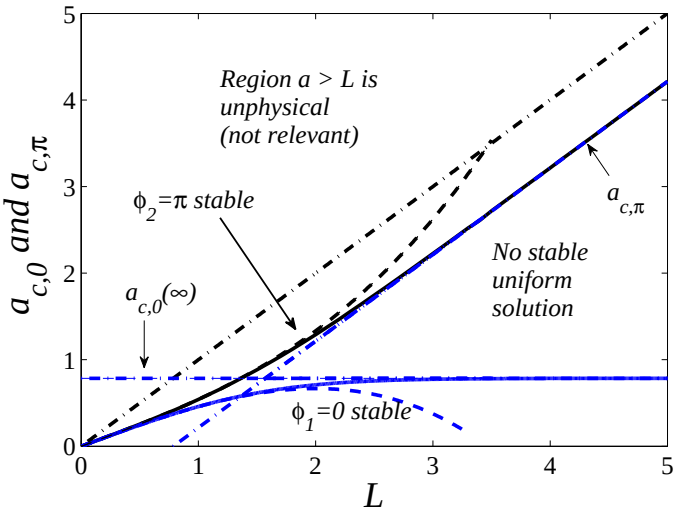

Figure 3.3: Instability region of the constant solutions $\widetilde{\phi} = 0$ and $\widetilde{\phi} = \pi$. Solid boundary curves are given by Eqs. (3.4.24) and (3.4.35). Dashed lines are analytical approximations given by (3.4.25) and (3.4.36). The lowest horizontal dashed-dotted line denotes the critical facet length $a_c, 0$ in the limit $L \to \infty$, while the inclined (blue) dashed-dotted represents the critical π-facet length (3.4.41) in the the limit $L \gg 1$.

3.4.3.3 The critical facet length $a_{c,\pi}$ as a function of the length of the π-junction

As discussed in the case of the linear stability of $\widetilde{\phi} = 0$, the first even mode of ground state solution (3.4.30) can be found by introducing $E = B_{15} = 0$, $a = a_{c,\pi}$, and applying the continuity condition at $x = \pm a_{c,\pi}$, we find that

$$B_{13} = \frac{A_{24}\cosh(a_{c,\pi})}{\cos(L - a_{c,\pi})}, \quad \text{and} \quad B_{13} = B_{16}. \tag{3.4.34}$$

As a result, the system (3.4.30) gives an implicit relation between $a_{c,\pi}$ and L as

$$\coth(a_{c,\pi}) \tan(L - a_{c,\pi}) = 1, \tag{3.4.35}$$

which gives the boundary of the stability region of the uniform solution $\widetilde{\phi} = \pi$. The plot of the relation (3.4.35) is presented by the upper bold line in Fig. 3.3.

3.4.3.4 Relation between $a_{c,\pi}$ and L for a small L

Now, we find an explicit relation between the critical π-facet length and the length of the π-junction by considering L small enough.

A Taylor series expansion of the relation (3.4.35) about $L = 0$ gives

$$a_{c,\pi} = \frac{L}{2} + \frac{1}{24}L^3 + \mathcal{O}(L^5). \tag{3.4.36}$$

The relation (3.4.36) of the π critical facet length in terms of increasing L, is depicted by the upper dashed line in Fig. 3.3. We observe that when L is close to zero, the relation (3.4.36) well approximates the expression (3.4.35).

3.4.3.5 Relation between $a_{c,\pi}$ and L in case of $L \gg 1$

Next, we consider the case when $L \gg 1$ and find relation between the π facet length, $a_{c,\pi}$, as a function of the half length L of the junction. To do so, we introduce a new variable $\widetilde{x}$ by

$$\widetilde{x} = \begin{cases} -(x + L), & x < 0, \\ L - x, & x > 0, \end{cases} \tag{3.4.37}$$

For this transformation, the system given by Eqs. (3.3.5), (3.3.2) and (3.4.2) respectively, takes the form

$$\phi_{\widetilde{x}\widetilde{x}} = \sin\left[\widetilde{\phi} + \theta(L - \widetilde{x})\right] - \gamma, \quad -L \leq \widetilde{x} \leq L, \tag{3.4.38}$$

$$\theta(\widetilde{x}) = \begin{cases} \pi, & -L < \widetilde{x} < -L + a, \\ 0, & -L + a < \widetilde{x} < L - a, \\ \pi, & L - a < \widetilde{x} < L, \end{cases} \tag{3.4.39}$$

$$V_{\widetilde{x}\widetilde{x}} = \left\{E + \cos\left[\widetilde{\phi} + \theta(L - \widetilde{x})\right]\right\} V, \quad -L \leq \widetilde{x} \leq L. \tag{3.4.40}$$

In other word, using the transformation (3.4.37), the 0-π-0 junction becomes a π-0-π-junction. Applying the continuity and boundary conditions (3.4.3) to (3.4.40), the "discrete" spectrum of the background $\widetilde{\phi} = \pi$ becomes the ” discrete” spectrum of the

constant $\widetilde{\phi} = 0$ solution discussed in Section 3.4.2.2, where the critical facet length is $\pi/4$.

Thus we conclude that when $L \gg 1$, the critical facet length $a_{c,\pi}$, for the uniform π solution, in terms of $\widetilde{x}$ is $\pi/4$. Substituting values in Eq. (3.4.37), one obtains that the critical facet length $a_{c,\pi}$ in terms of the variable x is given by

$$a_{c,\pi} = L - \frac{\pi}{4}. \tag{3.4.41}$$

Eq. (3.4.41) shows that when L becomes sufficiently large, $a_{c,\pi}$ will asymptotically approach $L - \pi/4$. This asymptotical behavior of $a_{c,\pi}$ is shown by the upper dashed dotted line in Figure 3.3.

3.4.4 Combined instability region

From the above discussion, it is clear that, unlike the infinite 0π-0 long Josephson junction, for the finite domain problem, there is a stability window in terms of the facet length a, where both the uniform zero and π backgrounds are stable. The plots of Eqs. (3.4.24) and (3.4.35), in terms of the half length L, of the junction, give a boundary to the stability window of the two solutions. These boundaries are plotted in Fig. 3.3, where then there is a region in which *both* the stationary solutions of the sine-Gordon (3.3.5) are unstable. This instability region lies in the junction where $a_{c,0} < a < a_{c,\pi}$. The ground state solutions in this combined instability region will be nonconstant in space, as we show later in this chapter.

3.5 Symmetries of the stability diagrams

Comparing Figs. 3.1 and 3.2, it is easy to observe that they are the same by reflection with respect to the line $a = L/2 = 1/2$. That is, the stability of the uniform solution $\widetilde{\phi} = 0$ at the half facet length a is the same as the stability of the stationary π solution at the half facet length $(L - a)$.

Looking in particular at the profiles of the solutions (3.4.11), (3.4.19), (3.4.26) and (3.4.30) versus the spatial variable x, one observes that

$$\phi(-L) = \phi(L), \quad \phi_x(-L) = \phi_x(L). \tag{3.5.1}$$

In other words, for the above mentioned particular solutions, the Neumann boundary conditions (5.2.4) at $x = \pm L$ can be replaced by periodic boundary conditions (3.5.1).

It may also be noted that for the periodic boundary conditions (3.5.1), the governing sine-Gordon model (3.3.1) is symmetric by rotation, i.e., it has cyclic symmetry, and $\theta \to \theta + \pi$. Due to this fact, there exists a symmetry between properties of the static and uniform 0 and π solutions. Using this symmetry, one can also conclude that for any L, the critical facet lengths $a_{c,0}$ and $a_{c,\pi}$ are related through the equation

$$a_{c,\pi} = L - a_{c,0}. \tag{3.5.2}$$

Due to the similarity to a periodic system, our problem in the undriven case ($\gamma = 0$) is the same as that considered by Buzdin and Koshelev [110]. As a consequence, Eqs. (3.4.19) and (3.4.24) and hence Eqs. (3.4.30) and (3.4.35) above are the same as Eqs. (3) and (4) of [110].

Despite the similarity, finite and periodic junctions also have some fundamental differences. These include the fact that continuous spectrum is present in periodic junctions with a band gap structure, see for instance, Susanto et al. [111]. This issue is addressed in Chapter 5 of this thesis.

3.6 Nonuniform ground states in the instability region

In the following, we investigate the nonuniform ground states in the instability region, where the facet length a is close to one of the critical facet lengths $a_{c,0}$ or $a_{c,\pi}$ ($0 < a - a_{c,0} \ll 1, 0 < a_{c,\pi} - a \ll 1$). For these purposes, we use different methods.

First, we use the Lindstedt-Poincaré method that was applied to analyse the ground state solution in the infinite domain (see Section 2.5.3.1). The main drawback found in applying this approach to the finite domain problem, is that there exist no secular term in regions I and III, and hence, there is no way to stretch the spatial variable in these regions. Consequently, the approximations obtained by this approach does not well approximate the corresponding numerical calculations.

Second, we use a modified Lindstedt-Poincaré method, where we consider the problem in a phase space, and aim to determine equations of the trajectories. The method well approximates the nonuniform ground states in the undriven case, but involves long calculations in finding simple explicit expressions for the driven problem.

The third method we use is a Lagrangian approach, which requires less labour but only gives good approximations in a region that is close to the critical facet lengths $a_{c,0}$ and $a_{c,\pi}$. We investigate the ground state close to each of the critical facet lengths separately.

3.6.1 Ground state in the region $0 < a - a_{c,0} \ll 1$

To analyse the ground states in the small instability region, we first consider the case when a is close to $a_{c,0}$.

3.6.2 Lindstedt-Poincaré method

One immediate way to analyse the approximate nonuniform ground state solutions in the combined instability region is to use the method of infinite domain discussed in Section 2.5.3. When discussing the ground states in the instability region close to $a_{c,0}$ in Chapter 2, we calculated the bounded solution in region II using Poincaré-Lindstedt method and the solutions in regions I, III were exponentially decaying. By applying the same technique to the finite domain, we can approximate the nonuniform ground state in the instability region close to $a_{c,0}$. In the following we briefly summarize the calculations.

Assuming

$$\phi = B\widetilde{\phi}, \quad \text{where} \quad |B| \ll 1, \tag{3.6.1}$$

a small perturbation of the constant background $\widetilde{\phi}$, the solution $\widetilde{\phi}^{(1)}$ of the sine-Gordon equation (3.3.5), for the undriven case, in region I is of the form

$$\widetilde{\phi}^{(1)}(x) = A_0 e^{x} + B_0 e^{-x}, \tag{3.6.2}$$

with A_0 and B_0 being the constants of integration. This solution should satisfy the boundary condition $\widetilde{\phi}_x^{(1)}(-L) = 0$, in which case we obtain $A_0 = B_0 e^{2L}$, and hence (3.6.2) is simplified to

$$\widetilde{\phi}^{(1)}(x) = B_0 \left(e^{x+2L} + e^{-x} \right). \tag{3.6.3}$$

The approximate solution $\widetilde{\phi}^{(2)}$ in region II for the undriven case, under the assumption (3.6.1), is obtained from Eq. (2.5.28)

$$\widetilde{\phi}^{(2)} = \cos(\omega x). \tag{3.6.4}$$

Here ω is the same as given by Eq. (2.5.27). By applying the continuity conditions (5.2.4) to the first and second region approximate solutions given by Eqs. (3.6.3) and (3.6.4), one respectively obtains

$$B_0 \left(e^{2L} + e^{2a} \right) = e^{a} \cos(\omega a), \tag{3.6.5a}$$

$$B_0 \left(e^{2L} - e^{2a} \right) = e^{a} \omega \sin(\omega a), \tag{3.6.5b}$$

from which by division, one may write

$$\frac{e^{2L}+e^{2a}}{e^{2L}-e^{2a}} = \frac{1}{\omega}\cot(\omega a)\,. \tag{3.6.6}$$

Now by embedding $a = kL$ where $k > 1/2$, into (3.6.6), using the formal series expansion, assuming L small, and solving for B, we obtain

$$B = \pm 4\sqrt{1-\sqrt{1-\frac{1}{k}}}. \tag{3.6.7}$$

Substituting the value of B_0 from (3.6.6) into Eq. (3.6.3), it is easy to write

$$\widetilde{\phi}^{(1)}(x) = \frac{e^{x+2L}+e^{-x}}{e^{a}+e^{2L-a}}\cos(\omega a)\,. \tag{3.6.8}$$

Now, by the help of Eqs. (3.6.1) and (3.6.8), we find that the solution in region I at the boundary $x = -L$ has the form

$$\phi^{(1)}(-L) = \frac{B\cos(\omega a)}{\cosh(L-a)}. \tag{3.6.9}$$

Similarly, using Eq. (2.5.28), for the solution $\phi^{(2)}$ in region II, we obtain

$$\phi^{(2)}(0) = B, \tag{3.6.10}$$

where B is given by Eq. (3.6.7). If one plots the approximation to the Josephson phase given by (3.6.9) and (3.6.10) as a function of half length of the π-junction, it will be observed that these approximations do not *well* approximate the corresponding numerics (this comparison is not presented here). We reason that this approximation is poor due to the spatial variable x in the first and third regions not being stretched as in region II. Thus, we need to look for an alternative method which can give a good approximation to its numerical counterpart.

3.6.3 Modified Lindstedt-Poincaré method

Let ϕ_1 be the approximate solution of the model (3.3.5) in region I. A Taylor series expansion of (3.3.5), assuming ϕ_1 small, up to the leading order term gives

$$\phi_{1xx} - \phi_1 + \gamma = 0.$$

Solution of this expression, satisfying the condition $\phi_x(-L) = 0$ is of the form $\phi_1 = C_3\cosh(x+L)+\gamma$, where C_3 is an integration constant. However, here we shall consider higher-order correction terms. To do so, we consider two problems.

Assuming ϕ_1 small, a Taylor series expansion of Eq. (3.3.5) about ϕ_1, up to the third correction term, one may write

$$\phi_{1xx} - \phi_1 + \frac{\phi_1^3}{6} + \gamma = 0, \quad -L < x < -a. \tag{3.6.11}$$

The solution of (3.6.11), satisfying the boundary condition $\phi_x(-L) = 0$, is of the form

$$\phi_1(x) = C_3 \cosh\left[\omega(x+L)\right] + \gamma, \quad -L < x < -a, \tag{3.6.12}$$

where $C_3 \ll 1$, $\omega = 1 + \epsilon\omega_1 + \mathcal{O}(\epsilon^2)$, $\epsilon \ll 1$ is a perturbation parameter and ω_1 is a constant to be determined.

As we know the idea of the Lindstedt-Poincaré method is to stretch the x-axis, where one approximates the periodic solution over its one period. However Poincaré method is for oscillatory problems and the stretched ω_1 is determined by suppressing the secular terms, see section 2.5.3. Here, we have a solution which is not in terms of oscillatory (trigonometric) solutions but rather it is in terms of hyperbolic functions. Hence, there do no exist secular terms in the present case. Therefore, for finding ω_1, we need another method such that the elementary function is a good approximation to the given solution.

Secondly, we want the approximate solution to be an accurate approximation of trajectory in phase space (ϕ, ψ). That is, using the idea of phase-plane analysis, we define

$$\phi_{1x} = \psi_1 = C_3\omega \sinh\left[\omega(x+L)\right], \tag{3.6.13}$$

so that Eq. (3.6.11) gives

$$\psi_{1x} = \phi_1 + \frac{\phi_1^3}{6} - \gamma. \tag{3.6.14}$$

Using the chain rule of differentiation, from Eqs. (3.6.13) and (3.6.14), we obtain

$$\frac{d\phi_1}{d\psi_1} = \frac{\psi_1}{\phi_1 - \phi_1^3/6 - \gamma}.$$

This equation, upon separating variables and integration yields

$$\frac{{\psi_1}^2}{2} = \frac{{\phi_1}^2}{2} - \frac{{\phi_1}^4}{24} - \gamma\phi_1 + C_4, \tag{3.6.15}$$

where C_4 is a constant of integration. From Eqs. (3.6.12) and (3.6.13), we find that $\phi_1(-L) = C_3 + \gamma$ and $\psi_1(-L) = 0$. These conditions give

$$C_4 = \frac{(C_3+\gamma)^4}{24} - \frac{(C_3+\gamma)^2}{2} + \gamma\left(C_3+\gamma\right).$$

Next, we substitute the value of C_4, into (3.6.15) and simple algebra yields

$$\begin{aligned}\psi_1{}^2 - \phi_1^2 + C_3^2 \;+\; & \gamma^2 + 2C_3\gamma\cosh\left[\omega(x+L)\right] \\ &= \frac{1}{12}\Big\{C_3^4\left(1-\cosh^4\left[\omega(x+L)\right]\right) + 4C_3^3\gamma\left(1-\cosh^3\left[\omega(x+L)\right]\right) \\ &\quad +6C_3^2\gamma^2\left(1-\cosh^2\left[\omega(x+L)\right]\right) + 4\gamma^3\left(1-\cosh\left[\omega(x+L)\right]\right)\Big\}.\end{aligned} \tag{3.6.16}$$

By using Eqs. (3.6.12), (3.6.13) and the identity $\cosh^2(x) - \sinh^2(x) = 1$, after neglecting smaller terms, we rewrite the above equation as

$$\psi_1{}^2 - \phi_1^2 + C_3^2 + \gamma^2 + 2C_3\gamma\cosh\left[\omega(x+L)\right] = -2\epsilon\omega_1 C_3^2\sinh^2\left[\omega(x+L)\right]. \tag{3.6.17}$$

A comparison of (3.6.16) and (3.6.17) and simplification gives

$$\begin{aligned}\epsilon\omega_1 \;=\; & -\frac{1}{24}\Big\{C_3^2\left(1+\cosh^2\left[\omega(x+L)\right]\right) - 4C_3\gamma\Big(\cosh\left[\omega(x+L)\right] \\ & +\frac{1}{1+\cosh\left[\omega(x+L)\right]}\Big) - 6\gamma^2 - \frac{4\gamma^3}{C_3}\left(\frac{1}{1+\cosh\left[\omega(x+L)\right]}\right)\Big\}.\end{aligned}$$

However, the right hand side depends upon x and the left hand side does not. To remove the x-dependency, one simple way is to average the two two sides over the region I.

The average of expressions given by (3.6.16) and (3.6.17) is obtained by integrating the last equation over the region I and dividing the resultant by its length $(L-a)$. Converting the fractions into proper form in the last equation and using double angle identities, the required average is, then, given by

$$\begin{aligned}\epsilon\omega_1 = \quad & -\frac{1}{24(L-a)}\int_{-L}^{-a}\Big\{\frac{C_3^2}{2}\Big(3+\cosh\left[2\omega(x+L)\right]\Big) + 4C_3\gamma\cosh\left[\omega(x+L)\right] + 6\gamma^2 \\ & +\frac{4\gamma}{C_3}\left(\frac{C_3^2+\gamma^2}{1+\cosh\left[\omega(x+L)\right]}\right)\Big\}dx.\end{aligned}$$

Evaluation of the above integral yields

$$\begin{aligned}\epsilon\omega_1 = \quad & -\frac{1}{24(L-a)}\Big\{\frac{C_3^2}{2}\Big(3\,(L-a) + \frac{\sinh\left[2\omega(L-a)\right]}{2\omega}\Big) + \frac{4C_3\gamma}{\omega}\sinh\left[\omega(L-a)\right] \\ & +6\gamma^2(L-a) + \frac{4\gamma}{C_3}\left(C_3^2+\gamma^2\right)\tanh\left[\frac{\omega}{2}(L-a)\right].\end{aligned} \tag{3.6.18}$$

Since $\omega = 1 + \epsilon\omega_1 + \mathcal{O}(\epsilon^2)$, the last equation is valid only for the scaling

$$a = \mathcal{O}(1), \quad L = \mathcal{O}(1), \quad \gamma = \sqrt{\epsilon}\widetilde{\gamma}, \quad C_3 = \sqrt{\epsilon}\widetilde{C}_3, \quad \widetilde{\gamma} = \mathcal{O}(1), \quad \widetilde{C}_3 = \mathcal{O}(1). \tag{3.6.19}$$

Using this scaling and a Taylor series expansion about $\epsilon = 0$, from Eq. (3.6.20), up to the leading order in ϵ, one obtains

$$\begin{aligned}\omega_1 &= -\frac{1}{24(L-a)}\left\{\frac{\widetilde{C}_3^2}{2}\left(3\,(L-a)+\frac{\sinh\left[2(L-a)\right]}{2}\right)+4\widetilde{C}_3\widetilde{\gamma}\sinh\left[(L-a)\right]\right.\\ &\left.+6\widetilde{\gamma}^2(L-a)+\frac{4\widetilde{\gamma}}{\widetilde{C}_3}\left(\widetilde{C}_3^2+\widetilde{\gamma}^2\right)\tanh\left[\frac{L-a}{2}\right]\right\},\end{aligned} \tag{3.6.20}$$

and the value of ω can be found accordingly.

Now, assume ϕ_2 to be the solution of the equation (3.3.5) in the region II. At leading order we have

$$\phi_{2xx}+\phi_2=0, \quad \text{so that} \quad \phi_2=\cos(x).$$

Substituting for ϕ_2 and using Taylor series expansion about $\phi_2 = 0$, we obtain the higher order approximation

$$\phi_{2xx}+\phi_2-\frac{\phi_2^3}{6}+\gamma=0. \tag{3.6.21}$$

Let us propose a general solution of this equation in the form

$$\phi_2=C_5\cos\left[\widetilde{\omega}x\right]-\gamma, \tag{3.6.22}$$

where C_5 is a constant to be determined later on and $\widetilde{\omega}=1+\epsilon\widetilde{\omega}_1+\mathcal{O}(\epsilon^2)$, with $\epsilon \ll 1$.

Following the method discussed above, we define $\phi_{2x}=\psi_2$, and find that

$$\begin{aligned}\psi_2^2+\phi_2^2-C_5^2-\gamma^2+2C_5\gamma\cos\left[\widetilde{\omega}x\right] &= \frac{1}{12}\left\{C_5^4\left(\cos^4\left[\widetilde{\omega}x\right]-1\right)-4C_5^3\gamma\left(\cos^3\left[\widetilde{\omega}x\right]-1\right)\right.\\ &+\left.6C_5^2\gamma^2\left(\cos^2\left[\widetilde{\omega}x\right]-1\right)-4C_5\gamma^3\left(\cos\left[\widetilde{\omega}x\right]-1\right)\right\},\end{aligned} \tag{3.6.23a}$$

$$\psi_2^2+\phi_2^2-C_5^2-\gamma^2+2C_5\gamma\cos\left[\widetilde{\omega}x\right] = 2\epsilon\omega_1C_5^2\sin^2\left[\widetilde{\omega}x\right]. \tag{3.6.23b}$$

Comparing Eq. (3.6.23a) with Eq. (3.6.23b), using trigonometric identities, and averaging the resultant equation over the interval II, we obtain

$$\epsilon\widetilde{\omega}_1=-\frac{1}{48a}\int_{-a}^{a}\left\{\frac{C_5^2}{2}\left(3+\cos\left[2\widetilde{\omega}x\right]\right)+4C_5\gamma\cos\left[\widetilde{\omega}x\right]-6\gamma^2+\frac{4\gamma}{C_5}\left(\frac{C_5^2+\gamma^2}{1+\cos\left[\widetilde{\omega}x\right]}\right)\right\}dx.$$

Evaluating the integral and using the same scaling as above, with $C_5 = \sqrt{\epsilon}\widetilde{C}_5$, by formal series expansion, up to the leading order in ϵ, it is easy to write

$$\widetilde{\omega}_1=-\frac{1}{48a}\left\{\frac{\widetilde{C}_5^2}{2}\left(6a+\sin(2a)\right)+8\widetilde{C}_5^2\widetilde{\gamma}\sin(a)-12a\widetilde{\gamma}^2+\frac{8\widetilde{\gamma}}{\widetilde{C}_5}\tan\left(\frac{a}{2}\right)\right\}. \tag{3.6.24}$$

Accordingly, we can find the expression of $\widetilde{\omega}$. Thus the modified Lindstedt-Poincaré method has stretched the spatial variable x in the region II.

Substituting the values of ω_1 and $\widetilde{\omega}_1$ into Eqs. (3.6.12) and (3.6.22) respectively and using the continuity conditions $\phi_1(-a) = \phi_2(-a)$ and $\phi_{1,x}(-a) = \phi_{2,x}(-a)$, we obtain

$$C_3 \cosh\left[\omega(L-a)\right] = C_5 \cos\left[\widetilde{\omega}a\right] - 2\gamma,, \tag{3.6.25a}$$

$$C_3\omega \sinh\left[\omega(L-a)\right] = C_5\widetilde{\omega} \sin\left[\widetilde{\omega}a\right]. \tag{3.6.25b}$$

From Eqs. (3.6.25a) and (3.6.25b), it is straight forward to write

$$\frac{1}{\omega}\coth\left[\omega(L-a)\right] = \frac{C_5\cos(\widetilde{\omega}a) - 2\gamma}{C_5\widetilde{\omega}\sin(\widetilde{\omega}a)}. \tag{3.6.26}$$

Taking the leading order terms in ω and $\widetilde{\omega}$, Eq. (3.6.25a), then gives

$$C_3 = \frac{C_5\cos(a) - 2\gamma}{\cosh(L-a)}. \tag{3.6.27}$$

3.6.3.1 Nonuniform ground states in the un-driven case

First we consider the case when the applied bias current (γ) is zero. Substituting C_3 into Eq. (3.6.26) and using Taylor series expansion assuming C_5 small, after simplification, one may obtains

$$\left[\cos(a)\tanh(L-a) - \sin(a)\right]C_5 + \left[G_1\left(\cosh(L-a) + \frac{\sinh(L-a)}{L-a}\right) + \frac{G_2G_3}{48}\right]C_5^3 = 0, \tag{3.6.28}$$

where

$$G_1 = -\frac{\cos^2(a)\left(6(L-a) + \sinh\left[2(L-a)\right]\right)}{96\cosh^3(L-a)},\ G_2 = 2a + \sin(2a),\ G_3 = \cos(a) + \frac{\sin(a)}{a}.$$

Solving (3.6.28), we obtain

$$C_5 = 0, \pm\sqrt{\frac{\sin(a) - \cos(a)\tanh(L-a)}{G_1\left[\cosh(L-a) + \sinh(L-a)/(L-a)\right] + G_2G_3/48}}. \tag{3.6.29}$$

Thus, our nonuniform ground state solution in the instability region $0 < a - a_{c,0} \ll 1$, in the undriven case, is given by

$$\phi(x) = \begin{cases} C_3\cosh\left[\omega\left(x+L\right)\right], & -L < x < -a, \\ C_5\cos\left(\widetilde{\omega}x\right), & |x| < a, \\ C_6\cosh\left[\omega\left(x-L\right)\right], & a < x < L, \end{cases} \tag{3.6.30}$$

where C_3 and C_5 are respectively given by Eqs. (3.6.27) and (3.6.29). The constant C_6 can be found by applying the continuity conditions $\phi(a^-) = \phi(a^+)$, $\phi_x(a^-) = \phi_x(a^+)$ and considering the leading order terms in $\widetilde{\omega}$ and ω to obtain

$$C_6 = \frac{C_5 \cos(a) - 2\gamma}{\cosh(L-a)}. \tag{3.6.31}$$

The approximation to the Josephson phase given by Eq. (3.6.30) at the points $x = -L$ and $x = 0$ are displayed by the lower dashed-dotted lines in Fig. 3.4. We observe that the numerical simulations (solid lines) are well approximated by the analytical work (3.6.30) when a is close to $a_{c,0}$.

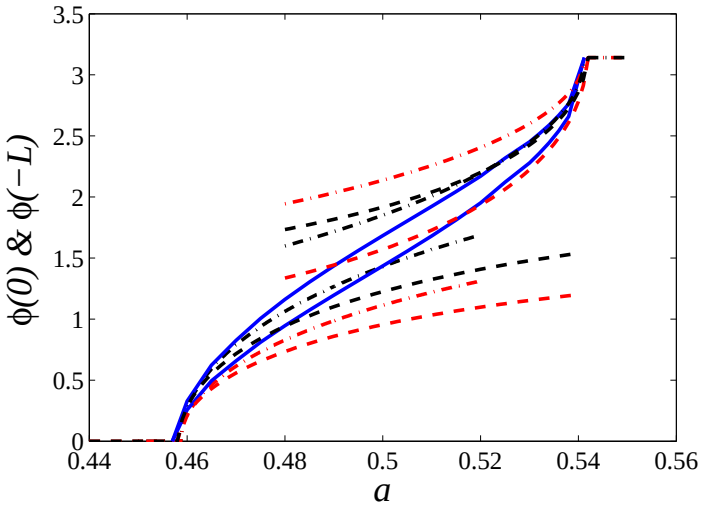

Figure 3.4: Plot of $\phi(0)$ and $\phi(L)$ of the nonuniform ground state obtained from numerical calculations (solid lines) as a function of the facet length a. The lower (upper) dashed dotted lines represent our analytical approximation given by the systems (3.6.30) and (3.6.34) respectively. The dash lines represent the approximation given by (3.6.39) and (3.7.7).

3.6.3.2 Nonuniform ground state in the driven case

Now we consider the case when the forcing term γ is not zero. Introducing the scaling (3.6.19) with

$$C_5 = \sqrt{\epsilon}\widetilde{C}_5, \quad \text{where} \quad \widetilde{C}_5 = \mathcal{O}(1), \tag{3.6.32}$$

and using the formal series expansion about ϵ, we obtain

$$\widetilde{C}_5 \left\{ \left(\frac{e^{2L} + e^{2a}}{e^{2L} - e^{2a}} \right) - \cos(a) \right\} + 2\gamma = 0. \tag{3.6.33}$$

This equation is linear in $\widetilde{C}_5$, whilst one would expect a cubic equation in $\widetilde{C}_5$, as we obtained in the case of infinite domain case (see Section 2.5.3.3). Due to complications in choosing the proper scaling and long calculations, our perturbation is not preferable. Thus we investigate the ground state solution using calculus of variation, which is easy and gives us a close approximation as will be discussed in Section 3.6.5.

3.6.4 Nonuniform state in the region $0 < |a_{c,\pi} - a| \ll 1$

Using method discussed in Section 3.6.1, it is easy to show that the dynamics of the nonuniform ground state in the instability region $0 < |a_{c,\pi} - a| \ll 1$ is given by

$$\phi(x) = \pi + \begin{cases} C_7 \cos\left[(1+\epsilon\omega_2)\,(x+L)\right] - \gamma, & -L < x < -a, \\ C_8 \cosh\left((1+\epsilon\widetilde{\omega}_2)x\right) + \gamma, & |x| < a, \\ C_9 \cos\left[(1+\epsilon\omega_2)\,(x-L)\right] - \gamma, & a < x < L. \end{cases} \tag{3.6.34}$$

The terms used here are defined as follows

$$\begin{aligned} \omega_2 &= \frac{-1}{24(L-a)}\left\{\frac{\widetilde{C}_7^2}{4}\left[6(L-a) + \sin\left[2(L-a)\right]\right] - 4\widetilde{C}_7\widetilde{\gamma}\sin(L-a) + 6\widetilde{\gamma}^2(L-a)\right. \\ &\quad \left. -\frac{4\widetilde{\gamma}}{C_7}\left(\widetilde{C}_7^2 + \widetilde{\gamma}^2\right)\tan\left(\frac{L-a}{2}\right)\right\}, \\ \widetilde{\omega}_2 &= \frac{-1}{48a}\left\{\frac{\widetilde{C}_8^2}{2}\left[6a + \sinh(a)\right] + \widetilde{C}_8\sinh(a) + 12\widetilde{\gamma}^2 a + \frac{8\widetilde{\gamma}}{\widetilde{C}_8}\left(\widetilde{C}_8^2 + \widetilde{\gamma}^2\right)\tanh\left(\frac{a}{2}\right)\right\}, \\ C_7 &= \frac{C_8\cosh(a) + 2\gamma}{\cos(L-a)},\ a = \mathcal{O}(1),\ L = \mathcal{O}(1),\ C_7 = \sqrt{\epsilon}\widetilde{C}_7,\ C_8 = \sqrt{\epsilon}\widetilde{C}_8,\ \gamma = \sqrt{\epsilon}\widetilde{\gamma}, \end{aligned}$$

and C_8 (in the undriven case) is given by

$$C_8 = 0,\ \pm\sqrt{\frac{\cos(a) - \sinh(a)\cot(L-a)}{G_4\left[\sinh(a)/\sin^2(L-a) + \cosh(a)/(L-a)\right] - G_5\left(G_6\cot(L-a) - \cosh(a)\right)}},$$

such that

$$G_4 = \frac{\cosh^2(a)\left[6(L-a) + \sinh\left[2(L-a)\right]\right]}{96\cos^2(L-a)},\ G_5 = \frac{6a + \sinh(a)}{96},\ G_6 = \cosh(a) + \frac{\sinh(a)}{a}.$$

The approximation to the Josephson phase given by Eqs. (3.6.30) and (3.6.34) are presented by the upper dashed-dotted lines in Fig. 3.4, where we have displayed only the case $\phi > 0$.

3.6.5 Lagrangian approach to the nonuniform ground state

Let us assume $V(x)$ is the first even solution of the eigenvalue problem (3.4.2) and $B(t) \ll 1$. Then $B(t)V(x)$ represents a small perturbation of the uniform solution $\widetilde{\phi}$. In

other words, to investigate the nonuniform ground state solution in the small instability region of a constant solution $\widetilde{\phi}$, we use the following ansatz

$$\phi(x,t) = \widetilde{\phi} + B(t)V(x). \tag{3.6.35}$$

3.6.5.1 The case of the uniform solution $\widetilde{\phi} = 0$

As we have calculated in Section 3.4.2.2, the first even solution $V(x)$ of the eigenvalue problem (3.4.2) about the zero constant background solution, satisfying the boundary conditions $V_x(\pm L) = 0$, has the form

$$V(x) = \begin{cases} D_1 \cosh\left[\widehat{\alpha}(x+L)\right], & (-L < x < -a), \\ D_2 \cos\left[\widehat{\beta}x\right], & (|x| < a), \\ D_3 \cosh\left[\widehat{\alpha}(x-L)\right], & (a < x < L), \end{cases} \tag{3.6.36}$$

with D_i being integration constants and $\widehat{\alpha}$, $\widehat{\beta}$ respectively given by Eqs. (2.4.8) and (2.4.12). The continuity conditions $V(-a^-) = V(-a^+)$, $V_x(-a^-) = V_x(-a^+)$, when applied to the system (3.6.39), respectively give

$$D_1 \cosh\left[\widehat{\alpha}(L-a)\right] - D_2 \cos\left[\widehat{\beta}a\right] = 0, \tag{3.6.37a}$$

$$D_1\widehat{\alpha} \sinh\left[\widehat{\alpha}(L-a)\right] + D_2\widehat{\beta} \sin\left[\widehat{\beta}a\right] = 0. \tag{3.6.37b}$$

Our region of interest starts from the point where the facet length a takes its critical value $a_{c,0}$. In such situation, the spectral parameter E becomes zero (see the lower panel of Fig. 3.1), and $a_{c,0}$ is given by Eq. (3.4.25). To find a nontrivial solution of Eqs. (3.6.37), we can fix one of the integration constants and find the second one. For instance, by setting $D_2 = 1$ and replacing a with $a_{c,0}$ into Eq. (3.6.37a), we find that

$$D_1 = \frac{\cos(a_{c,0})}{\cosh\left(L - a_{c,0}\right)}. \tag{3.6.38}$$

A similar trick can be used to calculate the constant D_3, where we found $D_3 = D_1$. Plugging values of the constants into the system (3.6.39), the ansatz (3.6.35) gives

$$\phi(x,t) = B(t) \begin{cases} \dfrac{\cos(a_{c,0})}{\cosh\left(L - a_{c,0}\right)} \cosh\left(x + L\right), & (a < |x| < L), \\ \cos\left(x\right), & (|x| < a). \end{cases} \tag{3.6.39}$$

Next, we substitute this value of ϕ (3.6.39) into the Lagrangian (3.3.4), which for the forced time-independent sine-Gordon equation, takes the form

$$\mathcal{L} = \int_{-L}^{L} \left[\frac{1}{2}\phi_t^2 - \frac{1}{2}\phi_x^2 - 1 + \cos(\phi + \theta) - \gamma\phi\right] dx. \tag{3.6.40}$$

Substituting the ansatz (3.6.39) into the Lagrangian (3.6.40), writing

$$a = \frac{L}{2} - kL^3, \tag{3.6.41}$$

where $k < 1/24$, and expanding about small L yields

$$\mathcal{L} = \left(L - \frac{L^3}{4}\right) B_t^2 - U. \tag{3.6.42}$$

Here the subscript represents a derivative with respect to t. The expression

$$U = 2L\left(1 - 2L^2k\right) + \frac{\gamma L}{4}\left(8 - L^2\right) B + \frac{L^3}{12}\left(24k - 1\right) B^2 - \frac{L^3}{36}\left(6k - 1\right) B^4, \tag{3.6.43}$$

in (3.6.42) represents the potential energy of the system and k is given by Eq. (3.6.41). This value of the potential energy, for the uniform solution $\widetilde{\phi} = 0$, is obtained by inserting (3.6.35) into

$$U = \int_{-L}^{L} \left[\frac{1}{2}\phi_x^2 + 1 - \cos(\phi + \theta) + \gamma\phi\right] dx,$$

and Taylor expanding the resulting expression about $|B(t)| \ll 1$.

Substituting the value of the Lagrangian $\mathcal{L}$, from Eq. (3.6.42), into the Euler-Lagrange equation (see, for example, Arfken et al. [112])

$$\frac{\partial \mathcal{L}}{\partial B} - \frac{d}{dt}\left(\frac{\partial \mathcal{L}}{\partial B_t}\right) = 0, \tag{3.6.44}$$

we obtain

$$B_{tt} = \frac{2U_B}{L\left(4 - L^2\right)}. \tag{3.6.45}$$

If B_0 denotes the time-independent solution of the Euler-Lagrange equation (3.6.45), then it is straightforward to show that B_0 is then given by the cubic equation $U_B = 0$, i.e.,

$$f(B_0) = 4L^2\left(6k - 1\right) B_0^3 + 6L^2\left(1 - 24k\right) B_0 + 9\left(L^2 - 8\right)\gamma = 0. \tag{3.6.46}$$

3.6.6 Nonuniform ground state solution in the absence of external current

Let us first consider the limiting solutions in the combined instability region in the undriven case. We notice that when there is no external current applied to the Josephson junction, i.e., when $\gamma = 0$, the roots of the Eq. (3.6.46) are given by

$$B_0^{(1,2)} = \pm\sqrt{\frac{3\left(24k - 1\right)}{2\left(6k - 1\right)}}, \quad B_0^{(3)} = 0. \tag{3.6.47}$$

Replacing $B(t)$ in Eq. (3.6.39) by one of the nonzero roots given by Eq. (3.6.47), we plot the profile of $\phi(x,t)$ at the points $x = -L$ and $x = 0$, in terms of the facet length a in

Fig. 3.4 for $\gamma = 0$ and $L = 1$. This shown by the lower dashed lines in the figure. It is noted that for $a < a_{c,0}$, both $\phi(-L)$ and $\phi(0)$ are zero, showing the stability of the uniform zero solution. A nonuniform ground state bifurcates from the point $a = a_{c,0}$. We also observe that when the facet length a in the instability region becomes large, the Josephson phase satisfies

$$|\phi(-L)| = \pi, \quad |\phi(0)| = \pi, \tag{3.6.48}$$

which means that the two nonzero roots of B_0 represents a pair of semifluxons.

To check our analytical results, we compare the approximation to the Josephson phase given by the system (3.6.39) with the corresponding numerical calculations. For a close to $a_{c,0}$, one can observe the numerical solutions are well approximated by the corresponding analytical approximation.

3.6.7 Nonuniform ground state solution in the presence of external current

Next, we study the influence of an applied bias current on the existence and stability of the nonuniform ground state.

For a general nonzero value of the applied bias current, γ, we solve the cubic equation (3.6.46) by the method [102]. It can be verified that with

$$\Delta = \sqrt{\frac{1-24k}{2\,(1-6k)}}, \quad h = -4L^2\,(1-24k)\,\Delta, \quad y_N = 9\gamma\left(L^2-8\right), \quad \Theta = \frac{1}{3}\arccos\left(-\frac{y_n}{h}\right), \tag{3.6.49}$$

the three roots are given by

$$B_0^{(n)} = 2\Delta\cos\left[\Theta + 2\,(n-1)\,\frac{\pi}{3}\right], \quad n = 1,2,3. \tag{3.6.50}$$

By substituting the roots (3.6.50) into the system (3.6.39), one can plot the profile of the Josephson phase $\phi(0)$ as a function of the applied bias current γ. This is shown by the lower dashed lines in Fig. 3.5, where we have taken $L = 1$ and $a = 0.495$. The analytical work is compared with the corresponding numerical solution (solid line), which for small γ are close to each other. By studying further the three roots (3.6.50), one finds that they do not persist for all γ. If γ is decreased away from zero, then there is a (negative) critical value of the bias current at which the $B_0^{(2)}$ collides with $B_0^{(3)}$ in a saddle node-bifurcation. Similarly, if γ is increased from zero, a (positive) critical value of γ is reached where a bifurcation occurs and the root $B_0^{(1)}$ collides with $B_0^{(3)}$. [4] In

[4] This is not shown here, as it is just the negative reflection of the collision of the roots $B_0^{(2)}$ and $B_0^{(3)}$. Fig. 3.5 shows only the "positive" ground state.

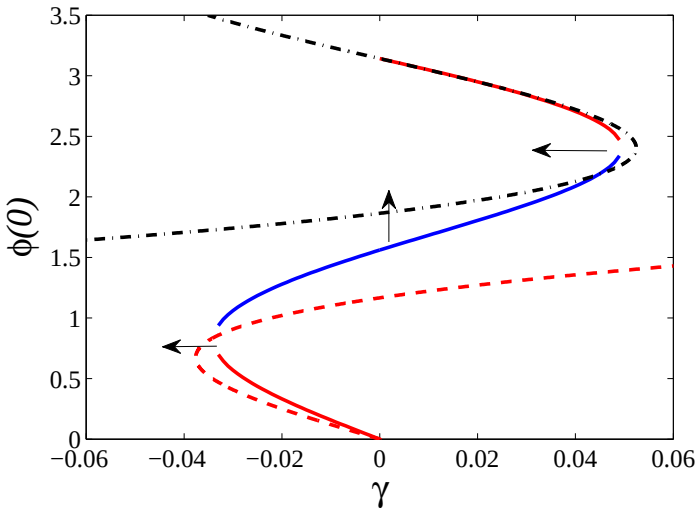

Figure 3.5: The existence diagram of the ground state. Plotted is $\phi(0)$ as a function of γ, obtained from numerical computations (solid lines) for $a = 0.495$ and $L = 1$. Shown in red is $\phi(0)$ as a function of a that corresponds to unstable solutions. The upper and lower red branch corresponds to solutions $\widetilde{\phi} = \pi$, 0, respectively.

other words, for these critical values of the bias current, the there is only root of the Eq. (3.6.50). Here, we denote the critical value of γ by $\gamma_{c,0}$.

Following [102] (see Chapter 2), we conclude that Eq. (3.6.50) has only one root under the condition

$$y_N^2 = h^2. \tag{3.6.51}$$

Substituting for y_N (with γ replaced with $\gamma_{c,0}$) and h from Eq. (3.6.49) into Eq. (3.6.51) and solving for $\gamma_{c,0}$, a simple manipulation gives

$$\gamma_{c,0} = \frac{2\sqrt{2}L^2\left(1-24k\right)^{3/2}}{9\sqrt{1-6k}\left(L^2-8\right)}. \tag{3.6.52}$$

This critical value can also be obtained by differentiating Eq. (3.6.46) with respect to B_0 and solving the corresponding equation for B_{0c}. In this case we find that

$$B_{0c}^{(1,2)} = \pm\sqrt{\frac{1-24k}{2\left(1-6k\right)}}. \tag{3.6.53}$$

Inserting B_{0c}, from Eq. (3.6.53) into Eq. (3.6.50) and solving for $\gamma_{c,0}$, we obtain (3.6.52).

The approximation to the critical applied bias current ($\gamma_{c,0}$) given by (3.6.52) is shown by the lower dash line in Fig. 3.6, where we have taken $L = 1$ and $a = 0.495$. Again the approximation to the critical bias current $\gamma_{c,0}$ given by Eq. (3.6.52) is close to its numerical counterpart whenever the facet length a is close to $a_{c,0}$.

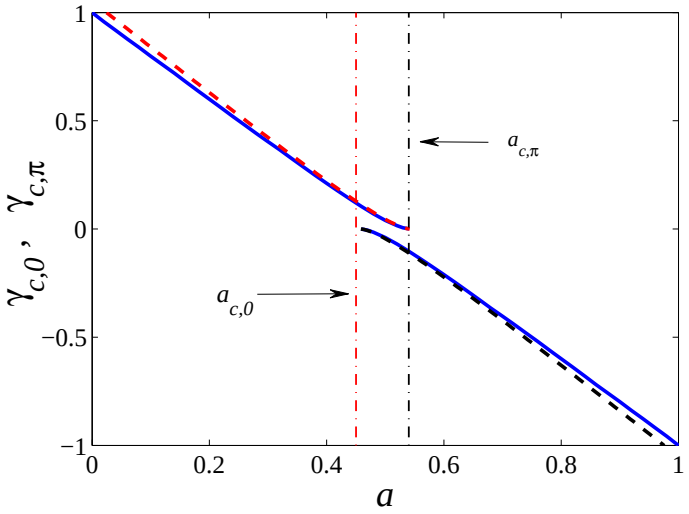

Figure 3.6: A comparison between the analytical approximation to critical bias currents $\gamma_{c,0}$ (the upper dashed line) and $\gamma_{c,\pi}$, (the lower dashed line) given respectively by the expressions (3.6.52) and (3.7.13), and the corresponding numerical solutions (solid lines), as a function of half of the length of π-junction.

3.7 Stability analysis of the critical eigenvalues

3.7.1 The case of the constant zero background

To study the stability of the stationary solutions (3.6.50), it is easy to verify that the potential energy H, given by Eq. (3.6.43) is locally minimized whenever $k < 1/24$. To obtain the critical eigenvalue (which is related to the smallest eigenfrequency) of the stable solutions, we write

$$B = B_0^{(n)} + \epsilon \widetilde{B}. \tag{3.7.1}$$

Using this ansatz and Taylor series expansion, assuming ϵ small, we write

$$U_B(B) = U_B(B_0^{(n)}) + \epsilon \widetilde{B} \left(U_{BB}\Big|_{B=B_0^{(n)}} \right) + \mathcal{O}(\epsilon^2). \tag{3.7.2}$$

Clearly $U_B(B_0^{(n)}) = 0$, as $B_0^{(n)}$ is a root of U_B. As a result, the Euler-Lagrange equation (3.6.45), after substituting in the U_B value from Eq. (3.7.2), to leading order, becomes

$$\widetilde{B}_{tt} = \frac{-2}{4L - L^3} \partial^2 U_B \Big|_{B=B^{(n)}} \widetilde{B}. \tag{3.7.3}$$

To calculate the eigenvalue of this equation, we put $\widetilde{B}_t = \widetilde{C}$, so that

$$\widetilde{C}_t = \frac{-2}{4L - L^3} U_{BB}\Big|_{B=B^{(n)}} \widetilde{B}, \tag{3.7.4}$$

and Eq. (3.7.3) can be expressed in the form of the following system

$$\begin{pmatrix} \widetilde{B}_t \\ \widetilde{C}_t \end{pmatrix} = \begin{pmatrix} 0 & 1 \\ \frac{-2}{4L-L^3} U_{BB}\Big|_{B=B^{(n)}} & 0 \end{pmatrix} \begin{pmatrix} \widetilde{B} \\ \widetilde{C} \end{pmatrix}. \tag{3.7.5}$$

The eigenvalue λ of the system (3.7.5) is given by

$$\begin{vmatrix} -\lambda & 1 \\ \frac{-2}{4L-L^3} U_{BB}\Big|_{B=B^{(n)}} & -\lambda \end{vmatrix} = 0.$$

From this, the critical eigenvalue of $B_0^{(n)}$ is calculated as

$$E = \frac{-2}{4L - L^3} U_{BB}\Big|_{B=B^{(n)}}, \tag{3.7.6}$$

with $E = \lambda^2$. Thus the critical eigenvalue is the negative square root of the oscillation frequency.

3.7.2 The case of the uniform $\widetilde{\phi} = \pi$ solution

In an identical fashion to the derivation of the dynamics of the Josephson phase ϕ in the instability region close to $a_{c,0}$, we find a similar instability region close to $a_{c,\pi}$, by exploiting the symmetry discussed in section 3.5. In the following, we briefly give the results.

The nonuniform ground state is described by the system

$$\phi = \pi + B(t) \begin{cases} \dfrac{\cosh(a_{c,\pi})}{\cosh(L - a_{c,\pi})} \cos(x + L), & (a < |x| < L), \\ \cosh(x), & (|x| < a). \end{cases} \tag{3.7.7}$$

With the help of (3.7.7) and assuming

$$a = \frac{L}{2} + kL^3, \tag{3.7.8}$$

such that $k < 1/24$,[5] and a formal series expansion, the Lagrangian (3.6.44) gives

$$\mathcal{L}_\pi = \left(L + \frac{L^3}{4}\right) B_t^2 - U_\pi,$$

[5] As mentioned earlier, for $k = 1/24$, (3.7.8) becomes the critical facet length, to the left of which π is unstable. So for the region of interest k must assume values less than $1/24$.

such that

$$U_\pi = 2L(1-2L^2k+\pi\gamma) + \frac{\gamma L}{4}\left(8+L^2\right)B + \frac{L^3}{12}(24k-1)B^2 - \frac{L^3}{36}(6k-1)B^4, \quad (3.7.9)$$

For this value of the potential energy, the Euler-Lagrange equation (3.6.44) gives

$$B_{tt} = \frac{2\partial_B U_\pi}{L(4+L^2)}. \quad (3.7.10)$$

Let us first consider the case of no applied bias current. It can be verified that when $\gamma = 0$, the time-independent roots of the equation

$$\partial_B U_\pi = 0, \quad (3.7.11)$$

are the same as given by Eq. (3.6.47). With these roots substituted into Eq. (3.7.7), the approximation to the nonuniform ground state $\phi(x)$ at the boundary $x = -L$ and the origin $x = 0$ are displayed by the upper dashed lines in Fig. 3.4. This approximation can also be obtained using the cyclic symmetry discussed in section 3.5. This symmetry can be clearly observed in Fig. 3.4, where the curves given by (3.6.39) and (3.7.7) are symmetric under rotation by π radians, with the center of rotation being $(a,\phi) = (L/2, \pi/2)$.

It can be seen from Fig. 3.4 that the approximation to the nonuniform ground states at the points $x = -L$ and $x = 0$, given by (3.7.7) well approximate the corresponding numerical solutions in the region where the facet length a is close to the critical facet length $a_{c,\pi}$.

In the undriven case where $\gamma \neq 0$, the time-independent roots B_0 of Eq. (3.7.10) are then given by the equation

$$4L^2(6k-1)B_0^3 - 6L^2(24k-1)B_0 - 9\gamma(L^2+8) = 0. \quad (3.7.12)$$

With the values given by Eq. (3.6.49) instead with $y_N = -9\gamma(L^2+8)$, the three roots of the equation (3.7.12) are given by Eq. (3.6.50). By plugging these roots into the system (3.7.7), one can then plot the ground states in the instability region where a is close to $a_{c,\pi}$ as a function of an applied bias current (see Fig. 3.5). There is a critical value of γ, where two roots merge. This value of the applied current is denoted by $\gamma_{c,\pi}$. This critical current can be obtained by the help of condition (3.6.51) as

$$\gamma_{c,\pi} = \frac{2\sqrt{2}L^2\left(24k-1\right)^{3/2}}{9\sqrt{6k-1}\left(L^2+8\right)} \quad (3.7.13)$$

where k is given by Eq. (3.7.8).

The upper dashed line in Fig. 3.6 represents the approximation to the second applied bias current, $\gamma_{c,\pi}$ given by Eq. (3.7.13), as a function of the facet length a. In the same figure, it is easy to observe that due to the cyclic symmetry, $\gamma_{c,\pi}$ can be obtained from $\gamma_{c,0}$ by rotating the curve by π radians, with the center of rotation being $(a, \gamma_{c,0}) = (L/2, 0)$.

In Figure 3.5, we plot our numerical solution $\phi(0)$ as a function of the applied bias current γ for $L = 1$ and $a = 0.495$. Starting from the point where $\gamma = 0$ and $\phi \approx 1.6$, first we decrease the applied bias current. As γ is reduced, the value of $\phi(0)$ also decreases up to a certain value of the bias current; the solution cannot be continued further, it terminates in a saddle node-bifurcation. Numerically, it is found that the saddle node-bifurcation is indeed due to a collision with a nonuniform solution connecting to $\widetilde{\phi} = 0$ and passing through the point $\gamma = 0$, as predicted by our analytical result [see (3.6.50)]. The value of $\gamma < 0$ at which bifurcation occurs is the aforementioned $\gamma_{c,0}$ given by Eq. (3.6.52). We show the bifurcation using our analytical results (3.6.50) as the lower dash lines.

Besides decreasing γ, one can also increase it. As γ increases, the value of $\phi(0)$ also increases. As the bias current is increased further, a saddle node-bifurcation occurs. We denote this critical value of the bias current by $\gamma_{c,\pi}$. Again, it can be observed, by following the upper branch of the bifurcation, that it corresponds to a collision between the nonuniform solution and the solution which comes from $\widetilde{\phi} = \pi$. The upper dashed lines show the bifurcation using our analytical results obtained from (3.6.50) exploiting the symmetry discussed in Section 3.5. The symmetry is clear in Fig. 3.5, where one can see that $\gamma(B_0)$ given by Eq. (3.6.50) is properly shifted by π, for the facet length $(L - a)$.

3.7.3 Nonuniform ground state for L large

Studying further the saddle-node-bifurcation between the nonuniform ground state and $\widetilde{\phi} = \pi$, we observe that it is not the typical collision that leads to the definition of $\gamma_{c,\pi}$ for any L. When L is relatively large, we find that the upper branch does not necessarily correspond to a uniform solution. This is depicted in Fig. 3.7, where we have considered $L = 10$ and $a = 3$.

Starting on the middle branch from $\gamma = 0$ and $\phi(0) \approx 2.9$, we increase the bias current. At the critical bias current $\gamma_{c,\pi}$, where $\gamma \approx 0.6$, we have a saddle node-bifurcation. Following the path from the bifurcation point, it is observed that the branch does not correspond to a uniform solution. If one decreases the applied bias current (γ), when

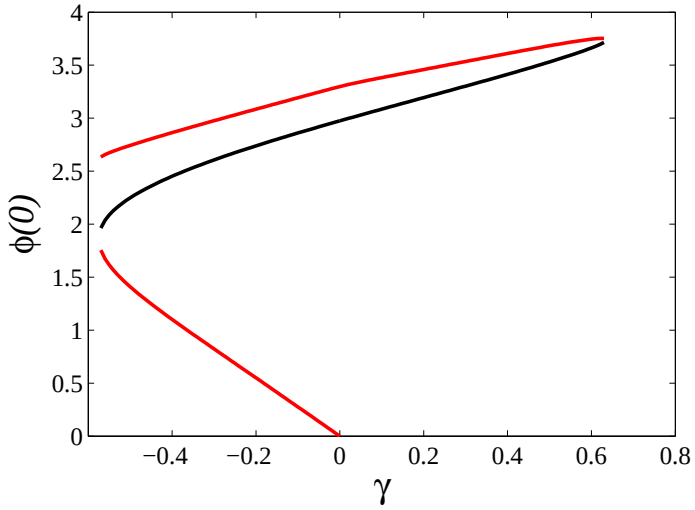

Figure 3.7: The profile of the nonuniform ground state solutions versus the bias current γ, where we have taken $L = 10$ and $a = 3$.

we reach $\gamma_{c,0}$, the solution terminates in a saddle node-bifurcation. Following the path, we reach the conclusion that this bifurcation is due to the collision between the nonuniform ground state and the uniform solution $\phi = 0$.

In the top panel of Figure 3.8, we plot the corresponding solutions for some values of the forcing term γ. Consider the profile of the Josephson phase ϕ in the un-driven case ($\gamma = 0$.) It can be immediately concluded that ϕ corresponds to a pair of semifluxons each of which is bound to a fluxon of the opposite sign, that is, a fluxon-antisemifluxon on the left hand side and a semifluxon-antifluxon on the right hand side. The profile of the Josephson phase ϕ is similar to the so-called type 3 semifluxons, defined by Susanto et al. [57] (see Figure 3 therein).

The value of $\gamma_{c,0}$ for $L \gg 1$, is approximately given by Eq. (2.5.50) (see Section 2.5.3.3), where $a_{c,0} \approx \pi/4$. Using the symmetry discussed in section 3.5, we can write $a_{c,\pi} \approx L - a_{c,0}$. In other words the critical bias currents $\gamma_{c,0}$ and $\gamma_{c,\pi}$, for large L can be approximated by

$$\gamma_{c,0} = -\sqrt{\frac{128}{27(\pi+1)}}\,(a - a_{c,0})^{3/2}, \tag{3.7.14a}$$

$$\gamma_{c,\pi} = \sqrt{\frac{128}{27(\pi+1)}}\,(a - a_{c,\pi})^{3/2}. \tag{3.7.14b}$$

This is in agreement with the expression of the critical bias current (2.5.50), obtained in the infinite domain problem.

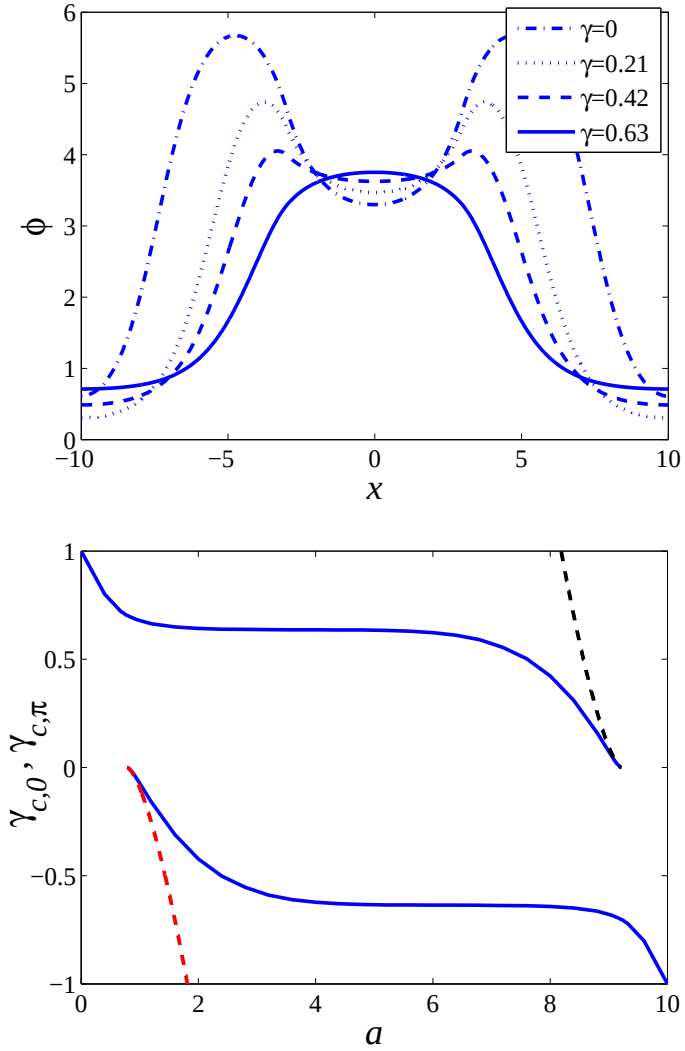

Figure 3.8: Top panel shows some of the nonuniform ground state solution corresponding to different values of the applied bias current γ. Bottom panel shows $\gamma_{c,0} < 0$ and $\gamma_{c,\pi} > 0$ as a function of a. Solid and dashed lines are numerical calculations and analytical approximations given by Eq. (3.7.14) respectively.

The analytical expressions given by Eq. (3.7.14) for $\gamma_{c,0}$ and $\gamma_{c,\pi}$ are presented by the dashed lines in the bottom panel of Figure 3.8, where the solid lines are the corresponding numerical calculations. The analytical approximations bear a good agreement to the corresponding numerics when the facet length is close to the critical facet lengths.

3.7.4 The stability analysis

Next, to study the stability of the critical eigenvalue, we perform the same calculations as discussed in Section 5.4. By inserting the ansatz (3.7.1) into the Euler Lagrange equation (3.7.10), the critical eigenvalue E of the stationary roots $B_0^{(n)}$ is calculated as

$$E = \frac{-2}{L\,(4+L^2)}\partial_B^2 U\Big|_{B=B^{(n)}}. \tag{3.7.15}$$

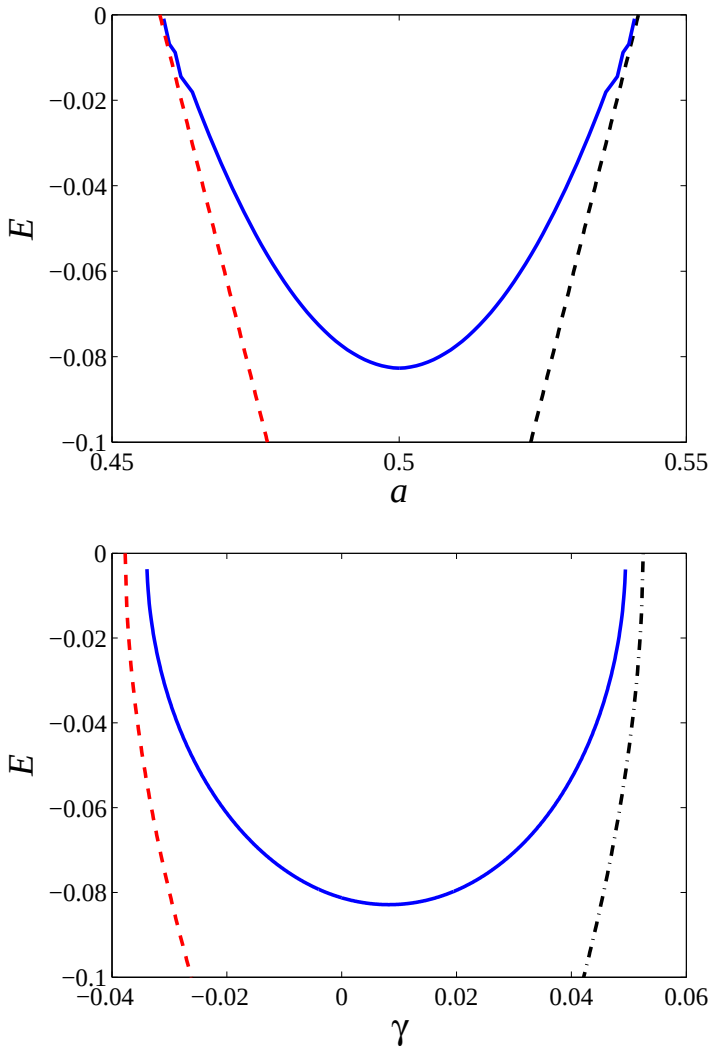

Figure 3.9: The top panel represents the comparison between the analytically obtained critical eigenvalues (dashed lines) given by Eqs. (3.7.6) (left) and (3.7.15) (right) as a function of a and their numerical counterparts (solid lines) in the un-driven case $(\gamma = 0)$ for $L = 1$. The bottom panel gives the plot of the same versus the applied bias current (γ) for $a = 0.495$ and $L = 1$.

Plotted in the upper panel of Figure 3.9 are the analytically obtained critical eigenva-

lues given by Eqs. (3.7.6) (left) and (3.7.15) (right) versus the facet length a, from which we see that when the facet length a is close to one of the critical values $a_{c,0}$ or $a_{c,\pi}$, the numerics (solid lines) are indeed well approximated by our analytical results.

In the lower panel of the same figure, we plot the critical eigenvalues of the nonuniform ground state as a function of γ for $a = 0.495$ and $L = 1$. Interestingly, we observe that the lowest eigenvalue is attained at a nonzero bias current. Therefore, it can be concluded that a nonuniform ground state can be made *more stable* by applying a bias current to it. In the same figure, we plot our approximations (3.7.6) and (3.7.15), which qualitatively agree with the corresponding numerical results.

One may ask about using 0-π-0 Josephson junctions to observe macroscopic quantum tunnelling and to build qubits. To answer the question, the reader is referred to the report by Goldobin et al. [67, 99] who consider quantum tunnelling of a semifluxon in a finite 0-π-junction, where it was concluded that finite 0-π-junctions do not provide a good playground to build a qubit. Goldobin et al. [67] consider quantum tunnelling of a semifluxon in an infinite 0-π-0 junction and a finite 0-π-junction, respectively. It was concluded that both setups provide a good playground to observe macroscopic tunnelling.

As for building a qubit, it will depend on the ratio between a and L. If $a \sim L$, the system considered here is not a promising one, because it requires the junction length to be very small. Goldobin et al. [99] have noted that in small length region the flux is too tiny to be detected by current technology. However, it has been stated that if $L \gg 1$ and a is small enough, finite 0-π-0 junctions can be good systems for qubits. It is then of interest to characterize the minimum value of L at which a finite 0-π-0 junction switches from being a good to a bad qubit system.

3.8 Conclusion

We have extended the ideas of Chapter 2 by considering a finitely long 0-π-0 Josephson junction, that is, a junction with two π-discontinuities in the phase, via a modified sine-Gordon equation. The existence and stability of the constant and static solutions of the model are studied. It is shown that there is a stability window in terms of the facet length a below (above) which the uniform zero (π) solution is stable. The relations between the critical facet lengths and the length of the junction are derived. We have shown that when the length of the junction is large enough, $a_{c,0}$ and $a_{c,\pi}$ respectively

approach $\pi/4$ and $L - \pi/4$, where $2L$ is the total length of the junction. Symmetry between the two types of uniform solution has been discussed.

We have shown that there is an instability region in which both the solutions are unstable. We have demonstrated that the ground state (corresponding to each constant solution) is a nonuniform therein. We investigated this nonuniform ground state solution using a Lindstedt-Poincaré method, a modified Lindstedt-Poincaré technique and a Lagrangian approach. The ground states in the combined instability region have been studied both in the absence and presence of an applied bias current. We have shown that like the infinite domain, semifluxons are spontaneously generated in the region of instability of the uniform solutions. The dependence of these semifluxons on the length of junction, the facet length and an applied bias current has been studied using an Euler-Lagrange approximation.

We have shown that in the region of instability, there exist two critical currents $\gamma_{c,0}$ and $\gamma_{c,\pi}$. There are two stable states solution and one unstable state in the region $|\gamma < |\min(|\gamma_{c,0}|, |\gamma_{c,\pi}|)$. When $\min(|\gamma_{c,0}|, |\gamma_{c,\pi}|) < |\gamma| < \max(|\gamma_{c,0}|, |\gamma_{c,\pi}|)$, we have one stable and one unstable solutions. There is no static ground state solution when $|\gamma| > \max(|\gamma_{c,0}|, |\gamma_{c,\pi}|)$.

We have also discussed the ground states in the instability region in the case where the length of the junction is large enough. The profile of the Josephson phase as a function of the spatial variable x for different values of the bias current is studied, and it is shown that when no current is flowing through the junction, the solution corresponds to a pair of semifluxons each of which is bound to a fluxon of the opposite signs (see the top panel of Fig. 3.8).

In addition the critical eigenvalue of the semifluxons has been discussed as well. It is observe that the lowest eigenvalue is attained in the situation where the applied bias current is nonzero. Numerical calculations are presented to support our analytical work.

CHAPTER 4

Analysis of 0-π disk-shaped Josephson junctions

In the previous chapters, we have analytically studied 0-π-0 long Josephson junctions on both infinite and finite domains, using a variety of asymptotic and variational techniques. In this chapter, we extend these ideas into two dimensions by considering a disk-shaped 0-π long Josephson junction. Parts of this chapter have been published in Ahmad et al. [113].

4.1 Introduction

The (1+1)-dimensional sine-Gordon model has been studied by a number of authors, see, for instance, Rajaraman [75], Drazin and Johnson [74], and Jackson [114] etc., where it was shown that it is fully integrable having some well-known exact solutions in the form of solitons. In different physical contexts, solitons may describe a variety objects. From a mathematical point of view, solitons are kinks (topological solitons) of the sine-Gordon model (see Section 1.5.1). Physically, if the phase-difference of the superconductors is denoted by $\phi(x,t)$, a kink in the context of long Josephson junctions corresponds to a vortex of supercurrent that is proportional to $\sin[\phi(x,t)]$, which creates a localized magnetic field $d\phi/dx$ with a total magnetic flux equal to a magnetic flux quantum. Investigation of solitons in long Josephson junctions (LJJs) have attracted a lot of attention in the last few decades. For a rather complete review and potential applications of solitons, see Ustinov [87] and references therein.

Traditionally, one investigates the most simple one-dimensional geometry, i.e. a (1+1)-dimensional sine-Gordon equation, in which only the phase variation in the x direction

is considered, while the phase dynamics in the y direction are neglected. This is justified when the width w of the junction in y direction is less than or approximately equal to the Josephson length (λ_J). In this case, the soliton can be viewed as a uniform flux tube going along the short y direction.

If one considers long Josephson junctions (LJJs) with both lateral sizes w (along y) and L (along x) greater than or approximately equal to the Josephson penetration depth (λ_J), then one should depart from the well-investigated (1+1)-dimensional sine-Gordon model and use a $(2+1)$-dimensional version of it, as originally proposed by Zagrodzinski [115]. This (2+1)-dimensional sine-Gordon equation is no longer fully integrable. In the literature, there are several approaches to obtaining different exact solutions of this $(2+1)$-dimensional model, for example the so-called Hirota method [116], which is also used by Gibbon and Zambotti [117], the auto-Bäcklund transformation of Konopelchenko et al. [118], exponentially decaying solutions of Schief [119], the Moutard transformation approach of Nimmo and Schief [120], and Lou et al. [121], the boundary integral equation of Dehghan and Mirzaei [122], the boundary element method of Mirzaei and Dehghan [123] and recently a differential quadrature method of Jiwari et al. [124].

A numerical study by Christiansen and Olsen [125], of spherically symmetric sine-Gordon equation in two and three spatial dimensions, suggested a solution in the form of kink-shaped ring waves (quasi-solitons). The authors named such solution a *ring wave* and found that this expanding soliton ring reaches a maximum size ($r = R_{max}$) and then shrinks to a minimum ($r \approx 0$). This phenomenon of expanding and shrinking of soliton ring was called *return effect*, which was later studied numerically by Samuelsen [126] using a Hamiltonian approach. There is another type of solution of such a symmetric sine-Gordon model, known as *pulson*, which can be understood as the generalization of the exact soliton-antisoliton bound state (the breather) solution of the (1+1)-dimensional sine-Gordon equation into higher dimensions. A pulson corresponds to the oscillations of the solution $\phi(r,t)$, as first reported by Makhankov [127] and later by Geicke [128], and Malomed [129]. Such pulsons were studied in the late seventies by Christiansen and Olsen [125, 130], who derived the return effect using a perturbation analysis.

In the (2+1)-dimensional sine-Gordon model, one still can observe solutions of the (1+1)-dimensional counterpart. Nonetheless, such (2+1)-dimensional solitons are still topologically equivalent to a simple flux line. On the other hand, in two spatial di-

mensions, one may also imagine solutions of a completely different topology, such as a flux line closed in a loop (ring). In a uniform system, such solitons are unstable even with initial velocity outwards (an expanding soliton ring), near the center and finally decaying into the trivial constant phase solution.

It is believed that the spatially uniform sine-Gordon equation has no radially symmetric (angle independent) static solitonic solutions in two or more spatial dimensions, as reported by Derrick [131]. In fact, the argument given therein applies only to three or more spatial dimensions and fails in two dimensions. Olsen and Samuelsen [132] demonstrated that, in two-dimensions, the static ring soliton is unstable and collapses to the center as it has infinite critical radius at zero bias. Goldobin et al. [133] have reported that any radially symmetric solution $\phi(r)$ of an N-dimensional sine-Gordon equation (see [131]) is equivalent to a solution $\phi(x)$ of a one-dimensional sine-Gordon equation with variable (Josephson junction) width $w(x) = (N-1)x$.

Christiansen and Lomdahl [134] numerically studied this model and observed the propagation of the wave along the direction of Josephson vortex. Recently, Gulevich et al. [47] have derived solutions of the unperturbed (2+1)-dimensional sine-Gordon model, which can be used for the description of propagation of waves having arbitrary shapes, along the y direction, especially when a soliton hits obstacles. There are several experimental works, e.g., see Koshelets and Shitov [135] and Torgashin et al. [136], and theocratical proposals, like those by Savel'ev et al. [137] and Yampol'skii et al. [138], which suggest the application of the properties of waves with arbitrary shapes along the Josephson vortex in high-frequency Josephson devices for the information transmission.

4.2 Overview

In this chapter, we consider a disk-shaped two-dimensional Josephson junction with concentric regions of $0-$ and $\pi-$ phase shifts. The junction has the inner circular π-part and the outer 0-part having respectively a radius from R_{min} to R_{mid} and a radius from R_{mid} to R_{max}, as sketched in Figure 4.1. This system is described by a perturbed $(2+1)$-dimensional sine-Gordon equation, which becomes effectively one dimensional in polar coordinates when one considers radially symmetric static solutions. We investigate the ground state of the system both in finite and semi-infinite domain. In particular, we analyze the existence and stability of different static solutions to find the

ground state of the system.

The chapter is organized as follows. In Section 4.3, we introduce the model that is used to illustrate the properties of the system under consideration. To discuss the stability of the uniform solutions, an eigenvalue problem is derived. In Section 4.4, we analyze the stability of uniform solutions of the system, in the case of no applied bias current and show that the uniform solutions are unstable in a certain parameter interval. Like the one-dimensional problem, we show that in the two dimensional problem, the uniform π solution can also be stable in a certain interval in the finite domain and is unstable when the domain is infinite. In the interval of parameters, where both uniform background states are unstable, we show that a semifluxon is spontaneously created. Using a Hamiltonian energy characterization, the existence and stability of nonuniform static solitons is discussed in Section 4.5 where, besides the undriven problem, we study the effect of an applied bias current on the existence of the nonuniform ground state. The critical eigenvalues of constant solutions, as functions of the facet length and an applied bias current are also discussed in the same section. Finally, in Section 5.7, we give a brief summary of the main results obtained in the Chapter.

4.3 Mathematical model

In order to study the dynamics of the Josephson phase in a two-dimensional long Josephson junction, we use the two-dimensional version of the $(1+1)$-dimensional perturbed sine-Gordon equation (1.5.5), namely (see, e.g., Ouroushev et al. [139], and Minzoni et al. [140])

$$\phi_{xx} + \phi_{yy} - \phi_{tt} = \sin\left[\phi + \theta(x,y)\right] + \alpha\phi_t - \gamma, \tag{4.3.1}$$

where $0 \leq x \leq L$ and $0 \leq y \leq W$ are the dimensions of the junction, $\phi(x,y,t)$ is a Josephson phase that is related to the magnetic flux B by the relation $B = d\phi/dx$, α is a dimensionless positive damping coefficient due to quasi-particle tunnelling, and γ is the applied bias current density, which is normalized to the critical current density J_c and assumed to be constant. The spatial variables x and y are measured in units of the Josephson penetration depth λ_J, and the time t is normalized to the inverse Josephson plasma frequency ω_p^{-1}, see for instance, Barone and Paterno [141].

Here, we consider the two-dimensional disk-shaped Josephson junction sketched in Figure 4.1. The origin of the coordinate system is the center of the disk, while $z = 0$ corresponds to the Josephson barrier which is assumed to be infinitesimal. Thus, Eq.

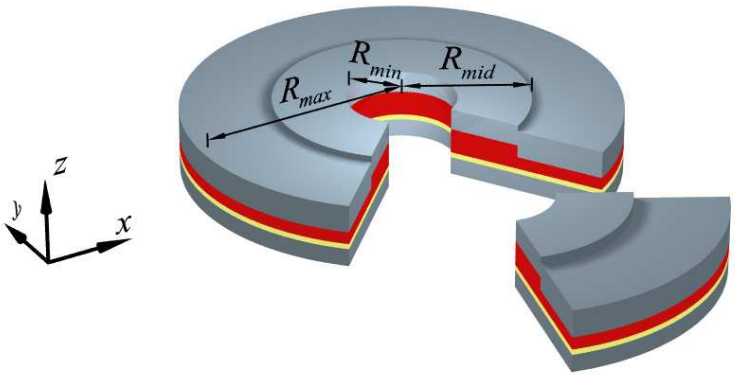

Figure 4.1: A sketch of the disk-shaped two dimensional $0-\pi$ Josephson junction considered herein.

(4.3.1) should be solved in the domain

$$R_{\min} < \sqrt{x^2+y^2} < R_{\max}.$$

The function $\theta(x,y)$ describes the position of an additional π shift and is given by

$$\theta(x,y) = \begin{cases} \pi, & R_{\min} < \sqrt{x^2+y^2} < R_{\mathrm{mid}}, \\ 0, & R_{\mathrm{mid}} < \sqrt{x^2+y^2} < R_{\max}. \end{cases} \tag{4.3.2}$$

In the following, we will limit ourselves to the case $R_{\min} = 0$.

Due to the geometry of the problem, it is convenient to work in polar coordinates. For this purpose, let us suppose $(r,\tilde{\theta})$ are the polar coordinates corresponding to the point (x,y) in the cartesian plane. Consequently, the model (4.3.1) reduces to

$$\phi_{rr} + \frac{1}{r}\phi_r + \frac{1}{r^2}\phi_{\tilde{\theta}\tilde{\theta}} - \phi_{tt} = \sin\left[\phi + \theta(r)\right] + \alpha\phi_t - \gamma. \tag{4.3.3}$$

The $\tilde{\theta}$-independent version of this equation, with $\alpha = \theta(r) = 0$, was used by Olsen and Samuelsen [132] to find 2π-kink ring waves solutions of a spherically symmetric sine-Gordon equation.

In polar coordinates, the function $\theta(r)$ can be rewritten as

$$\theta(r) = \begin{cases} \pi, & 0 < r < a, \\ 0, & a < r < L. \end{cases} \tag{4.3.4}$$

Here, for simplicity we have defined $R_{\mathrm{mid}} = a$ and $R_{\max} = L$. In spite of the phase jump at $r = a$, given by Eq. (4.3.4), we assume that the Josephson phase $\phi(r)$, and its derivative with respect to r, are continuous at the point $r = a$, i.e., we make use of the

following continuity conditions

$$\phi(a^-) = \phi(a^+), \quad \phi_r(a^-) = \phi_r(a^+). \tag{4.3.5}$$

The boundary conditions corresponding to a zero applied magnetic field read

$$\phi_r(L) = 0 \quad \phi_r(R_{\min}) = 0. \tag{4.3.6}$$

For the present problem, the one-dimensional Lagrangian (2.2.3) takes the form

$$\mathcal{L} = \int_0^{2\pi} \int_0^L \left\{ \frac{1}{2}\phi_t^2 - \frac{1}{2}\phi_r^2 - \frac{1}{2}\phi_{\tilde{\theta}}^2 - 1 + \cos\left[\phi + \theta(r)\right] - \gamma\phi \right\} r dr d\tilde{\theta}. \tag{4.3.7}$$

Subject to the boundary and continuity condition (4.3.5) and (4.3.6), the (2+1)-dimensional model (4.3.3) can be derived from the Lagrangian (4.3.7).

As in the previous chapters, we focus interest in static solutions, so for the existence of the solutions, we assume $\phi_t = 0$. In other words, the investigation of the solution is of the time-independent equation

$$\phi_{rr} + \frac{1}{r}\phi_r + \frac{1}{r^2}\phi_{\tilde{\theta}\tilde{\theta}} = \sin\left[\phi + \theta(r)\right] - \gamma. \tag{4.3.8}$$

In the present work we limit ourselves to the case where the solutions are radially symmetric, i.e., $\tilde{\theta}$-independent. Consequently (4.3.8) is converted into

$$\phi_{rr} + \frac{1}{r}\phi_r = \sin\left[\phi + \theta(r)\right] - \gamma. \tag{4.3.9}$$

4.3.1 Eigenvalue problem

Let us assume $\widetilde{\phi}(r, \tilde{\theta})$ is the static solution of the governing equation (4.3.3) in polar coordinates. To determine the linear stability of the solution $\widetilde{\phi}(r, \tilde{\theta})$, we assume $\epsilon\phi_1(r, \tilde{\theta}, t)$ to be a small perturbation of $\widetilde{\phi}$, where $\epsilon \ll 1$. In other words, we substitute

$$\phi(r, \tilde{\theta}, t) = \widetilde{\phi}(r, \tilde{\theta}) + \epsilon\phi_1(r, \tilde{\theta}, t), \tag{4.3.10}$$

into Eq. (4.3.3), using Taylor series expansion about $\epsilon = 0$, and retaining only the linear terms in ϵ, we obtain the linearised equation

$$\left\{ \partial_{rr} + \frac{1}{r}\partial_r + \frac{1}{r^2}\partial_{\tilde{\theta}\tilde{\theta}} \right\}\phi_1 = \left\{ \cos\left[\widetilde{\phi} + \theta(r)\right] + \partial_{tt} + \alpha\partial_t \right\}\phi_1. \tag{4.3.11}$$

This equation governs the dynamics of the small perturbation $\phi_1(r, \tilde{\theta})$. Since Eq. (4.3.11) is linear, we solve it by the method of separation of variables. As a result, the solution has the form

$$\phi_1 = e^{\lambda t}\widetilde{V}(r, \tilde{\theta}), \tag{4.3.12}$$

where $\lambda \in \mathbf{C}$. Using this assumption, we conclude from Eq. (4.3.10) that a static solution $\widetilde{\phi}$ is linearly stable whenever λ has a non-positive real parts.

By introducing Eq. (4.3.12) to (4.3.11), we obtain the following eigenvalue problem

$$\widetilde{V}_{rr} + \frac{1}{r}\widetilde{V}_r + \frac{1}{r^2}\widetilde{V}_{\tilde{\theta}\tilde{\theta}} = \left(E + \cos\left[\widetilde{\phi} + \theta(r)\right]\right)\widetilde{V}, \tag{4.3.13}$$

where E is given by the relation $E = \lambda^2 + \alpha\lambda$.

In the case where $\widetilde{\phi}$ is independent of the angular variable $\tilde{\theta}$, the method of separation of variables for partial differential equations, suggests the solution $\widetilde{V}$ of the eigenvalue problem (4.3.13) of the type

$$\widetilde{V}(r, \tilde{\theta}) = \cos\left(q\tilde{\theta}\right) V(r). \tag{4.3.14}$$

This covers all the $2\pi-$periodic functions in $\tilde{\theta}$ that can be represented by Fourier series. By substituting Eq. (4.3.14) into Eq. (4.3.13), our eigenvalue problem takes the form

$$V_{rr} + \frac{1}{r}V_r - \frac{q^2}{r^2}V = \{E + \cos\left[\widetilde{\phi} + \theta(r)\right]\}V. \tag{4.3.15}$$

It can be verified that the eigenvalue problem is self-adjoint, so the corresponding spectral parameter E is real, which in the present case, is a function of q.

The function $V(r)$ is subject to the continuity and boundary conditions that follow from Eqs. (4.3.5) and (4.3.6)

$$V(a^-) = V(a^+), \quad V_r(a^-) = V_r(a^+), \tag{4.3.16}$$

and

$$V_r(L) = 0, \quad V_r(R_{\min}) = 0 \tag{4.3.17}$$

Keeping in mind the discussion in Section 3.4, we note that an unstable (stable) solution in the non-dissipative system ($\alpha \neq 0$) remains unstable (stable) in the dissipative system ($\alpha = 0$). That is, α does not play any role in the stability analysis of a constant solution, therefore, without losing generality, in the following, we set

$$\alpha = 0, \tag{4.3.18}$$

unless stated otherwise. A uniform background solution is unstable whenever $E > 0$, or equivalently, if λ has a non-negative real part.

4.4 Existence and linear stability analysis of uniform solutions

We know that, for an undriven case ($\gamma = 0$), the model (4.3.9) allows two uniform and static solutions, namely $\widetilde{\phi} \equiv 0,\ \pi \pmod{2\pi}$. In the following, we discuss the existence and stability of these constant background solutions separately. To study the stability of the uniform solutions, one needs to solve the eigenvalue problem (4.3.15) subject to the continuity and boundary conditions (4.3.16) and (4.3.17). From a numerical calculation (see Fig. 7.1, and Section 7.4 in the Appendix), it appears that the critical eigenvalue of the solutions corresponds to $q = 0$. Therefore, in our analytical calculations below, we only consider the case $q = 0$.

4.4.1 Linear stability of the $\widetilde{\phi} = 0$ solution

We first take the constant solution $\widetilde{\phi} = 0$ into account. To discuss its linear stability we first discuss the so-called "continuous" spectrum which corresponds to the bounded solutions of the eigenvalue problem (4.3.15) in the inner and outer regions.

4.4.1.1 The "continuous" spectrum

Consider the region $0 < r < a$, where $\theta(r) = \pi$. Let $V^{(1)}(r)$ denote the solution to the eigenvalue problem (4.3.15) in this region. Then we obtain

$$V^{(1)}_{rr} + \frac{1}{r} V^{(1)}_{r} - (E-1) V^{(1)} = 0, \tag{4.4.1}$$

which is a Bessel equation of order zero with the solution

$$V^{(1)}(r) = B_1 \, \mathrm{J}_0\left(\hat{\beta} r\right) + B_1^* \, \mathrm{Y}_0\left(\hat{\beta} r\right), \tag{4.4.2}$$

with $\hat{\beta}$ given by Eq. (2.4.12). The terms J_0 and Y_0 represent Bessel functions of first and second kind that are respectively defined as (see, Abramowitz and Stegun [81])

$$\mathrm{J}_0 = \sum_{m=0}^{\infty} \frac{(-1)^{m-1} h_m}{2^{2m} (m!)^2} r^{2m},$$

$$\mathrm{Y}_0 = \mathrm{J}_0 \ln r + \sum_{m=0}^{\infty} \frac{(-1)^{m-1} h_m}{2^{2m} (m!)^2} r^{2m},$$

where h_m is defined as

$$h_m = 1 + \frac{1}{2} + \frac{1}{3} + \ldots + \frac{1}{m},\ m \in N.$$

The Bessel function of second kind $\mathrm{Y}_0(\hat{\beta}r)$ is unbounded at the point $r = 0$. In order to obtain a bounded solution of Eq. (4.4.1), we take $B_1^* = 0$ and are left with

$$V^{(1)}(r) = B_1 \mathrm{J}_0\left(\hat{\beta}r\right). \tag{4.4.3}$$

Let $V^{(2)}(r)$ be the solution to the eigenvalue problem (4.3.15) in the outer region $a < r < L$, where $\theta(r) = 0$. Consequently, Eq. (4.3.15) takes the form

$$V_{rr}^{(2)} + \frac{1}{r}V_r^{(2)} - (E+1)V^{(2)} = 0. \tag{4.4.4}$$

A general solution of this equation is

$$V^{(2)} = B_2 \mathrm{J}_0\left(\hat{\zeta}r\right) + B_3 \mathrm{Y}_0\left(\hat{\zeta}r\right), \tag{4.4.5}$$

where $\hat{\zeta}$ is the same as defined in (3.4.6).

Thus, the eigenfunctions of the "continuous" spectrum of the uniform zero solution are given by

$$V(r) = \begin{cases} B_1 \mathrm{J}_0\left(\hat{\beta}r\right), & 0 < r < a, \\ B_2 \mathrm{J}_0\left(\hat{\zeta}r\right) + B_3 \mathrm{Y}_0\left(\hat{\zeta}r\right), & a < r < L. \end{cases} \tag{4.4.6}$$

Applying the continuity and boundary conditions (4.3.16) and (4.3.17), we obtain a system of three homogenous equations of the form

$$S_1 \begin{pmatrix} B_1 \\ B_2 \\ B_3 \end{pmatrix} = 0, \tag{4.4.7}$$

where the coefficient S_1 matrix is defined by

$$S_1(E) = \begin{bmatrix} \mathrm{J}_0(\hat{\beta}a) & -\mathrm{J}_0(\hat{\zeta}a) & -\mathrm{Y}_0(\hat{\zeta}a) \\ -\mathrm{J}_1(\hat{\beta}a)\hat{\beta} & \mathrm{J}_1(\hat{\zeta}a)\hat{\zeta} & \mathrm{Y}_1(\hat{\zeta}a)\hat{\zeta} \\ 0 & -\mathrm{J}_1(\hat{\zeta}L)\hat{\zeta} & -\mathrm{Y}_1(\hat{\zeta}L)\hat{\zeta} \end{bmatrix}. \tag{4.4.8}$$

In order to find a nontrivial solution of the system, i.e., $(B_1, B_2, B_3)^T \neq \mathbf{0}$, we require

$$\det(S_1) = 0. \tag{4.4.9}$$

Figure 4.2 shows an implicit plot of the "continuous" spectrum E as a function of a for $L = 2$, from which we observe that E is negative in the "continuous" spectrum. This implies that there is no unstable eigenvalue for all a. The distribution of E eigenvalues becomes denser as L increases.

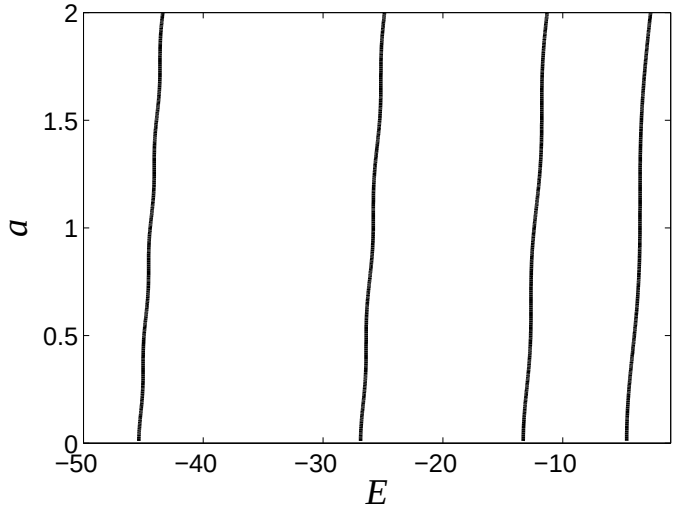

Figure 4.2: Plot of the "continuous" spectrum of the uniform solution $\widetilde{\phi} = 0$ as a function of the π region radius a for $L = 2$.

4.4.1.2 The "continuous" spectrum in the limit $L \to \infty$

Now we consider the set of bounded solutions of the eigenvalue problem (4.3.15) in the infinite domain. For this we suppose $r \gg 1, r \sim L$, where $\lim_{r\to\infty} \theta(r) = 0$. Substituting these assumptions, for the uniform solution $\widetilde{\phi} = 0$ into the eigenvalue problem (4.3.15), at the leading order we have

$$V_{rr} = (E + 1)\, V. \tag{4.4.10}$$

Solutions of this equation are bounded if and only if $E < -1$. Hence the continuous spectrum exists only on the imaginary axis, i.e., where λ is purely imaginary. Thus, we conclude that there is no unstable eigenvalue in the continuous spectrum of the uniform solution $\widetilde{\phi} = 0$. Nevertheless, it does not imply the linear stability of the uniform solution. In order to fully determine the linear stability we must also calculate the discrete spectrum of the uniform solution.

4.4.1.3 The discrete spectrum

As discussed in Section 2.4.1.2, the discrete spectrum of a uniform solution corresponds those values of the spectral parameter E for which the spectrum complements its "continuous" spectrum. The discrete spectrum corresponds to a bounded solution in the inner region and a square integrable solution in the outer region. In other words, the discrete spectrum of constant zero-background in the region $0 < r < a$ correspond to

a bounded solution in the inner region and a bounded and decaying solution in the outer region.

A simple calculation shows that a bounded solution of the eigenvalue problem (4.3.15) and $q = 0$, in the inner region $0 < r < a$, is given by

$$V^{(1)}(r) = B_4 \mathrm{J}_0(\hat{\beta} r), \tag{4.4.11}$$

with $\hat{\beta} a < j_{0,1}$, where $j_{0,1}$ is the smallest root of J_0 and B_4 is a constant of integration to be determined.

Again, in the region $a < r < L$, where $\theta(r) = 0$, the solution $V^{(2)}(r)$, of the eigenvalue problem (4.3.15), can be written in the form[1]

$$V^{(2)}(r) = B_5 \mathrm{J}_0\left(i\hat{\alpha} r\right) + B_6 \mathrm{Y}_0\left(i\hat{\alpha} r\right), \tag{4.4.12}$$

where $i^2 = -1$ and $\hat{\alpha}$ is given by (2.4.8).

To obtain a bounded and decaying solution in the outer region, we use the properties of Bessel functions [81]

$$\mathrm{J}_0\left(ir\sqrt{E+1}\right) = \mathrm{I}_0\left(r\sqrt{E+1}\right), \tag{4.4.13}$$

$$\mathrm{Re}\left[\mathrm{Y}_0\left(ir\sqrt{E+1}\right)\right] = -\frac{2}{\pi}\mathrm{K}_0\left(r\sqrt{E+1}\right). \tag{4.4.14}$$

Here

$$\mathrm{I}_0 = \sum_{m=0}^{\infty} \frac{r^{2m}}{2^{2m}(m!)^2}, \quad \text{and} \quad \mathrm{K}_0 = \mathrm{I}_0 \ln r - \frac{1}{4}r^2 + \frac{1}{128}r^4 - \frac{7}{13824}r^6 + ..., \tag{4.4.15}$$

are the modified Bessel functions of first and second kind respectively. Hence, a bounded and decaying solution to the eigenvalue problem in the outer region is

$$V^{(2)}(r) = B_5 \mathrm{I}_0(\hat{\alpha} r) - \frac{2B_6}{\pi}\mathrm{K}_0(\hat{\alpha} r). \tag{4.4.16}$$

Consequently, the eigenfunction corresponding to the discrete spectrum of the uniform solution $\widetilde{\phi} = 0$ is given by

$$V(r) = \begin{cases} B_4 \mathrm{J}_0(\hat{\beta} r), & 0 < r < a, \\ B_5 \mathrm{I}_0(\hat{\alpha} r) - \frac{2B_6}{\pi}\mathrm{K}_0(\hat{\alpha} r), & a < r < L. \end{cases} \tag{4.4.17}$$

Again by applying the continuity and boundary conditions (4.3.16) and (4.3.17), we obtain a system of three homogeneous equations of the form

$$S_2 \begin{pmatrix} B_4 \\ B_5 \\ B_6 \end{pmatrix} = \mathbf{0}, \tag{4.4.18}$$

[1] See also Section 2.4.1.2.

where

$$S_2(E) = \begin{bmatrix} \mathrm{J}_0(\hat{\beta}a) & -\mathrm{I}_0(\hat{\alpha}a) & \frac{2}{\pi}\mathrm{K}_0(\hat{\alpha}a) \\ \hat{\beta}\,\mathrm{J}_1(\hat{\beta}a) & -\hat{\alpha}\,\mathrm{I}_1(\hat{\alpha}a) & -\frac{2}{\pi}\hat{\alpha}\,\mathrm{K}_1(\hat{\alpha}a) \\ 0 & \hat{\alpha}\,\mathrm{I}_1(\hat{\alpha}L) & \frac{2}{\pi}\hat{\alpha}\,\mathrm{K}_1(\hat{\alpha}L) \end{bmatrix}, \tag{4.4.19}$$

is the coefficient matrix. For a nontrivial solution of (4.4.19), it is necessary for the coefficient matrix S_2 to satisfy

$$\det(S_2) = 0. \tag{4.4.20}$$

As the system (4.4.18) has three equations with three unknowns B_4, B_5, B_6, therefore, to obtain its nontrivial solution, we must assign a nonzero value to the constants B_i, $i = 4, 5, 6$. For example, taking $B_4 = 1$, we find that

$$\begin{aligned} B_5 &= \frac{\hat{\beta}\,\mathrm{K}_1(\hat{\alpha}L)\,\mathrm{J}_1(\hat{\beta}a)}{\hat{\alpha}\left[\mathrm{I}_1(\hat{\alpha}L)\,\mathrm{K}_1(\hat{\alpha}a) - \mathrm{I}_1(\hat{\alpha}a)\,\mathrm{K}_1(\hat{\alpha}L)\right]}, \\ B_6 &= -\frac{\pi\hat{\beta}\,\mathrm{I}_1(\hat{\alpha}L)\,\mathrm{J}_1(\hat{\beta}a)}{2\hat{\alpha}\left[\mathrm{I}_1(\hat{\alpha}L)\,\mathrm{K}_1(\hat{\alpha}a) - \mathrm{I}_1(\hat{\alpha}a)\,\mathrm{K}_1(\hat{\alpha}L)\right]}. \end{aligned}$$

The implicit plot of the zeros of the equation (4.4.20) is depicted in Figure 4.3. The plot shows that there is a critical value of the length a below which E is negative, i.e. the uniform zero solution is stable. At this particular value of the facet length, the spectral parameter E changes sign from negative to positive, which implies that the static zero solution becomes unstable. The value of the facet length at which the uniform zero solution changes stability is called the critical length for the uniform solution $\widetilde{\phi} = 0$ and is denoted by a_c^0.

The same plot can be obtained by introducing the values of the constants B_4, B_5, B_6 into the system (4.4.17) and plot $V(r)$ as a function of the facet length a for some value of L.

4.4.1.4 Relation between a_c^0 and L

Next, we express the critical facet length a_c^0 in terms of the length L of the Josephson junction. From our knowledge so far, we know that whenever the spectral parameter$E$ becomes zero, then the facet length a takes its critical value a_c^0. By substituting $E = 0$, $a = a_c^0$ into (4.4.20), the relation between a_c^0 and L can be written implicitly as

$$\frac{\mathrm{J}_0\left(a_c^0\right)}{\mathrm{J}_1\left(a_c^0\right)} = \frac{\mathrm{K}_1(L)\,\mathrm{I}_0(a_c^0) + \mathrm{I}_1(L)\,\mathrm{K}_0(a_c^0)}{\mathrm{I}_1(L)\,\mathrm{K}_1(a_c^0) - 2\,\mathrm{I}_1(a_c^0)\,\mathrm{K}_1(L)}. \tag{4.4.21}$$

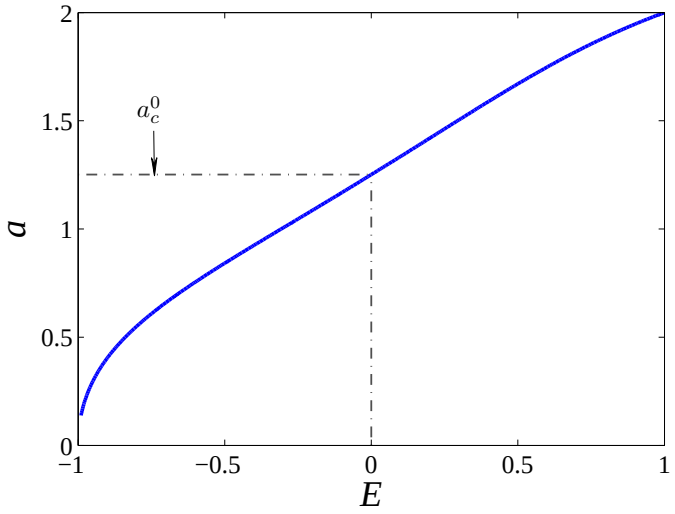

Figure 4.3: Plot of the roots of the system (4.4.20) i.e., the discrete spectrum of the uniform solution $\widetilde{\phi} = 0$ as a function of the facet length a, where we have taken the length of the junction $L = 2$.

This gives a boundary line separating the region of stability from that of instability of the zero solution and is shown by the lower solid line in Fig. 4.6.

Now consider the case when $L \to 0$. Expanding the implicit relation Eq. (4.4.21) by formal series expansion, we obtain an explicit dependence

$$a_c^0 = \frac{L}{\sqrt{2}} - \frac{2\ln(2) - 1}{16\sqrt{2}} L^3 + \mathcal{O}(L^5), \tag{4.4.22}$$

which represents a_c^0 as function of L. For example, when $L = 2$, one obtains $a_c^0 \approx 1.25$. The plot of this implicit relation in the (a, L)-plane is shown by the lower dashed line in Fig. 4.6.

4.4.2 Discrete spectrum of the zero background solution in the limit $L \to \infty$

Our analysis presented in the previous section is also valid in the limit $L \to \infty$. Nonetheless, below we consider this limit separately as the corresponding analytical calculations are simplified.

For a bounded solution $V^{(1)}(r)$ in the inner region, the eigenvalue problem (4.3.15) reduces to Eq. (4.4.1), whose solution is

$$V^{(1)}(r) = B_7 \mathrm{J}_0(\hat{\beta} r). \tag{4.4.23}$$

Similarly, if $V^{(2)}(r)$ represents the solution to the eigenvalue problem (4.3.15) in the outer region, then (4.3.15) takes the form of Eq. (4.4.4). Since the modified Bessel function

$\mathrm{I}_0(\hat{\alpha}r)$ is not defined when $r \to \infty$, so the bounded solution of Eq. (4.4.5), using the properties of the Bessel functions (see [81]), takes the form

$$V^{(2)}(r) = B_8\,\mathrm{K}_0(\hat{\alpha}r). \tag{4.4.24}$$

Consequently, with the help of the bounded solutions in the inner and outer regions, respectively given by Eqs. (4.4.23) and (4.4.24), the eigenfunction corresponding to the discrete spectrum of the stationary solution $\tilde{\phi} = 0$ reduces to

$$V(r) = \begin{cases} B_7\,\mathrm{J}_0\left(\hat{\beta}r\right), & 0 < r < a, \\ B_8\,\mathrm{K}_0\left(\hat{\alpha}r\right), & a < r < \infty. \end{cases} \tag{4.4.25}$$

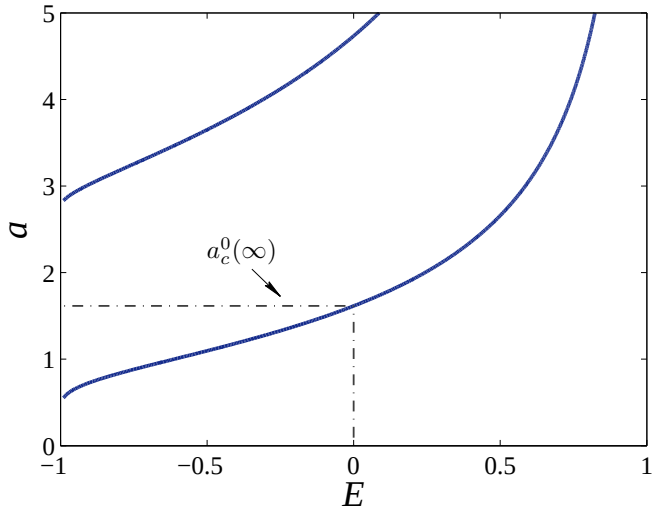

Figure 4.4: The discrete spectrum of the constant zero background solution for the case when L tends to infinity. The spectrum is obtained by plotting the zeros of the equation 4.4.28 in the (E, a)-plane.

Application of the continuity conditions to the system (4.4.25) leads to a homogeneous system of two equations of the form

$$S_3 \begin{pmatrix} B_7 \\ B_8 \end{pmatrix} = \mathbf{0}, \tag{4.4.26}$$

where the coefficient matrix S_3 is defined by

$$S_3(E) = \begin{bmatrix} \mathrm{J}_0\left(\hat{\beta}a\right) & -\mathrm{K}_0\left(\hat{\alpha}a\right) \\ -\mathrm{J}_1\left(\hat{\beta}a\right)\hat{\beta} & \mathrm{K}_1\left(\hat{\alpha}a\right)\hat{\alpha} \end{bmatrix}. \tag{4.4.27}$$

Again, the system (4.4.26) has a nontrivial solution when

$$\det(S_3) = 0. \tag{4.4.28}$$

The implicit plot of the zeros of determinant of the matrix S_3 (roots of Eq. (4.4.28)), in the (E, a)-plane, are depicted in Figure 4.4. From this figure, we observe that there is a critical value of the facet length a where the lowest E changes its sign, similarly to the case of finite L. This is the critical value of the facet length a in the infinite domain and is denoted by $a_c^0(\infty)$. We note that when L tends to infinity, then $a_c^0(\infty)$ is approximately equal to 1.615. This value of the critical a is obtained by substituting $E = 0$ into Eq. (4.4.28) and solving it for $a_c^0(\infty)$.

4.4.3 Linear stability of the constant π background

Next, we take into account the case of the uniform solution $\widetilde{\phi} = \pi$ and consider its linear stability. First we consider the case when the domain is finite and discuss the set of bounded solutions of the eigenvalue problem (4.3.15).

4.4.3.1 The "continuous" spectrum

First, we consider the inner region $0 < r < a$ where $\theta(r) = \pi$. In this region the eigenvalue problem (4.3.15) takes the form

$$V_{rr}^{(1)} + \frac{1}{r} V_r^{(1)} - (E+1)\, V^{(1)} = 0. \tag{4.4.29}$$

Eq. (4.4.29) is a Bessel equation of order zero whose general solution is given by

$$V^{(1)}(r) = B_9\, \mathrm{J}_0(\hat{\zeta} r) + B_{10}\, \mathrm{Y}_0(\hat{\zeta} r), \tag{4.4.30}$$

where $\hat{\zeta}$ is given by Eq. (3.4.6) and B_9, B_{10} are constants of integration to be determined. Since Y_0 is unbounded at the origin $r = 0$, therefore, to obtain a bounded $V^{(1)}$, one should set $B_{10} = 0$ in Eq. (4.4.30). Consequently, we write

$$V^{(1)}(r) = B_9\, \mathrm{J}_0(\hat{\zeta} r), \tag{4.4.31}$$

where B_9 is a constant yet to be determined. Similarly, in the outer region $a < r < L$, where $\theta(r) = 0$, the eigenvalue problem (4.3.15) reduces to

$$V_{rr}^{(2)} + \frac{1}{r} V_r^{(2)} - (E-1)\, V^{(2)} = 0. \tag{4.4.32}$$

The required general solution $V^{(2)}(r)$ satisfying this Bessel equation is

$$V^{(2)}(r) = B_{11}\, \mathrm{J}_0(\hat{\beta} r) + B_{12}\, \mathrm{Y}_0(\hat{\beta} r), \tag{4.4.33}$$

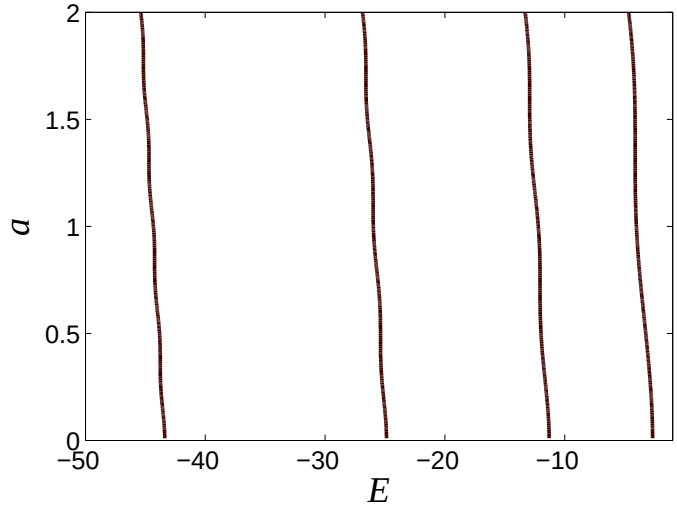

Figure 4.5: Plot of the "continuous" spectrum E of the uniform solution $\widetilde{\phi} = \pi$ as a function of a for $L = 2$, see (4.4.36).

where B_{11} and B_{12} are constants to be determined later, and $\hat{\beta}$ is given by Eq. (2.4.12). Using Eqs. (4.4.31) and (4.4.33), the eigenfunctions corresponding to the "continuous" spectrum of the uniform π solution are described by

$$V(r) = \begin{cases} B_9 \, \mathrm{J}_0(\hat{\zeta} r), & 0 < r < a, \\ B_{11} \, \mathrm{J}_0(\hat{\beta} r) + B_{12} \, \mathrm{Y}_0(\hat{\beta} r), & a < r < L. \end{cases} \tag{4.4.34}$$

This system, upon the application of the continuity and boundary conditions (4.3.16) and (4.3.6), yields a homogeneous system of three equations

$$S_4 \begin{pmatrix} B_9 \\ B_{11} \\ B_{12} \end{pmatrix} = \mathbf{0}, \tag{4.4.35}$$

with coefficient matrix S_4 given by

$$S_4(E) = \begin{bmatrix} \mathrm{J}_0(\hat{\zeta} a) & -\mathrm{J}_0(\hat{\beta} a) & -\mathrm{Y}_0(\hat{\beta} a) \\ -\mathrm{J}_1(\hat{\zeta} a)\hat{\zeta} & \mathrm{J}_1(\hat{\beta} a)\hat{\beta} & \mathrm{Y}_1(\hat{\beta} a)\hat{\beta} \\ 0 & -\mathrm{J}_1(\hat{\beta} L)\hat{\beta} & -\mathrm{Y}_1(\hat{\beta} L)\hat{\beta} \end{bmatrix}. \tag{4.4.36}$$

If one depicts the roots of the necessary condition for a nontrivial solution of the system (4.4.35) in the (E, a) plane, it will be observed that for a particular value of the length of the junction L, E is negative for all a, see Fig. 4.5, where we have taken $L = 2$. Again,

since $E < 0$ so that $\lambda \in i\mathbb{R}$. This implies that there is no unstable eigenvalue in the "continuous" spectrum of the static π background solution.

Rather than casting the system (4.4.35) into a matrix, the "continuous" spectrum can also be found alternatively as follows.

For a nontrivial solution of the system (4.4.35), we assign a nonzero value to the constants B_i's. For instance, we take $B_9 = 1$, and solve the last two equations for B_{10} and B_{11} which yields

$$B_{11} = \frac{\hat{\zeta}\, \mathrm{J}_1(\hat{\zeta}a)\, \mathrm{Y}_1(\hat{\beta}L)}{\hat{\beta}\left[\mathrm{Y}_1(\hat{\beta}L)\, \mathrm{J}_1(\hat{\beta}a) - \mathrm{Y}_1(\hat{\beta}a)\, \mathrm{J}_1(\hat{\beta}L)\right]}, \tag{4.4.37a}$$

$$B_{12} = -\frac{\hat{\zeta}\, \mathrm{J}_1(\hat{\beta}L)\, \mathrm{J}_1(\hat{\zeta}a)}{\hat{\beta}\left[\mathrm{Y}_1(\hat{\beta}L)\, \mathrm{J}_1(\hat{\beta}a) - \mathrm{Y}_1(\hat{\beta}a)\, \mathrm{J}_1(\hat{\beta}L)\right]}. \tag{4.4.37b}$$

Substituting these values into the system (4.4.34), and plotting the bounded solutions of the sysytem in the $(E, a)-$plane gives us the desired "continuous" spectrum of the uniform π background.

4.4.3.2 The "continuous" spectrum of $\widetilde{\phi} = \pi$ in the infinite domain

In the following, we show that, as in the one-dimensional problem in the infinite domain (see Section 2.4.2), in the two-dimensional case also, there is no stability region for the uniform solution $\widetilde{\phi} = \pi$ in the limit $L \to \infty$. This can be deduced from the "continuous" spectrum of the stationary solution π in the limit $L \sim r$ and $r \to \infty$, which is obtained by looking for the bounded solutions of the eigenvalue problem (4.3.15) in the limit $r \to \infty$, i.e. by finding a bounded $V(r)$ that satisfies

$$\lim_{r\to\infty}\left(V_{rr} + \frac{1}{r}V_r\right) = \lim_{r\to\infty}\left[E + \cos(\tilde{\phi} + \theta(r)\right] V. \tag{4.4.38}$$

It is clear from Eq. (4.3.4) that $\theta(r) = 0$ whenever $r \to \infty$. Substituting $\widetilde{\phi} = \pi$ into Eq. (4.4.38), one may write

$$V_{rr} = (E - 1)\, V. \tag{4.4.39}$$

Solutions of Eq. (4.4.39) are bounded if and only if $E < 1$. Hence, a part of the "continuous" spectrum lies on the imaginary axis and the interval on the real axis $-1 < \lambda < 1$. Since λ can take positive real values, from the stability ansatz (4.3.10), it immediately follows that $\tilde{\phi} = \pi$ is unstable everywhere.

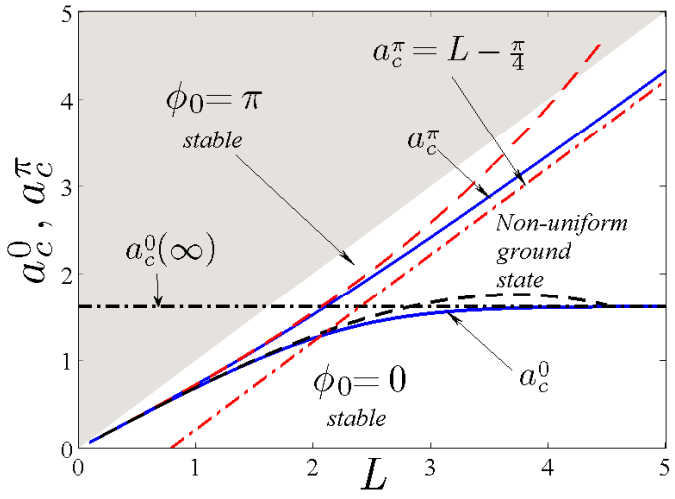

Figure 4.6: Boundary of stability of uniform $\widetilde{\phi} = 0$ and $\widetilde{\phi} = \pi$ solutions (solid lines). The numerics given by Eqs. (4.4.21) and (4.4.45) are shown by solid lines. Asymptotic behavior of a_c^0 and a_c^π given by Eqs. (4.4.22) and (4.4.51) are shown by dash-dotted lines. The approximations (4.4.22) and (4.4.46) are shown in dashed line. The gray region is physically irrelevant ($r > L$).

4.4.3.3 The "discrete" spectrum of $\widetilde{\phi} = \pi$ in the finite domain

To determine the linear stability of the uniform solution $\widetilde{\phi} = \pi$ in the finite domain, we need to find the spectrum that complements the "continuous" spectrum in the infinite domain. We know that such spectrum corresponds to bounded and decaying solutions of the eigenvalue problem (4.3.15) in the inner and outer regions.

Using the method in the previous sections and the properties of the Bessel functions (see Abramowitz and Stegun [81]), bounded and decaying solutions of the eigenvalue problem Eq. (4.3.15) are given by

$$V^{(1)}(r) = B_{13}\,\mathrm{I}_0(\hat{\alpha}r), \quad (r < a), \tag{4.4.40a}$$

$$V^{(2)}(r) = B_{14}\,\mathrm{J}_0(\hat{\beta}r) + B_{15}\,\mathrm{Y}_0(\hat{\beta}r), \quad (r > a), \tag{4.4.40b}$$

where $\hat{\alpha}$ and $\hat{\beta}$ are respectively given by Eqs. (2.4.8) and (2.4.12). The constants B_i, $i = 13, 14, 15$, are determined such that the system (4.4.40) has a nontrivial solution. Application of the continuity and boundary conditions (4.3.16) and (4.3.6) to (4.4.40) leads to a homogenous system of three equations of the form

$$S_5 \begin{pmatrix} B_{13} \\ B_{14} \\ B_{15} \end{pmatrix} = \mathbf{0}, \tag{4.4.41}$$

where

$$S_5(E) = \begin{bmatrix} \mathrm{I}_0(\hat{\alpha}a) & -\mathrm{J}_0(\hat{\beta}a) & -\mathrm{Y}_0(\hat{\beta}a) \\ \mathrm{I}_1(\hat{\alpha}a)\hat{\alpha} & \mathrm{J}_1(\hat{\beta}a)\hat{\beta} & \mathrm{Y}_1(\hat{\beta}a)\hat{\beta} \\ 0 & -\mathrm{J}_1(\hat{\beta}L)\hat{\beta} & -\mathrm{Y}_1(\hat{\beta}L)\hat{\beta} \end{bmatrix}. \tag{4.4.42}$$

The eigenvalue(s) are obtained by setting

$$\det(S_4(E)) = 0. \tag{4.4.43}$$

Figure 4.7 shows an implicit plot of such eigenvalue as a function of the facet length a for $L = 2$. From this figure, we observe that for a given L, there is a critical value of the facet length a, above which E is negative, i.e., the static $\widetilde{\phi} = \pi$ solution is stable, and below which E is positive showing the instability of the solution. This critical value of the facet length is denoted by a_c^{π}. For $L = 2$, we obtain $a_c^{\pi} \approx 1.5247$.

Alternatively, by setting $B_{13} = 1$, and using (4.3.5) and (4.3.6), one may obtain from (4.4.40)

$$B_{14} = \frac{\hat{\alpha}\,\mathrm{I}_1(\hat{\alpha}a)\,\mathrm{Y}_1(\hat{\beta}L)}{\hat{\beta}\left[\mathrm{Y}_1(\hat{\beta}L)\,\mathrm{J}_1(\hat{\beta}a) - \mathrm{Y}_1(\hat{\beta}a)\,\mathrm{J}_1(\hat{\beta}L)\right]}, \tag{4.4.44a}$$

$$B_{15} = -\frac{\hat{\alpha}\,\mathrm{I}_1(\hat{\alpha}a)\,\mathrm{I}_1(\hat{\beta}L)}{\hat{\beta}\left[\mathrm{Y}_1(\hat{\beta}L)\,\mathrm{J}_1(\hat{\beta}a) - \mathrm{Y}_1(\hat{\beta}a)\,\mathrm{J}_1(\hat{\beta}L)\right]}. \tag{4.4.44b}$$

After feeding the values of B_{13}, B_{14} and B_{15} from (4.4.44) into (4.4.40) and plotting the eigenvalues in the (E, a)-plane, we obtain the same "discrete" spectrum as given in Fig. 4.7.

4.4.3.4 The critical facet length a_c^{π} as a function of length L

The "discrete" spectrum of the static π-solution (see Fig. 4.7) shows that at the critical value a_c^{π} of facet length a, the spectral parameter E becomes zero. A relation between a_c^{π} and the length L can be found by substituting $E = 0$ and $a = a_c^{\pi}$ into the condition (4.4.43) and simplifying the resultant expression to obtain

$$\frac{\mathrm{I}_0(a_c^{\pi})}{\mathrm{I}_1(a_c^{\pi})} = \frac{\mathrm{Y}_1(L)\,\mathrm{J}_0(a_c^{\pi}) + \mathrm{J}_1(L)\,\mathrm{Y}_0(a_c^{\pi})}{\mathrm{J}_1(L)\,\mathrm{Y}_1(a_c^{\pi}) - \mathrm{J}_1(a_c^{\pi})\,\mathrm{Y}_1(L)}, \tag{4.4.45}$$

This gives an implicit relation between a_c^{π} and L for a general L. This relation gives a boundary of the region of stability instability of the uniform π background is depicted by the upper solid line in Fig. 4.6.

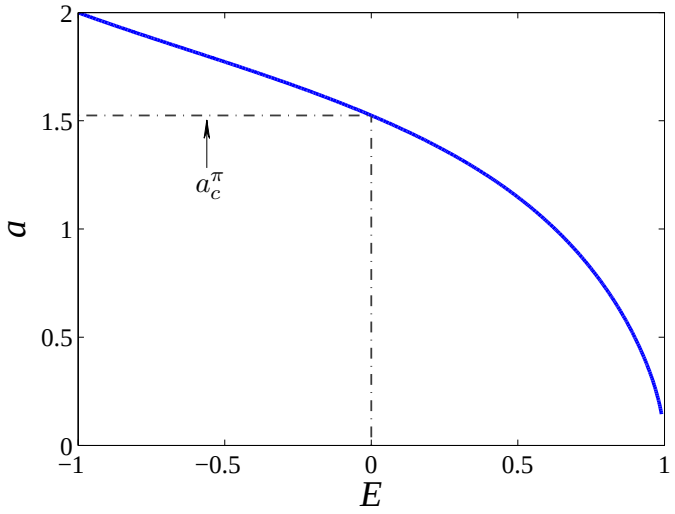

Figure 4.7: Plot of the discrete spectrum of the uniform solution $\widetilde{\phi} = \pi$ as a function of a for $L = 2$.

In the particular case where the length L of the π junction is small enough, i.e., when $L \to 0$, a Taylor expansion of the implicit relation (4.4.45) about L and ignoring the smaller terms, gives

$$a_c^\pi = \frac{L}{\sqrt{2}} + \frac{(2\ln 2 - 1)}{16\sqrt{2}} L^3 + \mathcal{O}(L^5), \tag{4.4.46}$$

which explicitly expresses a_c^π in terms of the length L. This explicit relation is depicted by the upper dashed line in Fig. 4.6. We observe that for L close to zero relations given by Eqs. (4.4.45) and (4.4.46) are in a close agreement.

4.4.3.5 The case when $L \gg 1$

Next, we consider the case when L is sufficiently large. From the discussion in the previous sections, it is clear that, when L is small and the discontinuity point a is close to 0 (L), the uniform solution $\widetilde{\phi} = 0$ (π) is stable.

In the following, we want to find the value of a where static solution π changes the stability in the case when $a \sim L$ and $L \gg 1$. To obtain the asymptotic boundary for the stability of π, we define a new radial variable $\widetilde{r}$ by

$$L - r = \widetilde{r}. \tag{4.4.47}$$

With this ansatz and using the chain rule for differentiation, our static sine-Gordon

model (4.3.9), and the eigenvalue problem (4.3.15) respectively becomes

$$\phi_{\widetilde{r}\widetilde{r}} - \frac{1}{L-\widetilde{r}}\phi_{\widetilde{r}} = \sin\left[\phi + \theta(L-\widetilde{r})\right] - \gamma, \tag{4.4.48a}$$

$$V_{\widetilde{r}\widetilde{r}} - \frac{1}{L-\widetilde{r}}V_{\widetilde{r}} - \frac{q^2 V}{(L-\widetilde{r})^2} = \left[E + \cos(\widetilde{\phi} + \theta(L-\widetilde{r}))\right] V, \tag{4.4.48b}$$

where $0 < \widetilde{r} < L$. The Josephson phase (4.3.4) in terms of the new variable $\widetilde{r}$ can be written as

$$\theta(\widetilde{r}) = \begin{cases} 0, & 0 < \widetilde{r} < a, \\ \pi, & a < \widetilde{r} < L. \end{cases} \tag{4.4.49}$$

Considering the region $0 < \widetilde{r} \ll L$, where $\theta(\widetilde{r}) = 0$, then for $L \gg 1$, the system (4.4.48) takes the form

$$\phi_{\widetilde{r}\widetilde{r}} = \sin\left[\phi + \theta(L-\widetilde{r})\right] - \gamma, \tag{4.4.50a}$$

$$V_{\widetilde{r}\widetilde{r}} = \left[E + \cos(\widetilde{\phi} + \theta(L-\widetilde{r}))\right] V. \tag{4.4.50b}$$

By applying the continuity and boundary conditions (4.3.16) and (4.3.17) for $\widetilde{r}$, the "discrete" spectrum reduces to the one-dimensional discrete spectrum of the uniform zero background in the infinite domain (see Section 2.4.1.2), where the critical a is $\pi/4$. Hence, the critical facet length for π solution in the limit $L \gg 1$ for the new radial parameter $\widetilde{r}$ is $\pi/4$. Consequently, the critical facet length $a_c^{\pi}(L)$ for the parameter r, by the help of Eq. (4.4.47), becomes

$$a_c^{\pi}(L) \approx L - \frac{\pi}{4}. \tag{4.4.51}$$

The asymptotic behavior of the critical facet length $a_c^{\pi}(L)$, given by Eq. (4.4.51), is presented by dash-dotted line in Fig. 4.6.

From the existence analysis of the uniform solutions, it is clear that, as in the finite one dimensional 0-π-0 long Josephson junctions, there is a critical a_c for both the uniform solutions beyond which their stability changes. Equations (4.4.21) and (4.4.45) give stability boundaries of both uniform solutions. In the region, where both uniform solutions are unstable, one expects a nonuniform ground state. This region of (in)stability is depicted in Fig. 4.6.

4.5 Ground state in the instability region of uniform solutions

In this section, we discuss the existence and the stability of the ground states of the Josephson junction when both uniform solutions are unstable.

It is important to note that from the case of one-dimensional long 0-π Josephson junctions, the bifurcation of the non-uniform ground states from the uniform solutions is supercritical (see Fig. 3.4). One would therefore expect a similar situation in the present case. Hence, at the critical values a_c the nonuniform ground states would satisfy the linearization of the governing equation (4.3.8) about the uniform solutions, which is the linear eigenvalue problem (4.3.15) at $E = 0$.

On the other hand, from the analysis of the uniform solutions, the critical eigenvalue of the solutions corresponds to a $\tilde{\theta}$- independent eigenfunction (see Fig. 7.1 and Section 7.4 in the Appendix). This then informs us that the non-uniform ground state should be $\widetilde{\theta}$-independent i.e., Eq. (4.3.9), which implies that in $\phi_{\tilde{\theta}} = 0$ in Eq. (4.3.8).

We study the ground states perturbatively using Euler-Lagrange approximations when a is in the vicinity of the critical facet length a_c^0 or a_c^π. For this, let us suppose $B(t)V(r)$, where $B(t) \ll 1$, be a small perturbation of the uniform solution $\widetilde{\phi}$, where $V(r)$ is an eigenfunction corresponding to the critical eigenvalue λ of a constant background $\widetilde{\phi}$ with a phase jump at the discontinuity point $r = a$. That is, to construct an approximate solution in the instability regions for the uniform solutions, we substitute

$$\phi(r,t) = \widetilde{\phi} + B(t)V(r), \tag{4.5.1}$$

into the $\tilde{\theta}$-independent Eq. (4.3.9) and obtain

$$rV_{rr} + V_r - r\cos\left[\widetilde{\phi} + \theta(r)\right] V = 0. \tag{4.5.2}$$

In the following, we deal with the case of each uniform solution separately.

4.5.1 Limiting solutions in the region $0 < a - a_c^0 \ll 1$

First we discuss the ground state solution bifurcating from the uniform solution $\widetilde{\phi} = 0$ in the instability region where a is close to a_c^0. To do so, we use a Hamiltonian approach.

4.5.1.1 Existence analysis

Consider the region $0 < r < a$, where $\theta(r) = \pi$. If $V^{(1)}(r)$ is a bounded solution of Eq. (4.5.2) in this region, then we find that

$$V^{(1)}(r) = B_{16}\,\mathrm{J}_0(r). \tag{4.5.3}$$

Similarly in the outer region, $a < r < L$, and the solution of (4.5.2) is given by

$$V^2(r) = B_{17}\,\mathrm{I}_0(r) + B_{18}\,\mathrm{K}_0(r), \tag{4.5.4}$$

where B_{16}, B_{17}, B_{18} are constants to be determined by applying the continuity and boundary conditions. Since $E = 0$, $a = a_c^0$. Thus by the help of conditions(4.3.16) and (4.3.17) from Eqs. (4.5.3) and (4.5.4), we obtain a system of three homogenous equations in the form

$$S_6 \mathbb{U} = \mathbf{0}, \tag{4.5.5}$$

where $\mathbb{U} = (B_{16}, B_{17}, B_{18})^T$ and the coefficient matrix S_6 is

$$S_6(E) = \begin{bmatrix} \mathrm{J}_0(a_c^0) & -\mathrm{I}_0(a_c^0) & -\mathrm{K}_0(a_c^0) \\ \mathrm{J}_1(a_c^0) & \mathrm{I}_1(a_c^0) & \mathrm{K}_1(a_c^0) \\ 0 & \mathrm{I}_1(L) & -\mathrm{K}_1(L) \end{bmatrix}. \tag{4.5.6}$$

The system (4.5.5) has a nontrivial solution if

$$\det(S_6) = 0, \tag{4.5.7}$$

which occurs when a_c^0 is given by Eq. (4.4.21). We define a solution vector by $\mathbb{U} = (B_{16}\ \ B_{17}\ \ B_{18})$, taking $B_{16} = 1$, whence

$$B_{17} = \frac{\mathrm{J}_1(a_c^0)\mathrm{K}_1(L)}{\mathrm{I}_1(L)\mathrm{K}_1(a_c^0) - \mathrm{I}_1(a_c^0)\mathrm{K}_1(L)}, \tag{4.5.8a}$$

$$B_{18} = \frac{\mathrm{I}_1(L)\,\mathrm{J}_1(a_c^0)}{\mathrm{I}_1(L)\mathrm{K}_1(a_c^0) - \mathrm{I}_1(a_c^0)\mathrm{K}_1(L)}. \tag{4.5.8b}$$

At the critical value of the facet length $a = a_c^0$, any multiple of $\mathbb{U}$ is also a solution of Eq. (4.5.5); such solutions only hold at $a = a_c^0$.

Now, for a close to a_c^0, we approximate $\phi(r,t)$ by

$$\phi(r,t) = B(t) \begin{cases} \mathrm{J}_0(r), & 0 < r < a, \\ B_{17}\,\mathrm{I}_0(r) + B_{18}\,\mathrm{K}_0(r), & a < r < L, \end{cases} \tag{4.5.9}$$

where the amplitude $B(t)$ will be determined by using variational calculus. When $a \neq a_c^0$, the equation (4.5.5) is not satisfied. Hence, the function (4.5.9) does not satisfy the continuity conditions Eq. (4.3.16) for $a > a_c^0$, and is therefore, termed an *approximate* solution. Hence, we expect it to give a good approximation when a is close to a_c^0 only.

Using the ansatz (4.5.9), the Lagrangian, $\mathcal{L}$ (4.3.7), becomes

$$\mathcal{L} = T - U, \tag{4.5.10}$$

where the kinetic energy T and the potential energy U of the junction are respectively given by

$$T = \frac{1}{2}\int_0^{2\pi}\int_0^L \phi_t^2\ r dr d\tilde{\theta}, \quad U = \int_0^{2\pi}\int_0^L \left(\frac{1}{2}\phi_r^2 + 1 - \cos\left[\phi + \theta(r)\right] + \gamma\phi\right)\ r dr d\tilde{\theta}.$$

These energies are respectively given by

$$T = (B_t)^2(Q_1+Q_2), \tag{4.5.11a}$$

$$U = a^2-\gamma(a\,\mathrm{J}_1(a)+M_7)B+(M_1-M_2+M_4+M_5)B^2 +(M_3-M_6)B^4, \tag{4.5.11b}$$

with the subscript denoting a derivative with respect to t and

$$Q_1 = \frac{a^2}{4}\left(\mathrm{J}_0^2(a)+\mathrm{J}_1^2(a)\right),$$

$$Q_2 = \frac{\mathrm{J}_1^2(a_c^0)}{2(\mathrm{I}_1(L)\,\mathrm{K}_1(a_c^0)-\mathrm{K}_1(L)\mathrm{I}_1^2(a_c^0)}\int_a^L\left(\mathrm{K}_1(L)\,\mathrm{I}_0(r)+\mathrm{I}_1(L)\,\mathrm{K}_0(r)\right)^2 rdr,$$

$$M_1 = \frac{a}{4}\left(a\,\mathrm{J}_1^2(a)-2\,\mathrm{J}_0(a)\,\mathrm{J}_1(a)+a\,\mathrm{J}_1^2(\mathrm{a})\right),$$

$$M_2 = \frac{a^2}{4}\left(\mathrm{J}_0^2(a)+\mathrm{J}_1^2(a)\right), \qquad M_3=\frac{1}{24}\int_0^a \mathrm{J}_0^4(r)rdr,$$

$$M_4 = \frac{\mathrm{J}_1^2\left(a_c^0\right)}{2\left(-\mathrm{I}_1\left(L\right)\mathrm{K}_1\left(a_c^0\right)+\mathrm{I}_1\left(a_c^0\right)\mathrm{K}_1\left(L\right)\right)^2}\int_a^L r\left(-\mathrm{K}_1\left(L\right)\mathrm{I}_1\left(r\right)+\mathrm{I}_1\left(L\right)\mathrm{K}_1\left(r\right)\right)^2 dr,$$

$$M_5 = \frac{1}{2}\int_a^L \eta^2 rdr, \quad M_6=\frac{1}{24}\int_a^L \eta^4 rdr, \quad \eta=\frac{\mathrm{J}_1(a_c^0)\left(\mathrm{K}_1(L)\,\mathrm{I}_0(r)+\mathrm{I}_1(L)\,\mathrm{K}_0(r)\right)}{\mathrm{I}_1(L)\,\mathrm{K}_1(a_c^0)-\mathrm{I}_1(a_c^0)\,\mathrm{K}_1(L)},$$

$$M_7 = \frac{\mathrm{J}_1(a_{cr,0})}{\mathrm{I}_1(L)\mathrm{K}_1(a_{cr,0})-\mathrm{I}_1(a_{cr,0})\mathrm{K}_1(L)}\Big\{(\mathrm{I}_1(L)(a(2\mathrm{K}_1(a)-\mathrm{K}_0(a)\mathrm{I}_1(a)-\mathrm{K}_1(a)\mathrm{I}_0(a)) +\mathrm{K}_1(L)(\mathrm{I}_1(L)\mathrm{I}_0(L)L-2a\mathrm{I}_1(a))+\mathrm{I}_0^2(L)\mathrm{K}_0(L)L)\Big\}.$$

By substituting the Lagrangian $\mathcal{L}$ (4.5.10) into the Euler-Lagrange equation (3.6.44), we obtain

$$B_{tt} = f(B), \tag{4.5.12}$$

where

$$f(B)=\frac{\gamma(a\,\mathrm{J}_1(a)+M_7)-2(M_1-M_2+M_4+M_5)B+4(M_6-M_3)B^3}{2(Q_1+Q_2)}. \tag{4.5.13}$$

The fixed points of this equation are given by setting its right hand side to zero, or equivalently by $U_B=0$.

4.5.1.2 The undriven case

First we study the roots of Eq. (4.5.13) in the absence of the forcing term γ. In this case, the roots of Eq. (4.5.13) are given by

$$B^{(1,2)}=\pm\sqrt{\frac{M_1-M_2+M_4+M_5}{2(M_6-M_3)}},\ B^{(3)}=0. \tag{4.5.14}$$

It can be verified that the potential energy U of the junction is locally minimized by $B^{(1)}$ and $B^{(2)}$. Hence, we obtain an approximation to the nonuniform ground state in the instability region of the constant zero solution. With the help of Eqs. (4.5.8), (4.5.14) and

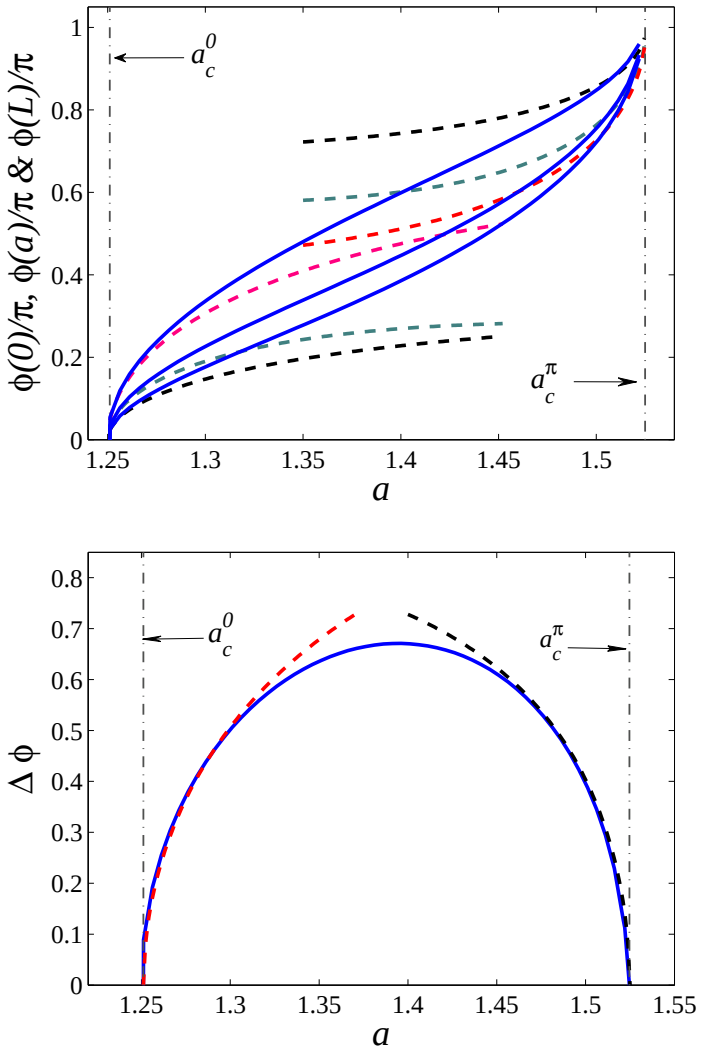

Figure 4.8: (Top panel) Comparison of the numerically obtained ground state phases $\phi(0)$, $\phi(a)$ and $\phi(L)$ (continuous lines) and analytical approximations as $a \to a_c^0$ (see Eqs. (4.5.9) and (4.5.14)), three lowest dotted lines, as $a \to a_c^\pi$ (see Eqs. (4.5.30) and (4.5.35)) ,three upper dotted lines, for $\gamma = 0$ and $L = 2$. Bottom panel: the difference of $\phi(L) - \phi(0)$ obtained numerically (solid) and analytically (dashed) in the vicinity of a_c^0 and a_c^π.

the system (4.5.9), we plot the nonuniform ground state at the points $r = 0$, $r = a$ and $r = L$ as a function of the facet length a, where a varies in the absence of an applied bias current, as shown in the top panel of Fig. 4.8.Good agreement can clearly be noticed when a is close to a_c^0. One can see that as $a \to a_c^0$, the whole solution $\widetilde{\phi}(r)$ tends to zero.

Thus $\phi(0)$, $\phi(a)$ and $\phi(L)$ tend to zero.

In the lower panel of the Figure 4.8, we plot the normalized magnetic flux, represented by $\Delta\phi = \phi(L) - \phi(0)$ as a function of a. It can be clearly observed that the magnetic flux is maximum in the center of the instability region and is zero for $a \leq a_c^0$ and $a \geq a_c^\pi$.

Similarly by taking $a = 1.3$ and $L = 2$, and substituting B from Eq. (4.5.14) and (4.5.8) into the nonuniform ground state solutions given by (4.5.9), we plot $\phi(r)$ against r in Fig 4.9. The top panel shows the profile of $\phi(r)$, in the one-dimensional representation, as a function of the radial parameter r, given by the system (4.5.9). The dashed lines represent the approximation to ground state solution in the instability region of the uniform solutions, given by Eq. (4.5.9) and the solid line gives the corresponding numerical counterpart. The lower panel of the same figure shows the plot of the original two-dimensional problem.

4.5.1.3 The driven case

In this subsection, we analyse the case of nonzero bias current. The general solutions to the cubic equation Eq. (4.5.13) in the presence of the forcing term ($0 < |\gamma| \ll 1$) can be found by using Nickall's method [102] which yields

$$B^{(n)} = 2\delta \cos\left(\Theta + (2n-1)\frac{\pi}{3}\right), \quad n = 1, 2, 3, \tag{4.5.15}$$

where

$$\begin{aligned}
\delta &= \sqrt{\frac{M_1 - M_2 + M_4 + M_5}{6(M_6 - M_3)}}, \\
h &= -\left(\frac{2}{3}\right)^{3/2} \frac{(M_1 - M_2 + M_4 + M_5)^{3/2}}{(M_6 - M_3)^{1/2}}, \\
\Theta &= \frac{1}{3}\arccos\left(-\frac{\gamma(a\,\mathrm{J}_1(a) + M_7)}{h}\right).
\end{aligned}$$

By introducing the roots (4.5.15) to the system (4.5.9), we are able to study the behaviour of the profile of the Josephson phase $\phi(r,t)$ in terms of the applied bias current γ for fixed values of the radial variable r, the facet length a and the size L of the π-junction. This is represented by the lower dashed lines of Fig. 4.10, where we have taken $a = 1.3$, $L = 2$ and $r = 0$. The analytical results are compared with the corresponding numerics (solid lines) where a good agreement is observed for ϕ near 0 and ϕ near π. Starting from the point where $\phi(0) = 0$ and $\gamma = 0$, as γ increases, one can see that there is a critical value of the current γ at which two solutions merge and disap-

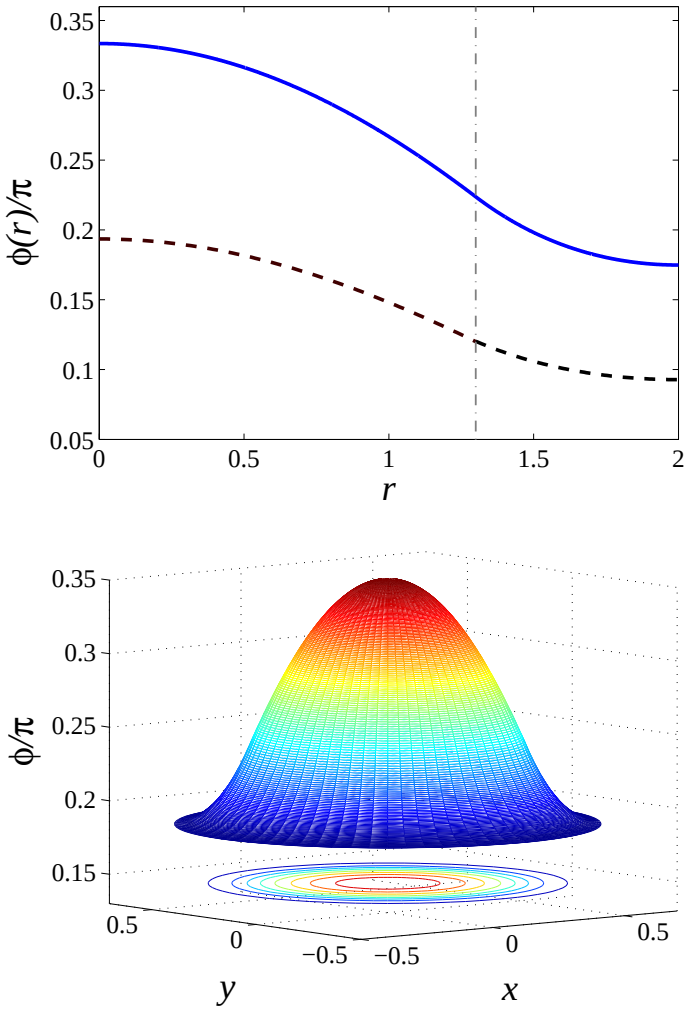

Figure 4.9: Top panel shows the numerically obtained ground state $\phi(r)$ for $L = 2$ and $a = 1.3$ in the 1D representation (solid) and its approximation (dashed). Shown in the bottom panel is the corresponding profile in the original two-dimensional problem.

pear in a saddle-node bifurcation. In the following, we denote this critical bias current by γ_c^0, which can be calculated as follows.

Differentiating Eq. (4.5.13) with respect to B and solving the resultant equation for the stationary points B, we obtain

$$B_{c_1,c_2} = \pm\sqrt{\frac{M_1 - M_2 + M_4 + M_5}{6(M_6 - M_3)}}. \tag{4.5.16}$$

These values of B locally minimize the potential energy U of the junction. The critical bias current γ_c^0 is then given by the inverse of $f(B)$ (4.5.13) evaluated at B_{c_1,c_2} (4.5.16),

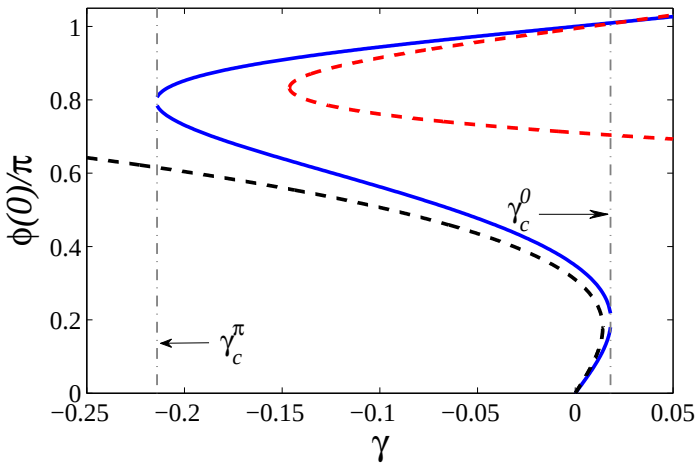

Figure 4.10: Plot of $\phi(0)$ as a function of γ, calculated numerically (solid) and approximated analytically (dashed) as given by Eq. (4.5.15) for both 0 and π uniform solutions . Here, we have taken $a = 1.3$ and $L = 2$.

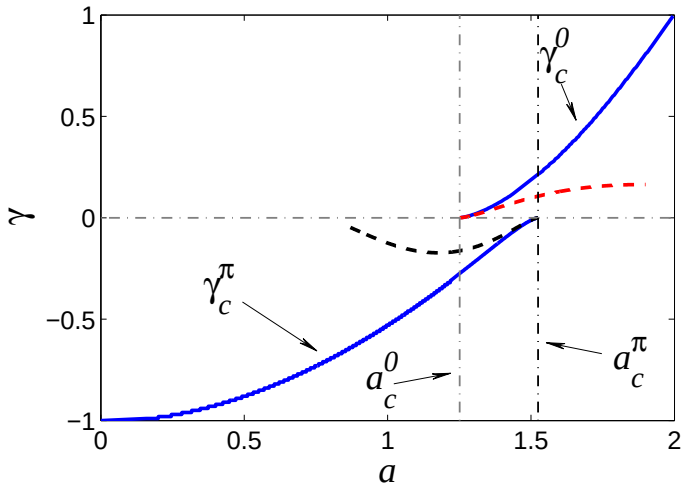

Figure 4.11: Comparisons of our analytical approximation of γ_c^0 given by Eq. (4.5.17) (dashed line) and γ_c^π given by Eq. (4.5.37) (dash-dotted line) as a function of a and the numerically obtained results, in both cases, $L = 2$.

i.e.

$$\gamma_c^0 = \pm \frac{4(M_6 - M_3)B_c^3 - 2\,(M_1 - M_2 + M_4 + M_5)\,B_c}{a\,\mathrm{J}_1(a) + M_7}. \tag{4.5.17}$$

Fig. 4.11 shows the profile of the approximation (upper dashed line) to the critical bias current γ_c^0, given by (4.5.17) as a function of the facet length a, where we have taken $L = 2$. Note that γ_c^0 is zero when the facet length a is less than or equal to a_c^0. For $a \geq a_c^0$ and close to a_c^0, the analytically obtained γ_c^0 is sufficiently close to its corresponding

numerical result (solid line).

4.5.1.4 Stability analysis

Next, we calculate the critical eigenfrequency of the non-uniform ground state. As in the analysis of uniform solutions, the critical eigenvalue of our nonuniform ground states corresponds to the case $q = 0$ (see Fig. 7.1).

To find the critical eigenvalue of the ground state analytically, we follow the steps discussed in Section 5.4. With $B^{(n)}$ given by (4.5.15), we substitute

$$B = B^{(n)} + \epsilon\tilde{B}, \quad \text{where} \quad |\epsilon| \ll 1, \tag{4.5.18}$$

into Eq. (4.5.12) and neglect the higher order terms in ϵ to obtain

$$\frac{d^2\tilde{B}}{dt^2} = -\frac{6(M_3-M_6)\left(B^{(n)}\right)^2+(M_1-M_2+M_4+M_5)}{Q_1+Q_2}\tilde{B}.$$

The critical eigenvalue of the ground state is therefore approximately given by

$$E = -\frac{6(M_3-M_6)\left(B^{(n)}\right)^2+(M_1-M_2+M_4+M_5)}{Q_1+Q_2}, \tag{4.5.19}$$

which is the negative of the square of the oscillation frequency of $\tilde{B}(t)$.

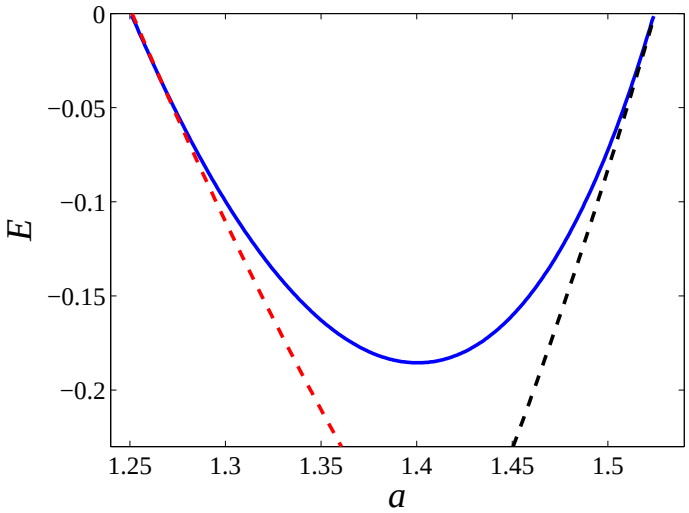

Figure 4.12: The critical eigenvalue at $\gamma = 0$ obtained numerically (solid line) and its approximations in the limits $a \to a_c^0$ (4.5.19) and $a \to a_c^\pi$ (4.5.38) (dashed lines). Here, $L = 2$.

A plot of the critical eigenvalue, given by (4.5.19), as a function of a for the case of $\gamma = 0$ is shown by the left dashed line in Fig. 4.12. The approximation is in close agreement with the numerical result (solid line), when the facet length is close to a_c^0.

The analytically obtained critical eigenvalues (4.5.19), corresponding to the stationary solution $\widetilde{\phi} = 0$, as a function of the applied bias current are presented by the right dashed line in Fig. 4.13. We again note that for the chosen parameter values, a good agreement between our approximation and numerical results is observed when a is close to a_c^0.

As in the case of the one-dimensional 0-π-0 finite Josephson junction, it can be observed from Fig. 4.13 also, that the critical eigenvalue is obtained at the point where the applied bias current is nonzero. In other words, the stability of the nonuniform ground state can be strengthened by applying an external current.

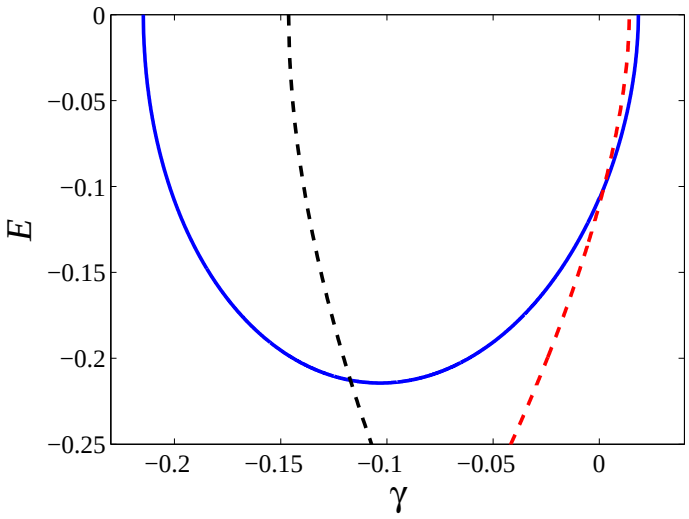

Figure 4.13: Solid lines show the bias-dependence of the critical eigenvalue $E_0(\gamma)$ calculated numerically for $a = 1.3$ and $L = 2$. Approximations about a_c^0 given by Eqs. (4.5.19) (right dashed line) and about a_c^π given by (4.5.38) (left dashed line) are shown by red and black dashed lines, respectively.

4.5.2 Limiting solutions in the instability region close to a_c^0 in the infinite domain

In the limit $L \to \infty$, a similar calculations can be performed as in the case of finite domain discussed above. Only in this case, for a close to $a_c^0(\infty)$, we approximate $\phi(r)$

by Eq. (4.5.1), where (see also Eq. (4.4.25)

$$V(r) = B \begin{cases} \mathrm{J}_0(r), & 0 < r < a, \\ \dfrac{\mathrm{J}_0\left(a_c^0(\infty)\right)}{\mathrm{K}_0\left(a_c^0(\infty)\right)} \mathrm{K}_0(r), & a < r < \infty. \end{cases} \tag{4.5.20}$$

This system is obtained by applying the continuity conditions (4.3.5) to the bounded solution given by (4.4.25). To obtain a nontrivial solution, the coefficient of the bounded solution in the inner region is fixed to unity and the coefficient of the bounded solution in the outer region is calculated. Again, we note that the solution given by the system (4.5.20) is approximate, as the solution vector is valid only at the point $a = a_c^0(\infty)$.

For an infinitely large π junction, from the Lagrangian (4.3.7) we obtain (4.5.10), with the kinetic and potential energies of the junction, respectively given by

$$T = \dot{B}^2 \left(Q_3 + Q_4\right), \tag{4.5.21}$$

$$U = a^2 - \gamma \left(a \mathrm{J}_1(a) + M_{14}\right) B + \left(M_8 - M_9 + M_{11} + M_{12}\right) B^2 + \left(M_{10} - M_{13}\right) B^4, \tag{4.5.22}$$

where we have defined

$$\begin{aligned}
Q_3 &= \frac{a^2}{2}\left(\left(\mathrm{J}_0(a)\right)^2 + \left(\mathrm{J}_1(a)\right)^2\right), \\
Q_4 &= \frac{a^2}{2}\frac{\left(-\left(\mathrm{K}_0(a)\right)^2 + \left(\mathrm{K}_1(a)\right)^2\right)\left(\mathrm{J}_0(a)\right)^2}{\left(\mathrm{K}_0(a)\right)^2}, \\
M_8 &= \frac{a}{4}\left(a\left(\mathrm{J}_0(a)\right)^2 - 2\mathrm{J}_0(a)\mathrm{J}_1(a) + a\left(\mathrm{J}_1(a)\right)^2\right), \\
M_9 &= \frac{a^2}{4}\left(\left(\mathrm{J}_0(a)\right)^2 + \left(\mathrm{J}_1(a)\right)^2\right), \qquad M_{10} = \frac{1}{24}\int_0^a \left(\mathrm{J}_0(r)\right)^4 r dr, \\
M_{11} &= -\frac{a\left(\mathrm{J}_0(a)\right)^2}{4}\eta_1, \quad \eta_1 = \frac{a\left(\mathrm{K}_1(a)\right)^2 - a\left(\mathrm{K}_0(a)\right)^2 - 2\mathrm{K}_1(a)\mathrm{K}_0(a)}{\left(\mathrm{K}_0(a)\right)^2}, \\
M_{12} &= \frac{a^2}{4}\frac{\left(-\left(\mathrm{K}_0(a)\right)^2 + \left(\mathrm{K}_1(a)\right)^2\right)\left(\mathrm{J}_0(a)\right)^2}{\left(\mathrm{K}_0(a)\right)^2}, \\
M_{13} &= \frac{1}{24}\int_a^\infty \frac{r\left(\mathrm{J}_0(a)\right)^4\left(\mathrm{K}_0(r)\right)^4}{\left(\mathrm{K}_0(a)\right)^4} dr, \qquad M_{14} = \frac{\mathrm{J}_0(a) a \mathrm{K}_1(a)}{\mathrm{K}_0(a)}.
\end{aligned}$$

Applying the Euler-Lagrange equation (3.6.44) to the effective Lagrangian (4.5.10) above yields

$$\frac{d^2B}{dt^2} = h(B), \tag{4.5.23}$$

where

$$h(B) = \frac{4\left(M_{10} - M_{13}\right)B^3 + 2\left(M_8 - M_9 + M_{11} + M_{12}\right)B - \gamma\left(a\mathrm{J}(1,a) + M_{14}\right)}{2(Q_3 + Q_4)}. \tag{4.5.24}$$

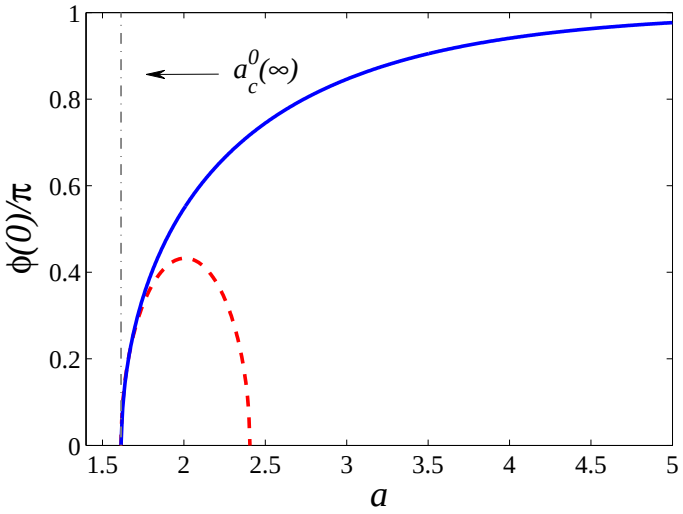

Figure 4.14: Comparison between the analytically obtained ground state solution at the point $r = 0$, given by Eqs. (4.5.20) and (4.5.25) and the corresponding numerical simulations, for the case of $L \to \infty$.

4.5.2.1 The undriven case

First we consider the case when $\gamma = 0$. In this case, the three roots of Eq. (4.5.24) are

$$B^{(1)} = 0,\ B^{(2,3)} = \pm\sqrt{\frac{M_8 - M_9 + M_{11} + M_{12}}{2\,(M_{13} - M_{10})}}. \tag{4.5.25}$$

Again, it can be verified that the roots $B^{(2)}$ or $B^{(3)}$ minimise the potential energy U. We substitute one of the roots $B^{(i)}$, $i = 2, 3$ into the system (4.5.20) and plot it as a function of the parameter a. In Fig. 4.14, we plot the analytically obtained $\phi(0)$, with the help of Eqs. (4.5.20) and (4.5.25), as a function of a and compare it with the numerically obtained nonuniform ground state. For a close to $a_c^0(\infty)$, the approximation and numerics are close. From the same figure, as $L \to \infty$, the numerically obtained $\phi(0)$ asymptotically approaches π.

4.5.2.2 The driven case

Now, we study the effect of the external current (γ) on the nonuniform ground state. When $\gamma \neq 0$, the stationary points of the equation (4.5.24) can be calculated from

$h(B) = 0$ which, with values

$$\begin{aligned}
\delta &= \sqrt{\frac{M_8 - M_9 + M_{11} + M_{12}}{6\,(M_{13} - M_{10})}}, \\
h &= -\left(\frac{2}{3}\right)^{3/2} \frac{(M_8 - M_9 + M_{11} + M_{12})^{3/2}}{(M_{13} - M_{10})^{1/2}}, \\
\Theta &= \frac{1}{3} \arccos\left(\frac{-(\gamma\,(a\,\mathrm{J}_1(a) + M_{20}))}{h}\right),
\end{aligned}$$

are explicitly given by (4.5.15) (see Nickalls [102]).

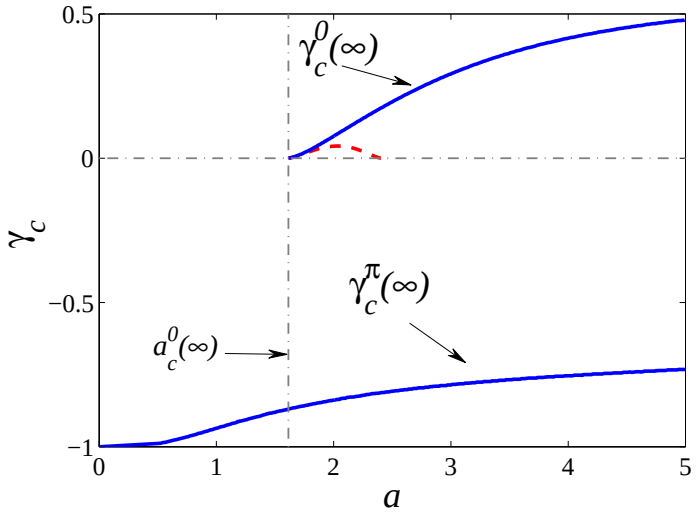

Figure 4.15: Plot of the analytically obtained critical bias current γ_c^0, given by Eq. (4.5.26) (dashed line)for $L \to \infty$. The upper solid line represents the same obtained from a numerical calculation. The lower solid line is the numerically obtained γ_c^π.

The critical bias current $\gamma_c^0(\infty)$ can also be calculated in a fashion similar to the finite domain case as

$$\gamma(B_c) = \frac{4\,(M_{10} - M_{13})\,B_c^3 + 2\,(M_8 - M_9 + M_{11} + M_{12})\,B_c}{(a\,\mathrm{J}_1(a) + M_{14})}, \tag{4.5.26}$$

where B_c is a root of $h'(B_c) = 0$, i.e.

$$B_c = \pm\sqrt{\frac{M_8 - M_9 + M_{11} + M_{12}}{6\,(M_{13} - M_{10})}}. \tag{4.5.27}$$

Plot of $\gamma_c^0(\infty)$, given by Eq. (4.5.26), as a function of the facet length a is depicted in Fig. 4.15 (dashed line), where it is observed that at the critical facet length $a_c^0(\infty)$, the critical current is zero. In the same figure, the numerically obtained $\gamma_c^0(\infty)$ is presented by the solid line.

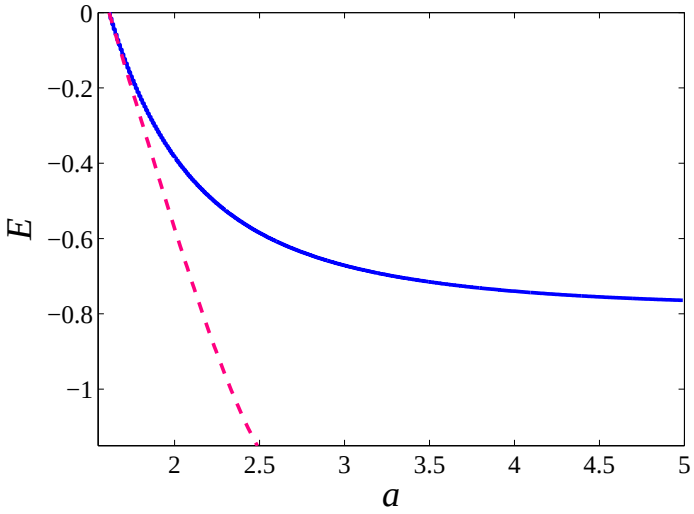

Figure 4.16: A comparison of analytically obtained critical eigenvalues (4.5.29) versus the facet length a for the case of $L \to \infty$ and the corresponding numerical counterpart (solid line). Here, we have considered the undriven case ($\gamma = 0$).

4.5.2.3 Stability analysis in the infinite domain

In order to study the stability of the smallest eigenvalue of the nonuniform ground state, we follow the method discussed in finite domain (see Section 4.5.1.4). By substituting (4.5.18) into Eq. (4.5.24) and discarding smaller terms, a simple analysis leads to

$$\frac{d^2\widetilde{B}}{dt^2} = -\frac{6\left(M_{13}-M_{10}\right)\left(B^{(n)}\right)^2-\left(M_8-M_9+M_{11}+M_{12}\right)}{\left(Q_3+Q_4\right)}\widetilde{B}. \tag{4.5.28}$$

From this, it can be calculated that the eigenfrequency is, approximately given by

$$E = -\frac{6\left(M_{13}-M_{10}\right)\left(B^{(n)}\right)^2-\left(M_8-M_9+M_{11}+M_{12}\right)}{\left(Q_3+Q_4\right)}. \tag{4.5.29}$$

The approximate critical eigenvalue, given by Eq. (4.5.29), as function of a is depicted in Fig. 4.16 for the instability region$a_c^0(\infty) \leq a$. The analytical approximation to the critical eigenvalue given by (4.5.29) are close to the numerical solution when a is close to its critical value $a_c^0(\infty)$.

A comparison between the approximation to E and the numerical value in the presence of an applied bias current is shown in Fig. 4.17, where we note again that the smallest E is attained at the point where $\gamma \neq 0$.

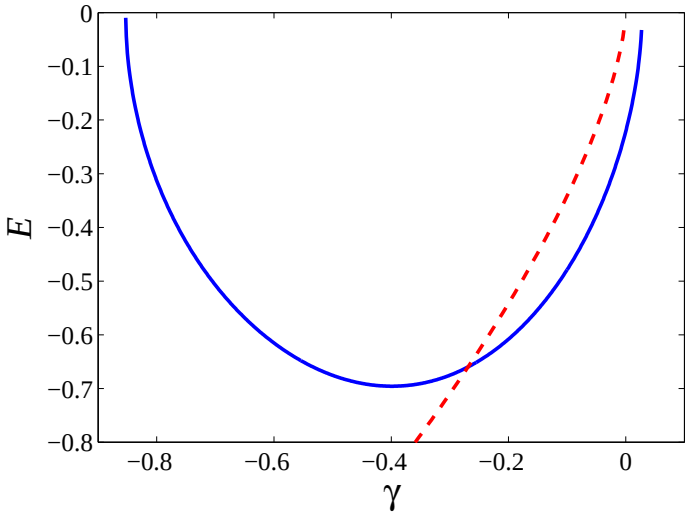

Figure 4.17: Comparison of the critical eigenvalues, analytically given by Eq. (4.5.29) (dashed line) and the numerical calculation (solid line), for the case of $L \to \infty$.

4.5.3 Nonuniform ground state solution in the region $a_c^\pi - a \ll 1$

We again consider the case of the finite domain and investigate the nonuniform ground state in the instability region, where the facet length varies close to the critical π-facet length a_c^π. We discuss the same problem and follow the method adopted for the investigation of the nonuniform ground states in a small instability region close to a_c^0. In the following we mention the main results.

4.5.3.1 Existence analysis

For a close to a_c^π, $\phi(r)$, with the help of (4.5.1), can be approximated by

$$\phi(r,t) = \pi - B(t) \begin{cases} B_{20}\, \mathrm{I}_0(r), & 0 < r < a, \\ B_{21}\, \mathrm{J}_0(r) + B_{22}\, \mathrm{Y}_0(r), & a < r < L, \end{cases} \tag{4.5.30}$$

where again, $B(t)$ will be calculated using variational calculus.

Setting $B_{20} = 1$, the constants B_{21} and B_{22} are then given by

$$B_{21} = \frac{\mathrm{I}_1\left(a_c^\pi\right) \mathrm{Y}_1\left(L\right)}{\mathrm{J}_1\left(L\right) \mathrm{Y}_1\left(a_c^\pi\right) - \mathrm{J}_1\left(a_c{}^\pi\right) \mathrm{Y}_1\left(L\right)}, \quad B_{22} = -\frac{\mathrm{J}_1\left(L\right) \mathrm{I}_1\left(a_c{}^\pi\right)}{\mathrm{J}_1\left(L\right) \mathrm{Y}_1\left(a_c^\pi\right) - \mathrm{J}_1\left(a_c{}^\pi\right) \mathrm{Y}_1\left(L\right)},$$

where a_c^π is given implicitly by Eq. (4.4.45).

With the values of B_i's determined, we substitute the ansatz (4.5.30) into the Lagrangian (4.3.7), and perform the integrations to calculate the energy of the Josephson junction

for a near to a_c^π. We find that the kinetic energy T_π of the system is

$$T_\pi = (Q_5 + Q_6)(B_t)^2, \tag{4.5.31}$$

where the subscript denotes a derivative and

$$\begin{aligned} Q_5 &= -\frac{a^2}{4}\left(-\left(\mathrm{I}_0(a)\right)^2 + \left(\mathrm{I}_1(a)\right)^2\right), \\ Q_6 &= \frac{\mathrm{I}_0(a_c^\pi)}{2}\int_a^L \left[\frac{\mathrm{Y}_1(L)\,\mathrm{J}_0(r) - \mathrm{J}_1(L)\mathrm{Y}_0(r)}{\mathrm{J}_1(L)\,\mathrm{Y}_1(a_c^\pi) - \mathrm{J}_1(a_c^\pi)\,\mathrm{Y}_1(L)}\right] rdr. \end{aligned}$$

In a similar fashion, by defining

$$\begin{aligned} M_{15} &= \frac{a^2}{4}\left[\left(\mathrm{I}_1(a)\right)^2 - \mathrm{I}_0(a)\,\mathrm{I}_2(a)\right], \qquad M_{16} = \frac{a^2}{4}\left[\mathrm{I}_1(a)^2 - \mathrm{I}_0(a)^2\right], \\ M_{17} &= \frac{1}{24}\int_0^a \left(\mathrm{I}_0(r)\right)^4 rdr, \qquad M_{18} = \frac{1}{2}\int_a^L R_1 rdr, \qquad M_{19} = \frac{1}{2}\int_a^L R_2^2 rdr, \\ M_{20} &= \frac{1}{24}\int_a^L R_2^4 rdr, \quad M_{21} = \int_a^L R_2 rdr, \quad R_1 = \left[\frac{\mathrm{I}_1(a_c^\pi)\left(\mathrm{J}_1(L)\,\mathrm{Y}_1(r) - \mathrm{Y}_1(L)\,\mathrm{J}_1(r)\right)}{\mathrm{J}_1(L)\,\mathrm{Y}_1(a_c^\pi) - \mathrm{Y}_1(L)\,\mathrm{J}_1(a_c^\pi)}\right]^2, \\ R_2 &= \frac{\mathrm{I}_1(a_c^\pi)(\mathrm{J}_1(L)\,\mathrm{Y}_0(r) - \mathrm{Y}_1(L)\,\mathrm{J}_0(r)}{\mathrm{Y}_1(L)\,\mathrm{J}_1(a_c^\pi) - \mathrm{J}_1(L)\mathrm{Y}_1(a_c^\pi)}, \end{aligned}$$

the total potential energy U_π, of the junction for a near a_c^π has the form

$$\begin{aligned} U_\pi &= \left[M_{20} - M_{17}\right]B^4 + \left(M_{15} + M_{16} + M_{18} - M_{19}\right)B^2 \\ &\quad -\frac{\gamma}{2}\left(a\left[a\pi + 2B\,\mathrm{I}_1(a)\right] + \pi\left(L^2 - a^2\right)B + 2M_{21}B\right) + L^2 - a^2. \end{aligned} \tag{4.5.32}$$

By introducing Eqs. (4.5.31) and (4.5.32) into the Lagrangian $\mathcal{L} = T_\pi - U_\pi$, the Euler-Lagrange equation (3.6.44) yields

$$\frac{d^2B}{dt^2} = g(B), \tag{4.5.33}$$

where

$$g(B) = \frac{\left[M_{20} - M_{17}\right]B^3 + 2\left[M_{15} + M_{16} + M_{18} - M_{19}\right]B - \gamma\left[2\mathrm{I}_1(a) + \frac{\pi}{2}(L^2 - a^2) + M_{21}\right]}{2(Q_3 + Q_4)}. \tag{4.5.34}$$

In the absence of an applied bias current, i.e., when $\gamma = 0$, the stationary solutions of Eq. (4.5.33) can be found by setting the right hand side of (4.5.34) to zero. This gives

$$B^{(1)} = 0, \;\; B^{(2,3)} = \pm\sqrt{\frac{M_{15} + M_{16} + M_{18} - M_{19}}{2(M_{17} - M_{20})}}. \tag{4.5.35}$$

The total potential energy (4.5.32) has a local minimum at the nonzero roots (4.5.35). Consider the non-zero positive root of Eq. (4.5.35), we study the behaviour of the non-uniform ground state solution in the region $0 < a_c^\pi - a \ll 1$. In particular we plot

the boundary points $r = 0$, $r = L$ and $r = a$. The plots of the Josephson phase at these points versus a are shown in the upper panel of Fig. 4.8. In the region $a \geq a_c^\pi$, all the solutions tend to the uniform π solution. We again notice a close relationship between the approximation to $\phi(r)$ (dashed lines) at the specified points, for $1 \gg a_c^\pi - a > 0$ and the corresponding numerical calculations (solid lines).

To study the ground state solutions in the instability region close to a_c^π, in the presence of an external force γ, the roots of the relation (4.5.35) are determined by the method discussed in [102]. With

$$\begin{aligned}
\delta &= \sqrt{\frac{M_{15}+M_{16}+M_{18}-M_{19}}{6\,(M_{20}-M_{17})}},\\
h &= -\left(\frac{2}{3}\right)^{3/2}\frac{(M_{15}+M_{16}+M_{18}-M_{19})^{3/2}}{\sqrt{M_{20}-M_{17}}},\\
\Theta &= \frac{1}{3}\arccos\left(\frac{\gamma\left(2\mathrm{I}_1(a)-\frac{\pi}{2}(L^2-a^2)+M_{21}\right)}{h}\right),
\end{aligned}$$

these roots are given by (4.5.15). The profiles of the ground state solutions (4.5.30), at the point $r = 0$, corresponding to these roots, as a function of the bias current γ are shown in the upper dashed lines of Fig. 4.10. If one starts from the point where $\gamma = 0$, $\phi(0) \approx 0.95\pi$, and the applied bias current is decreased, a decrease in $\phi(0)$ is noticed. After a certain value of $\gamma < 0$, a saddle node bifurcation occurs at $\gamma = -0.2$, $\phi(0) = 0.8\pi$, and the solution carries on at larger $\phi(0)$ and increasing γ. The bifurcation can be viewed as a collision between the nonuniform solution and the solution that bifurcates from the uniform π solution. In the following, this critical value of the bias current is denoted by γ_c^π, which can be calculated as follows.

Differentiating (4.5.34) with respect to B, and solving the expression $g'(B) = 0$, the stationary roots are given by

$$B_c = \pm\sqrt{\frac{M_{15}+M_{16}+M_{18}-M_{19}}{6(M_{17}-M_{20})}}. \tag{4.5.36}$$

Inserting B_c from Eq. (4.5.36) into (4.5.34) and solving $g(B) = 0$ for γ, gives the critical current as

$$\gamma_c^\pi = \frac{4(M_{20}-M_{17})B_c^3 + 2\,(M_{15}+M_{16}+M_{18}-M_{19})\,B_c}{2\mathrm{I}_1(a)+\frac{\pi}{2}(L^2-a^2)+M_{21}}. \tag{4.5.37}$$

Our analytically obtained value for γ_c^π (4.5.37), using the negative root of (4.5.36) is shown by the lower dashed line in Fig. 4.11 which is compared with its corresponding numerical γ_c^π (lower solid line), where we have taken $L = 2$. There is a close agreement between the analytical result and numerics in the vicinity of a_c^π. From the same figure,

it is clear that in the regions where $a_c^0 \leq a \leq a_c^\pi$, there are two nonuniform solutions. In the regions $a \leq a_c^0$ and $a \geq a_c^\pi$, there is only one nonuniform solution. We also note that at the critical value of the facet lengths, the corresponding critical currents γ_c^π and γ_c^0 are zero.

4.5.3.2 Stability analysis

We now study the stability of the stationary solutions given by (4.5.15) for the driven case corresponding to $\widetilde{\phi} = \pi$. For $\min(B^{(n)})$ and $\max(B^{(n)})$ the potential energy is locally minimized. Following the same steps as before, the critical eigenvalues of the stable solutions are calculated as

$$E = -\frac{6(M_{17}-M_{20})\left(B^{(n)}\right)^2-(M_{15}+M_{16}+M_{18}-M_{19})}{Q_5+Q_6}, \tag{4.5.38}$$

which are equal to the negative of the square of the oscillating frequency of $\tilde{B}(t)$. The right dashed line in Fig. 4.12 shows the critical eigenvalues (4.5.38) as a function of the facet length a, where it is observed the lowest eigenvalue is attained at a point of the instability region. In Fig. 4.13, the eigenvalues E (4.5.38) are presented in terms of the varying bias current, where we have considered the case where $L = 2$ and $a = 1.3$. The approximation (4.5.38) (left dashed line) qualitatively agrees with its numerical counterpart.

4.6 Excited states bifurcating from the uniform solutions

In Section 4.5, we discussed the nonuniform ground state in the combined instability region of the static solutions of the sine-Gordon model (4.3.8). We noticed that this nonuniform ground state is independent of $\widetilde{\theta}$ and has the same sign for all values of the radial parameter r, that is, the ground state in the instability region is sign-definite. In addition, the static sine-Gordon equation (4.3.8) may also have excited static states. For states bifurcating from the trivial solutions $\widetilde{\phi} = 0$ and $\widetilde{\phi} = \pi$ at $\gamma = 0$ in the instability region of the uniform solutions, a similar analysis can be performed as before. In Figs. 4.18–4.19, we present two examples of static excited states bifurcating from the trivial solution $\widetilde{\phi} \equiv 0$ for $R_{\text{mid}} = 7$ and $R_{\text{max}} = 10$ and their typical instability dynamics, supporting our conjecture.

In Fig. 4.18, we present the dynamics of a $\widetilde{\theta}-$independent excited state. This is an excited state in the sense that the solution is not sign-definite, i.e. it has one zero in the

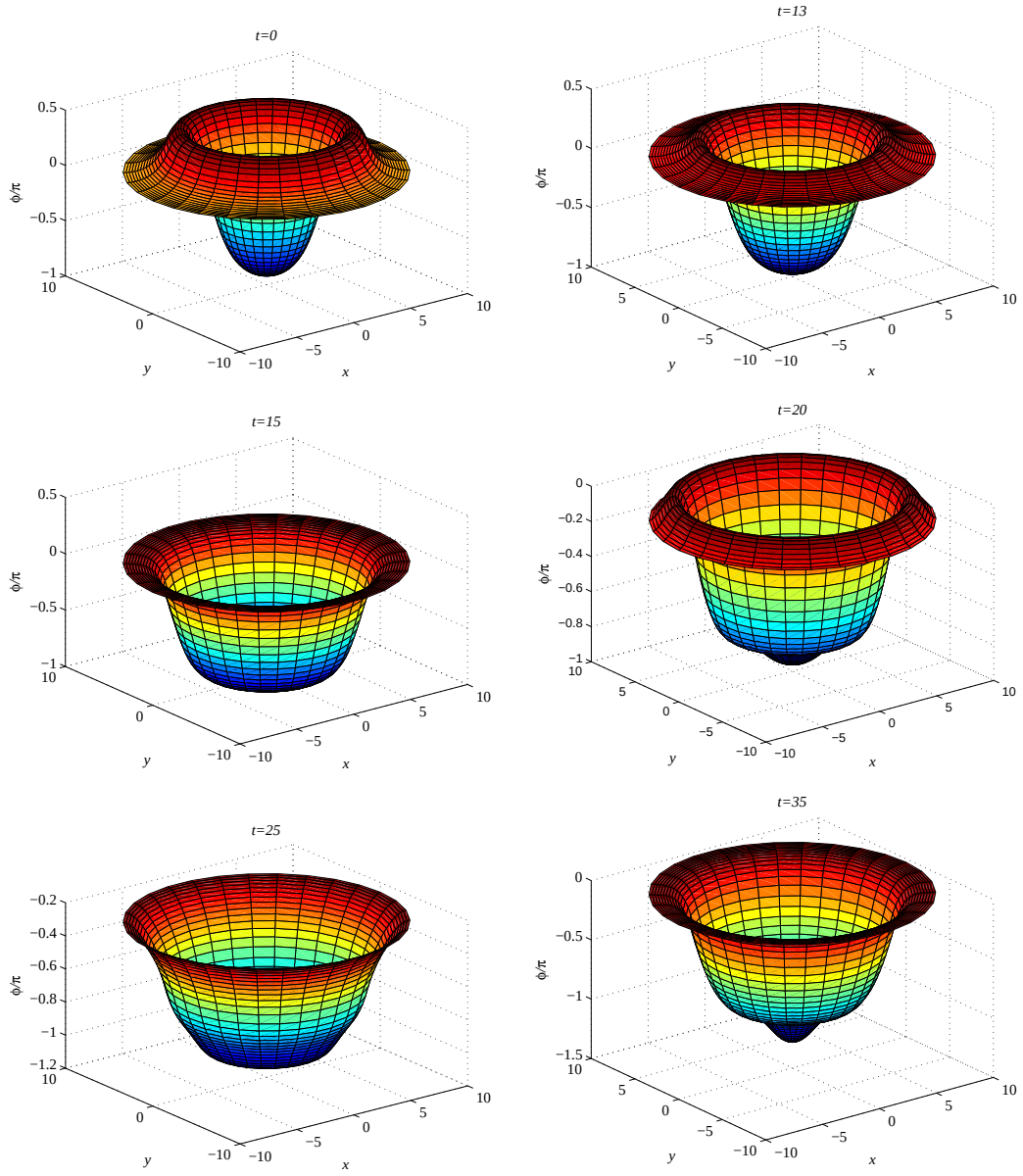

Figure 4.18: The typical evolution of the phase with the initial condition corresponding to a $\widetilde{\theta}$-independent excited state perturbed randomly with zero initial velocity. Here, $R_{\rm mid} = 7$ and $R_{\rm max} = 10$. The dissipation constant is set to $\alpha = 0.1$ to dissipate the radiation caused by the instability of the state. As time evolves, the solution tends to the ground state, see also Fig. 4.9.

radial direction. As for the excited state shown in Fig. 4.19, the state is sign-definite in the radial direction, but the state is not independent of the azimuthal direction ($\widetilde{\theta}$). Defining the vorticity Q as the wavenumber of the oscillation or rotation in the azimuthal direction, we note that the nonuniform ground state discussed above and the excited

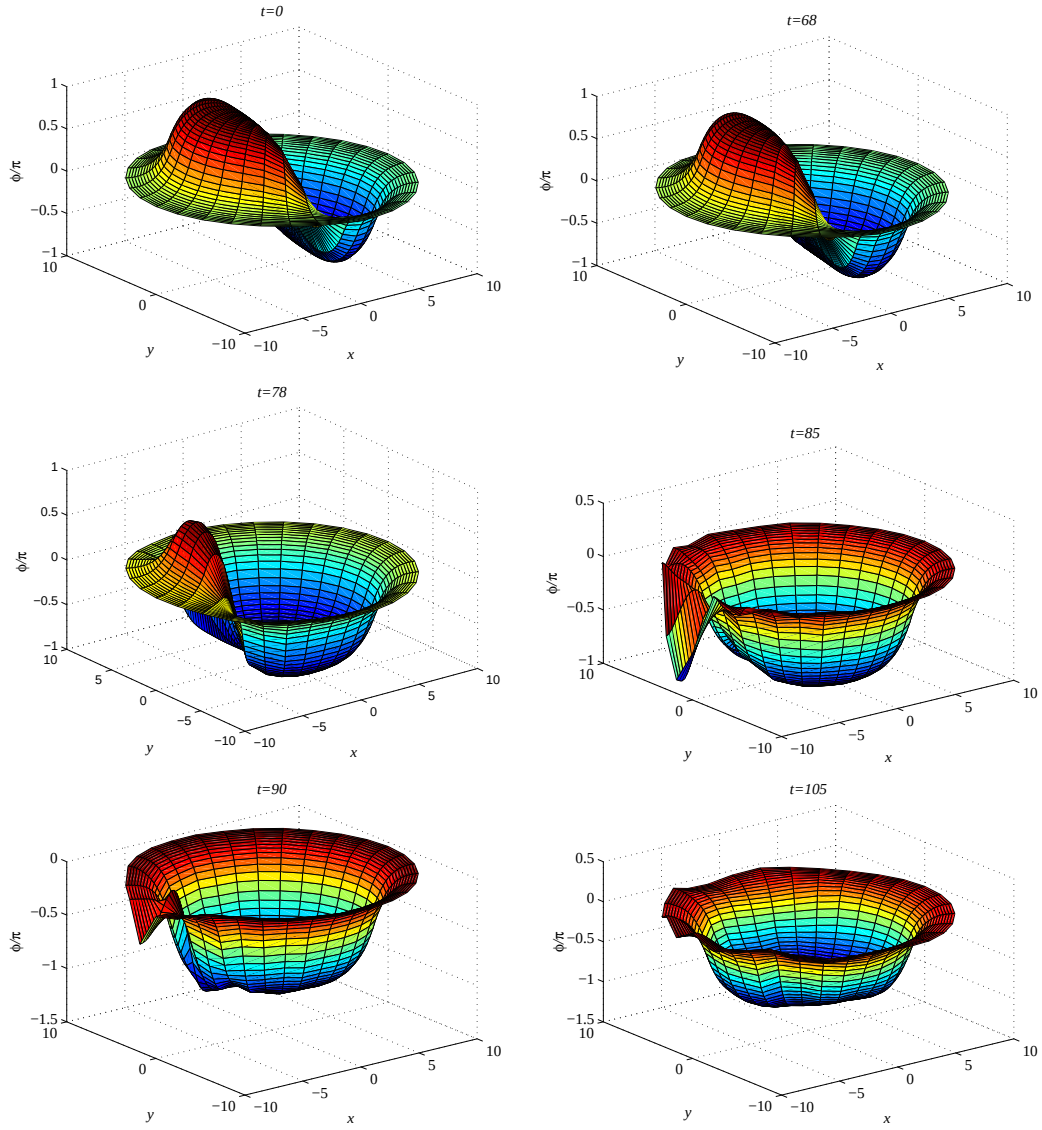

Figure 4.19: The same as Fig. 4.18, but for a static θ dependent excited state. As before, the solution also tends to the ground state as t increases due to damping ($\alpha > 0$).

state shown in Fig. 4.18 have $Q = 0$, while the excited state in Fig. 4.19 has vorticity $Q = 1$. We note that both excited states evolve into the ground state shown in Fig. 4.9.

4.7 Conclusions

In this chapter we have extended the ideas of an infinite and finite one dimensional long Josephson junctions, discussed in the last two chapters, into two dimensions. Here we have analytically investigated a two-dimensional disk-shaped 0-π Josephson junc-

tion in both finite and an semi-infinite domains. We have calculated the stability boundary of $\widetilde{\phi} = 0$ and $\widetilde{\phi} = \pi$ states. In the region of instability of both $\widetilde{\phi} = 0$ and $\widetilde{\phi} = \pi$ states a semifluxon having a shape of a ring is spontaneously generated. Using an Euler-Lagrange formalism we have shown that the existence of semifluxons depends on the radius $R_{\max}$ of the junction, the radius R_{mid} of 0-π boundary and on the applied bias current. Critical eigenvalues that determine the stability of semifluxon solutions have also been discussed. Analytical expressions are compared with numerical simulations. We have briefly discussed the existence of excited states bifurcating from $\widetilde{\phi} = 0$ and $\widetilde{\phi} = \pi$ states, which are conjectured to be unstable for the particular phase-shift structure discussed here.

CHAPTER 5

Band-gaps and gap breathers of long Josephson junctions with periodic phase shifts

In previous chapters, we analysed long Josephson junctions having a π-discontinuity in their superconducting phase difference and investigated the existence of semifluxons therein. In this chapter, we study a long Josephson junction that has an arbitrary κ discontinuities in its phase; i.e., the so-called 0-κ long Josephson junction. We discuss a periodic array of 0-κ discontinuities and analyse the band structures of the junction and gap-breathers that have oscillating frequencies in the band-gaps.

5.1 Introduction

The study of the propagation of a nonlinear wave in a periodic structure (e.g., a crystal) is a fascinating topic of research in solid state physics, optics and applied mathematics (see Kittel and McEuen [13], Kivshar and Agrawal [142], and Yang [143]). Periodic structures have important features, including the existence of multiple frequency gaps (also called Bloch bands or band-gaps) in the wave transmission spectra. These band-gaps play an important role in the physical properties of solids. By controlling the periodicity, the basic properties of a material can be altered and a material with desirable properties can be created. This process is not easy because of the fixed structure of crystals in nature and it requires e.g., a strong electric [144] or magnetic field [145] or pressure etc. To allow the control of the electronic properties of a material up to a wider extent, it would be interesting to construct and understand artificial periodic

structures with wide range varying properties during experiments. One proposal is to exploit Josephson junctions with periodic discontinuities.

In previous chapters, we have studied fractional vortices in long Josephson junctions with π-discontinuity points. The fractional vortices in junctions with $\pm\pi$-discontinuity are mirror symmetric, in that they carry a magnetic flux of either $\Phi_0/2$ or $-\Phi_0/2$. It is natural to ask what type of vortices can be created in a long Josephson junction with an arbitrary discontinuity? The possibility of creating an arbitrary phase shift in the Josephson phase was successfully studied experimentally by Goldobin et al. [46]. They showed that the phase shift can be tuned to be of any value κ and consequently, an arbitrary fractional magnetic flux quantum can be obtained in the junction. In such junctions, a pair of closely situated current injectors creates a κ-discontinuity, where κ and the current through the injectors are found to be proportional, as reported by Malomed and Ustinov [146].

If x is the coordinate along the Josephson junction and there is κ-phase discontinuity at $x = 0$, then the current-phase relation in the region $x > 0$ reduces to $I_s = I_c \sin(\phi + \kappa)$. It was demonstrated by Goldobin et al. [108] that by having a κ-discontinuity, a fractional vortex may spontaneously appear, to compensate the phase jump and is attached to the discontinuity. The eigenfrequency of this fractional vortex corresponds to oscillations of the magnetic flux of the vortex around the point of discontinuity and depends upon the parameter κ. It was reported that the eigenfrequency of a fractional vortex in a 0-κ Josephson junction depends upon the magnetic flux of the vortex and it lies within the band-gap [109].

Later, Susanto et al. [111] numerically studied a one-dimensional chain of fractional vortices in a long Josephson junctions having alternating $\pm\kappa$ discontinuities. They studied the small oscillations of fractional vortices and the corresponding energy bands in terms of the phase discontinuity κ. The points of bifurcation of the transitional curves from the energy-axis in the (energy, discontinuity)-plane, and the effect of an applied bias current on additional openings of the band-gaps in the continuous plasma bands still needed to be calculated analytically.

In this chapter, we consider a long Josephson junction with arbitrary periodic jump of κ in its phase and study the energy bands that correspond to the lattice oscillations. The electronic properties of such system can be controlled to a greater degree during experiment by varying the current or by choosing the inter vortex distance at the design time. Thus, the proposed periodic structure can be constructed and has applications in

solid state physics [147, 148].

The chapter is structured as follows: in Section 5.2, we present a mathematical model for the problem under consideration and find its periodic solutions in the regions of interest. Section 5.3 describes a detailed study of the existence of periodic solutions about the static solutions including the ground state solutions both in the absence and presence of the applied bias current. This section also deals with the dependence of the ground state solution on a coupling parameter a, and the arbitrary periodic discontinuity κ. In Section 5.4, we study the stability of the periodic solutions, we derive the expressions of the transitional curves, separating regions of allowed and forbidden bands. We study the points where the band-gap bifurcate and study the opening of the additional band-gaps in the presence of the applied bias current. We also find analytically expressions for the corresponding eigenfunctions. We discuss the breather solution of the sine-Gordon model bifurcating from transitional curves using a multiple scale expansion, and by using a rotating wave approximation, in Sections 5.5 and 5.6 respectively. Finally, Section 5.7 concludes the chapter.

5.2 Mathematical Model

We consider again the one-dimensional sine-Gordon equation (1.5.5) in such a way that the spatial variable x lies in the interval $-\infty < x < \infty$, and $\theta(x)$ represents periodic discontinuities of κ in $\phi(x,t)$, that is,

$$\theta(x) = \begin{cases} 0, & x \in (2na, (2n+1)a)\,, \\ \kappa, & x \in ((2n+1)a, 2(n+1)a)\,, \end{cases} \tag{5.2.1}$$

where $n \in \mathbb{Z}$, a is the distance between two consecutive discontinuities or the distance between two consecutive vortices (as shown in Figure 5.1) and $0 < \kappa < 2\pi$.

With the spatial variable x in the interval $-\infty < x < \infty$, and the additional shift $\theta(x)$ defined in (5.2.1), the sine-Gordon equation (1.5.5) is used for the description of the dynamics of the Josephson phase across the superconductors of an infinitely long Josephson junction with an arbitrary periodic phase jump of κ in Josephson phase, see for instance, Goldobin et al. [54] and Susanto et al. [111]. To study the dynamics the Josephson phase across the superconductors of such an infinitely long 0-κ Josephson junction, we will not take dissipation into account. In other words, in the following, we limit ourselves to the ideal case where $\alpha = 0$.

Looking at the structure of the additional periodic phase shift $\theta(x)$ given by Eq. (5.2.1),

it would be convenient to modify the problem under consideration into a simpler form. Thus to analyze the ground states of 0-κ long Josephson junctions with periodic phase shifts, without the loss of generality, we consider

$$\phi_{xx} - \phi_{tt} = \sin\left[\phi + \theta(x)\right] - \gamma, \quad (0 < x < 2a)\,, \tag{5.2.2}$$

where

$$\theta(x) = \begin{cases} 0, & (0 < x < a)\,, \\ \kappa, & (a < x < 2a)\,. \end{cases} \tag{5.2.3}$$

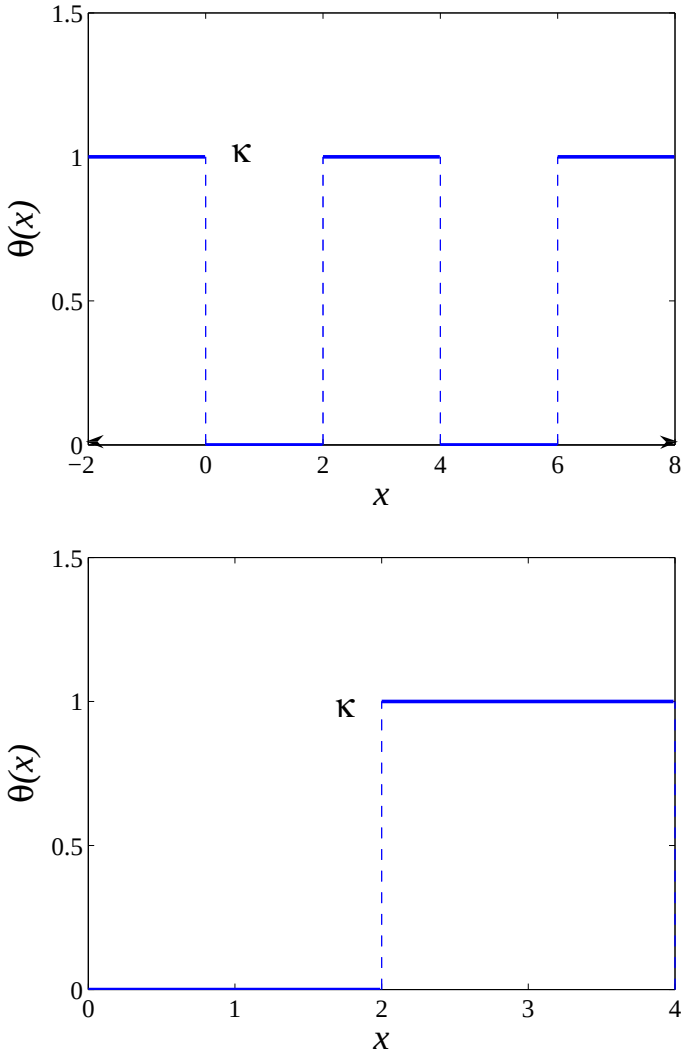

Figure 5.1: Plot of the additional phase shift of κ in the Josephson phase $\phi(x,t)$, given by Eqs. (5.2.1) (top) and (5.2.3) (bottom), where we have taken $\kappa = 1$ and $a = 2$.

Here all the parameters and variables are taken in the nondimensionalised form.

For practical purposes, we assume that the Josephson phase (ϕ) and the magnetic flux (ϕ_x) are continuous at the discontinuity $x = a$, and study the system described by Eqs. (5.2.2) and (5.2.3) subject to the following continuity and boundary conditions

$$\begin{aligned} \phi\left(a^{-}\right) &= \phi\left(a^{+}\right), \quad \phi_x\left(a^{-}\right) = \phi_x\left(a^{+}\right), \\ \phi\left(0^{+}\right) &= \phi\left(2a^{-}\right), \quad \phi_x\left(0^{+}\right) = \phi_x\left(2a^{-}\right). \end{aligned} \tag{5.2.4}$$

The stationary solutions of Eq. (5.2.2) are determined by solving the time independent-sine-Gordon equation

$$\phi_{xx} = \sin\left[\phi + \theta(x)\right] - \gamma. \tag{5.2.5}$$

This equation admits uniform solutions of the form

$$\widetilde{\phi} = \arcsin(\gamma) - \theta(x), \quad \widetilde{\phi} = \pi - \arcsin(\gamma) - \theta(x),$$

which, for small γ, can be approximated by

$$\widetilde{\phi} = \gamma - \theta(x), \quad \widetilde{\phi} = \pi - \theta(x) - \gamma.$$

Using the phase-shift (5.2.3), we find that the static and uniform solutions approximated as

$$\widetilde{\phi} = \gamma, \quad \widetilde{\phi} = \pi - \gamma, \quad (0 < x < a),$$

and

$$\widetilde{\phi} = \gamma - \kappa, \quad \widetilde{\phi} = \pi - \kappa - \gamma, \quad (a < x < 2a).$$

It can be verified that the uniform solutions satisfy the continuity conditions (5.2.4) only when $\gamma = 0$ and $\kappa \equiv 0,\ \pi \pmod{2\pi}$.

5.3 Existence analysis of periodic solutions

In the following, we deal with the periodic solutions about the uniform solutions of the static sine-Gordon model (5.2.5).

5.3.1 Existence of periodic solutions about 0 and $-\kappa$

In this subsection, we investigate the existence of the periodic solutions about the static 0-solution. We first study the existence of the periodic solutions in the presence of an

applied bias current ($\gamma \neq 0$), and discuss the results for the undriven case, $\gamma = 0$. To do this, we perform a perturbation analysis and assume

$$\phi(x) = \begin{cases} \widetilde{\phi}, & (0 < x < a)\,, \\ -\kappa + \widehat{\phi}, & (a < x < 2a)\,, \end{cases} \tag{5.3.1}$$

where $\widetilde{\phi} \ll 1$ and $\widehat{\phi} \ll 1$ are functions of x.

Inserting assumption (5.3.1) into our static sine-Gordon model (5.2.5), using Taylor series expansion about $\widetilde{\phi}$ and $\widehat{\phi}$ respectively in the two regions and neglecting the small terms, one finds that $\widetilde{\phi}$ and $\widehat{\phi}$ satisfy the system

$$\begin{cases} \widetilde{\phi}_{xx} - \widetilde{\phi} + \dfrac{\widetilde{\phi}^3}{6} + \gamma = 0, & (0 < x < a)\,, \\ \widehat{\phi}_{xx} - \widehat{\phi} + \dfrac{\widehat{\phi}^3}{6} + \gamma = 0, & (a < x < 2a)\,, \end{cases} \tag{5.3.2}$$

together with boundary conditions

$$\widetilde{\phi}(a) = \widehat{\phi}(a) - \kappa, \quad \widetilde{\phi}(0) = \widehat{\phi}(2a) - \kappa, \quad \widetilde{\phi}_x(a) = \widehat{\phi}_x(a), \quad \widetilde{\phi}_x(0) = \widehat{\phi}_x(2a).$$

Our aim is to determine the small perturbations $\widetilde{\phi}$ and $\widehat{\phi}$ in the respective regions. Motivated by the Poincare-Lindstedt method, to solve system (5.3.2), we propose an ansatz of the form (see Section 3.6.3 as well)

$$\widetilde{\phi} = \widetilde{A}\cosh\left[\widetilde{\omega}(x - x_1)\right] + \gamma, \quad (0 < x < a), \tag{5.3.3a}$$

$$\widehat{\phi} = \widehat{A}\cosh\left[\widehat{\omega}(x - x_2)\right] + \gamma, \quad (a < x < 2a), \tag{5.3.3b}$$

where $\widetilde{\omega} = 1 + \epsilon\widetilde{\omega}_1 + \mathcal{O}(\epsilon^2)$, $\widehat{\omega} = 1 + \epsilon\widehat{\omega}_1 + \mathcal{O}(\epsilon^2)$, $\widehat{A} \ll 1$, and $\widehat{A} \ll 1$. Here, $\widetilde{\omega}_1$ and $\widehat{\omega}_1$ are constant to be determined later. The terms x_1, x_2 in the above equations are arbitrary constants which can be chosen according to our convenience. We choose $x_1 = a/2$ and $x_2 = 3a/2$, so as to impose even symmetry about $x = a/2$ and about $x = 3a/2$.

To solve the first equation of the system (5.3.3), we introduce the scalings

$$a = \mathcal{O}(1), \quad \widetilde{A} = \sqrt{\epsilon}A + \mathcal{O}(\epsilon), \quad \gamma = \sqrt{\epsilon}\widetilde{\gamma} + \mathcal{O}(\epsilon), \quad \widetilde{\gamma} = \mathcal{O}(1), \quad A = \mathcal{O}(1), \tag{5.3.4}$$

where $\epsilon \ll 1$.

We consider problem in phase space $(\widetilde{\phi}, \widetilde{\phi}_x)$, and aim to desolve equations of trajectories therein. In order to solve the system (5.3.2) in the region $0 < x < a$, we define

$$\widetilde{\phi}_x = \widetilde{\psi}, \tag{5.3.5}$$

so that Eq. (5.3.3a) yields

$$\widetilde{\psi} = \widetilde{A}\widetilde{\omega}\sinh\left[\widetilde{\omega}(x - x_1)\right]. \tag{5.3.6}$$

Substituting Eqs. (5.3.3a) and (5.3.5) into the first equation of the system (5.3.2) and using the chain rule of differentiation, we obtain

$$\frac{d\widetilde{\psi}}{d\widetilde{\phi}} = \frac{\widetilde{\phi} - \widetilde{\phi}^3/6 - \gamma}{\widetilde{\psi}}. \tag{5.3.7}$$

This equation, upon separation of variables and integration, yields

$$\widetilde{\psi}^2 = \widetilde{\phi}^2 - \frac{\widetilde{\phi}^4}{12} - 2\gamma\widetilde{\phi} + 2C, \tag{5.3.8}$$

where C is an integration constant, which may be determined using $\widetilde{\phi}(x_1) = \widetilde{A} + \gamma$ and $\widetilde{\psi}(x_1) = 0$, i.e.,

$$C = \frac{\left(\widetilde{A} + \gamma\right)^4}{24} - \frac{\left(\widetilde{A} + \gamma\right)^2}{2} + \gamma\left(\widetilde{A} + \gamma\right). \tag{5.3.9}$$

With this value of C and simple algebra, Eq. (5.3.8) gives

$$\begin{aligned}\widetilde{\psi}^2 - \widetilde{\phi}^2 \quad + \quad & \widetilde{A}^2 + \gamma^2 + 2\widetilde{A}\gamma\cosh\left[\widetilde{\omega}(x - x_1)\right] = \frac{\widetilde{A}}{12}\Big\{\widetilde{A}^3\left(1 - \cosh^4\left[\widetilde{\omega}(x - x_1)\right]\right) \\ & + 4\widetilde{A}^2\gamma\left(1 - \cosh^3\left[\widetilde{\omega}(x - x_1)\right]\right) + 6\widetilde{A}\gamma^2\left(1 - \cosh^2\left[\widetilde{\omega}(x - x_1)\right]\right) \\ & + 4\gamma^3\left(1 - \cosh\left[\widetilde{\omega}(x - x_1)\right]\right)\Big\}.\end{aligned} \tag{5.3.10}$$

Again neglecting smaller terms in ϵ, and using a hyperbolic identity, by the help of Eqs. (5.3.3a) and (5.3.6), one can also write

$$\widetilde{\psi}^2 - \widetilde{\phi}^2 + \widetilde{A}^2 + \gamma^2 + 2\widetilde{A}\gamma\cosh\left(\widetilde{\omega}(x - x_1)\right) = -2\epsilon\widetilde{\omega}_1\widetilde{A}^2\sinh^2\left[\widetilde{\omega}(x - x_1)\right]. \tag{5.3.11}$$

By comparing Eqs. (5.3.10) and (5.3.11), and solving implicitly for $\epsilon\widetilde{\omega}_1$, we obtain that the difference of the right hand side of the two equations is dependent of the spatial variable x. To remove the x-dependency, we integrate the resulting equation over the interval $0 < x < a$ and divide the integrand by the length of the interval, which gives the average of the difference. Requiring this spatial average difference to be zero leads to

$$\begin{aligned}\epsilon\widetilde{\omega}_1 \quad = \quad & -\frac{1}{24a}\int_0^a \Bigg\{\frac{\widetilde{A}^2}{2}\left(3 + \cosh\left[2\widetilde{\omega}(x - x_1)\right]\right) + 4\widetilde{A}\gamma\cosh\left[\widetilde{\omega}(x - x_1)\right] \\ & + 6\gamma^2 + \frac{4\gamma}{\widetilde{A}}\left(\frac{\widetilde{A}^2 + \gamma^2}{1 + \cosh\left[\widetilde{\omega}(x - x_1)\right]}\right)\Bigg\}dx.\end{aligned}$$

Evaluating the integral and inserting the value of x_1 in the resulting equation, we find that ω_1 is given by the implicit relation

$$\begin{aligned}\epsilon\widetilde{\omega}_1 &= -\frac{1}{24a}\Bigg\{\frac{\widetilde{A}^2}{2}\left(3a+\frac{\sinh\left[(1+\epsilon\widetilde{\omega}_1)a\right]}{1+\epsilon\widetilde{\omega}_1}\right)+8\widetilde{A}\gamma\left(\frac{\sinh\left[(1+\epsilon\widetilde{\omega}_1]\,a/2\right)}{1+\epsilon\widetilde{\omega}_1}\right)\\ &\quad +6\gamma^2 a+8\gamma\left(\frac{\widetilde{A}^2+\gamma^2}{\widetilde{A}}\right)\frac{\tanh\left[(1+\epsilon\widetilde{\omega}_1)a/4\right]}{1+\epsilon\widetilde{\omega}_1}\Bigg\}.\end{aligned} \tag{5.3.12}$$

Using the scalings in (5.3.4) and expanding Eq. (5.3.12) and equating the coefficients of ϵ on both sides, for the leading order we obtain

$$\widetilde{\omega}_1=-\frac{1}{24a}\left\{\frac{A^2}{2}\left[3a+\sinh(a)\right]+8A\widetilde{\gamma}\sinh\left(\frac{a}{2}\right)+6\widetilde{\gamma}^2a+8\widetilde{\gamma}\left(\frac{A^2+\widetilde{\gamma}^2}{A}\right)\tanh\left(\frac{a}{4}\right)\right\}. \tag{5.3.13}$$

In a similar way, taking Eq. (5.3.3b) as the general solution of the second equation of the system (5.3.2) in the region $a<x<2a$, repeating the above calculations and taking $x_2=3a/2$, one may verify that $\widehat{\omega}_1$ in this case is given by

$$\widehat{\omega}_1=-\frac{1}{24a}\left\{\frac{\widehat{A}^2}{2}\left[3a+\sinh(a)\right]+8\widehat{A}\widetilde{\gamma}\sinh\left(\frac{a}{2}\right)+6\widetilde{\gamma}^2a+8\widetilde{\gamma}\left(\frac{\widehat{A}^2+\widetilde{\gamma}^2}{\widehat{A}}\right)\tanh\left(\frac{a}{4}\right)\right\}. \tag{5.3.14}$$

Substituting the values of ω_1 from Eqs. (5.3.13) and (5.3.14) into the general solutions (5.3.3a) and (5.3.3b) respectively and applying the conditions (5.2.4), we obtain a system of two equations for the two unknowns $\widetilde{A}$ and $\widehat{A}$,

$$\begin{cases}\left(\widetilde{A}-\widehat{A}\right)\cosh\left((1+\epsilon\widetilde{\omega}_1)\dfrac{a}{2}\right)+\kappa=0, & (0<x<a),\\ \left(\widetilde{A}+\widehat{A}\right)\sinh\left((1+\epsilon\widetilde{\omega}_1)\dfrac{a}{2}\right)=0, & (a<x<2a).\end{cases} \tag{5.3.15}$$

Since $a=\mathcal{O}(1)$ and $|\epsilon\widehat{\omega}_1|\ll 1$, therefore, the second equation of the system (5.3.15) holds if and only if

$$\widetilde{A}=-\widehat{A}. \tag{5.3.16}$$

As a result the first equation of the system (5.3.15) reduces to

$$\widetilde{A}\cosh\left((1+\epsilon\widetilde{\omega}_1)\frac{a}{2}\right)=-\frac{\kappa}{2}. \tag{5.3.17}$$

Substituting the value of ω_1 from (5.3.13) into (5.3.17), introducing the scaling (5.3.4) with $\kappa=\sqrt{\epsilon}\widetilde{\kappa}$, where $\widetilde{\kappa}=\mathcal{O}(1)$, expanding the resultant equation by Taylor series about $\epsilon=0$ and neglecting the smaller terms, we obtain

$$\begin{aligned}A &= -\frac{\widetilde{\kappa}}{2\cosh\left(a/2\right)}-\frac{1}{768\cosh^4\left(a/2\right)}\Bigg[\widetilde{\kappa}^3\left(3a+\sinh(a)\right)\sinh\left(\frac{a}{2}\right)\\ &\quad -16\widetilde{\kappa}^2\widetilde{\gamma}\left\{3\tanh\left(\frac{a}{4}\right)+\sinh\left(\frac{a}{2}\right)\right\}\sinh(a)-768\widetilde{\gamma}^3\mathrm{sech}^2\left(a/4\right)\cosh^3\left(a/2\right)\Bigg],\end{aligned} \tag{5.3.18}$$

and the corresponding $\widehat{A}$ can be found from Eq. (5.3.16). Consequently, the system described by Eq. (5.3.1) reduces to

$$\phi(x) = \begin{cases} \widetilde{A}\cosh\left((1+\epsilon\widetilde{\omega}_1)\left(x-\frac{a}{2}\right)\right)+\gamma, & (0<x<a)\,, \\ -\kappa-\widehat{A}\cosh\left((1+\epsilon\widehat{\omega}_1)\left(x-\frac{3a}{2}\right)\right)+\gamma, & (a<x<2a)\,. \end{cases} \tag{5.3.19}$$

Eq. (5.3.19) gives the ground state solution of system (5.3.2) in the driven case ($\gamma \neq 0$) (which we denote later on by ϕ_s in section 5.4). To analyze the dynamics of the system in the undriven case, we simply substitute $\gamma = 0$ into Eq. (5.3.19).

In Fig. 5.2, we have depicted the profile of the ground state solution ϕ, given by the system (5.2.2) – (5.2.3), as a function of the spatial variable x. The solid lines represent the numerically obtained $\phi(x)$ for $a = 1$ and $\kappa = 0.5$. The dashed lines represent the corresponding analytical approximation (5.3.19), for the same values of the inter-vortex distance a and the discontinuity κ.

The top panel represents the behaviour of the wave function $\phi(x)$ in the absence of an applied bias current γ. We notice that $\phi(x)$ oscillates and attains its maximum and minimum values respectively at the points $x = a/2$ and $x = 3a/2$, which are x_1 and x_2 respectively. In the undriven case, we observe a good agreement between the numerical calculation and the corresponding approximation (5.3.19). The lower panel of the same figure, shows the dynamics of the ground state solution ϕ versus x in the driven situation, where we take $\gamma = 0.2$. We also note that the approximation of the undriven case is closer than the driven case. Differences in the driven case are ~ 0.01 which is $\mathcal{O}(\epsilon^{3/2})$, given $\gamma = 0.2$. In both the cases, we note that the static solution $\phi(x)$ is sign-definite, that is, has the same sign for all x.

The approximations to the Josephson phase ϕ, given by the system (5.3.19), at $x = a/2$ (the upper branch) and $x = 3a/2$ (the lower branch) as functions of the distance a between two consecutive discontinuities, are shown in Fig. 5.3. The upper and lower panels represent the undriven and driven cases respectively. Consider the top panel of the figure; when $a = 0$, the two branches merge at the point where $\phi \approx -0.25$. This shows that the magnetic flux intensity $(\phi(3a/2) - \phi(a/2))$ is zero. As the distance a, between two consecutive discontinuities, increases, the gap between the two branches increases. This shows that the magnetic field increases with the increase in the facet length a. In other words, the strength of the magnetic field intensity is related to inter-vortex distance in Josephson junction. For larger inter-vortex distance, the

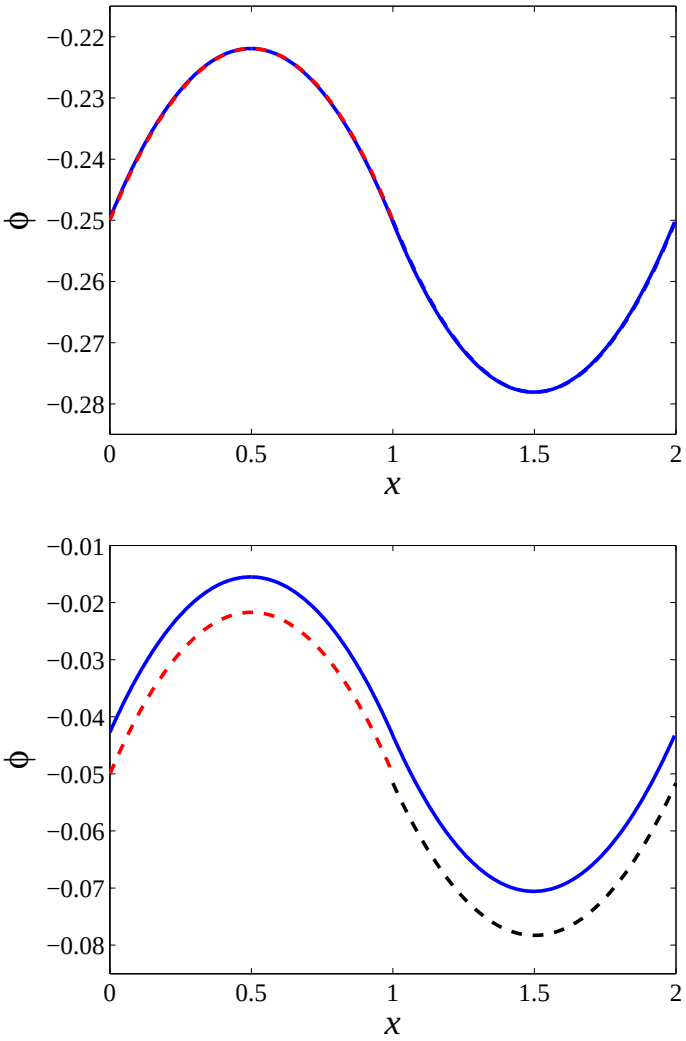

Figure 5.2: Comparison between the numerically obtained Josephson phase ϕ (solid lines) and the corresponding approximations (dotted lines) of the profile ϕ given by the system (5.3.19) in terms of the spatial variable x for the undriven (top) and the driven (bottom) cases. In the driven case we have taken $\gamma = 0.2$. Here the inter-vortex distance, a, is taken to be unity and $\kappa = 0.5$ in both the driven and undriven problems. The value of the discontinuity κ is taken to be 0.5.

magnetic flux is smaller and vice versa. We observe a rather good agreement between the approximations and numerics in this case. In the lower panel of the same figure, the profile of the ground state solution ϕ as a function of the inter-vortex distance a is plotted in the presence of the external force, where we have taken $\gamma = 0.2$. Again, one can observe that the magnetic flux, $\Delta\phi = \phi(3a/2) - \phi(a/2)$, is zero at $\phi \approx -0.041$, and increases with increasing a. A comparison between our approximations and the corres-

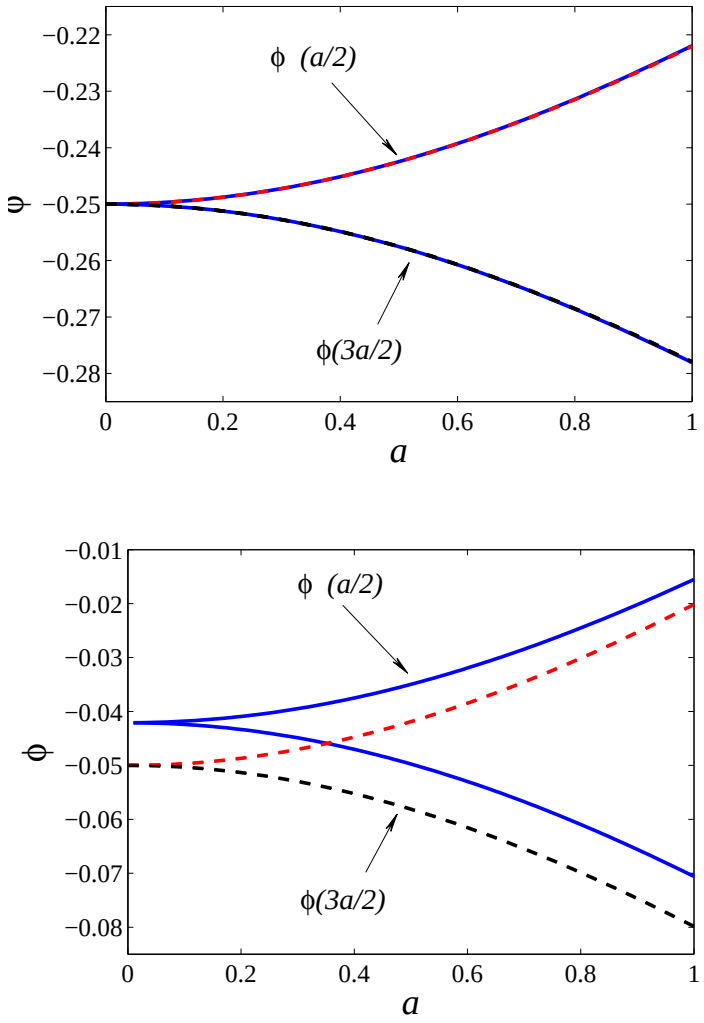

Figure 5.3: Plot of the approximations to the profile $\phi(a/2)$ and $\phi(3a/2)$, given by the system (5.3.19) at $\kappa = 0.5$, as a function of the the facet length a for the case of $\gamma = 0$ (top) and $\gamma = 0.2$ (bottom). Dashed lines are the approximation to the ground state solutions (5.3.19) and the solid lines are the corresponding numerical simulations.

ponding numerics is displayed in the same figure showing good qualitative agreement.

The effect of the applied bias current, γ, on the profile of the Josephson phase ϕ given by the system (5.3.19) is displayed by the lower dashed lines in Figure 5.4. For $\gamma = 0$ the Josephson phase emanates from the point $-\kappa$. The two branches correspond to $x = a/2$ and $x = 3a/2$. The Josephson phase ϕ increases with the increase in the bias current γ. For γ close to zero, the approximation to ground state solution, given by (5.3.19), well approximates its numerical counterpart.

5.3.2 Existence of periodic solutions about π and $\pi - \kappa$

Now we discuss the static solutions about the uniform solution π, $\pi - \kappa$. To discuss the existence of the periodic solutions about π, we assume

$$\phi = \pi + \begin{cases} \widetilde{\phi}, & (0 < x < a), \\ -\kappa + \widehat{\phi}, & (a < x < 2a), \end{cases} \tag{5.3.20}$$

where $\widetilde{\phi}$ and $\widehat{\phi}$ are small perturbations of the uniform solutions π and $\pi - \kappa$ respectively. Substituting the ansatz (5.3.20) into the system (5.2.5) and using a formal series expansion, up to the third correction term, we obtain

$$\begin{aligned} \widetilde{\phi}_{xx} + \widetilde{\phi} - \frac{\widetilde{\phi}^3}{6} + \gamma &= 0, \quad (0 < x < a), \\ \widehat{\phi}_{xx} + \widehat{\phi} - \frac{\widehat{\phi}^3}{6} + \gamma &= 0, \quad (a < x < 2a). \end{aligned} \tag{5.3.21}$$

This time, the solutions the system (5.3.21) are of the form

$$\widetilde{\phi} = \widetilde{B}\cos\left[\widetilde{\omega}\left(x - \frac{a}{2}\right)\right] - \gamma, \quad (0 < x < a), \tag{5.3.22a}$$

$$\widehat{\phi} = \widehat{B}\cos\left[\widehat{\omega}\left(x - \frac{3a}{2}\right)\right] - \gamma, \quad (a < x < 2a), \tag{5.3.22b}$$

where $\widetilde{\omega} = 1 + \epsilon\widetilde{\omega}_1 + \mathcal{O}(\epsilon^2)$, and $\widehat{\omega} = 1 + \epsilon\widehat{\omega}_1 + \mathcal{O}(\epsilon^2)$, $\widetilde{\omega}_1$. The terms $\widehat{\omega}_1$, $\widetilde{B} \ll 1$ and $\widehat{B} \ll 1$ in the system (5.3.22) are constants to be determined. First, we solve Eq. (5.3.22a). By giving the same reasoning as in the previous section, and the same scaling (5.3.4) along with

$$\widetilde{B} = \sqrt{\epsilon}B, \quad B = \mathcal{O}(1), \tag{5.3.23}$$

one may verify that the modified version of (5.3.13) becomes

$$\widetilde{\omega}_1 = \frac{-1}{48a}\left\{B^2\left(3a + \sin(a)\right) - 16B\widetilde{\gamma}\sin\left(\frac{a}{2}\right) + 12\widetilde{\gamma}^2 a - 16\widetilde{\gamma}\left(\frac{\widetilde{\gamma}^2}{B} + B\right)\tan\left(\frac{a}{4}\right)\right\}, \tag{5.3.24}$$

$$\begin{aligned} B = &-\frac{\widetilde{\kappa}}{2\cos\left(\frac{a}{2}\right)} + \frac{1}{768}\tan\left(\frac{a}{2}\right)\sec^3\left(\frac{a}{2}\right)\Bigg[\widetilde{\kappa}^3\left(3a + \sin(a)\right) + 32\widetilde{\gamma}\widetilde{\kappa}^2\Bigg\{\tan\left(\frac{a}{4}\right) + \\ &\sin\left(\frac{a}{2}\right)\Bigg\}\cos\left(\frac{a}{2}\right) + 16\widetilde{\gamma}^2\Bigg\{8\widetilde{\gamma}\tan\left(\frac{a}{4}\right)\cos\left(\frac{a}{2}\right) + 3a\widetilde{\kappa}\Bigg\}\cos^2\left(\frac{a}{2}\right)\Bigg]. \end{aligned} \tag{5.3.25}$$

Again by applying the conditions (5.2.4) to the system (5.3.22), we conclude that the constant $\widehat{B}$ is determined by the relation

$$\widetilde{B} = -\widehat{B}. \tag{5.3.26}$$

Similarly, considering the equation (5.3.22b), and following the same steps, we find

$$\widehat{\omega}_1 = \frac{-1}{48a}\left\{\widehat{B}^2\left(3a+\sin(a)\right) - 16B\widetilde{\gamma}\sin\left(\frac{a}{2}\right) + 12\widetilde{\gamma}^2 a - 16\widetilde{\gamma}\left(\frac{\widetilde{\gamma}^2}{\widehat{B}} + \widehat{B}\right)\tan\left(\frac{a}{4}\right)\right\}, \tag{5.3.27}$$

Introducing Eqs. (5.3.24), (5.3.26) and (5.3.27) to (5.3.22), we may write $\gamma_c \approx 0.96$.

$$\phi(x) = \pi + \begin{cases} \widetilde{B}\cos\left[\left(1+\epsilon\widetilde{\omega}_1\right)\left(x-\frac{a}{2}\right)\right] - \gamma, & (0 < x < a)\,, \\ -\kappa - \widetilde{B}\cos\left[\left(1+\epsilon\widehat{\omega}_1\right)\left(x-\frac{3a}{2}\right)\right] - \gamma, & (a < x < 2a)\,. \end{cases} \tag{5.3.28}$$

This gives the periodic solutions about π and $\pi - \kappa$ in the driven case. To obtain the solution in the undriven case, we simply put $\gamma = 0$ into the above system.

First we study the ground state solution about π and $\pi - \kappa$ in the presence of an applied bias current (γ). This is shown by the portion above the line $\phi \approx 1.31$ in Fig. 5.4. The two branches correspond to the value of the Josephson phase ϕ at the points $x = a/2$ (the lower branch) and $x = 3a/2$ (the upper branch). Here we have considered a unit distance between the two consecutive discontinuities and $\kappa = 0.5$. As the current increases, the Josephson phase ϕ decreases and the gap between the upper and lower branches becomes narrow. At a particular value of γ, the two branches coincide. Such solution ceases to exist if the bias current exceeds this particular value. This critical value of the bias current is denoted by γ_c. The value of the critical current is different for different values of the inter-vortex distance a, and the discontinuity κ. For $a = 1$, and $\kappa = 0.5$ we have found that

Below the line $\phi \approx 1.31$ is picture of the plot of the wave function ϕ as a function of the applied bias current given by the system (5.3.19). In this case, the upper and lower branches correspond to $x = a/2$ and $x = 3a/2$ respectively. When $\gamma = 0$ there are two periodic solutions, one emanating from the π-state (the upper lines) and the other from the 0-state (the lower lines). As the bias current increases, both the Josephson phases $\phi(a/2)$ and $\phi(3a/2)$ increase. This situation continues up to the point where the bias current attains its critical value γ_c.

At the critical bias current the branch corresponding to $x = a/2$ merges with the branch corresponding to $x = 3a/2$. At this point where $\gamma = \gamma_c$, the solution becomes unstable and turns around to a complementary unstable state (i.e., the solution corresponding to constant π background) at a saddle node bifurcation. From the same figure, we also notice that the graph of the solution corresponding to the zero background state is

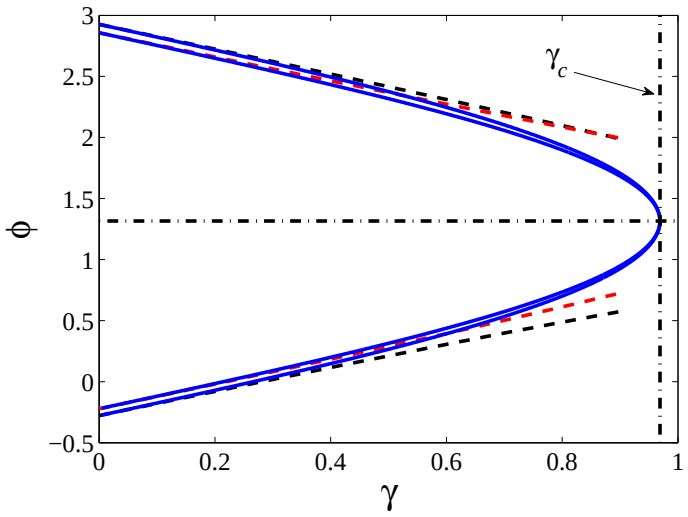

Figure 5.4: Comparison between the approximations to the profile of the wavefunctions $\phi(a/2)$ and $\phi(3a/2)$, (dotted lines) given by the systems (5.3.19) and (5.3.28) and the corresponding numerics (solid lines) as function of the applied bias current γ for $a = 1$ and $\kappa = 0.5$..

symmetric to the profile of its complementary state with respect to the horizontal line $\phi \approx 1.31$. The analytical approximation to the Josephson phase given by the systems (5.3.19)(lower dashed lines) and (5.3.28) upper dashed lines) are compared with the numerical counterparts, where one can see rather good agreement between them in the region where γ is close to zero.

The Josephson phase ϕ (5.3.28) as a function of the spatial variable x, both in the absence and presence of an applied bias current is shown by upper and lower panels of Fig. 5.5 respectively. We note that the solution is oscillating between its minimum and maximum values. These values are respectively attained the points $x = a/2$ and $x = 3a/2$. The solution is a sign-definite. Approximation to the ground state solution (5.3.28) is compared with the numerical solution. The same behaviour of the $\phi(x)$ is noted in the lower panel of the same figure, where we have taken $\gamma = 0.2$. Differences between the approximation and numerical calculation are of is $\sim \mathcal{O}(\epsilon^{3/2})$, given $\gamma = 0.2$ and $\gamma = \mathcal{O}(\epsilon^{1/2})$.

The top panel of Fig. 5.6 shows the profiles of ϕ as a function of the inter-vortex distance a for $\kappa = 0.5$ and $\gamma = 0$, where the upper and lower branches respectively correspond to the points $x = a/2$ and $x = 3a/2$. When the distance between the vortices is zero, then $\phi \approx 2.892$, and the magnetic flux ($\Delta\phi = \phi(3a/2) - \phi(a/2)$) is zero. As the inter-vortex distance increases, $\Delta\phi$ increases, showing an increase in the magnetic flux. In

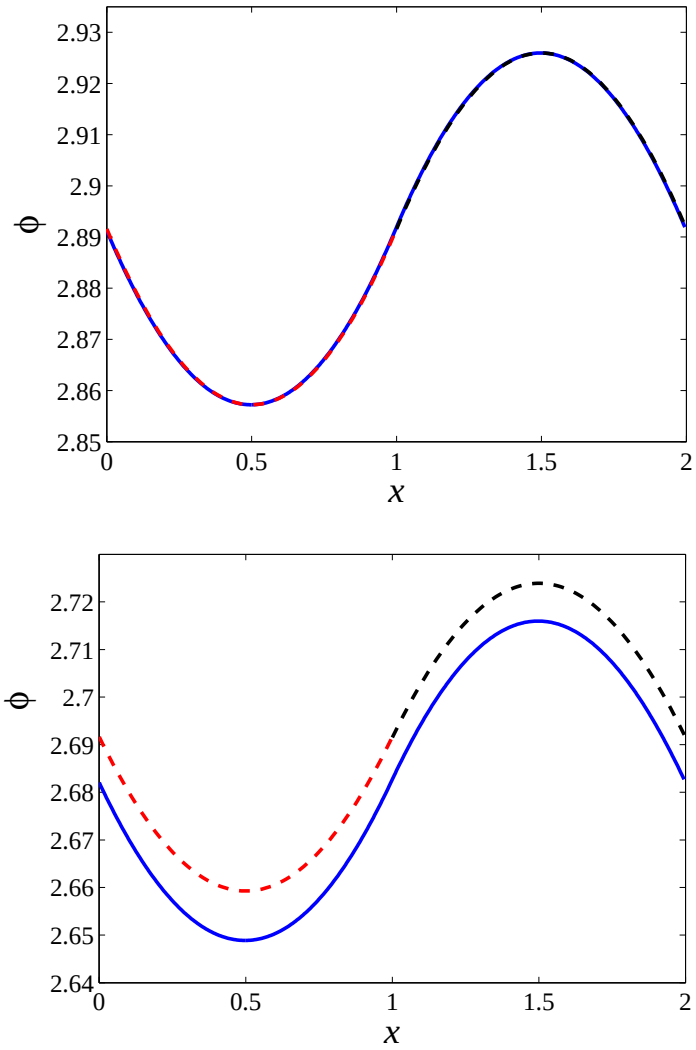

Figure 5.5: Comparison between the approximations (dashed lines) of the profile ϕ of the Josephson phase at $x = a/2$ and $x = 3a/2$ as a function of the spatial variable x given by system (5.3.28) and their corresponding numerics (solid lines). Here the discontinuity is 0.5, and discontinuities are taken to ba apart at a unit distance from each other. The lower panel represents the case where teh bias current is $\gamma = 0.2$, while $\gamma = 0$ in the upper panel.

this case, the approximation to the ground state solutions $\phi(a/2)$ and $\phi(3a/2)$ are in good agreement with the numerical calculations.

The lower panel of Fig. 5.6 represents the same profile but for the driven case, where $\gamma = 0.2$. In this case, the ground state solutions given by the systems (5.3.19) and (5.3.28) qualitatively agree with the corresponding numerics. The error is <0.01, which is of $\mathcal{O}(\epsilon^{3/2})$ since $\gamma \sim \sqrt{\epsilon}$ and $\gamma = 0.2$.

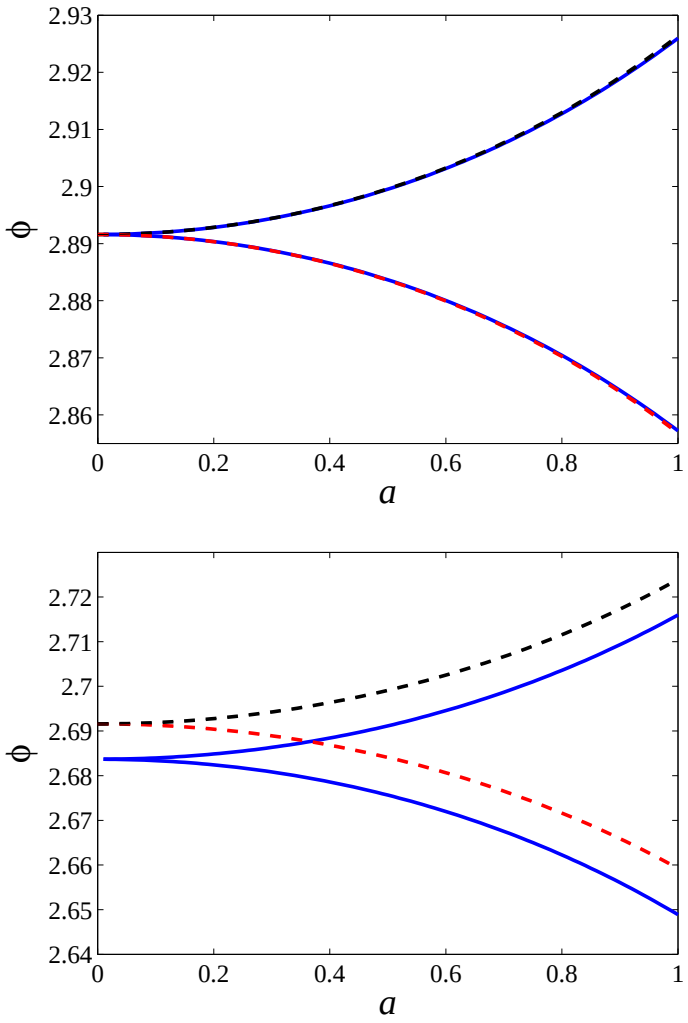

Figure 5.6: Comparison between the approximations (dashed lines) of the profile ϕ of the Josephson phase at $x = a/2$ and $x = 3a/2$ as a function of the inter-vortex distance a given by system (5.3.28) and their corresponding numerics (solid lines). The upper panel is the undriven case while the lower panel represents the driven case where we have taken $\gamma = 0.2$. The value of the discontinuity, κ, in both the cases is 0.5.

Next, we study the ground state solutions (5.3.19) and (5.3.28) in terms of the discontinuity κ both in the undriven and driven cases. The top panel of Figure 5.7 depicts the ground state solutions in the absence of the bias current $(\gamma = 0)$. It can be noted that when $\kappa = 0$, there is exactly solution $\phi = 0$ and $\phi = \pi$, each corresponding to the zero- and π-state. When the discontinuity, κ, in the phase increases, the solutions emanating from the $\phi = 0$ and $\phi = \pi$ decrease. For the 0-state (π-state) , the lower (upper) and upper (lower) branches correspond respectively to $x = a/2$ and $x = 3a/2$. At a certain

value of the discontinuity, the gaps between the two branches emanating from $\phi = 0$ and $\phi = \pi$ vanish at the points $\phi = -\pi$ and $\phi = 0$ respectively. Approximations to the Josephson phases (5.3.19) and (5.3.28) are compared with the numerical simulations.

The lower panel of Figure 5.7 represents the case of a nonzero bias current ($\gamma = 0.2$). Again, at the point $\kappa = 0$, there is one solution for the 0- and π-states. An increase of the discontinuity in the Josephson phase causes a decrease in solutions ϕ, in both the zero and π-states. Following the branches $\phi(a/2)$ and $\phi(3a/2)$ corresponding to the zero solution, one can observe that the solutions decrease up to a certain value of the discontinuity. This situation terminates after a critical value, κ_c is reached. At this particular discontinuity, κ_c, the anti-ferromagnetic (AFM) state becomes unstable and turns itself into its complementary state emanating from the constant $\phi = \pi$ solution, in a saddle node bifurcation.

For different values of the applied bias current and the inter-vortex distance a, there exists a different κ_c. For example, when $a = 1$, and $\gamma = 0.2$, we have found that $\kappa_c \approx 2.675$. There is no static ground state solution in the region where κ exceeds its critical value κ_c.

We note that in the case when there is no external current applied to the junction (γ=0), the approximation to Josephson phase $\phi(\kappa)$ analytically given by the systems (5.3.19) and (5.3.28) are in excellent agreement with their numerical counterparts. In the driven case when $\gamma = 0.2$, the numerical simulations are well approximated by our approximations in the region where κ is close to zero. The errors are ~ 0.01 which is $\mathcal{O}(\epsilon^{3/2})$, given $\gamma = \mathcal{O}(\epsilon^{1/2})$.

5.4 Stability analysis of the periodic solutions

5.4.1 Stability of the periodic solutions about the stationary 0-solution

In this section, we study the stability of the periodic solutions about $\phi = 0$. For this purpose, we perform perturbation analysis and assume

$$\phi(x,t) = \phi_s(x) + \epsilon e^{\lambda t} V(x), \quad (0 < x < 2a), \tag{5.4.1}$$

where $\epsilon \ll 1$ is perturbation parameter, $\lambda \in \mathbb{C}$, and $\phi_s(x)$ is the ground state solution about $\phi = 0$, approximately given by the system (5.3.19).

Introducing the assumption (5.4.1) into the sine Gordon model (5.2.2), expanding the resulting equation by Taylor's series about ϵ, and neglecting smaller terms leads to the

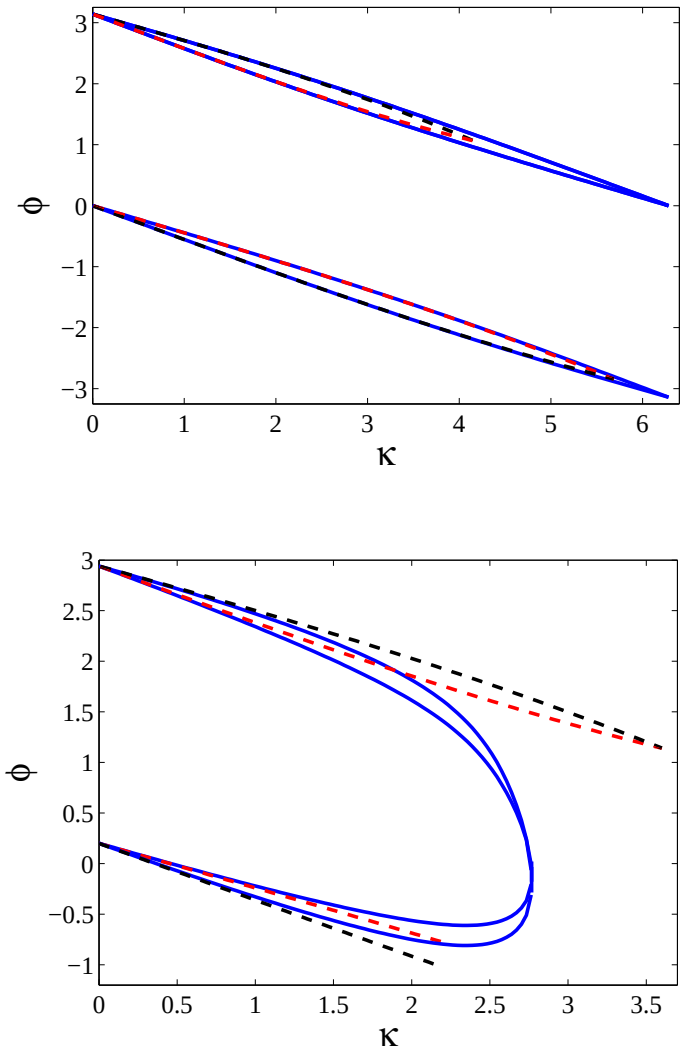

Figure 5.7: Plot of the approximations to the profiles $\phi(a/2)$ and $\phi(3a/2)$, given by the systems (5.3.19) (lower dashed lines) and (5.3.28) (upper dashed lines) as a function of the discontinuity κ, where the distance between consecutive discontinuities is unity. The upper panel of the Figure represents the case when there is no bias current applied to the system. The lower panel represents the driven case where we have taken $\gamma = 0.2$. The solid lines represent the corresponding numerical simulations.

eigenvalue problem at $\mathcal{O}(\epsilon)$

$$V_{xx} - \lambda^2 V = \cos(\phi_s + \theta)V, \quad (0 < x < 2a). \tag{5.4.2}$$

By the help of Eqs. (5.2.3) and (5.3.19) and a formal series expansion of $\cos(\phi_s + \theta(x))$,

up to second order in $\phi_s + \theta$, one may write

$$\cos(\phi_s+\theta) = \begin{cases} 1-\dfrac{1}{2}\left[A\cosh\left(\widetilde{\omega}\left(x-\dfrac{a}{2}\right)\right)+\gamma\right]^2, & (0<x<a), \\ 1-\dfrac{1}{2}\left[A\cosh\left(\widehat{\omega}\left(x-\dfrac{3a}{2}\right)\right)-\gamma\right]^2, & (a<x<2a), \end{cases} \tag{5.4.3}$$

where $\widetilde{\omega} = 1+\epsilon\widetilde{\omega}_1$, $\widehat{\omega} = 1+\epsilon\widehat{\omega}_1$ with quantities $\widetilde{\omega}_1$, $\widehat{\omega}_1$ and A being respectively given by Eqs. (5.3.13), (5.3.27), and (5.3.18). In order to simplify our calculations, we Fourier expand $\cos(\phi_s+\theta(x))$ in (5.4.3) above, and obtain

$$\cos(\phi_s+\theta(x)) = \frac{a_0}{2} + \sum_{n=0}^{\infty}\left\{R_{2n+1}\sin\left(\frac{(2n+1)\pi x}{a}\right) + R_{2n+2}\cos\left(\frac{(2n+2)\pi x}{a}\right)\right\}. \tag{5.4.4}$$

The first few terms of this expansion are

$$\begin{aligned} a_0 &= 2-\gamma^2-\frac{A^2}{2}\left(1+\frac{\sinh(\omega a)}{\omega a}\right), \\ R_1 &= -\frac{4\pi A\gamma\cosh(\omega a/2)}{\pi^2+\omega^2a^2}, \quad R_2 = -\frac{2A^2\omega a\sinh(\omega a)}{4\pi^2+4\omega^2a^2}, \\ R_3 &= -\frac{12\pi A\gamma\cosh(\omega a/2)}{9\pi^2+\omega^2a^2}, \quad R_4 = -\frac{2A^2\omega a\sinh(\omega a)}{16\pi^2+4w^2a^2}. \end{aligned}$$

From here onwards, we will be using these five terms as an approximation for the Fourier series of $\cos(\phi_s+\theta)$. Writing $E=\lambda^2$ and substituting Eq. (5.4.4) into Eq. (5.4.2), the eigenvalue problem (5.4.2), we obtain the following generalised Mathieu's equation

$$V_{xx} - \left[E+\frac{a_0}{2}+\sum_{n=0}^{\infty}\left\{R_{2n+1}\sin\left(\frac{(2n+1)\pi x}{a}\right)+R_{2n+2}\cos\left(\frac{(2n+2)\pi x}{a}\right)\right\}\right]V = 0. \tag{5.4.5}$$

From the stability ansatz (5.4.1), it is obvious that a solution is stable whenever λ is purely imaginary. Thus a solution is stable in the region where $E<0$ and is unstable otherwise.

5.4.2 Boundary of stability curves by perturbation

By using the scalings (5.3.4), we note that $a_0 = 1+\mathcal{O}(\epsilon)$. Let us define $\delta = \mathcal{O}(1)$, then by taking

$$E+1 = -\delta, \tag{5.4.6}$$

and introducing the scaling $R_i = -\epsilon r_i$, where $\epsilon \ll 1$ and $i = 1,\ldots 4$, the eigenvalue problem (5.4.5) takes the canonical form of the Mathieu's Equation

$$\begin{aligned} V_{xx} \quad &+\left[\delta+\epsilon\left\{E_0+r_1\sin\left(\frac{\pi x}{a}\right)+r_2\cos\left(\frac{2\pi x}{a}\right)+r_3\sin\left(\frac{3\pi x}{a}\right)\right.\right. \\ &\left.\left.+r_4\cos\left(\frac{4\pi x}{a}\right)\right\}\right]V = 0, \end{aligned} \tag{5.4.7}$$

where

$$E_0 = \frac{1}{2}\left[\tilde{\gamma}^2 + \frac{A^2}{2}\left(1 + \frac{\sinh(\omega a)}{\omega a}\right)\right]. \tag{5.4.8}$$

The general theory (Floquet analysis) of differential equations with periodic coefficients divides the (δ, κ)-plane into the regions of bounded solutions (allowed bands) and unbounded solutions (forbidden bands) of $V(x)$ as $x \to \infty$, see for instance, McLachlan [149] and Chicone [150]. The curves separating these regions are known as the *transition curves* or *Arnold tongues*. Floquet theory also confirms the existence of linearly increasing and periodic solutions (having periods $2a$ and $4a$) along the transition curves.

In the following, we focus our attention on obtaining approximate expressions for the Arnold tongues and the corresponding eigenfunctions V. We note that when $\epsilon = 0$, the necessary condition for the potential V to be $4a-$periodic is $\delta = (n\pi/2a)^2$, where $n \in \mathbb{Z}$. In other words, the Arnold tongues intersect the line $\kappa = 0$ at the critical points

$$\delta_c = \left(\frac{n\pi}{2a}\right)^2, \; n = 0, 1, 2, ... \tag{5.4.9}$$

We follow a perturbation technique, the so called method of strained parameters, see for example, Nayfeh and Mook [151], to investigate the boundary of boundedness of the periodic solutions. We find approximations which hold only on the transitional curves and hence do not give solution that holds in a small neighborhood of the Arnold tongues.

As discussed earlier, there exist periodic solutions of Eq. (5.4.7) on the transition curves having period $2a$ and $4a$. These periodic solutions and the transitional curves are determined in the form of the following perturbation series

$$V = V_0 + \epsilon V_1 + \epsilon^2 V_2 + \mathcal{O}(\epsilon^3), \tag{5.4.10a}$$

$$\delta = \left(\frac{n\pi}{2a}\right)^2 + \epsilon\delta_1 + \epsilon^2\delta_2 + \mathcal{O}(\epsilon^3), \tag{5.4.10b}$$

where $n \in \mathbb{Z}$. Putting Eqs. (5.4.10a) and (5.4.10b) into Eq. (5.4.7) and comparing the coefficients of ϵ on both sides of the resulting expression, we obtain

$$\mathcal{O}(\epsilon^0): \quad V_0'' + \left(\frac{n\pi}{2a}\right)^2 V_0 = 0, \tag{5.4.11a}$$

$$\mathcal{O}(\epsilon^1): \quad V_1'' + \left(\frac{n\pi}{2a}\right)^2 V_1 = -SV_0, \tag{5.4.11b}$$

$$\mathcal{O}(\epsilon^2): \quad V_2'' + \left(\frac{n\pi}{2a}\right)^2 V_2 = -\delta_2 V_0 - SV_1, \tag{5.4.11c}$$

where the primes denote derivatives with respect to x and

$$S = \delta_1 + E_0 + r_1 \sin\left(\frac{\pi x}{a}\right) + r_2 \cos\left(\frac{2\pi x}{a}\right) + r_3 \sin\left(\frac{3\pi x}{a}\right) + r_4 \cos\left(\frac{4\pi x}{a}\right).$$

In the following, we find the expressions for the boundary of allowed and forbidden bands for the first few non-negative values of n.

5.4.3 Transitional curves corresponding to $n = 0$

First, we find the transitional curve in (δ, κ)-plane for the case when $n = 0$. For this situation, Eq. (5.4.11a) is simplified to $V_0'' = 0$, whose periodic particular solution is given by

$$V_0 = A_0, \tag{5.4.12}$$

where A_0 is a constant of integration. Inserting this into Eq. (5.4.11b), one may write

$$V_1'' = -A_0\left[\delta_1 + E_0 + r_1 \sin\left(\frac{\pi x}{a}\right) + r_2 \cos\left(\frac{2\pi x}{a}\right) + r_3 \sin\left(\frac{3\pi x}{a}\right) + r_4 \cos\left(\frac{4\pi x}{a}\right)\right], \tag{5.4.13}$$

such that V_1 is expected to be periodic. To obtain such a V_1, we have to remove the secular terms in (5.4.13). To do so, we set $A_0\,(\delta_1 + E_0) = 0$. This implies that for a periodic V_1, we have either $A_0 = 0$ or $\delta_1 + E_0 = 0$. We are not interested in the first possibility as this implies V_0 will be trivial. To avoid this, we are forced to assure

$$\delta_1 = -E_0. \tag{5.4.14}$$

By inserting (5.4.14) into Eq. (5.4.13) and integrating twice with respect to x, the periodic particular solution of the resulting equation is given by

$$V_1 = A_0\left(\frac{a}{\pi}\right)^2\left[r_1 \sin\left(\frac{\pi x}{a}\right) + \frac{r_2}{4}\cos\left(\frac{2\pi x}{a}\right) + \frac{r_3}{9}\sin\left(\frac{3\pi x}{a}\right) + \frac{r_4}{16}\cos\left(\frac{4\pi x}{a}\right)\right]. \tag{5.4.15}$$

Substituting Eqs. (5.4.12) and (5.4.15) into Eq. (5.4.11c) and simplifying we may write

$$\begin{aligned} V_2'' &= -\delta_2 A_0 + A_0\left(\frac{a}{\pi}\right)^2\left[-S_1 + S_2 \sin\left(\frac{\pi x}{a}\right) + S_3 \cos\left(\frac{2\pi x}{a}\right) + S_4 \sin\left(\frac{3\pi x}{a}\right)\right. \\ &+ \left. S_5 \cos\left(\frac{4\pi x}{a}\right)\right], \end{aligned} \tag{5.4.16}$$

where the terms S_i are defined by

$$\begin{aligned} S_1 &= \frac{1}{2}\left(r_1^2 + \frac{r_2^2}{4} + \frac{r_3^2}{9} + \frac{r_4^2}{16}\right), \quad S_2 = \frac{1}{8}\left(5r_1r_2 - \frac{13r_2r_3}{9} + \frac{25r_3r_4}{16}\right), \\ S_3 &= \frac{r_1^2}{2} - \frac{5r_1r_3}{9} - \frac{5r_2r_4}{32}, \quad S_4 = \frac{r_1}{8}\left(5r_2 - \frac{17r_4}{4}\right), \quad S_5 = \frac{5r_1r_3}{9} - \frac{r_2^2}{8}. \end{aligned}$$

From (5.4.16), it is clear that the periodicity condition for V_2 demands

$$-\delta_2 A_0 - A_0\left(\frac{a}{\pi}\right)^2 S_1 = 0.$$

As mentioned above that $A_0 \neq 0$, hence the last expression yields

$$\delta_2 = -\left(\frac{a}{\pi}\right)^2 S_1. \tag{5.4.17}$$

With the help of Eqs. (5.4.14) and (5.4.17), Eq. (5.4.10b) gives

$$\delta = -\epsilon E_0 - \epsilon^2 \left(\frac{a}{\pi}\right)^2 S_1, \tag{5.4.18}$$

with E_0 given by (5.4.8), which is the expression for the boundary of the stability curve corresponding to $n = 0$. The approximation of the stability curve given by (5.4.18) is presented by the upper dashed lines in Figures 5.8, 5.9 and 5.10.

After the secular terms have been removed, the periodic solution of Eq. (5.4.16) becomes

$$V_2 = A_0 \left(\frac{a}{\pi}\right)^4 \left[S_2 \sin\left(\frac{\pi x}{a}\right) + \frac{S_3}{4}\cos\left(\frac{2\pi x}{a}\right) + \frac{S_4}{9}\sin\left(\frac{3\pi x}{a}\right) + \frac{S_5}{16}\cos\left(\frac{4\pi x}{a}\right)\right]. \tag{5.4.19}$$

By inserting Eqs. (5.4.12) and (5.4.15) into Eq. (5.4.10a), the corresponding equation for V can be found.

One may proceed further to obtain higher-order corrections of the transitional curve.

5.4.4 Arnold tongues bifurcating from $\delta = (\pi/2a)^2$

5.4.4.1 Leading order term

Next, we consider the case when $n = 1$. In this case the Arnold tongue bifurcates from the point $\delta = (\pi/2a)^2$ on the axis where $\kappa = 0$. The periodic solution of Eq. (5.4.11a) is given by

$$V_0 = A_0 \cos\left(\frac{\pi x}{2a}\right) + B_0 \sin\left(\frac{\pi x}{2a}\right). \tag{5.4.20}$$

Substituting this into Eq. (5.4.11b), we obtain

$$\begin{aligned} V_1'' + \left(\frac{\pi}{2a}\right)^2 V_1 \;=\; & -\left\{A_0\left(\delta_1 + E_0\right) + \frac{r_1}{2}B_0\right\}\cos\left(\frac{\pi x}{2a}\right) \\ & -\left\{B_0\left(\delta_1 + E_0\right) + \frac{r_1}{2}A_0\right\}\sin\left(\frac{\pi x}{2a}\right) + \frac{1}{2}\Bigg\{\left(r_1 B_0 - r_2 A_0\right)\cos\left(\frac{3\pi x}{2a}\right) \\ & -\left(r_1 A_0 - r_2 B_0\right)\sin\left(\frac{3\pi x}{2a}\right) - \left(r_2 A_0 + r_3 B_0\right)\cos\left(\frac{5\pi x}{2a}\right) \\ & -\left(r_2 B_0 + r_3 A_0\right)\sin\left(\frac{5\pi x}{2a}\right) + \left(r_3 B_0 - r_4 A_0\right)\cos\left(\frac{7\pi x}{2a}\right) \\ & -\left(r_3 A_0 - r_4 B_0\right)\sin\left(\frac{7\pi x}{2a}\right)\Bigg\}. \end{aligned} \tag{5.4.21}$$

To ensure that V_1 is periodic, the secular terms must vanish, which implies

$$A_0\left(\delta_1+E_0\right)+\frac{r_1}{2}B_0=0, \tag{5.4.22}$$

$$B_0\left(\delta_1+E_0\right)+\frac{r_1}{2}A_0=0. \tag{5.4.23}$$

Eq. (5.4.22) gives

$$A_0=-\frac{r_1}{2\left(\delta_1+E_0\right)}B_0. \tag{5.4.24}$$

Substituting the value of A_0 from Eq. (5.4.24) into Eq. (5.4.23), we find

$$\left[\left(\delta_1+E_0\right)^2-\left(\frac{r_1}{2}\right)^2\right]B_0=0.$$

This equation implies either $B_0=0$ or

$$\delta_1=-E_0\pm\frac{r_1}{2}. \tag{5.4.25}$$

Clearly for a nontrivial V_0, one must discard the possibility $B_0=0$. From expression (5.4.25) we deduce that corresponding to the two values of δ_1, there are two branches of the transitional curves emanating from the point $(\pi/2a)^2$, which we find in the following.

By considering the two cases in (5.4.25) separately, and inserting into Eq. (5.4.24), one can respectively obtain

$$A_0=\mp B_0. \tag{5.4.26}$$

It is easy to verify that by introducing (5.4.26) into Eq. (5.4.20), we can write

$$V_0=\mp B_0\left[\cos\left(\frac{\pi x}{2a}\right)\mp\sin\left(\frac{\pi x}{2a}\right)\right]. \tag{5.4.27}$$

5.4.4.2 First correction term

As a result, Eq. (5.4.21) reduces to

$$\begin{aligned}V_1''+\left(\frac{\pi}{2a}\right)^2V_1 \;=\; & \frac{B_0}{2}\Bigg[\left(r_1\pm r_2\right)\left\{\cos\left(\frac{3\pi x}{2a}\right)\pm\sin\left(\frac{3\pi x}{2a}\right)\right\}\\ & \pm\left(r_2\mp r_3\right)\left\{\cos\left(\frac{5\pi x}{2a}\right)\mp\sin\left(\frac{5\pi x}{2a}\right)\right\}\\ & +\left(r_3\pm r_4\right)\left\{\cos\left(\frac{7\pi x}{2a}\right)\pm\sin\left(\frac{7\pi x}{2a}\right)\right\}\Bigg].\end{aligned}$$

The particular periodic solution of this equation can be easily obtained by integrating it twice with respect to x as follows

$$\begin{aligned}V_1 \;=\; & -2B_0\left(\frac{a}{\pi}\right)^2\Bigg[\frac{r_1\pm r_2}{9}\left\{\cos\left(\frac{3\pi x}{2a}\right)\pm\sin\left(\frac{3\pi x}{2a}\right)\right\}\pm\frac{r_2-r_3}{25}\left\{\cos\left(\frac{5\pi x}{2a}\right)\mp\right.\\ & \left.\sin\left(\frac{5\pi x}{2a}\right)\right\}+\frac{r_3\pm r_4}{49}\left\{\cos\left(\frac{7\pi x}{2a}\right)\pm\sin\left(\frac{7\pi x}{2a}\right)\right\}\Bigg].\end{aligned} \tag{5.4.28}$$

5.4.4.3 Second correction term

Next, we insert Eqs. (5.4.27) and (5.4.28) into Eq. (5.4.11c) to obtain

$$\begin{aligned} V_2'' + \left(\frac{\pi}{2a}\right)^2 V_2 &= \left(\frac{a}{\pi}\right)^2 B_0 \Bigg\{ \left(S_6 \mp \left(\frac{\pi}{a}\right)^2 \delta_2\right) \left[\cos\left(\frac{\pi x}{2a}\right) \mp \sin\left(\frac{\pi x}{2a}\right)\right] \\ &\quad + S_7 \left[\cos\left(\frac{3\pi x}{2a}\right) \pm \sin\left(\frac{3\pi x}{2a}\right)\right] + S_8 \left[\cos\left(\frac{5\pi x}{2a}\right) \mp \sin\left(\frac{5\pi x}{2a}\right)\right] \\ &\quad + S_9 \left[\cos\left(\frac{7\pi x}{2a}\right) \pm \sin\left(\frac{7\pi x}{2a}\right)\right] \Bigg\}, \end{aligned} \tag{5.4.29}$$

where we have defined

$$\begin{aligned} S_6 &= \pm\frac{2r_3}{25}\left(r_2 \mp \frac{37r_3}{49}\right] - \frac{r_1}{9}\left(r_1 \pm 2r_2\right) \mp \frac{r_4}{49}\left(2r_3 \pm r_4\right) - \frac{34r_2^2}{225}, \\ S_7 &= \frac{2r_2}{9}\left(\frac{29r_3}{49} + \frac{8r_1}{25}\right) \pm \frac{r_1}{9}\left(r_1 + \frac{34r_3}{25}\right) \pm \frac{r_4}{25}\left(\frac{74r_2}{49} \mp r3\right), \\ S_8 &= \frac{r4}{9}\left(\frac{58r_1}{49} \pm r_2\right) \mp \frac{r_1}{9}\left(r_1 \pm \frac{16r_2}{25}\right) - \mp\frac{248r_1r_3}{1225}, \\ S_9 &= \frac{r_1}{49}\left(r_4 \mp \frac{24r_3}{25}\right) \pm \frac{r_2}{9}\left(r_2 \pm \frac{34r_1}{25}\right). \end{aligned}$$

To ensure that V_2 is periodic, we take

$$\delta_2 = \pm\left(\frac{a}{\pi}\right)^2 S_6. \tag{5.4.30}$$

Substituting the values of δ_1 and δ_2 respectively from (5.4.25) and (5.4.30) into Eq. (5.4.10b), we find that transitional curves emanating from the point $\delta = (\pi/2a)^2$ have the following form

$$\delta = \left(\frac{\pi}{2a}\right)^2 \pm \epsilon\left(\mp E_0 + \frac{r_1}{2}\right) \pm \epsilon^2\left(\frac{a}{\pi}\right)^2 S_6. \tag{5.4.31}$$

The transitional curves given by the expression (5.4.31) are depicted by the second and third dashed lines (from the top) in Figures 5.9 and 5.10.

By the help of Eq. (5.4.30) and Eq. (5.4.29), it is possible to verify that the particular solution is given by

$$\begin{aligned} V_2 &= -2\left(\frac{a}{\pi}\right)^4 B_0 \Bigg\{ \frac{S_7}{9}\left[\cos\left(\frac{3\pi x}{2a}\right) \pm \sin\left(\frac{3\pi x}{2a}\right)\right] + \frac{S_8}{25}\left[\cos\left(\frac{5\pi x}{2a}\right) \mp \sin\left(\frac{5\pi x}{2a}\right)\right] \\ &\quad + \frac{S_9}{49}\left[\cos\left(\frac{7\pi x}{2a}\right) \pm \sin\left(\frac{7\pi x}{2a}\right)\right] \Bigg\}. \end{aligned} \tag{5.4.32}$$

Once, the values of V_0, V_1 and V_2 from Eqs. (5.4.20), (5.4.28) and (5.4.32) respectively, have been introduced into Eq. (5.4.10a), one can find the expressions for the eigenfunction corresponding to the stability curves emanating from $(\pi/2a)^2$.

5.4.5 Arnold tongues corresponding to $n = 2, 3, 4$

To find the expressions for the Arnold tongues emanating from the points the points $(n\pi/2a)^2$, where $n = 2, 3, 4$, a similar analysis can be performed. We find that these stability curves have respectively the following expressions

$$\delta = \left(\frac{\pi}{a}\right)^2 - \epsilon\left(E_0 \mp \frac{r_2}{2}\right) + \epsilon^2\left(\frac{a}{\pi}\right)^2 S_{14}, \tag{5.4.33a}$$

$$\delta = \left(\frac{3\pi}{2a}\right)^2 - \epsilon\left(E_0 \mp \frac{r_3}{2}\right) + \epsilon^2\left(\frac{a}{\pi}\right)^2 S_{23}, \tag{5.4.33b}$$

$$\delta = \left(\frac{2\pi}{a}\right)^2 - \epsilon\left(E_0 \mp \frac{r_4}{2}\right) + \epsilon^2\left(\frac{\pi}{a}\right)^2 S_{31}. \tag{5.4.33c}$$

The approximation of the stability curves given by Eq. (5.4.33a) are presented by the third and fourth pairs of dashed lines (from the top) in Figures 5.9 and 5.10. The first equations in (5.4.33a) are presented by the second pairs of dashed lines (from the top) in Figure 5.8.

The S_i terms in the equations of (5.4.33) are defined by

$$\begin{aligned}
S_{14} &= -\frac{1}{4}\left(\frac{r_1^2}{4} \mp \frac{r_2^2}{9}\right) \pm \frac{r_2}{18}\left(\frac{r_2}{2} + r_4\right) \pm \frac{r_3}{8}\left(r_1 - \frac{5r_3}{8}\right), \\
S_{23} &= \mp\frac{2r_1}{25}\left(13r_1 \pm r_4\right) \pm 2r_2\left(r_1 - \frac{25r_2}{49}\right) - \frac{r_4^2}{25}, \\
S_{31} &= \frac{1}{4}\left(\frac{r_2^2}{16} + r_3^2\right) + \frac{r_1}{2}\left(\frac{5r_1}{9} \pm r_3\right).
\end{aligned}$$

The corresponding eigenfunctions are presented in the appendix (see Section 7.5).

5.4.6 Allowed and forbidden bands in the absence of external current

Let us first study the structure of the band-gaps in the (δ, κ)-plane, considering the case where the applied bias current (γ) is zero. In such a situation, the terms R_1 and R_3, defined in Section 5.4.1, become zero, which results in $r_1 = r_3 = 0$ (see Section 5.4.2). Consequently, the expressions for the Arnold tongues obtained in section 5.4.2 become much simpler. First, we consider the case of the band structure related to the 0-state. In the top panel of Figure 5.8, we present the band-gap structure, analytically given by Eqs. (5.4.18), (5.4.31), (5.4.33a), (5.4.33b), and (5.4.33c), as a function of the discontinuity κ, for a moderate value of the distance ($a = 3$) between the consecutive discontinuities in the Josephson phase. The figure reveals that when there is no discontinuity in the Josephson phase, i.e., $\kappa = 0$, the junction has a semi-infinite forbidden band (or plasma gap) for $-1 < E$. In other words, there does not exist any bounded periodic solution

in the region $E > -1$. The junction has a semi-infinite allowed band (also known as the continuous plasma band) in the region where the eigenfrequency $E < -1$. In this region, the periodic solution of the eigenvalue problem is stable (bounded).

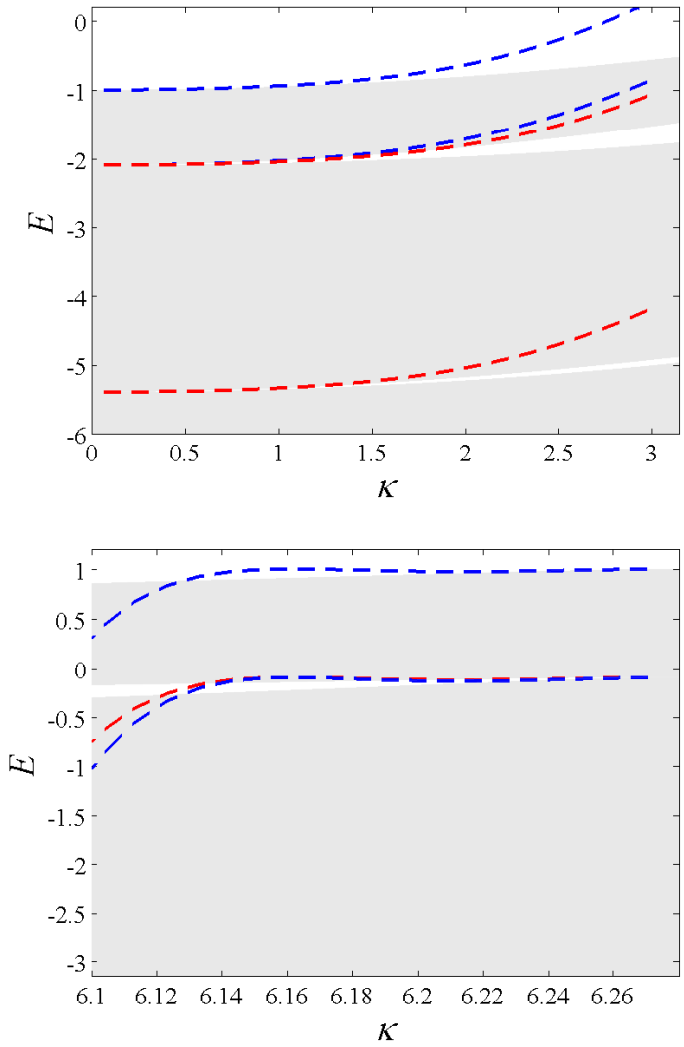

Figure 5.8: Comparison between the approximation of the Arnold tongues (dashed lines) given by Eqs. (5.4.18), (5.4.31), (5.4.33a), (5.4.33b), (5.4.33c) and the corresponding numerical solutions (grey regions) in the undriven case. Here we have considered a moderate value of inter-vortex distance $a = 3$. The upper panel represents the band-gap structure corresponding to the constant solution $\phi \equiv 0$, while the lower one is related to the uniform solution $\phi \equiv \pi$.

As the discontinuity, κ, in the Josephson phase increases, a pair of vortex and anti-vortex appears and the eigenfrequency splits into bands. Hence one can observe small gaps that appear in the continuous plasma band. The band gaps broaden in the direc-

tion of increasing κ. At $\kappa = \kappa_c(a)$ (which for $a = 3$ is approximately equal to 4.52), the state bifurcating from the constant zero solution becomes unstable and is converted to its counterpart solution which emanates from the uniform π-background. As a result, the κ-pair of vortices is converted to a pair of $2\pi - \kappa$ vortices, as depicted in the lower panel of Fig. 5.8.

It can be verified that the width of the band-gaps in the plasma bands depends upon the distance between two consecutive discontinuities in the junction. When the consecutive discontinuities are close to each other, i.e., when a is small, the opening in a band-gap is narrow, that is, the region of unboundedness is small enough in terms of an increasing discontinuity. The opening in the band-gap structure will broaden as one increase the distance between two consecutive vortices.

5.4.6.1 The effect of a bias current on Arnold tongues

Next, we study the effect of an applied bias current γ on the structure of the stability curves in the presence of an applied bias current for a moderate value of the parameter a, the distance between two consecutive vortices. The upper panel of Figure 5.9 shows the plot the transitional curves, obtained from our analytical work in Section 5.4.2, in the (κ, δ)-plane where we have taken $a = 3$ and $\gamma = 0.1$. It can immediately be seen from the figure that an application of external current to the junction causes the opening of additional band-gaps (forbidden bands) in band structure. As in the undriven case, when there is no discontinuity in the Josephson phase ($\kappa = 0$), an infinite plasma band (continuous spectrum) corresponding to the solution $\phi \equiv 0$ can be found in the region $E < -1$. As the discontinuity κ is increased, band-gaps are observed in the plasma bands. There are additional openings in the band-structure in the driven case, which emanate from the points $\delta = (m\pi/2a)^2$, where m is an even integer. The band-gap broadens with the increase in the phase-discontinuity. In the same figure, our analytical work (dashed lines) is compared with the corresponding numerical calculations. For a small discontinuity, one can see a rather good agreement between them. When κ attains its critical value, the stability curves switch to their complementary π-state.

By increasing the discontinuity in the phase, κ, one will observe that the openings of the band gap are broadened. For instance, we consider the case when $k = \pi$, and study the effect of a bias current on the band-gap structure, where we consider a moderate value of the inter-vortex distance $a = 3$. The dashed lines in the upper panel of Figure 5.10, are the approximation to the Arnold tongues given by Eqs. (5.4.18), (5.4.31), (5.4.33a),

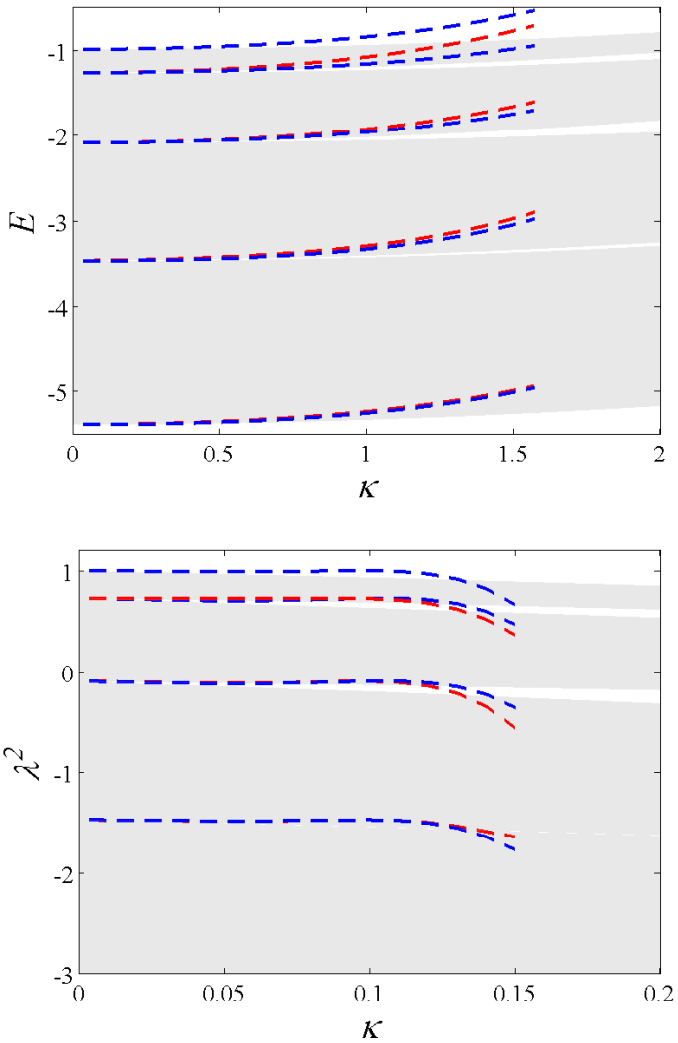

Figure 5.9: The structure of the band-gap in the (δ, κ)-plane in the presence of an applied bias current. The dashed lines are the approximations obtained by Eqs. (5.4.18), (5.4.31), (5.4.33a), (5.4.33b), and (5.4.33c), where we have taken $\gamma = 0.1$. In the upper panel represents the transitional curves corresponding to the solution $\phi = 0$, while the lower panel is the corresponding complementary state $\phi = \pi$.

(5.4.33b), and (5.4.33c), while the boundaries of the grey regions are the correspondng numerical simulations. We observe a qualitative agreement between the approximations and numerical solutions. The reason for this bad agreement is due to the fact that the approximation to the Arnold tongues are obtained by assuming κ small (see Section 5.3).

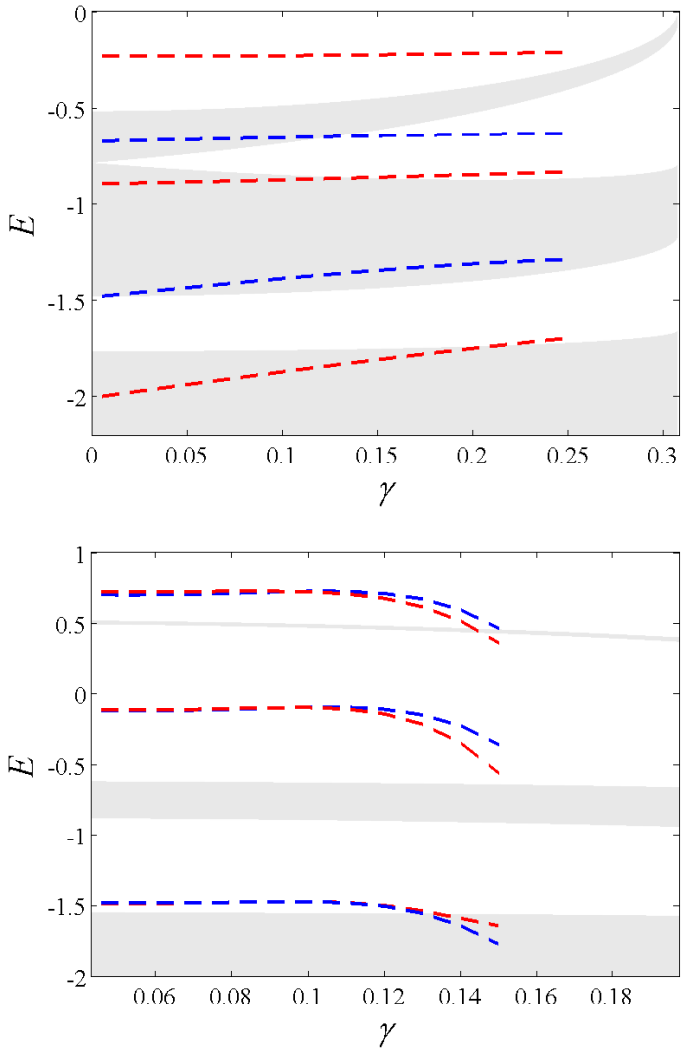

Figure 5.10: Stability curves versus the applied bias current about the periodic zero solution (upper) and the complementary π background (lower). Here, the coupling parameter $a = 3$ and the discontinuity κ is equal to π.

5.4.7 Stability of the periodic solutions about π

In this section, we study the stability of the periodic solutions about the static π-solution. To do so, a similar analysis can be performed. We use (5.2.3) and Fourier expand (5.3.28) to obtain (5.4.4), with the Fourier coefficients defined as

$$a_0 = -2 + \gamma^2 + \frac{B^2}{2}\left(1 + \frac{\sin(\omega a)}{\omega a}\right), \quad R_1 = -\frac{4\pi\gamma B\cos(\omega a/2)}{\pi^2 - \omega^2 a^2},$$
$$R_2 = \frac{-2a\omega B^2\sin(\omega a)}{4\pi^2 - 4a^2\omega^2}, \quad R_3 = -\frac{12\pi\gamma B\cos(\omega a/2)}{9\pi^2 - \omega^2 a^2}, \quad R_4 = \frac{-2a\omega B^2\sin(\omega a)}{16\pi^2 - 4a^2\omega^2}. \tag{5.4.34}$$

After perturbing the static solutions given by system (5.3.28) in the form (5.4.1), using the analysis and scaling of sections 5.4.1 and 5.4.2 along with the assumption

$$\delta = 1 - E, \quad E_0 = -\frac{1}{2}\left[1 + \frac{\widetilde{B}^2}{2}\left(1 + \frac{\sin(\omega a)}{\omega a}\right)\right], \quad B = \sqrt{\epsilon}\widetilde{B}, \tag{5.4.35}$$

Eq. (5.4.5) takes the canonical form of Mathieu's equation given by Eq. (5.4.7).

Using the values defined in Eq. (5.4.35) and by following the steps similar to Section 5.4.2, the same expressions for the Arnold tongues and the corresponding eigenfunctions can be derived.

The stability curves obtained for the undriven case, in the (κ, δ)-plane, for $a = 3$ are shown in the lower panel of Figure 5.8. It can be easily seen from the figure that the band-gap (forbidden band) lies in the region where $E > 1$. One can also deduce that in the case of absence of the discontinuities, the junction has a continuous plasma band in the region $E < 1$.

The effect of the bias current on the Arnold tongues, for $a = 3$ and $\gamma = 0.1$ is shown in the lower panel of Figure 5.9. It can be clearly observed from the figure that by applying a bias current, an additional forbidden band in the structure of the Arnold tongues can be created, similar to the zero stability case discussed in the last section. As κ increases, the forbidden bands widen. Our analytical results (dashed lines) are compared with the numerical simulations (grey regions), where we notice that a good agreement between them is found in the range where the discontinuity is small enough.

The behaviour of the Arnold tongues in the (δ, γ)-plane is displayed in the lower panel of Figure 5.10, where the discontinuity is taken to be π and the distance between consecutive discontinuities is moderate ($a = 3$). Similarly to the static $\phi = 0$ solution case, we notice that band-gaps are wide enough and there is a qualitative agreement between the numerics and asymptotic approximations.

5.5 Gap breathers

In section 1.5, we briefly discussed some solutions of the sine-Gordon equation. It is known that the model allows a special type of a solution in the form of a topological solitons called a kink (anti-kink). It is of interest to see what happens when a kink and an anti-kink interact, and study the *bound* state oscillation. This bound state of the two topological solitons forms what is known as a *breather* [89], [75]. For a rather complete review of breathers, see Maki and Takayama [152] and Kivshar and Malomed

[153] and references therein. A breather (also called a *bion*) is a localized solution of the sine-Gordon equation that oscillates periodically in time and decays exponentially in space.

As already mentioned in Chapter 1 that a kink (anti-kink) solution of a sine-Gordon equation represents a vortex (anti-vortex) of supercurrent in long Josephson junctions. Therefore, one can say that a breather solution corresponds a bound state of a vortex and anti-vortex in a long Josephson junction. Gulevich and Kusmartsev [154] have reported that besides the result of a fluxon and anti-fluxon interaction, a breather may also appear during the process of switching current measurements in annular Josephson junction. They also proposed a device that may be used to generate and trap breathers [155]. A breather can play an indeterminate role, i.e., it may cause a parasitic excitations or may be a good generator of electromagnetic waves propagating at frequencies in the terahertz (THz) range.

There are various papers, for example, those by Forinash and Willis [156], Ramos [157] and Kevrekidis et al. [158], which study breather solutions of sine-Gordon models. There are several numerical and theoretical reports, for instance, Karpman et al. [159] and Lomdahl et al. [160] respectively, which have shown that an external current can cause the decay of a sine-Gordon breather into a fluxon and anti-fluxon. Nevertheless, the aforementioned studies considered breathers with frequency in the semi-infinite plasma band. As our system admits high-frequency gaps, Josephson junctions with periodic phase-shifts support breathers with high oscillation-frequency, that is, gap breathers.

5.5.1 Asymptotic analysis

In this subsection, we derive a governing equation modelling the dynamics of such breather solutions. The amplitude of the breather is assumed to be small and its envelope, slowly varying in space. This motivates us to use a multiple scale method by introducing the new slow variables

$$y = \epsilon x, \quad \tau = \epsilon t, \quad T = \epsilon^2 t, \tag{5.5.1}$$

where ϵ is small. By the chain rule one obtains

$$\frac{d^2}{dx^2} \equiv \frac{\partial^2}{\partial x^2} + 2\epsilon \frac{\partial^2}{\partial x \partial y} + \epsilon^2 \frac{\partial^2}{\partial y^2}, \tag{5.5.2}$$

and

$$\frac{d^2}{dt^2} \equiv \frac{\partial^2}{\partial t^2} + 2\epsilon\frac{\partial^2}{\partial t\partial\tau} + \epsilon^2\left(\frac{\partial^2}{\partial\tau^2} + 2\frac{\partial^2}{\partial t\partial T}\right) + 2\epsilon^3\frac{\partial^2}{\partial\tau\partial T} + \epsilon^4\frac{\partial^2}{\partial T^2}. \tag{5.5.3}$$

Next, we assume an asymptotic expansion of the form

$$\begin{aligned}\phi &= \phi_s(x) + \epsilon V(x)\left\{e^{\lambda t}F(y,\tau,T) + c.c\right\} + \epsilon^2\Big\{W_0(x)\Big[G_0(y,\tau,T) + c.c\Big] \\ &+ W_1(x)\Big[e^{\lambda t}G_1(y,\tau,T) + c.c\Big] + W_2(x)\Big[e^{2\lambda t}G_2(y,\tau,T) + c.c\Big]\Big\} \\ &+ \epsilon^3\Big\{U_0(x)\Big[H_0(y,\tau,T) + c.c\Big] + U_1(x)\Big[e^{\lambda t}H_1(y,\tau,T) + c.c\Big] \\ &+ U_2(x)\Big[e^{2\lambda t}H_2(y,\tau,T) + c.c\Big] + U_3\Big[e^{3\lambda t}H_3(y,\tau,T) + c.c\Big]\Big\},\end{aligned} \tag{5.5.4}$$

where $\phi_s(x)$, given by (5.3.19), is the static ground state solution of the system (5.2.1), (5.2.4), (5.2.5), related to the uniform zero solution, and $V(x)$ represents an eigenfunction corresponding to the Arnold tongues about the zero-background solution, calculated in section 5.4.2, and $\lambda \in \mathbb{C}$ is given by (see Eq. (5.4.6))

$$\lambda = \sqrt{-1-\delta}, \tag{5.5.5}$$

and δ represents a transitional curve, calculated in Section 5.4.2. The terms F, G_i's and H_j's in (5.5.4) are slowly-varying and localized complex functions to be determined, and $W_i's$, $U_i's$ are bounded functions of the spatial variable x and $c.c$ denotes a complex conjugate.

Using the operators (5.5.2) and (5.5.3), we introduce the ansatz (5.5.4) to the time-dependent sine-Gordon equation (5.2.2), exploiting properties of complex numbers, using Taylor series expansion about $\epsilon \ll 1$, and equating the coefficients of each harmonic at each order of ϵ on both sides of the resultant equation, we obtain the following

set of equations

$$\mathcal{O}(\epsilon^0): \quad \phi_s'' = \sin[\phi_s + \theta(x)] - \gamma, \tag{5.5.6a}$$

$$\mathcal{O}(\epsilon): \quad \mathcal{L}V = 0, \tag{5.5.6b}$$

$$\mathcal{O}(\epsilon^2): \quad (\mathcal{L}W_0)(G_0 + \bar{G}_0) = -V^2|F|^2 \sin[\phi_s + \theta(x)], \tag{5.5.6c}$$

$$(\mathcal{L}W_1) G_1 - 2\lambda V F_\tau + 2V' F_y = 0, \tag{5.5.6d}$$

$$(\mathcal{M}W_2) G_2 + \frac{1}{2} V^2 F^2 \sin[\phi_s + \theta(x)] = 0, \tag{5.5.6e}$$

$$\mathcal{O}(\epsilon^3): \quad (\mathcal{K}U_0)(H_0 + \bar{H}_0) = -VW_1 (G_1 \bar{F} + \bar{G}_1 F) \sin[\phi_s + \theta(x)], \tag{5.5.6f}$$

$$(\mathcal{L}U_1) H_1 + V\left\{ W_0 (G_0 + \bar{G}_0) F + W_2 G_2 \bar{F} \right\} \sin[\phi_s + \theta(x)]$$

$$-2\lambda (W_1 G_{1\tau} + V F_T) + \frac{V^3}{2} F|F|^2 \cos[\phi_s + \theta(x)] + V F_{yy} + 2W_1' G_{1y} = 0, \tag{5.5.6g}$$

where $\mathcal{K}$, $\mathcal{L}$ and $\mathcal{M}$ respectively represent the differential operators

$$\begin{aligned} \mathcal{K} &\equiv \frac{d^2}{dx^2} - \cos[\phi_s + \theta(x)], \\ \mathcal{L} &\equiv \frac{d^2}{dx^2} - \left(\lambda^2 + \cos[\phi_s + \theta]\right), \\ \mathcal{M} &\equiv \frac{d^2}{dx^2} - \left(4\lambda^2 + \cos[\phi_s + \theta(x)]\right). \end{aligned} \tag{5.5.7}$$

Eqs. (5.5.6a) and (5.5.6b) are satisfied immediately by the static sine-Gordon equation (5.2.5) and the eigenvalue problem (5.4.2) respectively and so may be discarded.

We proceed to derive the set of governing equations. First we consider the equations obtained from $\mathcal{O}(\epsilon^2)$. Eq. (5.5.6c) can be rewritten as

$$\frac{G_0 + \bar{G}_0}{|F|^2} = k_0 = -\frac{V^2 \sin[\phi_s + \theta(x)]}{\mathcal{K}W_0}. \tag{5.5.8}$$

Because the left hand side of (5.5.8) is a ratio of terms which are functions of (y, τ, T), while the right hand side is that of terms of functions of x, this situation is justified only if the ratios on both sides are equal to a constant, say k_0. By writing

$$\widetilde{W}_0 = k_0 W_0, \tag{5.5.9}$$

the right hand side of Eq. (5.5.8), when equated to k_0, can be cast into the form

$$\mathcal{K}\widetilde{W}_0 = -V^2 \sin(\phi_s + \theta). \tag{5.5.10}$$

Next, we consider Eq. (5.5.6d). According to Fredholm's theorem the necessary and sufficient condition for Eq. (5.5.6d) to have a solution is that its right hand side is orthogonal to the null space of the adjoint of the operator $\mathcal{L}$ [161]. In other words, Eq.

(5.5.6d) has a solution if and only if

$$2\left(\lambda V F_\tau - V^{'} F_y\right) \perp \mathcal{N}(\mathcal{L}^*), \tag{5.5.11}$$

where $\mathcal{N}(\mathcal{L}^*)$ denotes the null space of $\mathcal{L}$. Since $\mathcal{L}$ is self-adjoint, V is also in the null space of $\mathcal{L}^*$. Using the definition of orthogonality and inner product, Eq. (5.5.11) reduces to

$$2\int_0^{2a} V\left(\lambda V F_\tau - V^{'} F_y\right) dx = 0. \tag{5.5.12}$$

As V is $2a-$periodic, it follows that the product of V with its derivative, when integrated over the period vanishes. As a result Eq. (5.5.12) simplifies to

$$2\lambda F_\tau \int_0^{2a} V^2 dx = 0. \tag{5.5.13}$$

Since the eigenvalue λ is nonzero and the square of the potential V when integrated over the period gives a nonzero value, it follows that Eq. (5.5.13) holds if and only if, the temporal derivative of the function F is zero, i.e.,

$$F_\tau = 0. \tag{5.5.14}$$

This is our first solvability condition which tells us that the function $F(y, \tau, T)$ is independent of the variable τ. Hence we obtain $F = F(y, T)$.

With the first solvability condition (5.5.14), Eq. (5.5.6d) is simplified to

$$\left(\mathcal{L} W_1\right) G_1 = -2V^{'} F_y. \tag{5.5.15}$$

Again, this equation holds if and only if, for a real constant k_1, we have

$$G_1 = k_1 F_y. \tag{5.5.16}$$

Similarly, if one defines

$$W_1 = k_1 \widetilde{W}_1, \tag{5.5.17}$$

and substitute (5.5.16) into Eq. (5.5.15), it can be easily cast into the form

$$\mathcal{L}\widetilde{W}_1 = -2V^{'}. \tag{5.5.18}$$

Next, we consider Eq. (5.5.6e), which for a real constant k_2, can be written as

$$\frac{G_2}{F^2} = -\frac{V^2 \sin\left[\phi_s + \theta(x)\right]}{2\left(\mathcal{M} W_2\right)} = k_2. \tag{5.5.19}$$

By equating the functions of x in (5.5.19) to the constant k_2 and defining

$$\widetilde{W}_2 = k_2 W_2, \tag{5.5.20}$$

one arrives at

$$\mathcal{M}\widetilde{W}_2 = -\frac{1}{2}V^2 \sin\left[\phi_s + \theta(x)\right]. \tag{5.5.21}$$

Finally, we consider the equation with the first harmonic in equations of order ϵ^3, namely (5.5.6g), use (5.5.8), (5.5.9), (5.5.16), (5.5.17), (5.5.19) and (5.5.20) along with the first solvability condition (5.5.14) to obtain

$$\begin{aligned}(\mathcal{L}U_1)\, H_1 &= 2V\lambda F_T - (2\widetilde{W}_1' + V)F_{yy} - \Big[V\left(\widetilde{W}_0 + \widetilde{W}_2\right)\sin\left[\phi_s + \theta(x)\right] \\ &+ \frac{V^3}{2}\cos\left[\phi_s + \theta(x)\right]\Big]F|F|^2. \end{aligned} \tag{5.5.22}$$

Eq. (5.5.22) possesses a solution if and only Fredholm's condition is satisfied [161], i.e., if and only if the right hand side is orthogonal to V. Multiplying (5.5.22) with V and integrating over the interval $0 \le x \le 2a$, we obtain the nonlinear Schrödinger (NLS) equation

$$QF|F|^2 + UF_{yy} - (2\lambda U_2)\, F_T = 0, \tag{5.5.23}$$

where $Q = Q_1 + Q_2 + Q_3$, and $U = U_1 + U_2$, with

$$\begin{aligned} Q_1 &= \int_0^{2a} V^2\widetilde{W}_0 \sin\left[\phi_s + \theta(x)\right] dx, \quad Q_2 = \int_0^{2a} V^2\widetilde{W}_2 \sin\left(\phi_s + \theta\right) dx, \\ Q_3 &= \frac{1}{2}\int_0^{2a} V^4 \cos\left[\phi_s + \theta(x)\right] dx, \quad U_1 = 2\int_0^{2a} V\widetilde{W}_1' dx, \quad U_2 = \int_0^{2a} V^2 dx. \end{aligned} \tag{5.5.24}$$

This equation appears in a wide range of physical problems, which admits soliton solutions, see Remoissenet [14] and Scott [70].

As described in [162], the nonlinear Schrödinger equation (5.5.23) admits a bright soliton solution if the coefficients Q and U have the same sign. On the other hand, it has a dark soliton or a hole soliton, if the coefficients Q and U have the opposite signs. Thus, to know about the nature of the soliton solutions admitted by the nonlinear Schrödinger equation (5.5.23), one needs to solve Eqs. (5.5.10), (5.5.18) and (5.5.21).

5.5.2 Failure of perturbation expansions

In the following, we show that the results of perturbation expansions derived in Sections 5.3–5.4 cannot be used to determine of the coefficients of the nonlinear Schrödinger equation (5.5.23).

While investigating the transitional curves in Section 5.4.2, we demonstrated that V is the only bounded eigenfunction corresponding to an eigenvalue λ along a curve. In

Section 5.5.1, we also showed that this V is in the null space of the operator $\mathcal{L}$. It follows that the dimension of the null space of $\mathcal{L}$ is one.

Now consider the relation (5.5.18). The right hand side of the equation satisfies the Fredholm's theorem because the integral of the product of the null space of $\mathcal{L}$ and its derivative, over the interval $0 \leq x \leq 2a$ is zero. Hence, (5.5.18) admits a bounded solution. Nevertheless, Eq. (5.5.18) cannot be solved perturbatively, as shown below.

Consider Eq. (5.5.18) and assume a bounded solution of the form

$$\widetilde{W}_1 = \widetilde{W}_1^{(0)} + \widehat{\epsilon}\widetilde{W}_1^{(1)} + \widehat{\epsilon}^2\widetilde{W}_1^{(2)} + \ldots, \tag{5.5.25}$$

where $\widehat{\epsilon}$ is small. Introducing (5.5.25) into Eq. (5.5.18) and equating the coefficients of $\widehat{\epsilon}$ on both sides, we obtain for the lowest-order equations

$$(\widetilde{W}_1^0)_{xx} + \left(\frac{\pi}{2a}\right)^2 \widetilde{W}_1^0 = B_0\left(\frac{\pi}{a}\right)\left\{\cos\left(\frac{\pi x}{2a}\right) + \sin\left(\frac{\pi x}{2a}\right)\right\}, \tag{5.5.26}$$

where we have used the expression of V given by Eqs. (5.4.27), (5.4.28) and (5.4.32).

Clearly the dimension of the differential operator on the left hand side of this equation is 2, so there are two bounded solutions.

Now analysing Eq. (5.5.26), it is clear that the equation has a solution growing in x, as $B_0 \neq 0$ (see Section 5.4.4). As a result, we are unable to find a bounded solution $\widetilde{W}_0$ (and hence a bounded $\widetilde{W}_1$) that satisfies Eq. (5.5.18) using expansion (5.5.25). To use the approximations presented in Sections 5.3–5.4, we use another approach as below.

5.6 Gap breathers by a rotating wave approximation method

In this section, we apply the method of the rotating wave approximation to investigate the breather solution of the sine-Gordon model. This approximation is used frequently in atom optics (see, e.g., Christopher and Peter [163] and Frasca [164]). In this approximation, only terms in an equation that are resonant with the fundamental frequency are retained and the terms which oscillate rapidly are neglected, see, for instance, Scott [70].

To use the rotating wave approximation method, we assume $\widetilde{\epsilon}$ is a small parameter and $F(y,T)$ is a localized and slowly varying complex function, where $y = \widetilde{\epsilon}x$ and $T = \widetilde{\epsilon}^2 t$ are slow spatial and temporal variables respectively. We make the ansatz

$$\phi(x,t) = \phi_s + \widetilde{\epsilon}V(x)\left(e^{\lambda t}F(y,T) + c.c\right) + \mathcal{O}(\widetilde{\epsilon}^2), \tag{5.6.1}$$

represents a small perturbation of the static ground state solution ϕ_s given by (5.3.19), where $\lambda \in \mathbb{C}$ is given by (5.5.5).

Substituting the ansatz into the sine-Gordon model (5.2.2) and comparing the coefficients of $e^{\lambda t}$ on both sides of the resulting expression leads to

$$(\mathcal{L}V)\,F + 2\widetilde{\epsilon}V^{'}F_y + \widetilde{\epsilon}^2\left(VF_{yy} - 2\lambda VF_T + \frac{V^3}{2}\cos\left[\phi_s + \theta(x)\right]F|F|^2\right) + \mathcal{O}(\widetilde{\epsilon}^3) = 0, \tag{5.6.2}$$

where the operator $\mathcal{L}$ is given by (5.5.7).

As before, for the last equation to be solvable, $V(x)$ must be an eigenfunction of $\mathcal{L}$ corresponding to a transitional curve in the (δ, κ)-plane (see Section 5.4.2). Multiplying (5.6.2) by V and integrating one obtains

$$2\left(F_{yy} - 2\lambda F_T\right)\int_0^{2a} V^2 dx + F|F|^2\int_0^{2a}\left(V^4\cos\left[\phi_s + \theta(x)\right]\right)dx = 0. \tag{5.6.3}$$

Using the notation from (5.5.24), the expression (5.6.3) takes the form of a nonlinear Schrödinger equation

$$Q_3 F|F|^2 + U_2 F_{yy} - (2i\omega U_2)\,F_T = 0, \tag{5.6.4}$$

where $\lambda = i\omega$ is pure imaginary.

It can be easily observed that $Q_3 > 0$ and $U_2 > 0$, at least when $|\phi_s| \ll 1$. Hence, we are indeed looking for bright soliton solutions, which are calculated in the following subsection.

5.6.1 Bright soliton solution

As discussed by Scott [70], a bright soliton solution of (5.6.4) has the form

$$F(y,T) = Ae^{i\Omega T}\text{sech}\,(\beta y)\,. \tag{5.6.5}$$

Substituting Eq. (5.6.5) into the Schrödinger equation (5.6.4), simple manipulation leads to

$$F(y,T) = \pm 2\sqrt{\frac{\Omega U_2\sqrt{1+\delta}}{Q_3}}e^{i\Omega T}\,\text{sech}\left(y\sqrt{2\Omega\sqrt{1+\delta}}\right), \tag{5.6.6}$$

treating Ω as a free parameter.

To check the validity of this approximation, the solution (5.6.1) at $t = 0$, should be used as initial condition to the original sine-Gordon equation and the change in the profile of the corresponding breather calculated. This work is suggested for future investigation.

5.7 Conclusion

We have considered a long Josephson junction with periodic arbitrary phase shift in the superconducting Josephson phase. Using a perturbation technique, the existence of stationary periodic solutions are discussed both in the absence and presence of an external current. We demonstrated that the solutions with minimum energy depend upon the discontinuity κ and the facet length a. We found that there is a critical value of the applied bias current and the discontinuity, above which each solution will merge into its complementary counterpart.

The magnetic flux of the system is studied in terms of increasing inter-vortex distance in the undriven and driven cases. We have shown that the magnetic flux depends upon the distance between the consecutive vortices. The greater the distance between consecutive discontinuities, the greater the magnetic flux is, and vice versa.

When there is no discontinuity in the Josephson phase, the system has a semi-infinite plasma band (or a continuous allowed band) in terms of the spectral parameter E. We have shown that as the discontinuities are introduced, one finds forbidden bands in the plasma bands. The expressions for the Arnold tongues which separate an allowed band from a forbidden band have been derived. In addition, it is observed that when one applies an external current to the system, additional band-gaps will emanate from the points $(n\pi/2a)^2$, where n is an even integer. These openings expand with the increase in discontinuity. Our results also show that the band-gaps become wider as the distance between discontinuities increases.

In addition to the band structure, we have also derived an equation for breather solutions with oscillation frequency in the band-gaps using multiple scale expansions. A rotating wave approach has also been used to derive a similar equation for gap soliton solutions.

CHAPTER 6

Conclusions and Future work

This thesis has investigated semifluxons analytically, these being π-kink solutions of the sine-Gordon model, of the unconventional long Josephson junctions, that is, long Josephson junctions (LLJs) with phase shifts. In the following, we briefly summarize the main results of the work done throughout the study.

6.1 Summary

Chapter 1 started with a brief history of superconductivity and recent progress in the topic. Josephson junctions and related terms were introduced followed by some applications of long Josephson junctions. Fundamental results related to the Josephson junctions having π-shift in the phase were discussed. Several papers on the manufacturing of π-junctions were reviewed. In Section 1.3.3 we discussed some important papers regarding the Josephson junctions consisting of both zero and π-parts, i.e., the so-called 0-π-Josephson junctions. Semifluxons in 0-π long Josephson junctions and their possible applications in the real world were discussed in the same section.

We derived a mathematical model, namely the sine-Gordon equation, used for the description of dynamics of the Josephson phase across the nonsuperconducting barrier of long Josephson junctions. The famous kink solution of the unperturbed sine-Gordon equation was presented in Section 1.5. Breather solutions of the model and some physical applications of the kink (Josephson vortex) solution were presented in the subsequent sections. The chapter was concluded by a brief overview of the thesis.

In Chapter 2, we theoretically studied the static properties of semifluxons in an infinitely long Josephson junction with two π-phase discontinuities, the so-called 0-π-0 long Josephson junction. In Section 2.3, we studied the existence of the static and uni-

form solutions of the system, where it was shown that the uniform solutions satisfy the continuity conditions only when there is no external current applied to the junction. To study the linear stability of the stationary solutions permitted by the system, an eigenvalue problem was derived. It was concluded that the dissipative parameter, α, does not play a role in the stability of a static solution. Two types of possible solutions, corresponding to the continuous and the discrete spectra, of the eigenvalue problem were discussed. Our investigation showed that there is a critical value $a_c = \pi/4$, of the facet length a, above which the constant zero solution becomes unstable. The uniform π-solution, on the other hand, was shown to be unstable for all parameter values.

A non-constant ground state was found to exist in the region where the constant solutions of the system are unstable. This ground state solution was analysed using a Hamiltonian approach and a perturbation technique in Sections 2.5.1 and 2.5.3, respectively. It was observed that there are two ground states bifurcating from the zero background solution. An asymptotic analysis has been used to construct the ground states in the region where the facet length is slightly larger than the zero-critical facet length. In Section 2.5.3.1, we investigated the non-uniform ground state solution in the absence of an applied bias current, which has the form of static semifluxons.

The effect of an applied bias current on the non-constant ground state solutions was discussed in Section 2.5.3.3. Two critical currents $\pm\gamma_{c,0}$ and $\pm\gamma_{c,\pi}$ were found in the instability region. It was concluded that the ground state solution exists in the region where the bias current γ takes values between $\pm\gamma_{c,0}$ and that there are no static solutions in the region where $|\gamma_{c,\pi}| < |\gamma|$. An explicit relation for the critical current $\pm\gamma_{c,0}$ in terms of the facet length and its critical value was obtained using a perturbation technique. We noted that the critical forces $|\pm\gamma_{c,0}|$ asymptotically approach $2/\pi$ when the facet length a becomes sufficiently large. There is one static ground state solution of the system in the region $\gamma_{c,0} < \gamma < \gamma_{c,\pi}$.

The ideas of Chapter 2 were extended to a finite domain by considering a finite 0-π-0 long Josephson junction in Chapter 3. The analysis considered a sine-Gordon model with spatial variable $-L < x < L$, where $2L$ is the total length of the junction. The existence and stability of the stationary solutions of the model were studied in Section 3.4. The analysis of the "continuous" spectrum of the static and uniform solutions showed that there is no unstable eigenvalue in this spectrum. On the other hand, from the "discrete" spectrum of the zero background solution we found that, similar to the infinite domain, a critical facet length $a_{c,0}$ can be found in the finite domain as well,

above which the uniform zero solution is unstable. Analytical expressions for this critical facet length $a_{c,0}$ in terms of half of the junction length has been derived for large and small L. It has been demonstrated that in the case of sufficiently large L, the zero critical facet length asymptotically approaches $\pi/4$, the value for the infinitely long 0-π-0 Josephson junctions.

While studying the uniform π solution of the finite system, we found that, unlike the infinite domain problem, in the finite domain problem, there is a stability window in terms of the facet length above which the uniform π background solution becomes stable, that is $a > a_{c,\pi}$. The critical facet length $a_{c,\pi}$ has been expressed analytically for large and small L. It was deduced that whenever L becomes large, $a_{c,\pi}$ approaches $L - \pi/4$.

From the stability analysis of the uniform solutions of the system, in Section 3.5, the stability region of $\widetilde{\phi} = 0$ and $\widetilde{\phi} = \pi$ was found to be the same following a reflection in the line $a = L/2 = 1/2$ and that the critical lengths, for any value of L can be related through the equation $a_{c,\pi} = L - a_{c,0}$.

Plots of $a_{c,0}$ and $a_{c,\pi}$ a function of the junction's length gave a region where both the uniform 0- and π-solutions are unstable. The non-constant ground state solutions in the combined instability region were investigated using the Poincare-Lindstedt method, a modified Poincare-Lindstedt technique and a Lagrangian approach. It was observed that when there is no bias current applied to the junction, i.e., when $\gamma = 0$, there correspond to ground state solutions to each of the uniform solutions $\widetilde{\phi} = 0, \quad \widetilde{\phi} = \pi$. We observed that the ground state solutions correspond to a pair of semifluxons of positive and negative polarities. Using an Euler-Lagrange approximation, we demonstrated that these semifluxons depend on the length of junction and the facet length.

While studying the nonuniform ground states in the presence of an applied bias current, we investigated two ground states that bifurcate from the constant backgrounds. Two critical forces $\pm\gamma_{c,0}$ and $\pm\gamma_{c,\pi}$ were found to exist. It was deduced that there is one ground state solution corresponding to each of the constant solutions in the regions where $|\gamma| < |\gamma_{c,0}|$ and $|\gamma| < |\gamma_{c,\pi}|$. No static ground state solution was found to exist in the regions $|\gamma| > |\gamma_{c,0}|$ and $|\gamma| > |\gamma_{c,\pi}|$. We also deduced that at the critical currents $\pm\gamma_{c,0}$ and $\pm\gamma_{c,\pi}$, the ground states bifurcating from the uniform solutions merge into a nonconstant solution. The behaviour of these critical currents for varying facet length was studied as well. We noticed that the critical forces $\gamma_{c,0}$ and $\gamma_{c,\pi}$ are zero at $a_{c,0}$ and $a_{c,\pi}$.

In addition to junctions with small length $2L$, we also discussed the nonconstant solutions in the case where the length of the junction is large enough. In this situation, we reached at the conclusion that a ground state solution may not emanate from a constant background. We also studied the profile of the Josephson phase as a function of the spatial variable x for different values of the bias current, where it was concluded that when there is no applied bias current, the solution corresponds to a pair of semifluxons each of which is bound to a fluxon.

We studied the stability of a constant background and showed that the junction can be made more stable by applying a bias current.

The ideas of Chapters 2 and 3 have been extended into two dimensions in Chapter 4, by considering a two-dimensional disk-shaped 0-π long Josephson junction both on a finite and an infinite domain. In Section 4.3, the mathematical model used for the description of the dynamics of 0-π long Josephson junction was explained. By using polar coordinates and limiting the study to angularly symmetric solutions, the problem under consideration took the form of one-dimensional 0-π long Josephson junction. The existence and linear stability analysis of the constant backgrounds admitted by the system was studied in Section 4.4. It was shown that like the one-dimensional 0-π-0 finite long Josephson junction, there is no unstable eigenvalue in the "continuous" spectra of the uniform solutions, when one considers the two-dimensional 0-π finite long Josephson junction.

Like the previous chapters, we observed that there exists a stability region in terms of the facet length a in which the uniform zero solution is stable. The critical facet length $a_{c,0}$ as a function of L was derived for small and large L. The π-background solution which is unstable in the limit $L \to \infty$, was shown to be stable in a certain region of the facet length a in the finite domain. We showed that there is an interval of a where the constant solutions of the system are unstable. Unlike the one-dimensional problem, the stability regions of the constant solutions, in the present case, are not symmetric. The nonuniform ground states close to either critical facet lengths were investigated using a Lagrangian approach.

We studied the nonuniform ground state in the combined instability region in the undriven case, and found two ground states that bifurcate from the constant solutions. It was deduced that the ground states correspond to semifluxons. The bifurcation of ground states emanating from the constant backgrounds was supercritical. The profiles of the ground state solutions were studied. We found that the normalized magnetic flux

is is zero in regions where a uniform solution is stable and is maximum in the combined instability region.

In addition, we have studied the nonuniform ground states in the presence of an applied bias current, where we found critical forces, namely $\pm\gamma_{c,0}$, at which the ground state solutions emanating from the zero background terminate at a saddle node bifurcation. Similarly, the ground state solutions emanating from the constant π solution were to terminate at the critical forces $\pm\gamma_{c,\pi}$. Analytical expressions for these critical forces were studied and found in terms of the facet length a. We concluded that the critical currents $\gamma_{c,0}$ and $\gamma_{c,\pi}$ are zero at the critical facet lengths. The nonuniform ground state solutions in the vicinity of the critical facet length a_0^∞ were investigated on an infinite domain using the same Lagrangian approach.

The critical eigenvalues of each solution, in terms of the facet length and an applied bias current, was studied both in finite and infinite domain. The minimum of the critical eigenvalue was attained at a nonzero value of the bias current.

In addition to the ground states, we studied excited states bifurcating from the stationary solutions in Section 4.6. Unlike the nonuniform ground states, the excited states were not sign definite. The dynamics of $\widetilde{\theta}$-independent and $\widetilde{\theta}$-dependent excited states were presented from which it was deduced that both types of excited states evolve into the ground states, where $\widetilde{\theta}$ represents the angular variable in a polar co-ordinate system.

In Chapter 5, we investigated a long Josephson junction with periodic discontinuity in its phase. After discussing the governing equation in Section 5.2, the existence of static solutions was studied using a modified Poincare-Linstedt technique both in the absence and presence of an applied bias current. The analysis suggested that the magnetic flux increases whenever the distance between the discontinuities (vortices) increases and vice versa. The stationary periodic solutions in the presence of an external current were studied, where a critical values of the applied bias current γ_c was found above which a solution switches to its complementary counterpart. This critical current was found to depend on the distance between the vortices. While studying the stationary solutions in terms of the discontinuity, a critical value of the discontinuity was determined above which the zero solution merges to the π solution and vice versa. We also observed that the ground state solutions depend on the inter-vortex distance and the discontinuity. In addition, the magnetic flux in terms of increasing inter-vortex distance in the absence and presence of an applied bias current was studied, where it

was shown that the magnetic flux increases whenever the distance between two consecutive discontinuities increases.

In Section 5.4, we discussed the stability of the stationary periodic solutions using a perturbation technique. The analysis showed that when the system has no discontinuity, the zero solution has a semi-infinite continuous plasma band in the region $E < -1$. Band-gaps were formed in the allowed bands when one introduces discontinuity in the system. We found that when there is no current applied to the junction, these band-gaps emanate from the points $(p/2a)^2$, where p is an even integer. We observed that the band-gap widens when the discontinuity increases. The band-gaps as a function of inter-vortex distance a were studied as well. It was noticed that the band-gaps are narrow when a is small and vice versa. We also noted that when the discontinuity exceeds a critical value, the zero solution merges with complementary π-solution. On the other hand, the static π solution of the system has an allowed band in the region $E < 1$.

The effect of an applied bias current on the band structure was studied as well. We noticed that a bias current causes additional band-gaps in the band structure, which emanate from the point $(n/2a)^2$, where n is odd. Expressions of the transitional curves and the eigenfunctions corresponding to each curve of an Arnold tongue were analytically calculated using a perturbation technique.

Taking a stable solution of the system and using multiple scale expansions, an equation for a breather solution with an oscillating frequency in the band-gaps has been derived. Rotating wave method was used in Section 5.6, to derive a similar equation for gap solitons where it is suggested that we have a bright soliton solution.

6.2 Future Work

In the course of this study, we have identified several problems which require further work. These include the investigation of the existence and stability analysis of the stationary solutions of 0-π disk-shaped two-dimensional Josephson junctions when $R_{\text{min}} \neq 0$ in the phase shift (4.3.2) (see Fig. 4.1). In other words, one may investigate a 0-π disk-shaped two-dimensional long Josephson junction having no hole in the inner part. The second possible investigation would be the case where a zero phase-shifts in the junction in the regions $0 < \sqrt{x^2+y^2} < R_{\text{mid}}$ and $R_{\text{mid}} < \sqrt{x^2+y^2} < R_{\text{max}}$ and a π-phase shift in the region $R_{\text{mid}} < \sqrt{x^2+y^2} < R_{\text{max}}$, i.e., a disk-shaped 0-$\pi$-0 long Josephson junction, in two dimensions, both on a finite and an infinite domains. The

study of such Josephson junctions are of important from the physical point of view, since such junctions have recently been successfully fabricated using Superconductor-insulator-ferromagnet-superconductor (SIFS) technology Gulevich et al. [47].

Another interesting study would be the investigation of a 0-π disk-shaped two-dimensional Josephson junction whose solutions are not angularly symmetric.

Another future work is to investigate further the problem of Chapter 5, i.e., to numerically solve Eq. (5.5.18). The validity of the nonlinear Schrödinger equation (5.5.23) in approximating the breather solution is still an open question.

In addition to the multiple scale expansion approach above, gap breather solutions of the sine-Gordon equation (5.2.2) with a shift of κ (5.2.3) in the Josephson phase will be analysed using a couple-mode theory (see for example, M de Sterke and Sipe [165], Yulin and Skryabin [166], Efremidis and Christodoulides [167]).

These problems will be addressed in the near future.

CHAPTER 7

Appendix

In this appendix, we recap some elementary results from Lagrangian mechanics, the Calculus of Variations, Linear Algebra and nonlinear differential equations.

7.1 Derivation of the sine-Gordon model from a Lagrangian

In this section, we show that the sine-Gordon model (1.4.12) in the non-dissipative form, that is, with $\alpha = 0$, can be derived from the Lagrangian, see for example, Goldstein et al. [168] and Synge and Griffith [169]

$$\mathcal{L}(\phi) = \int_{-\infty}^{\infty}\int_{-\infty}^{\infty}\left[\frac{1}{2}\phi_t^2 - \frac{1}{2}\phi_x^2 - 1 + \cos(\phi) - \gamma\phi\right] dxdt. \tag{7.1.1}$$

Replacing ϕ by $\phi + \epsilon V$ in Eq. (7.1.1), where $\phi + \epsilon V$ with $\epsilon \ll 1$ is a small perturbation , then up to the leading order of ϵ, one can write from the last equation

$$\begin{aligned}\mathcal{L}(\phi + \epsilon V) &= \int_{-\infty}^{\infty}\int_{-\infty}^{\infty}\left[\frac{1}{2}\phi_t^2 - \frac{1}{2}\phi_x^2 - 1 + \cos(\phi) - \gamma\phi\right] dxdt \\ &\quad + \epsilon\int_{-\infty}^{\infty}\int_{-\infty}^{\infty}\left[\phi_t V_t - \phi_x V_x - V\sin(\phi) - \gamma V\right] dxdt.\end{aligned}$$

From this equation the *Fréchet derivative* of the Lagrangian $\mathcal{L}$ can be found as

$$\left[\frac{\partial\mathcal{L}}{\partial\phi}\right](V) = \lim_{\epsilon\to 0}\frac{\mathcal{L}(\phi+\epsilon V) - \mathcal{L}(\phi)}{\epsilon} = \int_{-\infty}^{\infty}\int_{-\infty}^{\infty}\left[\phi_t V_t - \phi_x V_x - V\sin(\phi) - \gamma V\right] dxdt. \tag{7.1.2}$$

To find the extreme values of the energy, we require this to be zero for all functions $V(x,t)$, hence

$$\left[\frac{\partial\mathcal{L}}{\partial\phi}\right](V) = 0,$$

and consequently Eq. (7.1.2) yields

$$\int_{-\infty}^{\infty}\int_{-\infty}^{\infty}\left[\phi_t V_t - \phi_x V_x - V\sin(\phi) - \gamma V\right] dxdt = 0.$$

Integration by parts leads to

$$\begin{aligned}&\int_{-\infty}^{\infty}\left(\phi_t V(t)\Big|_{-\infty}^{\infty}-\int_{-\infty}^{\infty}\phi_{tt}Vdt\right)dx\\ =\;&\int_{-\infty}^{\infty}\left(\phi_x V(x)\Big|_{-\infty}^{\infty}-\int_{-\infty}^{\infty}\phi_{xx}Vdx\right)dt+\int_{-\infty}^{\infty}\int_{-\infty}^{\infty}\left[V\sin(\phi)+\gamma V\right]dxdt.\end{aligned}$$

Imposing the conditions $V(\pm\infty)=0$ and simplifying the equation, we obtain the non-dissipative sine-Gordon model

$$\phi_{xx}-\phi_{tt}=\sin(\phi)-\gamma.$$

7.2 Self adjointness of the operator $\mathcal{D}$

We show that the differential operator $\mathcal{D}=\dfrac{d^2}{dx^2}-[E+\cos(\tilde{\phi}+\theta)]$ is self adjoint. Let $U=U(x)$ and $V=V(x)$ be two twice differentiable functions. To show the self adjointness of the operator $\mathcal{D}$, we need to show that

$$<\mathcal{D}U,V>=<U,\mathcal{D}^{\dagger}V>, \tag{7.2.1}$$

where $\mathcal{D}^{\dagger}$ is the adjoint operator of $\mathcal{D}$, and $<,>$ represents the inner product. Using the definition of an inner product, we have

$$<\mathcal{D}U,V>=\int_{-\infty}^{\infty}\left[\frac{d^2U}{dx^2}-\left(E+\cos\left[\tilde{\phi}+\theta\right]\right)U\right]Vdx=I_1+I_2, \tag{7.2.2}$$

where

$$I_1=\int_{-\infty}^{\infty}\frac{d^2U}{dx^2}Vdx,\;I_2=\int_{-\infty}^{\infty}\left[E+\cos\left(\tilde{\phi}+\theta\right)\right]UVdx.$$

Using integration by parts, we have

$$I_1=V\frac{dU}{dx}\Big|_{-\infty}^{\infty}-\int_{-\infty}^{\infty}\frac{dV}{dx}\frac{dU}{dx}. \tag{7.2.3}$$

Assuming $U(\pm\infty)=0$, $V(\pm\infty)=0$, it is simple to write, from Eq. (7.2.3)

$$I_1=\int_{-\infty}^{\infty}\frac{d^2V}{dx^2}Udx. \tag{7.2.4}$$

Substituting for I_1 from (7.2.4), Eq. (7.2.2), after a simple manipulation, gives

$$<\mathcal{D}U,V>=\int_{-\infty}^{\infty}U\left[\frac{d^2V}{dx^2}-\left(E+\cos\left[\tilde{\phi}+\theta\right]\right)V\right]dx=<U,\mathcal{D}^{\dagger}V>. \tag{7.2.5}$$

This implies that $\mathcal{D}=\mathcal{D}^{\dagger}$, and the result is proved.

7.3 Eigenvalues of self-adjoint operator

In the following, we show that the eigenvalues corresponding to a self-adjoint differential operator are real [170]. The argument is similar to that used to prove eigenvalues of real symmetric matrices are real, see e.g., Halmos [171].

For this purpose, let us suppose that λ be a complex eigenvalue of a self-adjoint operator $\mathcal{D}$, then one can write

$$\mathcal{D}\phi = \lambda\phi, \tag{7.3.1}$$

where ϕ is the corresponding eigenfunction. Since $\mathcal{D}$ is self-adjoint, it follows that if $\mathcal{D}^\dagger$ denotes its adjoint then we have $\mathcal{D}^\dagger = \mathcal{D}$. In terms of an inner product, this can be written as

$$< \mathcal{D}\phi, \phi > \quad = \quad < \phi, \mathcal{D}^\dagger\phi > \tag{7.3.2}$$

Now using the properties of inner product space, and making use of Eqs. (7.3.1) and (7.3.2), one can write

$$\begin{aligned} \lambda < \phi, \phi > \; &= \; < \lambda\phi, \phi > \; = \; < \mathcal{D}\phi, \phi > \; = \; < \phi, \mathcal{D}^\dagger\phi > \\ &= \; < \phi, \mathcal{D}\phi > \; = \; < \overline{\mathcal{D}\phi}, \overline{\phi} > \; = \; < \overline{\lambda\phi}, \overline{\phi} > \\ &= \; \overline{\lambda} \; < \overline{\phi}, \overline{\phi} > \; = \; \overline{\lambda} < \phi, \phi > . \end{aligned}$$

That is

$$\lambda < \phi, \phi > \quad = \quad \overline{\lambda} < \phi, \phi >,$$

and since $\phi \neq 0$, this holds if and only if

$$\lambda = \overline{\lambda}.$$

This implies that λ has a zero imaginary part, or equivalently λ is real.

7.4 Numerical Schemes and angular stability

In this section, we briefly discuss the numerical schemes used to numerically solve the $\widetilde{\theta}$-independent equation (4.3.9).

Using a Taylor series expansion, one can approximate the first and second order derivatives as

$$\phi_r \approx \frac{\phi_{i+1} - \phi_{i-1}}{2\Delta r}, \quad \phi_{rr} \approx \frac{\phi_{i+1} - 2\phi_i + \phi_{i-1}}{(\Delta r)^2}. \tag{7.4.1}$$

To solve the $\widetilde{\theta}$-independent equation (4.3.9), which can be rewritten as

$$\frac{1}{r}\left(r\phi_r\right)_r = \sin(\phi+\theta) - \gamma, \tag{7.4.2}$$

we use a finite difference method. With the help of (7.4.1), and following Strikwerda [172], one may write,

$$\left(r\phi_r\right)_r = \phi_r + r\phi_{rr} \approx \frac{\phi_{i+1}-\phi_{i-1}}{2\Delta r} + r_i\left(\frac{\phi_{i+1}-2\phi_i+\phi_{i-1}}{(\Delta r)^2}\right).$$

With a simple manipulation, this expression can be cast to the form

$$\left(r\phi_r\right)_r \approx \left[\left(r_i+\frac{\Delta r}{2}\right)\frac{\phi_{i+1}-\phi_i}{\Delta r} - \left(r_i-\frac{\Delta r}{2}\right)\frac{\phi_i-\phi_{i-1}}{\Delta r}\right].$$

Thus Eq. (7.4.2) may be written as

$$\frac{1}{r_i}\left[\left(r_i+\frac{\Delta r}{2}\right)\frac{\phi_{i+1}-\phi_i}{\Delta r} - \left(r_i-\frac{\Delta r}{2}\right)\frac{\phi_i-\phi_{i-1}}{\Delta r}\right] = \sin\left[\phi_i+\theta_i\right] - \gamma, \tag{7.4.3}$$

where ϕ_i and θ_i, $i = 1,\ldots,I$, are the grid functions approximating $\phi(i\Delta r)$ and $\theta(i\Delta r)$ and $\Delta r = L/(I+1)$. The Dirichlet boundary condition at $r = L$ is approximated by

$$\phi_{I+1} = \phi_I. \tag{7.4.4}$$

The most particular feature of polar coordinates is the condition that must be imposed at $r = 0$. To derive our condition at the origin, we follow the method described in [172]. Integrating (7.4.2) over a small disk of radius ϵ yields

$$\int_0^\epsilon \left(\sin\left(\phi+\theta\right) - \gamma\right) r\, dr = \int_0^\epsilon \left(r\phi_r\right)_r\, dr,$$

where we have evaluated the integral over the angular variable θ as ϕ is independent of θ. By assuming that in the small disk, ϕ is independent of the radial variable r, the integrals can be approximated by

$$\left[\sin(\phi_0+\theta_0) - \gamma\right]\left(\frac{\Delta r}{2}\right)^2 = \phi_1 - \phi_0, \tag{7.4.5}$$

where $\phi \approx \phi_0$ and $\theta = \theta_0 = \theta_1$. In the equation above, we have taken $\epsilon = \Delta r/2$ and approximated ϕ_r by a forward difference. Equations (7.4.3)–(7.4.5) form a complete set of algebraic equations, which is solved using a Newton-Raphson method.

The eigenvalue problem (4.3.15) is also solved numerically using a similar method. It is necessary to note that the same calculation to obtain a condition at the origin as before should not be applied directly to the equation. Instead, we first rewrite the equation as

$$r\left(rV_r\right)_r - q^2V - r^2\cos(\phi+\theta)V = r^2EV. \tag{7.4.6}$$

Integrating each term over a small disk yields

$$\begin{aligned}
\int_0^\epsilon r\,(rV_r)_r\; r\,dr &= \epsilon^3 V_r - 2\int_0^\epsilon r^2 V_r\,dr \\
&= \epsilon^3 V_r - 2\left(\epsilon^2 V - 2\int_0^\epsilon rV\,dr\right) \\
&\approx \frac{\Delta r^2}{8}(V_1 - V_0), \\
\int_0^\epsilon q^2 V\, r\,dr &\approx \frac{\Delta r^2}{8} q^2 V_0, \\
\int_0^\epsilon \left(r^2\cos(\phi+\theta)V\right)\; r\,dr &\approx \frac{\Delta r^4}{64}\cos(\phi_0+\tilde{\theta}_0)V_0, \\
\int_0^\epsilon \left(r^2 EV\right)\; r\,dr &\approx \frac{\Delta r^4}{64} EV_0.
\end{aligned}$$

The finite difference version of (7.4.6) at the origin is therefore given by

$$V_1 - \left(1 + q^2 + \frac{\Delta r^2}{8}\cos(\phi_0+\theta_0)\right)V_0 = \frac{\Delta r^2}{8} EV_0. \tag{7.4.7}$$

The boundary condition at $r = L$ follows from (7.4.4), i.e.

$$V_{I+1} = V_I. \tag{7.4.8}$$

At the inner points, the eigenvalue problem (7.4.6) is approximated by

$$r_i\left[\left(r_i + \frac{\Delta r}{2}\right)\frac{V_{i+1}-V_i}{\Delta r} - \left(r_i - \frac{\Delta r}{2}\right)\frac{V_i - V_{i-1}}{\Delta r}\right]\frac{1}{\Delta r} - q^2 V_i - r_i^2\cos(\phi_i+\theta_i)V_i = r_i^2 EV_i. \tag{7.4.9}$$

Equations (7.4.9) with boundary conditions (7.4.7) and (7.4.8) form a generalized algebraic eigenvalue problem, that has to be solved simultaneously for $\{V_i\}_{i=0}^I$ and E.

We solve the two-dimensional time-independent equation (4.3.8) using a Newton-Raphson method and numerically integrate the time-dependent one (4.3.3) using a Runge-Kutta method with a similar boundary condition at the singularity $r = 0$ [172].

We have used the method explained above to solve the eigenvalue problem (4.3.15). Shown in Figure 7.1 is the critical eigenvalue, i.e. the maximum E, of the system's ground state as a function of the radius a of the π region for three different values of q, with $L = 2$ and $\gamma = 0$. We note that the case $q = 0$ indeed gives the largest eigenvalue.

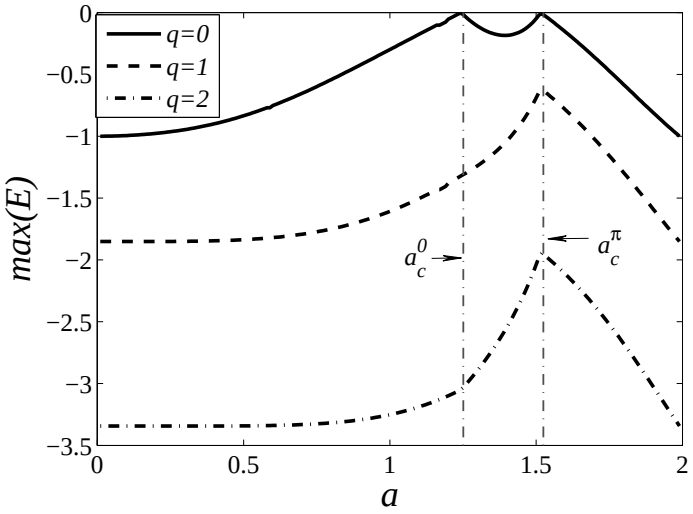

Figure 7.1: The critical eigenvalue of the system's ground state as a function of a for three different values of q as indicated in the legend. Here, $\gamma = 0$ and $L = 2$. Note that between a_c^0 and a_c^π the ground state is not uniform.

7.5 The eigenfunctions corresponding to the Arnold tongues related to $n = 2, 3, 4$

The expressions for the eigenfunctions corresponding to the transitional curves bifurcating from the point $\delta = (n\pi/2a)^2$ in the (δ, κ)-plane, for $n = 2, 3, 4$, are calculated as follows

$$
\begin{aligned}
V_0 &= B_0 \sin\left(\frac{\pi x}{a}\right), \\
V_1 &= -\frac{B_0}{2}\left(\frac{a}{\pi}\right)^2\left\{\frac{r_1 - r_3}{4}\cos\left(\frac{2\pi x}{a}\right) - \frac{r_2 - r_4}{9}\sin\left(\frac{3\pi x}{a}\right) + \frac{r_3}{16}\cos\left(\frac{4\pi x}{a}\right)\right\}, \\
V_2 &= -B_0\left(\frac{a}{\pi}\right)^4\left\{\frac{S_{15}}{4}\cos\left(\frac{2\pi x}{a}\right) + \frac{S_{16}}{9}\sin\left(\frac{3\pi x}{a}\right) + \frac{S_{17}}{16}\cos\left(\frac{4\pi x}{a}\right)\right\},
\end{aligned}
$$

$$
\begin{aligned}
V_0 &= A_0 \cos\left(\frac{\pi x}{a}\right), \\
V_1 &= -\frac{A_0}{2}\left(\frac{a}{\pi}\right)^2\left\{\frac{(r_1 + r_3)}{4}\sin\left(\frac{2\pi x}{a}\right) + \frac{(r_2 + r_4)}{9}\cos\left(\frac{3\pi x}{a}\right) + \frac{r_3}{16}\sin\left(\frac{4\pi x}{a}\right)\right\}, \\
V_2 &= -A_0\left(\frac{a}{\pi}\right)^4\left\{S_{19}\sin\left(\frac{2\pi x}{a}\right) + S_{20}\cos\left(\frac{3\pi x}{a}\right) + S_{21}\sin\left(\frac{4\pi x}{a}\right)\right\},
\end{aligned}
$$

$$
\begin{aligned}
V_0 &= -B_0\left\{\cos\left(\frac{3\pi x}{a}\right) - \sin\left(\frac{3\pi x}{a}\right)\right\},\\
V_1 &= -2B_0\left(\frac{a}{\pi}\right)^2\left\{(r_2 - r_1)\left[\cos\left(\frac{\pi x}{2a}\right) + \sin\left(\frac{\pi x}{2a}\right)\right] + \frac{r_1 + r_4}{25}\left[\cos\left(\frac{4\pi x}{2a}\right)\right.\right.\\
&+ \left.\left.\sin\left(\frac{5\pi x}{2a}\right)\right] + \frac{r_2}{49}\left[\cos\left(\frac{7\pi x}{2a}\right) - \sin\left(\frac{7\pi x}{2a}\right)\right]\right\},\\
V_2 &= 4B_0\left(\frac{a}{\pi}\right)^4\left\{S_{22}\left[\cos\left(\frac{\pi x}{2a}\right) + \sin\left(\frac{\pi x}{2a}\right)\right] + S_{24}\left[\cos\left(\frac{5\pi x}{2a}\right) + \sin\left(\frac{5\pi x}{2a}\right)\right]\right.\\
&\left. + S_{25}\left[\cos\left(\frac{7\pi x}{2a}\right) - \sin\left(\frac{7\pi x}{2a}\right)\right]\right\},
\end{aligned}
$$

$$
\begin{aligned}
V_0 &= B_0\left[\cos\left(\frac{3\pi x}{2a}\right) + \sin\left(\frac{3\pi x}{2a}\right)\right],\\
V_1 &= 2B_0\left(\frac{a}{\pi}\right)^2\left\{(r_1 + r_2)\left[\cos\left(\frac{\pi x}{2a}\right) - \sin\left(\frac{\pi x}{2a}\right)\right] - \frac{r_1 - r_4}{25}\left[\cos\left(\frac{4\pi x}{2a}\right)\right.\right.\\
&- \left.\left.\sin\left(\frac{5\pi x}{2a}\right)\right] + \frac{r_2}{49}\left[\cos\left(\frac{7\pi x}{2a}\right) + \sin\left(\frac{7\pi x}{2a}\right)\right]\right\},\\
V_2 &= -4B_0\left(\frac{a}{\pi}\right)^4\left\{S_{26}\left[\cos\left(\frac{\pi x}{2a}\right) - \sin\left(\frac{\pi x}{2a}\right)\right] + S_{28}\left[\cos\left(\frac{5\pi x}{2a}\right) - \sin\left(\frac{5\pi x}{2a}\right)\right]\right.\\
&\left. - S_{29}\left[\cos\left(\frac{7\pi x}{2a}\right) - \sin\left(\frac{7\pi x}{2a}\right)\right]\right\},
\end{aligned}
$$

$$
\begin{aligned}
V_0 &= B_0\sin\left(\frac{\pi x}{a}\right),\\
V_1 &= \frac{B_0}{2}\left(\frac{\pi}{a}\right)^2\left\{(r_1 + r_3)\cos\left(\frac{\pi x}{a}\right) - \frac{r_1}{9}\cos\left(\frac{3\pi x}{a}\right) + \frac{r_2}{16}\sin\left(\frac{4\pi x}{a}\right)\right\},\\
V_2 &= -B_0\left(\frac{\pi}{a}\right)^4\left\{S_{30}\cos\left(\frac{\pi x}{a}\right) + \frac{S_{31}}{9}\cos\left(\frac{3\pi x}{a}\right) + \frac{S_{33}}{16}\sin\left(\frac{4\pi x}{a}\right)\right\}.
\end{aligned}
$$

$$
\begin{aligned}
V_0 &= A_0\cos\left(\frac{\pi x}{a}\right),\\
V_1 &= \frac{A_0}{2}\left(\frac{\pi}{a}\right)^2\left\{(r_1 - r_3)\sin\left(\frac{\pi x}{a}\right) - \frac{r_1}{9}\sin\left(\frac{3\pi x}{a}\right) - \frac{r_2}{16}\cos\left(\frac{4\pi x}{a}\right)\right\},\\
V_2 &= -A_0\left(\frac{\pi}{a}\right)^4\left\{S_{34}\sin\left(\frac{\pi x}{a}\right) + \frac{S_{35}}{9}\sin\left(\frac{3\pi x}{a}\right) + \frac{S_{37}}{16}\cos\left(\frac{4\pi x}{a}\right)\right\}.
\end{aligned}
$$

The terms S_i in the above expressions are defined as

$$S_{14} = -\frac{1}{4}\left(\frac{r_1^2}{4} - \frac{r_2^2}{9}\right) + \frac{r_2}{18}\left(\frac{r_2}{2} + r_4\right) + \frac{r_3}{8}\left(r_1 - \frac{5r_3}{8}\right),$$

$$S_{15} = \frac{r_1}{144}\left(5r_2 + 13r_4\right) - \frac{r_3}{16}\left(\frac{r_2}{4} + r_4\right), \quad S_{16} = \frac{r_1}{16}\left(r_1 - \frac{5r_3}{4}\right) - \frac{r_2}{36}\left(r_2 - r_4\right),$$

$$S_{17} = \frac{r_1}{36}\left(\frac{13r_2}{4} - r_4\right) - \frac{3r_2r_3}{64},$$

$$S_{18} = -\frac{1}{4}\left(\frac{r_1^2}{4} + \frac{r_2^2}{9}\right) - \frac{r_2}{18}\left(\frac{r_2}{2} + r_4\right) - \frac{r_3}{8}\left(r_1 + \frac{5r_3}{8}\right),$$

$$S_{19} = \frac{13r_1}{144}\left(r_2 + r_4\right) + \frac{r_3}{16}\left(3r_2 + r_4\right), \quad S_{20} = \frac{r_1}{16}\left(r_1 + \frac{3r_3}{4}\right) + \frac{r_2}{36}\left(r_2 + r_4\right),$$

$$S_{21} = -\frac{r_1}{36}\left(\frac{13r_2}{4} + r_4\right) - \frac{3r_2r_3}{64},$$

$$S_{22} = r_1\left(\frac{26r_2r_2}{25} - r_1\right) + \frac{2r_2}{49}\left(24r_3 + \frac{37r_4}{25}\right) - \frac{r_3}{25}\left(24r_1 - r_4\right),$$

$$S_{23} = -\frac{2r_1}{25}\left(13r_1 + r_4\right) + 2r_2\left(r_1 - \frac{25r_2}{49}\right) - \frac{r_4^2}{25},$$

$$S_{24} = r_2\left(r_2 + r_3\right) - \frac{r_3}{25}\left(24r_1 - r_4\right) - \frac{50r_1r_2}{49},$$

$$S_{25} = \frac{r_1}{25}\left(r_1 - 26r_4\right) + r_3\left(r_1 - \frac{48r_2}{49}\right) + r_2r_4,$$

$$S_{26} = r_1\left(\frac{26r_2r_2}{25} + r_1\right) - \frac{2r_2}{49}\left(\frac{37r_4 - 24r_3}{25}\right) + \frac{r_3}{25}\left(24r_1 + r_4\right),$$

$$S_{28} = -r_2\left(r_2 - r_3\right) + \frac{r_3}{25}\left(24r_1 + r_4\right) - \frac{50r_1r_2}{49},$$

$$S_{29} = \frac{r_1}{25}\left(r_1 - 26r_4\right) - r_3\left(r_1 + \frac{48r_2}{49}\right) - r_2r_4, \quad S_{30} = \frac{2r_1}{9}\left(r_2 + r_4\right) + \frac{r_3}{4}\left(\frac{17r_2}{16}r_4\right),$$

$$S_{31} = \frac{1}{4}\left(\frac{r_2^2}{16} + r_3^2\right) + \frac{r_1}{2}\left(\frac{5r_1}{9} + r_3\right), \quad S_{32} = r_4\left(\frac{2r_1}{9} + \frac{r_3}{4}\right) + \frac{r_2}{4}\left(\frac{17r_1}{16} + r_3\right),$$

$$S_{33} = \frac{r_3}{4}\left(r_1 + r_3\right) + \frac{1}{4}\left(\frac{r_2r_4}{16} - \frac{r_1^2}{9}\right), \quad S_{34} = \frac{52r_1}{18}\left(r_2 - r_4\right) - \frac{r_3}{4}\left(\frac{17r_2}{16} - r_4\right),$$

$$S_{35} = \frac{1}{4}\left(\frac{r_2^2}{16} + r_3^2\right) + \frac{r_1}{2}\left(\frac{5r_1}{9} - r_3\right), \quad S_{36} = r_4\left(\frac{2r_1}{9} - \frac{r_3}{4}\right) - \frac{r_2}{4}\left(\frac{17r_1}{16} - r_3\right),$$

$$S_{37} = \frac{r_3}{4}\left(r_1 - r_3\right) + \frac{1}{4}\left(\frac{r_2r_4}{16} - \frac{r_1^2}{9}\right).$$

Bibliography

[1] RA Millikan and ES Bishop. *Elements of electricity: a practical discussion of the fundamental laws and phenomena of electricity and their practical applications in the business and industrial world*. American Technical Society, (1917).

[2] HK Onnes. Investigations into the properties of substances at low temperatures, which have led, amongst other things, to the preparation of liquid helium. *Nobel Lecture*, (1913). http://nobelprize.org/physics/laureates/1913/onnes-lecture.pdf.

[3] W Meissner and R Ochsenfeld. Ein neuer effekt bei eintritt der supraleitf "ahigkeit. *Naturwissenschaften*, 21:787–788, (1933).

[4] F London and H London. The electromagnetic equations of the supraconductor. *Proc Roy Soc Lond. A*, 149:71–88, (1935).

[5] LD Landau and VL Ginzburg. On the theory of Superconductivity. *Zh. Eksp. Teor. Fiz*, 20:546–68, (1950).

[6] H Fröhlich. Theory of the superconducting state 1. The ground state at the absolute zero of temperature. *Phys. Rev.*, 79:845–856, (1950).

[7] LN Cooper. Bound electron pairs in a degenerate Fermi gas. *Phys. Rev.*, 104(4): 1189–1190, (1956).

[8] J Bardeen, LN Cooper, and JR Schrieffer. Theory of superconductivity. *Phy Rev*, 108:1175–1204, (1957).

[9] BD Josephson. Possible new effects in superconductive tunnelling. *Phys. Letts.*, 1:251–253, (1962).

[10] JG Bednorz and KA Müller. Possible high T_c superconductivity in the Ba La Cu O system. *Zeit. für Phys. B*, 64:189–193, (1986).

[11] A Schilling, M Cantoni, D Guo, and HR Ott. Superconductivity above 130 K in the Hg-Ba-Ca-Cu-O system. *Nature 363, 56*, 58, (1993).

[12] Y Kamihara, H Hiramatsu, M Hirano, R Kawamura, H Yanagi, T Kamiya, and H Hosono. Iron-based layered superconductor: LaOFeP. *J. Am. Chem. Soc*, 128: 10012–10013, (2006).

[13] C Kittel and P McEuen. *Introduction to Solid State Physics*. Wiley, New York, 1976.

[14] M Remoissenet. *Waves Called Solitons: Concepts and Experiments*. Springer Verlag, Berlin, 1999.

[15] BV Vasiliev. About the London penetration depth. *arXiv:1101.0330*, 2011.

[16] M Tinkham. *Introduction to Superconductivity*. Dover Publications, Mineola, 2004.

[17] LB Ioffe, VB Geshkenbein, MV Feigel'Man, AL Fauchere, and G Blatter. Environmentally decoupled sds-wave Josephson junctions for quantum computing. *Nature*, 398:679–681, 1999.

[18] T Yamashita, K Tanikawa, S Takahashi, and S Maekawa. Superconducting π qubit with a ferromagnetic Josephson junction. *Phys. Rev. Letts.*, 95:97001, 2005.

[19] Y Nakamura, YA Pashkin, and JS Tsai. Coherent control of macroscopic quantum states in a single-Cooper-pair box. *Nature*, 398:786–788, 1999.

[20] JM Martinis, S Nam, J Aumentado, and C Urbina. Rabi oscillations in a large Josephson-junction qubit. *Phys. Rev. Letts.*, 89:117901, 2002.

[21] JE Mooij, TP Orlando, L Levitov, L Tian, CH Van der Wal, and S Lloyd. Josephson persistent-current qubit. *Science*, 285:1036, 1999.

[22] MA Nielsen, I Chuang, and LK Grover. Quantum computation and quantum information. *Am. J. Phys.*, 70:558, 2002.

[23] PG Gennes. *The Superconductivity of metals and alloys*. Addison-Wesley, New York, 1966.

[24] JM Rowell, PW Anderson, and DE Thomas. Image of the phonon spectrum in the tunneling characteristic between superconductors. *Phys. Rev. Lett.*, 10:334–336, 1963.

[25] LN Bulaevskii, VV Kuzii, and AA Sobyanin. Superconducting system with weak coupling to the current in the ground state. *Soviet Journal of Experimental and Theoretical Phys. Letts.*, 25:290, 1977.

[26] DJ Van Harlingen. Phase-sensitive tests of the symmetry of the pairing state in the high-temperature superconductors−evidence for $d_{x^2-y^2}$ symmetry. *Rev. of Mod. Phys.*, 67:515, 1995.

[27] JJA Baselmans, AF Morpurgo, BJ Van Wees, and TM Klapwijk. Reversing the direction of the supercurrent in a controllable Josephson junction. *Nature*, 397: 43–45, 1999.

[28] VV Ryazanov, VA Oboznov, AY Rusanov, AV Veretennikov, AA Golubov, and J Aarts. Coupling of two superconductors through a ferromagnet: evidence for a π junction. *Phys. Rev. Lett.*, 86:2427–2430, 2001.

[29] E Terzioglu, D Gupta, and MR Beasley. Complementary Josephson junction circuits. *IEEE Transactions on Applied Superconductivity*, 7:3642–3645, 1997.

[30] E Terzioglu and MR Beasley. Complementary Josephson junction devices and circuits: A possible new approach to superconducting electronics. *IEEE Transactions on applied superconductivity*, 8, 1998.

[31] G Testa, A Monaco, E Esposito, E Sarnelli, DJ Kang, SH Mennema, EJ Tarte, and MG Blamire. Midgap state-based π-junctions for digital applications. *Applied Phys. Letts.*, 85:1202, 2004.

[32] H Sellier, C Baraduc, F Lefloch, and R Calemczuk. Half-integer Shapiro steps at the 0-π crossover of a ferromagnetic Josephson junction. *Phys. Rev. Lett.*, 92: 257005, 2004.

[33] VV Ryazanov, VA Oboznov, AV Veretennikov, and AY Rusanov. Intrinsically frustrated superconducting array of superconductor-ferromagnet-superconductor π junctions. *Phys. Rev. B*, 65:020501, 2001.

[34] A Bauer, J Bentner, M Aprili, ML Della Rocca, M Reinwald, W Wegscheider, and C Strunk. Spontaneous supercurrent induced by ferromagnetic π junctions. *Phys. Rev. Lett.*, 92:217001, 2004.

[35] Y Blum, A Tsukernik, M Karpovski, and A Palevski. Oscillations of the superconducting critical current in Nb-Cu-Ni-Cu-Nb junctions. *Phys. Rev. Lett.*, 89:187004, 2002.

[36] AI Buzdin, LN Bulaevskii, and SV Panyukov. Critical-current oscillations as a function of the exchange field and thickness of the ferromagnetic metal (F) in an SFS Josephson junction. *JETP Lett*, 35:103–104, 1982.

[37] AI Buzdin. Proximity effects in superconductor-ferromagnet heterostructures. *Reviews of modern physics*, 77:935, 2005.

[38] T Kontos, M Aprili, J Lesueur, F Genet, B Stephanidis, and R Boursier. Josephson junction through a thin ferromagnetic layer: negative coupling. *Phys. Rev. Lett.*, 89:137007, 2002.

[39] M Weides, M Kemmler, H Kohlstedt, R Waser, D Koelle, R Kleiner, and E Goldobin. $0 - \pi$ Josephson Tunnel Junctions with Ferromagnetic Barrier. *Phyical Review Letts.*, 97:247001, Dec 2006.

[40] CC Tsuei and JR Kirtley. Pairing symmetry in cuprate superconductors. *Rev. of Mod. Phys.*, 72:969, 2000.

[41] CC Tsuei and JR Kirtley. Phase-sensitive evidence for d-wave pairing symmetry in electron-doped cuprate superconductors. *Phys. Rev. Letts.*, 85:182–185, 2000.

[42] YS Barash, H Burkhardt, and D Rainer. Low-temperature anomaly in the Josephson critical current of junctions in d-wave superconductors. *Phys. Rev. Lett.*, 77: 4070–4073, 1996.

[43] E Il'Ichev, M Grajcar, R Hlubina, RPJ IJsselsteijn, HE Hoenig, HG Meyer, A Golubov, MHS Amin, AM Zagoskin, and AN Omelyanchouk. Degenerate ground state in a Mesoscopic Y Ba_2 Cu_3 O_{7-x} grain boundary Josephson junction. *Phys. Rev. Lett.*, 86:5369–5372, 2001.

[44] HJH Smilde, DHA Blank, GJ Gerritsma, H Hilgenkamp, and H Rogalla. *d*-Wave Induced Josephson Current Counterflow in $YBa_2Cu_3O_7$/Nb Zigzag Junctions. *Phys. Rev. Lett.*, 88:57004, 2002.

[45] H-J H Smilde D H A Blank G Rijnders H Rogalla JR Kirtley H Hilgenkamp, Ariando and CC Tsuei. Ordering and manipulation of the magnetic moments in large-scale superconducting π-loop arrays. *Naure*, 422:50–53, 2003.

[46] E Goldobin, A Sterck, T Gaber, D Koelle, and R Kleiner. Dynamics of semifluxons in Nb long Josephson 0-π junctions. *Phys. Rev. Letts.*, 92:57005, 2004.

[47] DR Gulevich, FV Kusmartsev, S Savel'ev, VA Yampol'skii, and F Nori. Shape and wobbling wave excitations in Josephson junctions: exact solutions of the (2+ 1)-dimensional sine-Gordon model. *Phys. Rev. B*, 80:094509, 2009.

[48] W Braunisch, N Knauf, V Kataev, S Neuhausen, A Grütz, A Kock, B Roden, D Khomskii, and D Wohlleben. Paramagnetic Meissner effect in Bi high-temperature superconductors. *Phys. Rev. Letts.*, 68:1908–1911, 1992.

[49] M Sigrist and T M Rice. Paramagnetic Effect in High T_c Superconductors-A Hint for *d*-Wave Superconductivity. *Journal of the Physical Society of Japan*, 61:4283–4286, 1992.

[50] T Ortlepp, O Mielke, CJM Verwijs, KFK Foo, H Rogalla, FH Uhlmann, and H Hilgenkamp. Flip-flopping fractional flux quanta. *Science*, 312:1495, 2006.

[51] CM Pegrum. Can a fraction of a quantum be better than a whole one? *Science(Washington)*, 312:1483–1484, 2006.

[52] AB Kuklov, VS Boyko, and J Malinsky. Instability in the current-biased 0-π Josephson junction. *Phys. Rev. B*, 51:11965, 1995.

[53] LN Bulaevskii, VV Kuzii, AA Sobyanin, and PN Lebedev. On possibility of the spontaneous magnetic flux in a Josephson junction containing magnetic impurities. *Solid State Communications*, 25:1053–1057, 1978.

[54] E Goldobin, D Koelle, and R Kleiner. Semifluxons in long Josephson 0-π-junctions. *Phys. Rev. B*, 66:100508, 2002.

[55] JH Xu, JH Miller Jr, and CS Ting. π-vortex state in a long 0-π Josephson junction. *Phys. Rev. B*, 51:11958–11961, 1995.

[56] E Goldobin, D Koelle, and R Kleiner. Ground states and bias-current-induced rearrangement of semifluxons in 0-π long Josephson junctions. *Phys. Rev. B*, 67.

[57] H Susanto, SA van Gils, TPP Visser, Ariando, HJH Smilde, and H Hilgenkamp. Static semifluxons in a long Josephson junction with π-discontinuity points. *Phys. Rev. B*, 68:104501, 2003.

[58] JR Kirtley, KA Moler, and DJ Scalapino. Spontaneous flux and magnetic-interference patterns in 0-π Josephson junctions. *Phys. Rev. B*, 56:886, 1997.

[59] JR Kirtley, CC Tsuei, Martin Rupp, JZ Sun, Lock See Yu-Jahnes, A Gupta, MB Ketchen, KA Moler, and M Bhushan. Direct Imaging of Integer and Half-Integer Josephson Vortices in High-T_c Grain Boundaries. *Phys. Rev. Lett..*, 76:1336–1339, Feb 1996.

[60] JR Kirtley, CC Tsuei, and KA Moler. Temperature dependence of the half-integer magnetic flux quantum. *Science*, 285:1373, 1999.

[61] A Sugimoto, T Yamaguchi, and I Iguchi. Temperature dependence of half flux quantum in Y Ba_2 Cu_3 O_{7-y} tricrystal thin film observed by scanning SQUID microscopy. *Physica C*, 367:28–32, 2002.

[62] C Gürlich, S Scharinger, M Weides, H Kohlstedt, RG Mints, E Goldobin, D Koelle, and R Kleiner. Visualizing supercurrents in ferromagnetic Josephson junctions with various arrangements of 0 and π segments. *Phys. Rev. B*, 81:094502, 2010.

[63] H Farhan-Hassan and FV Kusmartsev. Spontaneous Movable Semifluxons–New Phenomenon arising in Nano-Electronic Superconducting System. In *Journal of Physics: Conference Series*, volume 248, page 012058. IOP Publishing, 2010.

[64] DR Gulevich and FV Kusmartsev. Flux cloning in Josephson transmission lines. *Phys. Rev. Lett.*, 97:17004, 2006.

[65] WQ Chen and FC Zhang. π-phase shift at the interface of two pnictide superconductors with antiphase s-wave pairing. *Phys. Rev. B*, 83:212501, 2011.

[66] E Goldobin, A Sterck, T Gaber, D Koelle, and R Kleiner. Dynamics of Semifluxons in Nb Long Josephson $0-\pi$ Junctions. *Phys. Rev. Lett..*, 92:057005, Feb 2004.

[67] E Goldobin, K Vogel, WP Schleich, D Koelle, and R Kleiner. Coherent superpositions of single semifluxon states in a 0-π Josephson junction. *Phys. Rev. B*, 81: 054514, 2010.

[68] A Barone and G Paterno. *The Josephson Effect*. John Wiley & Sons, New York, 1982.

[69] Alwyn C Scott. *Active and Nonlinear Wave Propogation in Electronics*. John Wiley & Sons, New York, 1970.

[70] A Scott. *Nonlinear Science: Emergence and Dynamics of Coherent Structures*. Oxford University Press, New York, 2003.

[71] JC Swihart. Field solution for a thin-film superconducting strip transmission line. *Journal of Applied Physics*, 32:461, 1961.

[72] A Seeger, H Donth, and A Kochendörfer. Theorie der Versetzungen in eindimensionalen Atomreihen. *Zeitschrift für Physik A Hadrons and Nuclei*, 134:173–193, 1953.

[73] JK Perring and THR Skyrme. A model unified field equation. *Nuclear Physics*, 31: 550–555, 1962.

[74] PG Drazin and RS Johnson. *Solitons: an introduction*. Cambridge University Press, Cambridge, 1989.

[75] R Rajaraman. *Solitons and Instantons: an Introduction to Solitons and Instantons in Quantum Field Theory*. Elsevier, Amstardam, 1982.

[76] A Enneper. U ber asymptotische Linien. *Nachr. Konigl. Gesellsch. d. Wiss. Gottingen*, page 493, 1870.

[77] PS Lomdahl, OH Soerensen, and PL Christiansen. Soliton excitations in Josephson tunnel junctions. *Phys. Rev. B*, 25:5737, 1982.

[78] B. Dueholm, OA Levring, J. Mygind, N.F. Pedersen, OH Soerensen, and M. Cirillo. Multisoliton excitations in long Josephson junctions. *Phys. Rev. Letts.*, 46: 1299–1302, 1981.

[79] Z Hermon, A Shnirman, and E Ben-Jacob. Dephasing length and coherence of a quantum soliton in an ideal long Josephson junction. *Phys. Rev. Letts.*, 74:4915–4918, 1995.

[80] T Kato and M Imada. Macroscopic quantum tunneling of a fluxon in a long Josephson junction. *Journal of the Physical Society of Japan*, 65:2963–2975, 1996.

[81] M Abramowitz and IA Stegun. *Handbook of Mathematical Functions*. Dover publications, Mineola, 1964.

[82] Alexey Ustinov. Lectures on Dynamics and Applications of Josephson Fluxons. (2002).

[83] A Wallraff, A Lukashenko, J Lisenfeld, A Kemp, MV Fistul, Y Koval, and AV Ustinov. Quantum dynamics of a single vortex. *Nature*, 425:155–158, 2003.

[84] Y Bugoslavsky, GK Perkins, X Qi, LF Cohen, and AD Caplin. Vortex dynamics in superconducting MgB_2 and prospects for applications. *Nature*, 410:563–565, 2001.

[85] S Savel'Ev and F Nori. Experimentally realizable devices for controlling the motion of magnetic flux quanta in anisotropic superconductors. *Nature Materials*, 1: 179–184, 2002.

[86] KK Likharev. *Dynamics of Josephson junctions and circuits*. Gordon and Breach, Amsterdam, 1986.

[87] AV Ustinov. Solitons in Josephson junctions. *Physica D*, 123:315–329, 1998.

[88] KE Lonngren and A Scott. *Solitons in action: proceedings of a workshop sponsored by the Mathematics Division, Army Research Office held at Redstone Arsenal October 26-27, 1977*. Academic Press, 1978.

[89] DW McLaughlin and AC Scott. Perturbation analysis of fluxon dynamics. *Phys. Rev. A*, 18:1652, 1978.

[90] NF Pedersen. In SE Trullinger, VE Zakharov, and VL Pokrovsky, editors, Solitons. *Elsevier, Amsterdam*, 120:469, 1986.

[91] RD Parmentier. The New Superconducting Electronics Ed H Weinstock and RW Ralston, 1993.

[92] NW McLachlan. *Ordinary nonlinear differential equations in engineering and physical sciences*. Clarendon Prss, Oxford, 1956.

[93] DK Arrowsmith. *An Introduction to Dynamical Systems*. Cambridge University Press, 1990.

[94] Takeo Kato and Masatoshi Imada. Vortices and Quantum tunneling in current-biased $0 - \pi - 0$ Josephson junctions of d-wave Superconductors. *Journal of the Physical Society of Japan*, 66:1445–1449, 1997.

[95] CS Owen and DJ Scalapino. Vortex Structure and Critical Currents in Josephson Junctions. *Phys. Rev.*, 164:538–544, 1967.

[96] T Kato. *Perturbation Theory for Linear Operators*. Springer, New York, 1966.

[97] LD Landau and EM Lifshitz. *Quanutum Mechanics, Non-relativisitic Theory*, volume 3. Pergamon Press, Oxford, 1973.

[98] RL Liboff. *Introductory Quantum Mechanics*. Addison-Wesley Reading, MA, 1998.

[99] E Goldobin, K Vogel, O Crasser, R Walser, WP Schleich, D Koelle, and R Kleiner. Quantum tunneling of semifluxons in a 0-π-0 long Josephson junction. *Phys. Rev. B*, 72:054527, 2005.

[100] AH Nayfeh and DT Mook. *Perturbation methods*, volume 6. John Wiley & Sons, New York, 1979.

[101] VG Kogan, JR Clem, and JR Kirtley. Josephson vortices at tricrystal boundaries. *Phys. Rev. B*, 61:9122–9129, 2000.

[102] RWD Nickalls. A new approach to solving the cubic: Cardan's solution revealed. *The Mathematical Gazette*, 77:354–359, 1993.

[103] S Ahmad, H Susanto, and JAD Wattis. Existence and stability analysis of finite 0-π-0 Josephson junctions. *Phys. Rev. B*, 80:064515, 2009.

[104] A Zenchuk and E Goldobin. Analysis of ground states of 0-π long Josephson junctions. *Phys. Rev. B*, 69:024515, 2004.

[105] A Dewes, T Gaber, D Koelle, R Kleiner, and E Goldobin. Semifluxon molecule under control. *Phys. Rev. Letts.*, 101:247001, 2008.

[106] JA Boschker. Manipulation and on-chip readout of fractional flux quanta. Master's thesis, University of Twente, Netherlands, 2006.

[107] AB Kuklov, VS Boyko, and J Malinsky. Instability in the current-biased 0-π Josephson junction: Erratum. *Phys. Rev. B*, 55:11878, 1997.

[108] E Goldobin, D Koelle, and R Kleiner. Ground states of one and two fractional vortices in long Josephson 0-κ junctions. *Phys. Rev. B*, 70:174519, 2004.

[109] E Goldobin, H Susanto, D Koelle, R Kleiner, and SA Van Gils. Oscillatory eigenmodes and stability of one and two arbitrary fractional vortices in long Josephson 0-κ junctions. *Phys. Rev. B*, 71:104518, 2005.

[110] A Buzdin and AE Koshelev. Periodic alternating 0-and π-junction structures as realization of φ-Josephson junctions. *Phys. Rev. B*, 67:220504, 2003.

[111] H Susanto, E Goldobin, D Koelle, R Kleiner, and SA van Gils. Controllable plasma energy bands in a one-dimensional crystal of fractional Josephson vortices. *Phys. Rev. B*, 71:174510, 2005.

[112] GB Arfken, HJ Weber, and H Weber. *Mathematical Methods for Physicists*, volume 148. Academic press New York, 1995.

[113] S Ahmad, H Susanto, JAD Wattis, and E Goldobin. Existence and stability analysis of semifluxons in disk-shaped two-dimensional 0-π Josephson junctions. *Phys. Rev. B*, 82:174504, 2010.

[114] E A Jackson. *Perspectives of nonlinear dynamics*, volume 2. Cambridge University Press, 1989.

[115] J Zagrodzinski. The solutions of the two-dimensional sine-gordon equation. *Phyics Letts. A*, 57:213–214, 1976.

[116] R Hirota. Exact three-soliton solution of the two-Dimensional sine-Gordon Equation. *Journal of the Physical Society of Japan*, 35, 1973.

[117] JD Gibbon and G Zambotti. The interaction of n-dimensional soliton wave fronts. *Il Nuovo Cimento B*, 28:1–17, 1975.

[118] BG Konopelchenko, W Schief, and C Rogers. A (2+1)-dimensional sine-Gordon system: its auto-Bäcklund transformation. *Phys. Letts. A*, 172:39–48, 1992.

[119] WK Schief. On localized solitonic solutions of a (2+1)-dimensional sine-Gordon system. *Journal of Physics A: Mathematical and General*, 25:L1351, 1992.

[120] JJC Nimmo and WK Schief. Superposition principles associated with the Moutard transformation: an integrable discretization of a (2+ 1)–dimensional sine–Gordon system. *Proceedings of the Royal Society of London. Series A: Mathematical, Physical and Engineering Sciences*, 453:255, 1997.

[121] S Lou, C Chen, and X Tang. (2+ 1)-dimensional (M+ N)-component AKNS system: Painlevé integrability, infinitely many symmetries, similarity reductions and exact solutions. *Journal of Mathematical Physics*, 43:4078, 2002.

[122] M. Dehghan and D. Mirzaei. The boundary integral equation approach for numerical solution of the one-dimensional sine-Gordon equation. *Numerical Methods for Partial Differential Equations*, 24:1405–1415, 2008.

[123] D Mirzaei and M Dehghan. Boundary element solution of the two-dimensional sine-Gordon equation using continuous linear elements. *Engineering analysis with boundary elements*, 33:12–24, 2009.

[124] R Jiwari, S Pandit, and RC Mittal. Numerical simulation of two-dimensional sine-Gordon solitons by differential quadrature method. *Computer Physics Communications*, 183:600–616, 2011.

[125] PL Christiansen and OH Olsen. Return effect for rotationally symmetric solitary wave solutions to the sine-Gordon equation. *Phys. Letts. A*, 68:185–188, 1978.

[126] MR Samuelsen. Approximate rotationally symmetric solutions to the sine-Gordon equation. *Phys. Letts. A*, 74:21–22, 1979.

[127] VG Makhankov. Dynamics of classical solitons (in non-integrable systems). *Physics reports*, 35:1–128, 1978.

[128] J Geicke. Cylindrical pulsons in nonlinear relativistic wave equations. *Physica Scripta*, 29:431, 1984.

[129] BA Malomed. Decay of shrinking solitons in multidimensional sine-Gordon equation. *Physica D*, 24:155–171, 1987.

[130] PL Christiansen and OH Olsen. Ring-shaped quasi-soliton solutions to the two- and three-dimensional sine-Gordon equation. *Physica Scripta*, 20:531, 1979.

[131] GH Derrick. Comments on nonlinear wave equations as models for elementary particles. *Journal of Mathematical Physics*, 5:1252, 1964.

[132] OH Olsen and MR Samuelsen. The influence of an external field on solutions to the spherically symmetric sine-Gordon equation. *Physica Scripta*, 23:1033, 1981.

[133] E Goldobin, A Sterck, and D Koelle. Josephson vortex in a ratchet potential: theory. *Phys. Rev. E*, 63:031111, 2001.

[134] PL Christiansen and PS Lomdahl. Numerical study of (2+1) dimensional sine-Gordon solitons. *Physica D*, 2:482–494, 1981.

[135] VP Koshelets and SV Shitov. Integrated superconducting receivers. *Superconductor Science and Technology*, 13:R53, 2000.

[136] MY Torgashin, VP Koshelets, PN Dmitriev, AB Ermakov, LV Filippenko, and PA Yagoubov. Superconducting integrated receiver based on Nb-AlN-NbN-Nb Circuits. *Applied Superconductivity, IEEE Transactions on*, 17:379–382, 2007.

[137] S Savel'ev, AL Rakhmanov, and F Nori. Quantum terahertz electrodynamics and macroscopic quantum tunneling in layered superconductors. *Phys. Rev. Letts.*, 98: 77002, 2007.

[138] VA Yampol'skii, DR Gulevich, S Savel'ev, and F Nori. Surface plasma waves across the layers of intrinsic Josephson junctions. *Arxiv preprint cond-mat.supr-con:0808.1384*, 2008.

[139] D Ouroushev, N Martinov, and A Grigorov. An approach for solving the two-dimensional sine-Gordon equation. *Journal of Physics A: Mathematical and General*, 24:L527, 1991.

[140] AA Minzoni, NF Smyth, and AL Worthy. Pulse evolution for a two-dimensional sine-Gordon equation. *Physica D*, 159:101–123, 2001.

[141] A Barone and G Paterno. The Josephson Effect. *Physics and Applications*, 1984.

[142] YS Kivshar and GP Agrawal. *Optical Solitons: From Fibers to Photonic Crystals*. Academic Press, California, USA, 2003.

[143] J Yang. *Nonlinear waves in Integrable and Nonintegrable Systems*, volume 16. Society for Industrial and Applied Mathematics, Philadelphia, USA, 2010.

[144] EI Rashba. Properties of Semiconductors with an extremum loop. 1. Cyclotron and combinational resonance in a magnetic field perpendicular to the plane of the loop. *Soviet Physics Solid State*, 2:1109–1122, 1960.

[145] UC Coskun, TC Wei, S Vishveshwara, PM Goldbart, and A Bezryadin. h/e magnetic flux modulation of the energy gap in nanotube quantum dots. *Science*, 304: 1132, 2004.

[146] BA Malomed and AV Ustinov. Creation of classical and quantum fluxons by a current dipole in a long Josephson junction. *Phys. Rev. B*, 69:064502, 2004.

[147] NW Ashcroft and ND Mermin. *Solid State Physics*, volume 3000. Holt Saunders, Philadelphia, 1976.

[148] C Giacovazzo, HL Monaco, G Artioli, D Viterbo, G Ferraris, G Gilli, G Zannotti, and M Catti. *Fundamentals of Crystallography*. Oxford University Press Inc, New York, USA, 2002.

[149] NW McLachlan. *Theory and Application of Mathieu Functions*. Clarendon Press, Oxford, 1947.

[150] C C Chicone. *Ordinary differential equations with applications*, volume 34. Springer Verlag, New York, 2006.

[151] AH Nayfeh and DT Mook. *Nonlinear Oscillations*. John Wiley & Sons, New York, 1979.

[152] K Maki and H Takayama. Quantum-statistical mechanics of extended objects. II. Breathers in the sine-Gordon system. *Phys. Rev. B*, 20:5002, 1979.

[153] YS Kivshar and BA Malomed. Dynamics of solitons in Nearly Integrable Systems. *Rev. of Mod. Phys.*, 61:763, 1989.

[154] D Gulevich and F Kusmartsev. Switching phenomena in an annular Josephson junction. *Physica C*, 435:87–91, 2006.

[155] DR Gulevich and FV Kusmartsev. New phenomena in long Josephson junctions. *Superconductor Science and Technology*, 20:S60, 2007.

[156] K Forinash and CR Willis. Nonlinear response of the sine-Gordon breather to an ac driver. *Physica D*, 149:95–106, 2001.

[157] JI Ramos. The sine-Gordon equation in the finite line. *Applied mathematics and computation*, 124:45–93, 2001.

[158] PG Kevrekidis, A Saxena, and AR Bishop. Interaction between sine-Gordon breathers. *Phys. Rev. E*, 64:026613, 2001.

[159] VI Karpman, NA Ryabova, and VV Solov'ev. Numerical investigations of the fluxon-antifluxon system in a long Josephson junction. *Phys. Letts. A*, 92:255–257, 1982.

[160] PS Lomdahl, OH Olsen, and MR Samuelsen. Breather-kink-antikink-pair conversion in the driven sine-Gordon system. *Phys. Rev. A*, 29:350, 1984.

[161] I Stakgold and MJ Holst. *Green's functions and Boundary Value Problems*. Wiley New York, 1998.

[162] RK Dodd, HC Morris, and JC Eilbeck. *Soliton and nonlinear wave equations*. Academic Press, New York, NY, USA, 1982.

[163] CG Christopher and LK Peter. *Introductory Quantum Optics*. Cambridge University, Cambridge, 2005.

[164] M Frasca. A modern review of the two-level approximation. *Annals of Physics*, 306:193–208, 2003.

[165] C M de Sterke and JE Sipe. Gap Solitons. *Progress in Optics*, 33:203–260, 1994.

[166] AV Yulin and DV Skryabin. Out-of-gap Bose-Einstein solitons in optical lattices. *Phys. Rev. A*, 67:023611, 2003.

[167] NK Efremidis and DN Christodoulides. Lattice solitons in Bose-Einstein condensates. *Phys. Rev. A*, 67:063608, 2003.

[168] H Goldstein, C Poole, and J Safko. *Classical Mechanics*. Addison-Wesley, New York, 2002.

[169] JL Synge and BA Griffith. *Principles of Mechanics*. McGraw-Hill Book Company, Inc., 1959.

[170] E Kreyszig. *Introductory Functional Analysis with Applications*. Wiley, New York, 1978.

[171] PR Halmos. *Finite-dimensional vector spaces*. Springer Verlag, New York, 1958.

[172] JC Strikwerda. *Finite Difference Schemes and Partial Differential Equations*. SIAM, Philadelphia, 2004.